THESIS

THE ROLE OF DYNAMIC ICE-BREAKUP ON BANK EROSION AND LATERAL MIGRATION OF THE MIDDLE SUSITNA RIVER, ALASKA

Submitted by

Renee A. Vandermause

Department of Civil and Environmental Engineering

In partial fulfillment of the requirements

For the Degree of Master of Science

Colorado State University

Fort Collins, Colorado

Summer 2018

Master's Committee:

Advisor: Robert Ettema
Co-Advisor: Lyle Zevenbergen

Sara Rathburn

ABSTRACT

THE ROLE OF DYNAMIC ICE-BREAKUP ON BANK EROSION AND LATERAL MIGRATION OF THE MIDDLE SUSITNA RIVER, ALASKA

Rivers in northern, boreal regions experience frigid winters and ice formation that influence several geomorphic processes including bank erosion and lateral channel migration. Not only are the ice-driven processes complex and highly variable in time and space, but they are difficult to observe due to the logistical challenges of conducting fieldwork when the rivers are frozen in the winter and during ice breakup in the spring. Yet, characterizing and quantifying the processes that drive bank erosion, whether during the summer open-water period or when ice is in the channel, is important for predicting channel dynamics in the boreal rivers where there is a mixed ice-fluvial regime. Of particular importance is understanding the erosional processes that form or maintain complex channel and riparian systems which in turn provide diverse aquatic habitat for a range of salmonid species. This study capitalized on an extensive archive of field data and observations, of which the author was involved, to quantify the extent to which channel change is driven by ice and fluvial processes on the Susitna River, a large gravel-cobble bed river in south-central Alaska. As bank erosion is a key element of channel change, this study focused on bank erosion along the middle reach of Susitna River located downstream of a proposed dam site.

Using aerial photography and videography over two one-year periods, 2011 to 2012 (included a thermal ice-breakup) and 2012 to 2013 (included a dynamic ice-breakup), the study identified short-term erosion rates for distinct geomorphic reaches, determined the amount of erosion by the type of geomorphic surface, and quantified when the most bank erosion occurred

annually; whether during the open-water season or when ice was in the channel, particularly during ice-breakup. The aerial imagery was supplemented by observations and data collected along the Middle Susitna River over two field seasons. The study also used a synthesis of observations and 2-D depth averaged fluvial modeling using SRH-2D to characterize processes that drive bank erosion.

This study found that the majority of bank erosion, 54 to 61 percent by sub-reach, occurs or is initiated over a short period of time during dynamic breakup of the river's ice cover. The dominant erosion process is attributable to the combination of relatively high-water discharge and the presence of ice floes and ice rubble. Vegetated bars and terrace margins were the most susceptible to bank erosion, notably by impacting ice floes. Erosion of banks adjoining floodplain surfaces, partly protected by vegetation rootmats and by shear walls of smaller ice rubble, accounted for less overall erosion than vegetated bars or terraces. Wide sub-reaches with multiple channels were prone to ice-jamming, diversion of flow conveying ice into side channels, and localized pockets of subsequent bank erosion. Bank erosion occurred less in predominantly single-channel reaches than in the predominantly multi-channel reaches.

Rates of bank erosion along the Middle Susitna River are relatively low in comparison to bank erosion rates measured along gravel-bed rivers generally. This may partly be explained by the low frequency of dynamic, ice-breakup events that initiate large-scale bank erosion. It may also be due to protective effects of ice that inhibit bank erosion such as formation of gravel-cobble pavements at bank toes, or protective effects from vegetation such as root-reinforced top of bank layers that slump over cantilevered banks effectively providing vegetated rip-rap to an exposed bank face.

ACKNOWLEDGEMENTS

The list of people to thank for their support, comments, and meals spent discussing this thesis is numerous. A simple list of names does not do their efforts justice, but will have to suffice.

I would first like to thank my thesis-committee members, Dr. Rob Ettema, Dr. Lyle Zevenbergen, and Dr. Sara Rathburn. I remember writing to Rob from a coffee shop in Seattle over three years ago, asking if he would be interested in taking me on as a student, and exploring a thesis topic on the Susitna River. Rob replied with grace and curiosity and has made it possible for me to complete my studies at Colorado State University. I thank him profusely for his guidance, encouragement, and attentiveness. I currently work with Lyle at Tetra Tech and was lucky enough to spend a couple field sessions with him in Alaska in 2013. Lyle has always been open to questions and discussions, sharing his expertise freely; he has created an incredible atmosphere in which to learn and collaborate. I thank him for his ability to listen, inspire curiosity, and share a good laugh.

I'd also like to thank Dr. Mike Harvey; an unofficial advisor. Mike was one of the first people who encouraged me to attend graduate school and find a thesis topic on the Susitna River. Few words can describe the incredible mentorship he has provided over the last five years, beginning with my first field lessons on the Susitna in 2013. To quote a familiar author of Mike's, William Shakespeare, "I can no other answer make, but thanks; and thanks; and ever thanks."

A huge thank-you to Bill Fullerton, for hiring me as part of the Tetra Tech Hydraulics and Hydrology team in Seattle in 2012. I joined the team on the heels of a contract win doing work in Alaska. I indicated my interest in working in Alaska, asking Bill to send me even if I had to sleep under a tipped over canoe. Bill proceeded to give me every opportunity to work in Alaska over the next two summers, which proved to be one of the greatest gifts. His continued support through

graduate school, and dedication to help me finish school while also working part-time, has been fundamental.

Matthew Moore has provided immense help in pulling together data, models, and giving me a crash course in SRH-2D. Brad Trabant and Allie Mcrae have graciously helped develop figures. Travis Hardee has provided figure support, multiple proof reads of my thesis, and multiple renditions of my presentation. Kathy Vanderwal Dube was the best field roommate I could have asked for. Many a night was spent giggling, killing mosquitos, and sharing wonder.

Many thanks to my friends and family, who have provided me with continued support, hoo-rah, and love. In particular, thank you to my sister, Chelse, who has been an incredible rock, and helped push me back on track after some delays.

Lastly, my gratitude is extended to the mighty Susitna River: for being such a remarkable playground and teacher. You are a constant reminder of the importance in paying attention.

TABLE OF CONTENTS

LIST OF TABLES

LIST OF FIGURES

CHAPTER 1: INTRODUCTION

1.1 Introduction

Many studies report observations of the effects of ice on bank erosion (e.g. Marusenko, 1956; Smith 1980; Beltaos, 1995, Zabilanksy et al., 2002; Prowse and Culp, 2003). Specifically, studies have summarized the effect of increased erosion during the ice-break up period from ice-run gouging, abrasion (e.g. Ettema and Kempema, 2012), and ice-jam release waves (Beltaos, 2018; Beltaos et al., 2018). Other studies have attempted to locally quantify the extent of erosion driven by ice processes such as at a meander bend (e.g. Ashton and Bredthauer, 1986). However, the question of how much erosion is controlled or driven by the presence of an ice-regime on the reach-scale has been raised, though not explicitly answered. For example, the extent of ice-driven erosion has often been implicitly included in the broader question: do channels in boreal environments exhibit an ice-scoured morphology not explained by typical fluvial models? Some channels in northern river environments display channel configurations not significantly outside the norm of hydraulic geometry relationships for fluvial environments (Bray, 1982), others display enlarged channel conditions (e.g. Smith, 1979; Smith, 1980; Boucher, 2008; Boucher et al., 2009, Boucher et al., 2012) while still others are equivocal (Uunila and Church, 2015). Inherent to this broader question is defining the extent and frequency that ice-induced processes are driving erosion. Certainly, the answer to these questions are watershed specific, and in some cases, may be sub-watershed specific (e.g. Best et al., 2005; Boucher, 2008).

In many boreal rivers, the most erosion resulting from ice-induced processes occurs during the ice-breakup period in the spring (e.g. Beltaos et al., 2018; Walker and Hudson, 2003). However, the nature of ice-breakups varies from year-to-year and even among sub-reaches in a single year. Generally, ice-breakup is categorized into two designations: “thermal” ice-breakup,

which indicates ice has been weakened from solar radiation and rising temperatures; and, "dynamic" ice-breakup, which indicates the ice has maintained strength, is capable of forming in-channel ice jams, ice-runs, and very high bed and bank shear-stresses (Beltaos et al., 2018). It is the latter, dynamic ice-breakups, which are capable of causing substantial erosion, shearing of floodplain vegetation, flooding, and subsequent damage to roadways and properties. Ecologically, dynamic breakup processes may be fundamental to flooding side channel and side sloughs for aquatic habitat (Prowse and Culp, 2003) or resetting vegetation at heads of secondary channels to maintain channel connectivity.

Therefore, it is particularly important to understand the processes that drive erosion, whether during ice-breakup events or during open-water flows, not only to characterize spatially and temporally the capacity for a channel to erode its banks but also for prediction of future channel changes due to climatic or anthropogenic influences. Boreal rivers where erosional processes are driven by the influence of ice, may be significantly modified by a shrinking cryosphere (McNamara and Kane, 2009). Warmer air temperature during winter could result in a reduced ice strength and/or more thermal (less erosive) ice-breakups in some watersheds. In other watersheds, there may be more frequent and damaging ice-related erosive processes due to enhanced mid-winter jamming and higher spring flows (Beltaos and Burrell, 2005). Anthropogenic changes, such as the construction of dam, would change the downstream magnitude and temperature of water flow, affecting the formation and breakup of an ice-regime. Rivers whose erosional processes primarily occur due to the influence of in-channel ice could have the magnitude and/or frequency of dynamic ice breakup events reduced. This could have significant implications for the formation or maintenance of side channels and side sloughs that provide preferential conditions for migratory fish habitat, especially salmon.

Yet, quantifying the erosive effects of ice, especially at the reach-scale, is a complex undertaking, often complicated by the remoteness of river reaches in far-northern locations and further complicated for large rivers. The generation of datasets throughout the annual stages of river-ice, including ice formation, presence, and breakup is typically costly and dangerous.

However, wide-ranging studies of the Susitna River, Alaska, performed as part of proposed hydroelectric projects in the 1980s (Alaska Power Authority [APA], 1984) and the proposed construction of a 215m-high, hydroelectric dam (Alaska Energy Authority [AEA], 2012) between 2012-2015, yielded an extensive, publically-available dataset of the ice-covered and ice-free periods. Data was collected locally and on the reach-scale over hundreds of kilometers of the Susitna River. The most recent dataset was collected between 2011 through 2015 and the oldest dataset extends back to 1951.

This thesis capitalized on the existing dataset to quantify the extent that erosion is driven by ice-processes on a large, free-flowing, coarse-bed river. Specifically, this thesis focused on ice-related erosion of the river banks along the middle geomorphic segment of the Susitna River, and sought to address the following questions:

1. When annually does the majority of bank erosion occur: during the open-water season or when ice is in the channel?
2. What processes cause the channel banks to erode?
3. To what extent, and why, do the erosion processes vary along the study reach?
4. How do short-term rates compare to long-term rates of erosion and how do these rates compare to other gravel-bed channels globally?

1.2 **Study Site**

The Susitna River is a predominantly gravel- and cobble-bed river, subject to long, frigid winter weather conditions. As shown in Figure 1-1, the river originates in the Alaskan Range and is sub-divided into four large-scale geomorphic segments as it flows approximately 580 km to Cook Inlet near Anchorage, Alaska (Tetra Tech, 2015a). The most downstream, southerly geomorphic segments, including the Lower and Middle Susitna Rivers, do not flow through permafrost terrain.

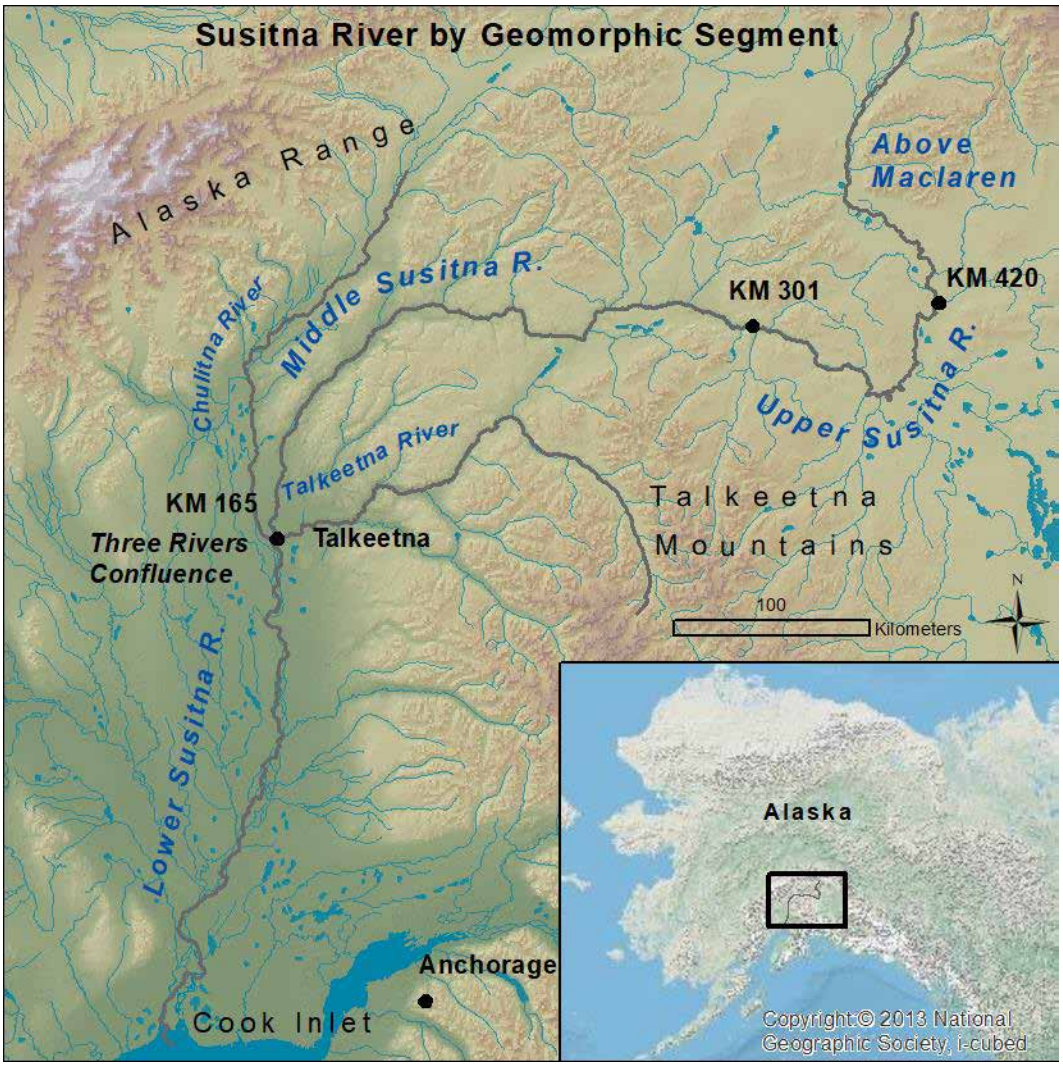

Figure 1-1. Geomorphic Segments along the Susitna River, Alaska.

The first geomorphic segment, referred to as the Above Maclaren segment, ranges from the headwaters to nearly 160 km downstream at the confluence of the Susitna River with a large tributary, the Maclaren River. Along this segment, the Susitna River flows through a series of glacier-fed, braid plains, and moraine and bedrock constrictions, and has primarily a sand bed. There are few vegetated mid-channel islands in expansion zones.

The second geomorphic segment, referred to as the Upper River, extends nearly 120 km downstream from the Maclaren River to the proposed dam site. Through this segment, the river has an inherited, non-alluvial planform confined by bedrock and glacial deposits. The river has a cobble-bed and is predominantly single channel with some, though limited, vegetated mid-channel islands.

The third segment, referred to as the Middle River, extends 135 km downstream from the proposed dam site until the Susitna River confluences with its next two major tributaries, the Chulitna and Talkeetna Rivers, referred to as the Three Rivers Confluence. Through this segment, the river is gravel-bed and flows through a series of valley floor expansions zones that include a suite of alluvial floodplain and terrace surfaces. The river alternates between primarily single channel reaches to multi-channel reaches. The Middle River is the focal segment of the present study.

The fourth and last geomorphic segment of the Susitna River is referred to as the Lower River. This segment extends 165 km from the Three Rivers Confluence to the mouth of the Susitna River at Cook Inlet. The Lower River is nearly three times as wide as any other geomorphic segments, primarily due to the flow contributions of the Chulitna and Talkeetna Rivers and the sediment contribution of the Chulitna River. Further, the Lower River has a gravel-bed that flows

through anastomosed sub-reaches with vegetated island complexes and sub-reaches of expansive braid plans.

1.3 Approach

The geomorphic segments are further divided into geomorphic reaches (Tetra Tech, 2015a). Two reaches of the Middle Susitna River were selected for observation and analysis of ice-related erosion of channel banks. The reaches were selected for three reasons:

1. They include multi-channel reaches, with constrictions, expansion zones, and mid-channel islands prone to ice-jam development;
2. They include single channel reaches where the flow is mainly constrained in the streamwise direction, and for which there is limited lateral capacity for ice and sediment storage; and,
3. The selected reaches have a large amount of available data, are distinct in geomorphic character, and the most downstream boundary is located far enough upstream of the Three Rivers Confluence (Figure 1-1; approximately 5 miles upstream) that any backwater effects due to the confluence are limited.

Using the two representative reaches of the Middle Susitna River, a three-part approach was adopted to investigate the study questions. Part 1, illustrates common bank forms in the study area that vary by geomorphic surface, and presents erosional conceptual models that identify possible erosional mechanisms that may lead to the observed bank forms. Part 2, quantifies the extent of erosion on the reach-scale, links erosion to types of geomorphic surfaces, and attributes the erosion to the various erosional processes identified in Part 1. Part 3, compares short-term and long-term erosion rates and provides suggestions for the general frequency of erosive events.

The three-part approach for the sub-reaches is outlined below:

Part 1: Observations and Conceptual Models

a. Use observations to characterize the common bank forms along the reach.

b. Link the common bank forms to possible erosion processes, to identify the main ice-related processes causing bank erosion and creating the common bank forms along the Middle Reach.

Part 2: Quantitative Analysis

a. Determine the extents of short-term erosion through aerial photography analyses. This step was performed in GIS by overlaying digitized vegetated channel features that span a thermal ice-breakup event (2011 to 2012) and a dynamic ice-breakup event (2012 to 2013). Prominent features were grouped into three categories of geomorphic surface: vegetated bar, active floodplain, and terrace.

b. At the erosion locations identified in Part 2a, review reconnaissance videos and photographs within the one-year period during distinct time periods (freeze-up, breakup, and the open-water season during summer and fall) to determine the time period (i.e. primary hydrologic regime) during which bank erosion occurred.

c. Identify the likely dominant bank-erosion processes by linking the extent of erosion and the time period of erosion to the erosional processes identified in Part 1b.

Part 3: Comparison of Erosion Rates

a. Compare the estimates of existing long-term erosion rates to the short-term erosion rates determined in Part 2a.

b. Relate these rates to representative rates of erosion reported for gravel-bed channels.

1.4 The Susitna-Watana Hydroelectric Project

Though this thesis does not address how the Susitna-Watana Hydroelectric Project (Project) may impact the Susitna River, it is useful here to briefly describe the project.

A hydroelectric project was initially proposed for the Susitna River in 1980 by Alaska Power Authority. Two dams were proposed; one located in Devils Canyon (roughly 80 km upstream of the town of Talkeetna) and another an additional 55 km upstream where the river is confined by bedrock. Studies to collect baseline data along the Susitna River downstream of both dams lasted for four years and included collection of aerial photography, survey data, flow measurements, sediment transport measurements, and field observations of geomorphic surfaces, channel form, and ice processes. Due in part to a reduction in oil prices, the project was halted in 1985 and archived with Alaska Resources Library and Information Services.

Alaska Energy Authority, previously known as Alaska Power Authority, reinitiated a proposal for a hydroelectric project located on the Susitna River in 2011. This more recent proposal, known as the Susitna-Watana Hydroelectric Project (FERC No. 14241) included only one dam, located about 145 km upstream of the town of Talkeetna, would stand approximately 215 m in height, and include a reservoir that would extend up to 64 km upstream. Units are presented in terms of River Kilometers (RK). However, a river stationing system was developed as part of the Project in terms of mile units and designated as Project River Miles, which begin at Cook Inlet and extended upstream nearly to the glaciers. For reference, Project River Miles will be noted as River Miles (RM) and may occasionally be presented in addition to as River Kilometers (in parenthesis).

The proposed project prompted many environmental, social, and cultural studies in order to identify the project's various potential impacts. In the course of identifying and assessing these

impacts, the project generated an extensive archive of information regarding bank and channel conditions along the Susitna River, especially along the Middle Susitna River, or "Middle River," which is thought likely to be most affected by the hydroelectric project. The primary studies utilized in this thesis included the Geomorphology Study and Fluvial Geomorphology Modeling Study (both contracted to Tetra Tech, Inc. of which the author was part of the team), the Ice Processes Study (contracted to HDR Alaska, Inc.), and the Riparian Vegetation and Aquatic Habitat Study (both contracted to R2 Resources, Inc.). The author spent two summers collecting data in support of the Geomorphology and Fluvial Geomorphology Studies. In addition, she used the publically available dataset to quantify the extent and causation of channel change within the Middle River. The cumulative datasets are located at gis.suhydro.org. Technical memorandums and progress reports as part of the Project are posted at http://www.susitna-watanahydro.org/type/documents/.

CHAPTER 2: PHYSICAL CHARACTERISTICS OF THE MIDDLE SUSITNA RIVER

This study seeks to determine ice effects on channel-bank stability along the Middle Susitna River. As a result, it is useful to describe in detail the physical characteristics of the river and to assess how some of the characteristics have changed over time.

2.1 Location

The Susitna River is a sand-, gravel-, and cobble-bed river that drains the glaciated southern end of the Alaska Range to Cook Inlet, approximately 580 km downstream. As part of the Susitna-Watana Hydroelectric Project, the Middle River was further subdivided into eight geomorphic reaches (Tetra Tech, 2015a). The present study investigated two of them – Middle River Geomorphic Reach 6 (Reach 6) and Middle River Geomorphic Reach (Reach 7) – located downstream of Devils Canyon and upstream of the Three Rivers Confluence. Figure 2-1 shows the study area and identifies the two reaches, which span 51.8 km of the Middle River, from RK 225.4 to RK 173.6.

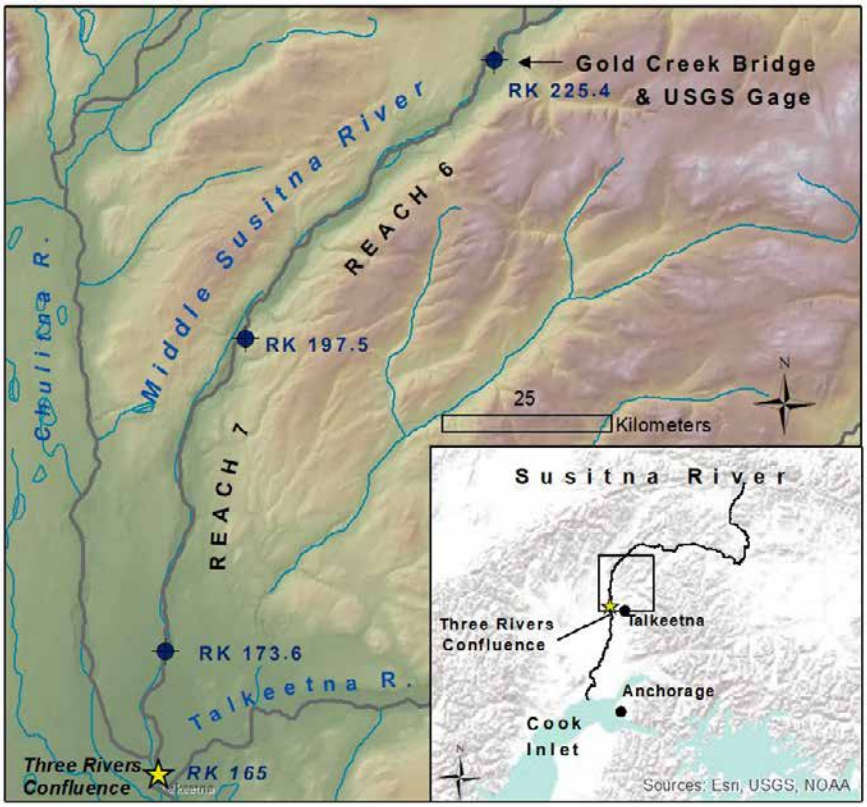

Figure 2-1. Study area along the Susitna River, Alaska. (Data source: ESRI Basemaps).

2.2 Geologic and Geomorphic Settings

The study area is bounded by Cretaceous-age Kahiltna Flysch (fine-grained turbidites) with inset undifferentiated Upper Pleistocene-age moraines, kames, and lacustrine deposits (Tetra Tech, 2015a). The average river gradient is 0.0016 to 0.0020. The sinuosity, ratio of the channel length to valley length, ranges from 1.05 to 1.09. The active channel is about 260 m to 300 m wide, while the valley bottom width ranges from 625 m to about 720 m. A railroad on the east side of the river provides some, though limited, lateral constraint through a portion of the reach, reducing the valley bottom width by roughly 40 m, ranging from 580 m to 680 m wide. The channel bed armor, sampled at the heads of mid-channel bars and islands, is composed of gravel and cobbles with a median grain size of 60-65 mm. Surface armor samples, collected beneath the ice cover during

winter, along the thalweg of the channel yielded slightly higher median grain sizes of 65 mm to 94 mm (Tetra Tech, 2014a). The median grain size of subsurface samples, taken at the heads of mid-channels bar and islands, was 30 mm; on average 83 percent of the sample was gravel, 16 percent was sand, and one percent was composed of silt/clay.

The delineation and characterization of the geomorphic reaches was developed by Tetra Tech (2015a), and are based on the Schumm (2005) classification scheme, which considers channel planform, constraints, confinement, gradient, and bed materials. A summary of geomorphic characteristics for the two study reaches is presented in Table 2-1. Single channel and multi-channel sections of the river are presented in Figure 2-2.

Table 2-1. Geomorphic characteristics of studied reaches along the Middle Susitna River.

	Geomorphic Characteristics				
	Length (km)	Bed Slope	Valley Bottom Width (m)	Active Channel Width (m)	Number of Channels
Reach 6	27.8	0.0020	715	300	2.4 +/- 1.1
Reach 7	24.0	0.0016	625	260	1.8 +/- 1

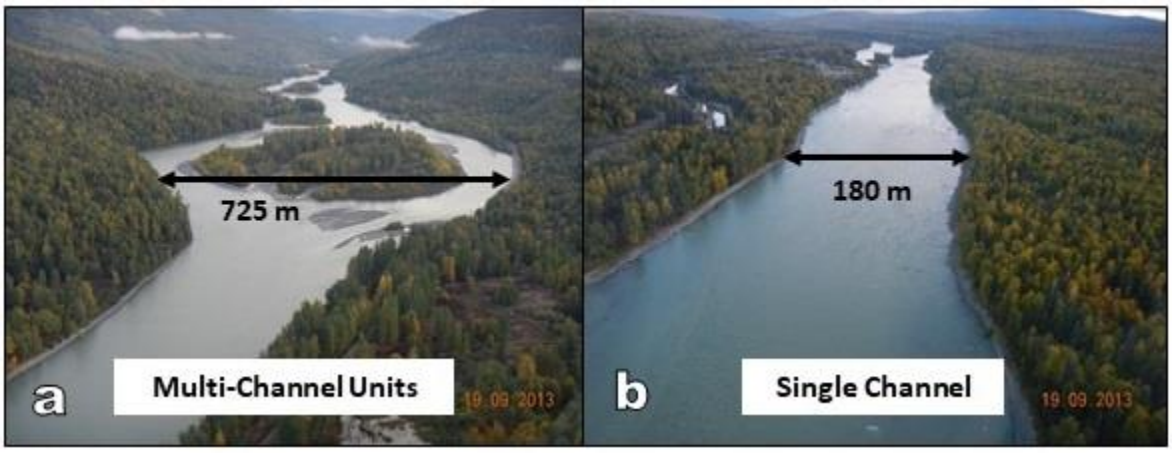

Figure 2-2. Aerial view upstream in Middle Susitna River: (a) a multi-channel reach with mid-channel bars and island; and (b) a single channel reach with bank attached floodplain and limited in-channel sediment storage.

Reach 6, from RK 225.4 to 197.5 (the upstream boundary was reduced from RK 238.9 in Tetra Tech (2015a) to RK 225.4 for this analysis), is predominantly a laterally confined multiple channel reach with sediment storage in mid-channel bars, vegetated islands, and continuous floodplain segments. The average active channel width is 300 m while valley bottom width averages 715 m (675 m in some areas due to a railroad). Bed slope through the reach is 0.002. The reach contains the widest valley bottom area in the Middle Susitna River (aside from just upstream of the Three Rivers Confluence) and is composed of a series of multi-channel units containing a range of channel conditions, fast and deep main channel, shallower side channels, and shallow sloughs, and a range of geomorphic surfaces, gravel bars, vegetated bars, low-lying floodplain units with young vegetation (less than 30 years old), and higher floodplain units with more mature vegetation (greater than 30 years old and up to 150 years old).

Reach 7, from RK 197.5 to Mile 173.6, is predominantly a laterally confined single channel with limited sediment storage in mid-channel bars, vegetated islands, and non-continuous bank-attached floodplain segments. Average active alluvial width is 260 m while valley bottom width averages 625 m (580 m in some areas due to a railroad). Bed slope through the reach averages 0.0016. As this reach is more confined, there is a less diverse range in channel conditions and geomorphic surfaces compared to Reach 6.

2.3 River Flows and Temperature

The contributing drainage area of the Susitna River at the closest gaging station is approximately 16,000 km^2; the gage is at Gold Creek (RK 225.4; Gage No. 15292000), located at the upstream end of Reach 6. The average annual flow of the Susitna River at Gold Creek is 277 m^3/s with high seasonal variability (Tetra Tech, 2013a). The average monthly, air temperature is near 0ºC in October and fluctuates between -4ºC and -12ºC through the winter (Figure 2-3).

Flows remain low through the ice-covered period with an average monthly low in March of approximately 40 m^3/s. By April, air temperatures have risen to just above freezing and continue to rise to roughly 16ºC by July. Peak flows correspond with the rise in temperature and melting of snow through the basin, with an average monthly flow of 745 m^3/s in June. Average monthly flows are plotted with the open-water peak flow recurrence intervals at the Gold Creek Gage in Figure 2-4. Monthly flows were averaged from August 1949 through December 2013 providing a 63-year period of record. Typical ice cover, ice breakup window, and open-water periods are also illustrated in Figure 2-4; the periods were determined from observations made in the 1980s and from 2011 to 2014.

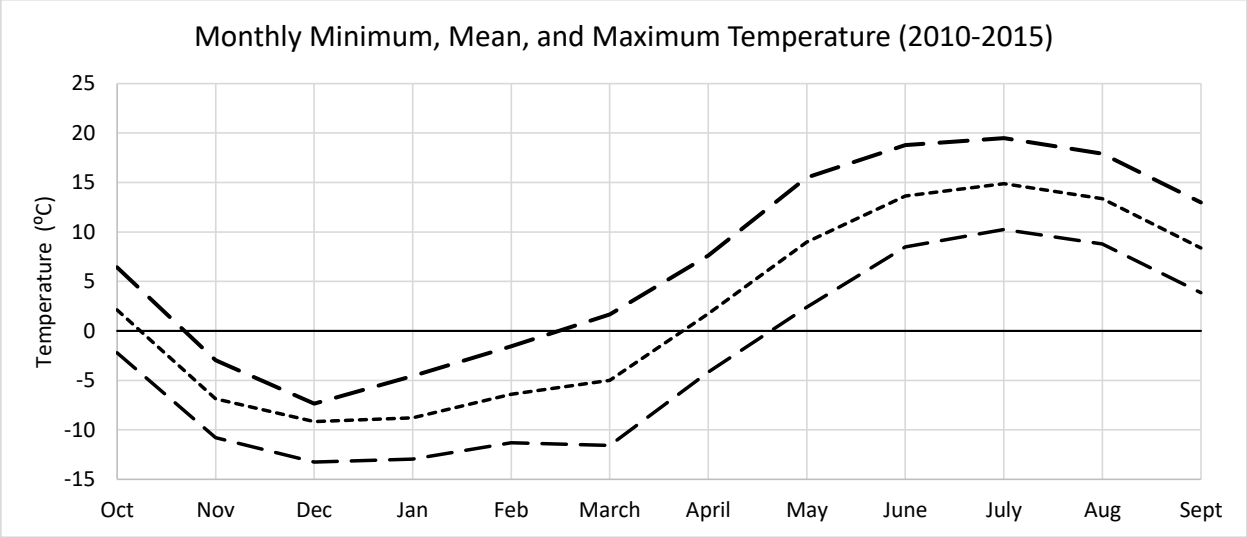

Figure 2-3. Monthly mean, minimum, and maximum values of air temperatures at Talkeetna Airport, near the Middle Reach. Data source: NOAA (2010-2015).

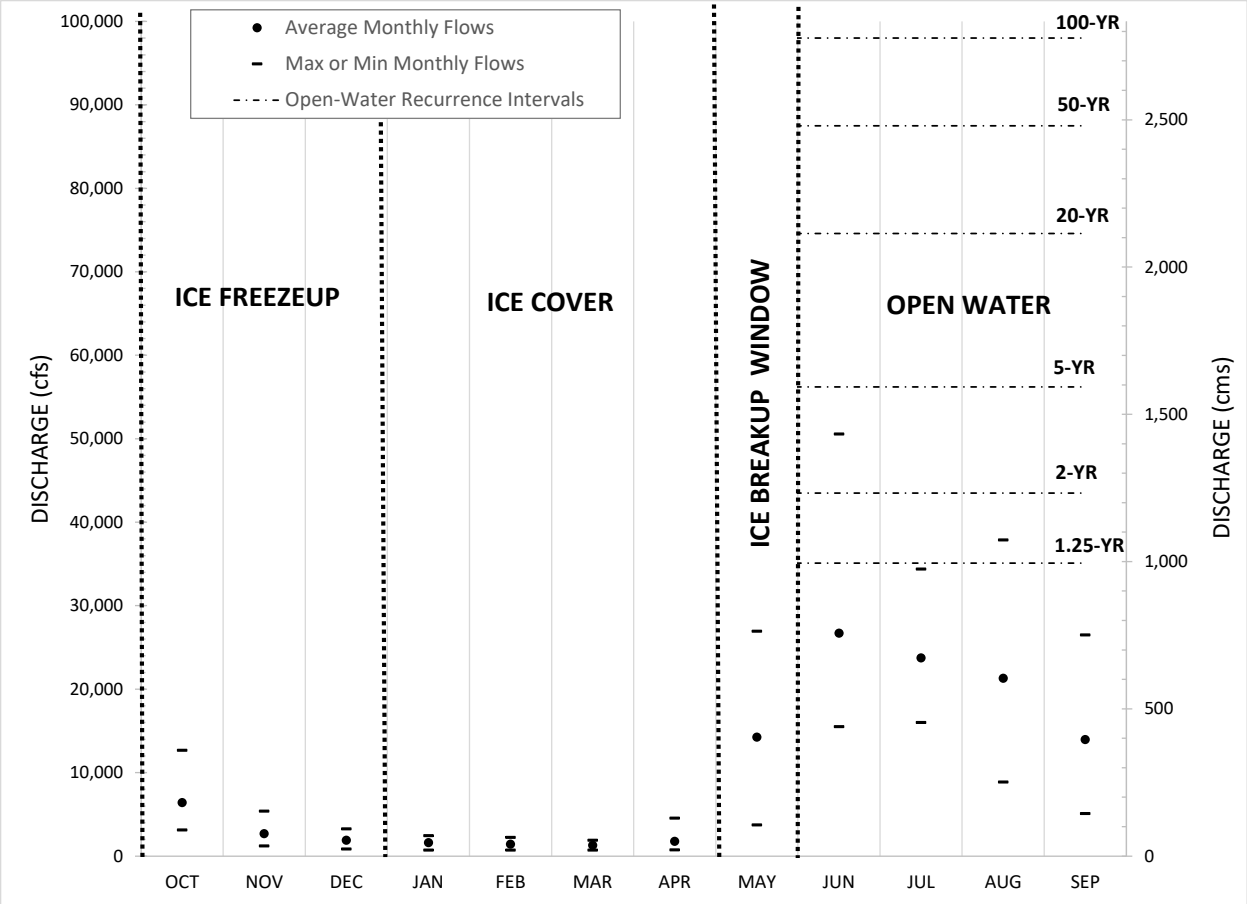

Figure 2-4. Monthly minimum, average, and maximum flows with open water peak flow recurrence intervals through the Middle Susitna River at Gold Creek Gage (USGS No. 15292000) from August 1949 through December 2013.

2.4 **Ice Processes**

Three phases of in-channel ice are elaborated in the ensuing section: ice cover formation, ice cover, and ice cover breakup. Each phase has been well documented as part of the proposed hydroelectric project in the 1980s (APA, 1984) and the more recent proposed project between 2012-2015 (AEA, 2012). A brief and general description of each phase is provided from the existing literature on the subject (Artic Environmental Information and Data Center, 1984; HDR Alaska, Inc., 2014a, 2014b, 2014c, 2014d, 2015; R&M Consultants, Inc, 1981; 1984). More thorough and localized descriptions of each phase are elaborated in the above cited references and

can also be found within other related reports at http://www.arlis.org/susitnadocfinder/ for studies from the 1980s and http://www.susitna-watanahydro.org/type/documents/ for studies between 2012-2015.

***Freeze-up**:* Floating frazil and anchor ice is typically observed in the Middle River when average daily air temperatures reach 0°C at Talkeetna Airport (HDR Alaska, Inc., 2015a). Frazil and anchor ice are largely generated upstream in Devils (RK 267 to 248) and Vee, also known as "Watana" (RK 365 to RK 362) Canyons. This ice accumulates in loosely bounded slush floes and either passes through the Middle River into the Lower River and down to Cook Inlet or may melt away. Once discharge drops to around 142 cms at the Gold Creek gage (RK 225) around late October or early November, ice-cover progression begins, starting in the Lower River (HDR Alaska, Inc., 2015a).

Border ice usually begins to form by the accumulation of frozen slush layers along the banks before the passage of the ice front. An ice bridge usually forms upstream of the Three River's Confluence (downstream extent of the Middle Susitna River) and becomes the leading edge of an ice front that eventually progresses upstream into the Middle River. Ice-cover progression along the Middle River begins as early as late October in very cold years, but has occurred as late as January in relatively warm years (HDR Alaska, Inc., 2015a). Ice cover formation along the Middle River usually occurs sometime in November and progresses upstream to Gold Creek by mid-December. Discharge decreases through December, averaging 40 to 70 m^3/s at Gold Creek gage. Despite the very low discharges, the increased resistance due to the ice cover can cause the flow stage to increase between 1 to 2.5 m (HDR Alaska, Inc., 2015a).

***Ice Cover*:** While the ice cover typically remains stable through the winter, open water leads persist. Two kinds of leads can be observed (HDR Alaska, Inc., 2014d):

1. Velocity or hydraulic leads form where the flow velocity is fast and turbulent; and,
2. Thermal leads occur where there is groundwater upwelling, notably along the toe of main channel banks, and in sloughs and side channels.

Ice thickness measurements were conducted by HDR Alaska, Inc. (2014b) in early March 2013 at RK 200.2 (RM 124.4) in Reach 6 and RK 187.8 (RM 116.7) in Reach 7. Measurements in Reach 6 yielded ice thicknesses from 0.7 to 1.4 m with anchor-ice and frazil accumulation of 0 to 2.9 m below the ice cover. Measurements at the Reach 7 site yielded ice thicknesses of 0.5 to 1.0 m with anchor-ice and frazil accumulation of 0 to 2.1 m below the ice cover.

***Breakup*:** A pre-breakup period usually occurs sometime in April, when snowmelt begins at lower elevations in the basin (Artic Environmental Information and Data Center, 1984). As water levels rise due to snowmelt, and precipitation, overflow often occurs onto the ice. Standing water appears in depressions on the ice cover, which eventually deteriorate into open leads (Arctic Environmental Information and Data Center, 1984a).

The breakup period typically occurs between late April and late May (HDR Alaska, Inc., 2015). Thermal ice-breakups occur when there is a gradual thaw of the ice-cover and the ice cover mostly melts in place; in contrast, dynamic breakups occur when there is a rapid thaw and sharp increase in discharge. During dynamic ice-breakups, broken pieces of the ice cover are conveyed downstream, often forming ice-jams (HDR Alaska, Inc., 2014c).

Water levels can increase rapidly behind an ice jam, spilling water and ice into side channels, sloughs, and onto the floodplain. With the absence of other high pulse flows to flush the ice out of the side channels or slough, they typically will melt in place, leaving a layer of silt and sediment that accumulated on top of the ice floes. In contrast, continued high flows and breakup jam flooding can flush the ice floes from the side channels and overbank, causing fluvial

entrainment of bank materials, as well as driving ice floes and large ice blocks into banks and trees (HDR Alaska, Inc., 2014c). This process of ice jam formation and release occurs until all the jams are swept downstream and only rafted ice blocks remain in some side channels, sloughs, gravel bars, and overbanks where they melt in place (HDR Alaska, Inc., 2014c).

2.5 Ice Effects on Water Flow

Not only can in-channel ice cause water levels to be much higher than the largest open-water floods, but the onset of an ice-induced flood can occur much faster than open-water floods. Additionally, the release of flow from behind an ice-jam may well produce local peak discharges approaching extreme open water flooding. Capturing the effects of ice on water flow, in particular the effects of ice-jam breakup on the flow hydrographs, is possible if jamming occurs near gaging stations. Surges of water from ice jam breaks may create a wave akin to a dam break (Beltaos, 1995) and are capable of causing significant local erosion (Arctic Environmental Information and Data Center, 1984b).

2.6 Sediment Transport and Sediment Supply

Sediment transport through the Middle Susitna River is supply-limited and largely wash load dominated. Estimates of the annual sediment loads at the USGS gaging station at Gold Creek average a total sediment load of 3.4 million (M) tons where the wash load of silt and clay is about 57 percent of the total load, the sand load is about 42 percent of the total load and the gravel bed load accounts for the remaining 1 percent. Tributaries to this reach are mostly clear water with negligible wash loads, some sand, and greater amounts of gravel. Gravel sediment loading from tributaries exceeds transport capacity at the lower end of the Middle River, but sediment storage occurs mostly in the tributary fans and not on the Susitna River channel bed (Tetra Tech, 2014b).

Two factors substantially reduce sediment transport during winter: the supply of silt and clay decreases with the freezing of the glacial headwaters; and, water flow reduces and becomes unable to transport sand and gravels. Rates of sediment transport during ice breakup are unknown. However, observations indicate that at least localized transport of sand and gravels occur. Sand, gravel, and cobbles get ramped up bank faces and deposited on top of the floodplain, in addition to scour holes and disparate piles of sand and gravel along gravel bars and the bottom of banks. Localized transport may occur primarily during breakup when greater velocities and depths occur at sites along the river.

While the Susitna River receives a large amount of gravels from tributaries, many of the other sediment sources (sediment ranging from silts to boulders) originate from mass wasting of slopes, bank undercutting, and erosion of outwash terraces and moraines. Other than erosion from bank surfaces, sand and silt supply originates from the geomorphic segment just downstream of the glacial headwaters (Tetra Tech, 2014d).

The effective discharge for the Middle Susitna River, determined as the flow class or bin that transports the largest quantity of sediment (using data on bed-material load at Gold Creek gage), is approximately 765 m^3/s (27,000 m^3/s), and occurs nearly on an annual basis (Tetra Tech 2014d). Bed-material load, determined as the summation of the sand load and the gravel load, comprises predominantly sand. The effective water discharge for moving the gravel load, determined due to its importance in forming channel bed geometry and the basal layer of vertically accreted geomorphic surfaces, is approximately 2,237 m^3/s (79,000 ft^3/s), and occurs between the 20- to 50-yr peak flows.

2.7 Vertical Stability

The latest morphologically significant event in the Susitna River Basin was during the Little Ice Age, a Holocene-age glacial event that peaked in 1750 and begin to recede sometime between 1800 to 1850 (Luckman, 2000; Calkin et al., 2001; Reyes et al., 2006). Dendrochronology of present-day terrace surfaces along the Middle River is consistent with the timeline of glacial retreat, and dates of vegetation establishment of some of the oldest Cottonwood trees range between 1800 and 1850. Channel degradation since 1850 has left a large number of terraces throughout the Middle River, occupying nearly one-third of the total valley bottom area of Reaches 6 and 7, and over one-half of the non-channel valley area.

Since the early 1980s, when survey data were collected through the Middle River, there has been no reach-wide degradation or aggradation trends (Tetra Tech, 2014e). A 2014 analysis compared cross-sections from the 1980s to those surveyed in 2012 and 2013 for changes in average bed elevation and flow area at the 2-year peak flow. Over the 51.8 km study area that spans Reach 6 and 7, a total of 18 cross-sections were compared. In general, 61 percent had changes in average bed elevation less than 0.3 m while 44 percent had minimal changes in flow area (i.e. less than 40 m^2). Comparisons of channel width indicate that 82 percent had width changes (either narrowing or enlarging) of less than 45 m or less; this amounts to approximately 15 to 17 percent of the average channel width. Only 18 percent had width changes greater than 45 m over the 30-year period of comparison.

2.8 Lateral Stability

Since the first period of aerial photography record, starting in 1951, the Middle Susitna River has experienced rather modest, reach-scale channel changes. The channel has essentially maintained its planform, and only rarely have entire islands been completely eroded. Long-term rates of channel change in the form of lateral bank retreat are relatively low compared to the size of the river (10 percent or less of the channel width). Previous analysis of bed material mobilization concluded the channel bed was infrequently mobilized, evidenced by low gravel transport rates (Tetra Tech, 2014b), a relatively stable channel planform with mid-channel bars and vegetated islands, and an armored gravel and cobble bed (Tetra Tech, 2015a). Investigations of fluvial shear stresses at the base of known bank erosion locations where up to 30 m of lateral bank retreat had occurred, revealed even the highest open-water flows did not exceed the critical shear threshold for bed material mobilization (Tetra Tech, 2015b).

Two analyses were performed to identify the locations and rates of erosion. The first analysis overlaid aerial photographs between two approximately 30-year periods to identify conversion of vegetated floodplain units to un-vegetated channel units (Tetra Tech, 2014f). This analysis identified long-term erosion on the reach-scale with an accuracy of approximately 10 m of width per one meter of feature length. The second analysis compared surveyed cross-section data to LiDAR-derived data to identify lateral bank retreat between the cross-sectional surveys and subsequent LiDAR flights (Tetra Tech, 2015b). This analysis identified short-term erosion at specific locations with an accuracy of approximately one meter.

Long-term rates of channel change over two 30-year periods, determined from aerial photography overlays (Tetra Tech, 2014f), are relatively low compared to the size of the river (approximately 5 percent of the total reach area or less). There is variation in the long-term rates

of channel change by differing geomorphic reaches within the Middle River. Historic erosion rates as a percent of total reach area were nearly double for predominantly multi-channel reaches in wider valley bottoms than the predominantly single channel reaches through narrower valley bottoms.

The total erosion over the period of analysis, determined in unit area, was converted into erosion values as unit width (i.e., amount of lateral bank retreat), in some of the most dynamic, valley bottom sub-reaches; the erosion area values from Tetra Tech (2014f) were divided by the sub-reach length to generate an average width of erosion. The results are summarized in Table 2-2. While reach-long averages of lateral bank retreat are low, averaging approximately 1 m/yr, reach-long erosion rates over the streamwise distance where erosion occurred were slightly greater, and averaged approximately 2 m/yr. Localized lateral retreat through these same sub-reaches was much greater, with erosion widths of up to 70 m. However, overall, erosion widths over two 30-year periods were less than 10 percent of the active channel width.

Table 2-2. Erosion rates in Middle Susitna River sub-reaches.

Time Period:	1951 - 1983 (32 years)	1983-2012 (29 years)
Wide Valley Bottom Region - RK 210 to RK 206.2		
Active channel width	420 m	345 m
Average bank retreat over entire length (3.8km)	40 m	33 m
Average bank retreat of only streamwise length that has eroded	57 m	33 m
Narrow Valley Bottom Region - RK 185.6 to RK 183.0		
Active channel width	280 m	290 m
Average bank retreat over entire length (2.6km)	24 m	6 m
Average bank retreat of only streamwise length that has eroded	29 m	12 m

Limited channel change is further corroborated between the 2012 and 2013 channel surveys and the 2014 LiDAR (flown between May 21 and June 3, 2014). If the channel eroded between the surveys and the LiDAR collection, then a gap in the topographic data would be identified. Of the 60 surveyed cross-sections collected in 2012 and 2013 through Reach 6 and 7, between the survey date and the LiDAR date, 45 percent were subjected to a 2-yr peak flow (1,232 cms), a nearly 20-yr peak flow and a nearly 50-yr peak flow (2,478 cms); 15 percent were subjected to a 2-yr peak flow and nearly 50-yr peak flow, while 40 percent were subjected to a 2-yr peak flow. Of all the cross-sections, only one (RK 194.3) experienced significant erosion that was detected when comparing the survey data to the 2014 LiDAR data. The bank eroded approximately 12 m and was also identified in the sequential aerial photography analysis, described in Section 5.2.1.

The interaction between the resistive bank properties and applied external forces within the riverine zone determine the annual rates of bank retreat. Given the large hydraulic stresses generated by this river, one might expect to see more lateral bank retreat than has been observed. Resistive properties include areas of confinement by bedrock, vegetation type and composition, bank height and composition, rooting characteristics, and bank angle. External forces include hydraulic and ice forces, both of which are a function of channel form. The interactions among these various components build a complex and interconnected picture of channel change and stability, especially when viewed at the reach scale.

2.9 Riparian Vegetation and Geomorphic Surfaces

2.9.1 *Overall*

The riparian vegetation and geomorphic surfaces of the Middle River are intimately connected. Riparian vegetation was classified by ABR, Inc. (2014) and R2 Consultants, Inc. (2014)

using classification established in Viereck et al. (1992). Geomorphic surface mapping was performed by Tetra Tech (2014g). Overall, vegetation along the Middle Susitna River is predominantly composed of spruce-paper birch forests, poplar (i.e., Cottonwood) forests, willow-alder scrub, and fern and umbel meadows. The distribution of vegetation is primarily determined by topography (i.e., various geomorphic surfaces), flood frequency and disturbance regimes. As terrace surfaces occupy more than one-half of the non-channel valley bottom area, slightly less than one-half of the valley bottom area is composed of surfaces linked to the active hydrologic regime. A geomorphic succession model of surfaces in the active hydrologic regime was initially presented in Tetra Tech (2014g), and included geomorphic surface heights and stratigraphy, brief riparian vegetation descriptions, and approximate surface ages. The geomorphic succession model is expanded in Figure 2-5 below to include surface overtopping frequencies, updates to riparian vegetation descriptions, and the thickness of the fine-grained bank material above the gravel core.

Overall, the active river corridor is characterized by willow-alder shrub at lower, more frequently inundated locations categorized as vegetated bars, followed by poplar forests on a range of young and old floodplain surfaces that shift into spruce-poplar forests and spruce-paper birch forests with age. Meadows, open spruce-poplar forests and open spruce-paper birch woodlands are common on terrace features.

Disturbance regimes are processes that remove or impact local riparian communities, typically shifting the community into an earlier successional state (R2, 2014). On the Susitna River, flooding and ice processes disturb all geomorphic surfaces, but some to a greater (e.g. vegetated bars) or lesser degree (e.g. active floodplains).

2.9.2 *Geomorphic Surfaces and Succession Model*

Geomorphic surfaces were mapped as part of Tetra Tech (2014g). The surface heights were measured above a summer open-water 70th percentile flow (510 m^3/s; 18,000 ft^3/s) during the summer field seasons in 2013 and 2014 as part of the Susitna-Watana Geomorphology and Fluvial Geomorphology Studies (Tetra Tech, 2014h, 2015b). This flow was selected as it was predominantly the flow that occurred during the majority of the geomorphic surface mapping effort. The primary basal unit of all geomorphic surfaces is the un-vegetated gravel bar (Tetra Tech, 2014g), later referred to as the basal gravel core, which is approximately 0.6 m to 1 m high. Bed-material sampling on gravel bars resulted in a median surface grain size of 60-65 mm and median subsurface grain size of 30 mm. The approximate overtopping discharge of gravel bars in multi-channel complexes ranges from 700 m^3/s to 850 m^3/s (approximately 25,000 ft^3/s to 30,000 ft^3/s); the elevation of such complexes approximately correspond to the elevation of the gravel-sand contact in bank profiles of hydrologically active geomorphic surfaces. Gravel bars are overtopped on an annual basis, typically between June and August.

The deposition of 0.3 m to 0.6 m of predominantly sand-size material, together with seedling establishment, creates vegetated bars approximately 1 to 1.3 m in height above the bank toe. Initial vegetation establishment consists of closed tall willow and alder shrubs that over 10-20 years develop into tall willow shrubs and open poplar woodland with balsam poplars less than 10 m in height and 0.15 m in diameter at breast height. Disturbance regimes include water flow and ice-processes (elaborated in Section 5.1.3 *Erosional Processes Conceptual Model*). Vegetated bars are overtopped between the 2- to 5-yr open-water recurrence intervals and show significant signs of mechanical shearing of vegetation by ice. The approximate age of the surface ranges from 10 to 60 years.

Continued sediment deposition leads to the development of a young floodplain surface that averages 1.5 to 1.8 m in height above the bank toe, whereby 0.75 m to 1.2 m of the upper bank layer is composed of sand and silty sand above the gravel core. Vegetation is characterized by closed pole balsam poplar forests and as the vegetation begins to age, and thin, shifts into open pole balsam poplar forests with poplars about 0.3m in diameter at breast height, open poplar woodland-alder shrub, and open poplar woodland-willow shrub. Disturbance regimes include water flow and various ice-processes. Young floodplains are overtopped slightly less than the 5-yr recurrence interval and show signs of mechanical shearing by ice, tree-ice scars, and knocked over trees from ice-rubble. Ages of balsam poplar on the surface range from 30-60 years.

Slowed, but continued sediment deposition on the young floodplain surface, creates a mature floodplain surface that is approximately 1.8 to 2.1 m in height above the bank toe, whereby sand and silty sand layers constitute approximately 0.9 to 1.5 m of the bank layers above the gravel core. Vegetation is characterized mostly by open timber balsam poplar forest and open spruce-balsam poplar forest. Disturbance regimes include water flow, ice-processes, and wind. Mature floodplains are overtopped between the 20- to 50-yr recurrence intervals and show signs of ice-induced erosive processes including tree-ice scars, knocked over trees from ice-rubble, gouged bank faces and floodplain material, and gullies from possible ice-jam induced flooding (as described in Smith and Pearce, 2002). A minimum age of establishment is approximately 60 years, while the age of some balsam poplar and white spruce are up to 160 years.

Though there is little change in the surface height, an aging of vegetation indicates a shift from mature floodplain to old floodplain. Vegetation is characterized as open timber balsam poplar forests, open spruce-paper-birch forests, spruce balsam poplar woodlands, and closed tall willow shrub. Overall tree density is low and balsam poplars are decadent where some date up to 180

years. The dendrochronology provides a minimum age for the surface and suggests the old floodplain surfaces were formed and were more fluvially active after the Little Ice Age recession, which occurred sometime between the mid-1700s and mid-1800s (Luckman, 2000; Calkin et al. 2001; Reyes et al. 2006). Disturbance regimes include water flow, ice-processes, and wind. Old floodplains are overtopped around the 50-yr recurrence interval and shows signs of ice-induced process including tree-ice scars, gouged bank faces and floodplain material, and gullies from possible ice-jam induced flooding.

Terraces, defined as surfaces that are no longer hydrologically active geomorphic surfaces, were defined on the Susitna River as surfaces that are at least 1.5 m above the current 100-yr water surface elevation (Tetra Tech, 2015c). Vegetation is similar to that of an Old Floodplain and includes open spruce-balsam forest and open spruce-paper birch woodlands. Paper birches, that establish on the root-balls of wind-thrown poplars (Kevin Fetherston, R2 Resources, personal communication), are more prevalent on terraces. The age of paper birches can be added to the age of decadent poplars, and provide an extension of time since vegetation establishment. One white spruce tree on a terrace surface dates to the beginning of the 1800s. The surfaces are typically 2.7 to 3 m in height above the bank toe, whereby the basal gravel layer is thicker and higher in elevation than the hydrologically active lower geomorphic surfaces. A sand-dominated depositional unit above the basal gravel layer ranges from 1.15 m to 1.8 m, approximately 0.3 m greater in thickness than the fine-grained bank thickness in the more hydrologically active geomorphic surfaces. The thickness of both the basal gravel layer and the sand-dominated depositional layer indicate a paleo surface and an approximate timeframe of river degradation between the establishment of the existing terrace surfaces to the establishment of the Old Floodplains (sometime in the early to mid-1800s).

The similitude in bank composition, surface vegetation, and channel planform indicate the present day terraces and old floodplain units are geomorphically similar features, but were hydrologically active at different times. While Pb210 sediment cores were collected on some terrace surfaces in the Middle River, aging the terrace surfaces from Pb210 proved problematic as there is low clay content on the Susitna River to which Pb210 binds itself, such that reliable dating can only extend approximately 60 years from the present day (Rolf Aalto, University of Exeter, personal communication). It is possible to identify the minimum age of a geomorphic surface by aging vegetation establishment. This is performed by summing the ages of poplars (that tend to establish early in the formation of the surface) and the ages of birches (that tend to form on higher, less inundated surfaces, as the tree canopy thins). This method provides a minimum age of the terrace surface of greater than 200 years. However, this technique can be problematic as the riparian succession model could have been interrupted or reset by ice processes or flooding, in which the likelihood of disturbance is higher for older geomorphic surfaces. It is likely the establishment age of the terrace surfaces is greater than 200 years.

The Little Ice Age is estimated to have peaked in the mid-1700s and receded sometime in the early to mid-1800s (Luckman, 2000; Calkin et al. 2001; Reyes et al. 2006). This timeframe corresponds well with an aggradational period following the peak of glacial advance, which provided a surplus of sediment supply, and adequate transport capacity as the glaciers began to recede and melt, that were able to construct active floodplain surfaces that now form the modern-day terraces. As both flows and sediment supply began to recede, degradation on the Middle Susitna River, brought the river to approximately its modern-day elevation. Differences in elevation between the gravel-sand contact in the present-day terraces versus the old floodplains, suggests river degradation following the aggradational period caused by the Little Ice Age. The

similarity of bank composition, height and vegetation type and succession between the old floodplains and modern day mature floodplains, suggests there has been little vertical channel adjustment since the establishment of the old floodplain surfaces sometime in the 1800s.

While the Little Ice Age was a morphologically significant event in the Middle Susitna River, causing short-term aggradation and subsequent degradation, it was a geologically short-term modification in channel adjustment compared to the relaxation time since Pleistocene glaciation (Church and Slaymaker, 1989). The present-day river elevation may likely be similar to that immediately before the Little Ice Age.

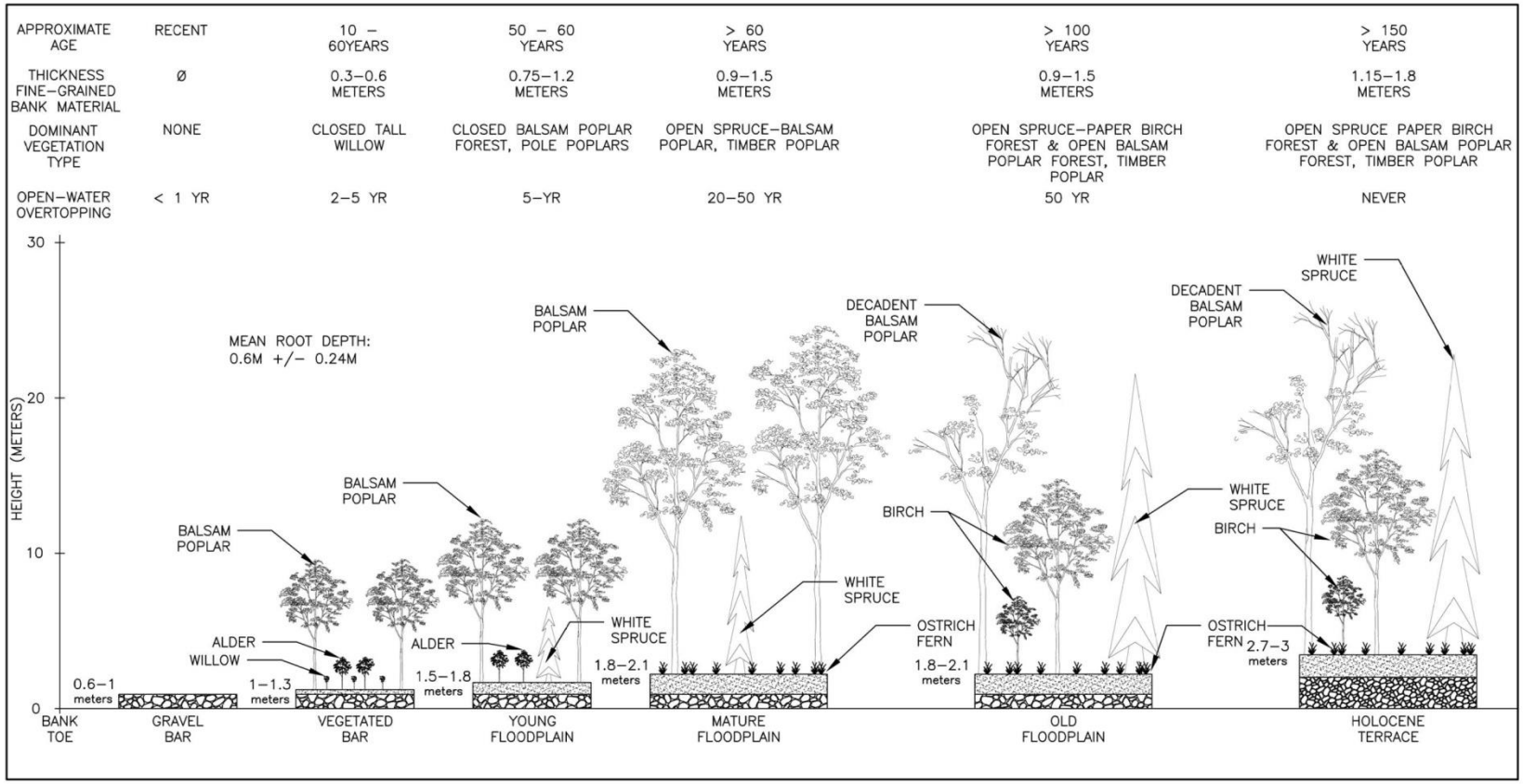

Figure 2-5. Geomorphic succession of typical geomorphic surfaces in the Middle Susitna River. Figure adapted from Tetra Tech (2014g).

CHAPTER 3: LITERATURE REVIEW

Winter processes in fluvial systems have become better understood in the last half century, but their geomorphic effects on the channel system remain unclear. The effectiveness of driving forces to cause bank erosion in northern environments are complicated due to changing thermal properties of resisting forces (e.g., McNamara and Kane, 2009). Though it is generally accepted that the ice breakup regime can exhibit the highest energy events experienced on a river system, it is unclear for boreal rivers not in permafrost terrain whether reach-scale erosional processes are exacerbated by ice-processes or predominantly driven by them.

The timing of erosion within the year typically aids identification of the leading erosional processes. However, as Scott (1978) elaborates, the timing of the most bank erosion in boreal rivers is far from uniform. Lateral bank erosion on the Colville River, Alaska (Walker and Arnborg, 1966; Walker and Hudson, 2003) and Mackenzie River delta (Outhet, 1974), both rivers set within permafrost terrain, has been documented to occur primarily during or shortly after ice-breakup flooding. In contrast, lateral erosion on Banks Islands in the Canadian Arctic (Miles, 1976) was predominantly found to occur during the open-water season.

Scott (1978) suggests that drainage area may be an indicator of whether ice breakup processes may exhibit dominant erosive processes, though he indicates the correlation may be overly simplistic and other variables are likely also responsible. This suggestion is, in part, substantiated by Smith's (1980) analysis of large rivers in Alberta. Smith (1980) found a geomorphic threshold that resulted in ice-enlarged river channels, and by definition, increased bank erosion due to ice-induced erosion processes, for rivers with bankfull discharges greater than 500 cms; all rivers above this threshold were known to experience ice jams and ice runs. The smaller rivers considered in Smith's (1980) study did not experience ice drives and had a mean

bankfull return period of 2.15 years, more common of fluvial rivers in temperate regions. Additionally, in a study of the Necopastic River, Quebec, Boucher et al. (2012) found ice-enlarged channel reaches to be a function of drainage area and ice jam frequency. Channel reaches greater than a particular drainage area threshold and experienced ice jams and ice runs at least once every 5 years, were found to have enlarged channels, indicative of increased lateral bank erosion.

Yet the dominant causes of erosion on other large boreal rivers are inconclusive (Abramov, 1957; Czudek and Demek, 1970; Scott, 1978; Kellerhals and Church, 1980; Uunila and Church, 2015). In some cases, more frigid winters may result in less erosion during spring breakup, because frozen bed and bank material reduces erosion (McNamara, 2012). In other cases, jam-related flooding causes flow to spill into overbank regions and thereby may even lead to channel narrowing (Uunila, 1997).

The following sections aim to identify the range of erosion processes acting along a boreal gravel-bed river not set in permafrost terrain. Specific erosion processes are summarized in the framework listed in Table 3-1. Erosion resistance properties are presented in Table 3-2. These tables include the timeframe within the year of the specific erosional or protective process, the leading effects of the process, controlling factors, and literature references.

External erosion processes due to frigid winter conditions are elaborated in Section 3.2. Bank weakening processes are identified within the erosion processes framework. However, they are not further described within this chapter.

There is extensive literature of fluvial effects on bank erosion. Whereas some fluvial effects are included within this chapter, readers are referred, for example, to Thorne (1982) for more thorough descriptions. Erosion processes not described herein may be more relevant for other river systems; for example, slope aspect in boreal environments (Ritchie and Walker, 1974), thermo-

erosional niching from permafrost (Scott, 1978; Church and Miles, 1982; Lawson, 1983), thawing of permafrost (Walker and Hudson, 2003), or thermal expansion of ice sheets (Gerard, 1989).

It is noted that long-term erosion studies have been performed for other Alaskan rivers including the Matanuska River (Curran and McTeague, 2011) and the Tanana River (Collins, 1990). However, direct comparison of erosion processes or rates of the Matanuska and Tanana rivers to the Susitna River are not possible due to fundamental differences in geomorphic form; the Matanuska River is a braided river, and the study area on the Tanana River is a wide anastomosed channel reach, both more similar to the Lower Susitna River (below the Three Rivers Confluence in Figure 1-1), rather than the Middle Susitna River which is the topic of this study.

3.1 Erosional Processes Framework

This study developed a framework for characterizing erosion process in terms of the driving and resisting forces of erosion. The two primary categories of erosion are based on Thorne (1982). Erosion processes specific to rivers in boreal environments are collated from a range of studies.

The following processes occur in a gravel-bed river that experiences frigid winter processes:

1. Erosion occurs via entrainment,
    a. (1a) bank material is directly entrained by flow and transported downstream;
    b. (1b) bank material is directly entrained by ice-rubble;
    c. (1c) an applied force at the base of the bank is sufficient to mobilize the gravel boundary material and cause gravitational failure of the bank; or,
    d. (1d) an applied force at the top of bank or in the overbank is sufficient to incise into the bank material.

2. Or erosion occurs by weakening and weathering based on given soil (and climate) conditions due to,
    a. (2a) strength reduction caused by saturation and water-level drawdown, ice pressure in the pores due to freeze and thaw, or leaching of cohesive particles by water movement through the bank; or,
    b. (2b) removal of bank material with detaching bank-attached ice.

To resist applied forces or stabilize a bank from weakening and weathering processes, the following processes should be considered:

3. Banks exhibit a suite of protective processes including,
    a. an armored bank toe
    b. ice-scoured pavement
    c. presence of root-reinforced organic layer from vegetation
    d. ice-cover
    e. frozen banks
    f. bank-attached ice

Specific erosional processes are summarized in Table 3-1. Erosion resistance properties are summarized in Table 3-2.

Table 3-1. Summary table of erosional processes on a boreal river.

Mechanism	Framework Number / How	When	What	Controlling Factors	References
Entrainment of bank and bed materials	**1a Directly by flow along bank face**	Open-water period when banks are unfrozen	Bank sediments directly entrained by flow on bank	Bank composition, presence of vegetation, transport capacity	Hooke, 1979; Thorne and Tovey, 1981; Thorne, 1982
		Banks still frozen but open-water hydraulic conditions	Thermo-erosional niching whereby flow entrains frozen bank material creating an erosional niche. The upper frozen "shelf" eventually fails due to its own weight.	Presence of permafrost	Church and Miles, 1982; Collins ,1990; Lawson, 1983;
	1b Directly by ice along bank face	Ice breakup when banks are unfrozen	Ice rubble abrades bank directly entraining bank material	Thermal properties of bank, floating ice to form jams and ice runs, strength of ice rubble	Ettema, 2002; Ettema and Kempema, 2012; Smith, 1979; Smith, 1980;
	1c Scour (in channel margin at bank toe)	Open-water period	Bank toe is mobilized	Grain size at toe of bank	Nanson and Hicken, 1986
		Winter period with ice cover	Flow is concentrated along bank from ice-cover and in-channel ice	Bank composition, thermal state of bank	Lawson et al., 1986; Prowse, 2001; Zabilanksy et al., 2002
		Ice-breakup	*Ice Jam Release.* Lateral pressure of ice against banks coupled with downstream movement from ice-jam release scours away bank material	Discharge, channel width and slope, hydraulic resistance, strength characteristics of jam, ice volume, water temperature, strength and thickness of ice cover	Arctic Environmental Information and Data Center, 1984b; Beltaos, 1995; Boucher et al., 2009
			Moving Ice Block. Failing ice cover in ice-jam creates consolidation phases in ice blocks that induces surge waves downstream. The surge waves are capable of breaking off shore-fast ice that is then ramped into banks	Presence of ice jam to back up ice-blocks, solar radiation to weaken ice blocks	Arctic Environmental Information and Data Center, 1984b; Michel 1971

Mechanism	Framework Number / How	When	What	Controlling Factors	References
			Ice-Induced Flow Diversion	Diversion of flow by ice jams excaberates erosion at typically stable channel areas (i.e. inside of bends)	Gerard 1989
	1d Scour (on floodplain surface)	Ice-breakup	*Ice Jam.* High mainstem flows backed up by an ice jam can cause overbank flooding that incises into bank/floodplain. Further degrades existing secondary channels or dissects floodplain forming new channels.	Presence of ice jam, decaying ice cover (warming temperatures), precipitation event, channel morphology	Arctic Environmental Information and Data Center, 1984b; Dupre and Thompson, 1979; Ettema, 2002; Mackay et al., 1974; Prowse, 2001; Prowse and Culp, 2003; Smith and Pearce, 2002; Zabilanksy et al., 2002
Bank Strength Reduction	**2a Pore-water pressure**	Open-water period when banks are unfrozen on falling limb of a flood hydrograph	Bank material is thoroughly saturated causing collapse and slumping	Soil moisture conditions	Hooke, 1979; Thorne 1982
		Spring when banks subject to freeze-thaw cycling	Freeze-thaw weakens bank materials	Soil moisture conditions, temperature	Ferrick et al., 2005
	2b Bank-attached ice	Ice breakup	Collapsing bankfast ice can remove bank material and vegetation	Bank angle, location of water table adjacent to bank, drop in flow stage	Ettema, 2002; Ettema and Kempema 2012; Zabilanksy et al., 2002;

Table 3-2. Summary table of erosion resistance properties**.**

Mechanism	Framework Number / How	When	What	Controlling Factors	References
Bank Protection	**3a Gravel / Cobble Armoring**	Year-round	Selective scouring of fine-grained sediment and selective deposition of coarse grained sediment. Feature is mobilized at a critical discharge	Hydraulics	Bunte and Abt, 2001
	3b Gravel / Cobble Pavement	Year-round	Tightly packed gravels, cobbles and boulders that are often not mobilized.	Presence of ice rubble to shear along channel bed	Church and Miles, 1982; Mackay and MacKay, 1977; Prowse and Culp, 2003
	3c Vegetation	Year-round	Vegetation provides root-reinforcement to bank material increasing overall bank stability	Groundwater, precipitation, presence and frequency of disturbance regimes (fluvial and ice)	Bätz et al., 2016; Church and Miles, 1982; Outhet, 1974; Pollen and Simon, 2005; Simon and Collison 2002; Smith, 1976
	3d Ice cover	Ice cover	Presence of an ice cover reduces local velocity gradient and thereby local shear stress values	Formation of ice cover	Zabilanksy et. al, 2002
	3e Frozen Banks	Ice-freezeup, ice-cover, ice-breakup	Frozen banks prevent fluvial entrainment and bed scour	Thermal properties of bank	Scott, 1978; Oatley, 2002; Walker and Hudson, 2003; Best et al., 2005
	3f Bank-attached ice or Shear wall	Ice-freezeup, ice-cover, ice-breakup	Bank attached ice shields the bank from flowing water and ice rubble	Near-bank flow velocity, bank height, location of water table adjacent to bank	Outhet, 1974; Ettema, 2002; Ettema and Kempema, 2012

3.2 Ice-Induced Applied Erosion Mechanisms

3.2.1 *Flow Concentration under an Ice Cover*

The build-up of frazil and anchor-ice deposits beneath an ice cover cause the development of sub-ice channels that act to locally concentrate flow (Lawson et al. 1986, Beltaos, 1995); it should be noted that the processes whereby frazil and anchor-ice form are presently ill-defined. Often, sub-ice channels preferentially align along the deepest and/or fastest portions of the channel (Prowse 2001). Lawson et al. (1986) found this process to cause seasonal changes in morphology on the gravel- bed Tanana River, Alaska, whereby the bed profile slightly degraded during the ice-cover period from concentration of flow. Post- breakup flows with larger amounts of sediment in transport were then found to cause aggradation. Similarly, in the Fort Peck reach of the sand-bed Missouri River, Zabilanksy et al. (2002) found flow concentration below an ice cover to locally hasten bank erosion. This phenomenon may be more common in channels where the channel bed and bank toe are mobilized relatively frequently.

3.2.2 *Ice Jams*

Three erosive processes can be linked to the formation and maintenance or destruction of an ice jam; the processes include flow diversion, water surge and ice-runs. This section elaborates the three processes.

During the formation and maintenance of an ice jam, large and rapid increases can occur in the upstream water stage. This process leads to the diversion of flow and subsequent overtopping of side channel and side slough berms, or overbanks. Within a single channel, diversion of flow can cause extensive bed scour or bank erosion near the inside of a bend (e.g. Smith, 1980; Prowse and Culp, 2003). Diversion of flow into secondary channels occurs for anabranching or braided river channels (Beltaos, 1995) and has been documented to cause bed scour (MacKay et al., 1974),

yet the literature is sparse for how this process may exacerbate erosion, other than local ice abrasion along banks.

The failure of an ice-jam leads to the release of a surge wave, which has been compared to the surge of a wave akin to a dam break (Beltaos, 1995). Surges released from ice-jam breaks can trigger downstream mechanical breakup (Beltaos, 2007) observations indicate waves have reached up to 5 m/s (Beltaos and Burrell, 2005). Observations from Prowse (1986) indicate an ice rubble front during an ice-breakup on the Liard River moved at an average velocity of 5 m/s for nearly 18 km.

The abrasive action of ice rubble released from an ice jam has been observed to exacerbate local bank erosion (e.g., Beltaos, 1995), though the extent of erosion of the reach-scale has not been quantified. Ice runs can produce downstream jamming, failure and surging, which in particularly dynamic ice breakups, may continue until the ice is mostly flushed from the channel. Certain morphologic features cause ice runs to either arrest, stall, or dampen; this includes sharp bends or channel constrictions for arresting or stalling ice runs (Smith, 1980; Gerard, 1989) and the enlargement of flow area for dampening ice runs (Gerard, 1989; Beltaos, 1995). As a result, certain areas of channels may be more prone to erosion from the abrasive action of ice runs. Such areas include the outside of bends or heads of islands (Beltaos, 1995); i.e., areas where channel morphology forces flow velocity to change in direction.

It is noted that the integrity of ice blocks to form jams and erode banks is more dependent on solar radiation than warming temperatures (Gerard, 1989); warm temperatures raise the surface of the ice sheet to 0ºC, causing the surface to melt and gradually thin. Solar radiation, however, penetrates the ice sheet, such that warmer temperatures are absorbed deeper than the surface layer

and cause internal melt (Gerard, 1989). These processes cannot begin until the snow cover has melted.

3.2.3 *Moving Ice Block*

Forces against a structure are a function of the mass and velocity of ice floes. The maximum force an ice floe can exert upon on an object it collides with is the force required to break the ice; this force is determined using the ice's compressive strength or flexural strength, ice thickness, and geometry of the contact structure.

As the ice-cover breaks apart, ice rubble is transported downstream and able to exert mechanical shear against objects it comes in contact with. Abrasion of ice rubble along banks has been documented to exacerbate local erosion, affecting channel form (Boucher et al., 2012). Best et al. (2005) suggest that the presence of floating ice, which resulted in more frequent ice-jamming, may aggravate bank erosion and cause channel widening on the Kuparauk River, Alaska. Ice-jamming in the Necopastic River, Quebec, specifically the abrasion of ice along banks, has been shown to enhance bank erosion and enlarge channel geometry. Channel reaches along the Necopastic River that were sufficiently large in drainage area (greater than 100km^2) and were subject to ice-jams at a minimum frequency (at least once every five years), developed an ice-scoured channel form (Boucher et al., 2009); bank profiles consisted of a steep talus typically set above a vegetated, ice-scarred, narrow bench that was above the bankfull stage. Similar benches have been observed on other boreal rivers including the Peace River and may be a product of both ice-scour and flow regulation (Uunila and Church, 2015).

3.3 Erosion Resistance Properties

3.3.1 *Gravel/Cobble Armoring*

Along gravel-bed channels, boulder pavements may form differently than does bed armoring. Boulder pavements are believed to develop as a result of ice processes; cobbles and boulders are tightly packed into a finer-grained matrix, coarse materials may be difficult to pluck by hand, and the feature may not extend laterally or longitudinally along the entire channel bed. In contrast, coarse-bed armoring occurs via selective scouring of fine-grained materials, selective deposition of coarse grained materials, and based on the current hydrologic regime can become mobile (Sutherland, 1987; Bunte and Abt, 2001). Boulder pavements may persist for over a century (Mackay and MacKay, 1977) and have been observed on many northern rivers (e.g. Kindle 1918; Wentworth, 1932; Mackay and MacKay, 1977; Prowse and Culp, 2003; Uunila and Church, 2015). These features act to stabilize the bank toe thereby limiting bank erosion driven by toe scour.

3.3.2 *Vegetation*

It is generally understood that vegetation can have a stabilizing effect on channel banks and morphology (e.g., Bätz et al., 2016; Fischenich and Allen, 2000; Gurnell and Petts, 2002; Millar 2000). Accordingly, vegetation is often used as an erosion-control method (e.g., Schiechtl, 1980). Various studies have attempted to quantify a bank's increased resistance to erosion due to vegetation (Smith, 1976; Simon and Collison, 2002; Pollen and Simon 2005). However, vegetation may also increase infiltration and thereby soil moisture content, and thereby potentially geotechnically destabilize a bank; this effect may be more problematic in arid regions with incised channels (Simon and Collison, 2002). Simon and Collison (2002) indicate that the mechanical benefits of vegetation on bank stability tend to outweigh destabilizing effects from changing soil moisture content, however there may be rare instances in which the hydrologic effects of

vegetation outweigh the mechanical. Antecedent soil moisture does play a role in soil stability, where a drier period and subsequent higher matric suction increased soil stability for mixed trees while reducing soil stability for grasses due to the increased infiltration.

The mechanical effects of vegetation have been more clearly quantified. For example, Smith (1976) found cohesive soil (silt) with 16 to 18 percent by volume of roots and a 5-cm root mat, to have 20,000 times more resistance to erosion than the same soil with no vegetation. In a field experiment, Simon and Collison (2002) found various species of tree roots to increase bank soil strength by 2000- 8000 Pa and grass roots to increase soil strength from 6,000-18,000 Pa, which supports the view that smaller roots tend to have more tensile strength than do larger roots. However, combining the effects of root area per unit area of soil and root diameter-tensile strength, it was found that most of the strength for woody species came from the larger diameter roots (>5mm), indicating that root area is more important than root strength (Simon and Collison 2002). Vegetation may have a stabilizing effect when subjected to forces by water, but when impacted by ice rubble, this effect may be diminished (e.g., Prowse and Culp, 2003).

3.3.3 *Ice cover*

The additional flow resistance caused by the presence of an ice cover usually increases flow stage, reduces the average flow velocity, and decreases the hydraulic radius. These actions reduce the effective shear stress, and thereby reduce the flow's capacity to convey any eroded sediment from the sediment source (Zabilanksy et al., 2002). On the Missouri River, this process caused some local transient bars to form near an erosion location that were eventually washed downstream after breakup (Zabilanksy et. al., 2002). One consequence of this action is altered alignment of flow channels.

3.3.4 *Frozen Banks and Bedfast Ice*

Ice becomes attached to a channel bed (i.e., bedfast ice) particularly in shallow channels (Ashton, 1986). The presence of ice alters the time of year for bed-sediment mobilization, so that scour or erosion cannot take place until after ice has lifted from the bed or, for fully frozen streams, the bed and bank materials have thawed (Scott 1978; Oatley, 2002; Walker and Hudson, 2003; Best et al., 2005). Ice runs tend not to occur in channel reaches with bedfast ice (Ashton, 1986) which is believed to be a result of channel ice type (Best et al., 2005); ice runs occur where there is floating ice that can subsequently cause ice jams, ice runs, and enhanced bank erosion (Best et al., 2005).

3.3.5 *Shorefast Ice*

Once the ice begins to breakup the presence of shorefast ice, or, the formation of shear walls from an ice run, may also act to protect a bank from erosion (e.g. Prowse and Culp, 2003; Ettema and Kempema, 2012).

CHAPTER 4: METHODS

A three-part approach was used to address the objectives of this study. Recapping briefly, Part 1 synthesizes bank observations along the selected sub-reaches and presents conceptual erosion models for differing hydrologic regimes that may lead to the observed bank forms. Part 2 is a bank-erosion analysis focusing on the extent of short-term erosion, the type of geomorphic surface eroding, and locating where the erosion occurs. Additionally, this analysis identifies the hydrologic regime during which the erosion mainly occurs; i.e., open-water conditions or when ice is in the river. Of importance in this regard is linking erosion to specific hydrologic events during the year. Part 3 then compares short-term erosion identified in Part 2 to existing records of long-term erosion along the Middle River.

4.1 Part 1: Observations and Conceptual Models

Part 1 has three-subsections. Section 4.1.1 presents bank observations through the observation of geomorphic reaches – Reaches 6 and 7. This sub-section of the thesis includes photographs and descriptions of various bank forms along the sub-reaches, as well as acquiring observations of ice-effects along banks. Section 4.1.2 describes the most common bank forms in the sub-reaches. Section 4.1.3 presents a schematic of possible erosional processes throughout the year along with conceptual models of the common erosional processes that may lead to the bank forms observed along the Middle Susitna River study reaches. The subs-sections are elaborated below.

4.1.1 *Reach-wide Bank Observations*

Bank observations collected between 2013 and 2014 are collated along the study reaches. Typical bank forms are described, including bank-toe conditions, bank-soil stratification, and top-of-bank conditions. Further, common effects of ice on banks are presented.

4.1.2 *Common Profiles of Eroding Bank*

The most commonly observed bank forms are presented and described with the aid of a series of figures.

4.1.3 *Erosional Processes Conceptual Model*

A schematic for the time-frame of erosional processes based on the primary hydrologic regime within the year (ice freeze-up, ice-cover, ice-breakup, and open-water) was developed. Conceptual erosion models for the dominant observed and theorized erosional processes were identified. The erosion models illustrate the erosional processes that can cause the common bank forms observed along the Middle Susitna River.

4.2 **Part 2: Erosion Analysis**

An erosion analysis was performed to quantify the extent of short-term erosion and identify under which hydrologic regime erosion occurred. To distinguish the possible erosive effects of various open-water flow events and ice-induced erosive processes, the short-term erosion analysis was performed over two, one-year periods with distinctly different hydrologic regimes including varying open-water peak flow events and types of ice-breakup. The erosion analysis used sequences of aerial photographs and videos obtained from aerial flights flown periodically between the aerial photography flights.

To identify whether fluvial or ice-induced processes were driving bank erosion, short-term channel changes were categorized into approximate time period “bins” within the year: ice freeze-

up, ice breakup, and the open-water period. This task entailed reviewing aerial reconnaissance videos to determine the timing of erosion. The reconnaissance videos were flown during ice freeze-up, during the ice-cover period, before ice breakup, during ice breakup, and after ice-breakup when all ice was flushed from the river. The locations of erosion were reviewed during each time period to identify when erosion occurred.

4.2.1 *Sequential Aerial Photography Analysis*

Aerial photographs were collected in June 2011, September 2012, and September 2013. Details of each sequence of photographs are described below. The aerial photographs were ortho-rectified to facilitate accurate estimation of changes in land-surface extent. Ortho-rectification involved adjusting image displacements caused by the presence of ridges or depressions in the terrain, or by camera geometry, so that objects appear to be viewed directly from above.

4.2.1.1 *Aerial Photographs*

The Matanuska-Susitna Borough acquired aerial photographs that covered the Susitna River Basin in June 2011. The photographs were ortho-rectified, multispectral, 4-band images showing the river and banks at 0.3 m resolution (Matanuska-Susitna Borough, 2011). Aerial flights of the downstream portion of Reach 6 and all of Reach 7 were flown on May 25, 2011 when the flow at the Gold Creek gage was 867 m^3/s (30,600 ft^3/s). Aerial flights of the upstream portion of Reach 6 were flown on June 18 and July 21, 2011 when the flow at the Gold Creek gage was 505m^3/s (17,900 ft^3/s), and 520 m^3/s (18,300 ft^3/s), respectively. The gold creek gage, located at RK 225, is shown in Figure 2-1.

Aerial photographs of the Susitna River were collected in 2012 by Tetra Tech (2013b). The photographs were ortho-rectified, 4-band imagery at 0.3 m resolution or better pixel resolution.

Aerial flights of Sub-reach 6 and 7 were flown on September 10, 2012 when flow at the Gold Creek gage was 365 m^3/s (12,900 ft^3/s).

Aerial photographs of the Susitna River were collected in 2013 by Tetra Tech (2014i). The photographs were ortho-rectified, 4-band imagery at 0.3 m pixel resolution. Aerial flights of Reach 6 and 7 were flown on September 24, 2013 when the flow at the Gold Creek gage was 320 m^3/s (11,300 ft^3/s).

4.2.1.2 *Hydrologic Record between Aerial Photograph Datasets*

Immediately following the 2011 aerial flight, flow at the Gold Creek gage was slightly larger than a 2-yr recurrence interval flow event (1,255 m^3/s; 43,900 ft^3/s) due to the spring runoff. Through the rest of the summer to freeze-up, flows were less than the 1.25-yr recurrence interval. The winter was followed by intermittent, above-freezing temperatures in April and cool temperatures in May. This temperature variation led to the slow thermal decay and breakup of the ice cover (HDR Alaska, Inc., 2014a). The 2012 ice-breakup was categorized as a thermal ice-breakup due to the low discharges and weak ice cover that was unable to form large jams. A month later, the spring snowmelt runoff yielded a flow slightly less than the 2-yr peak flow event that was followed by another flow event between the 2- to 5-yr recurrence interval. Flows continued to drop through the rest of the summer and into September by the time the 2012 aerial imagery was collected. The hydrograph between the 2011-2012 aerial imagery flights is shown in Figure 4-1.

The 2012 aerial photographs were collected on September 10, 2012 (365 m^3/s; 12,900 ft^3/s) and were soon followed by heavy rains that yielded a nearly 20-yr recurrence interval flow on September 22 (2,005 m^3/s; 70,800 ft^3/s). Subsequent flows dropped leading into freeze-up in mid-October and early November. The 2012-2013 winter was followed by a cool spring that sustained

much of the snow and ice cover through the basin (HDR Alaska, Inc., 2014a). Gradual warming temperatures in mid-May caused some deterioration in the snow and ice cover, resulting in some jamming and flooding of sloughs through the Middle River. The end of May brought a sharp increase in temperatures that resulted in rapid snowmelt and subsequent increase in discharge. Rising flows and a competent ice cover lead to a dynamic ice breakup. The Middle River was largely ice-free by May 29, 2013 (1,820 m^3/s; 64,300 ft^3/s) and flows continued to rise to a nearly 50-yr recurrence interval peak open-water flow by June 2 (2,460 m^3/s; 86,800 ft^3/s). Precipitation in late August yielded a flow slightly larger than the 2-yr recurrence interval. Flows continued to drop by the time aerial imagery was flown on September 24, 2013 (320 m^3/s; 11,300 ft^3/s). The hydrograph between the 2012-2013 aerial-photography flights is shown in Figure 4-2.

Both one-year time periods experienced multiple flows higher than the 2-yr recurrence interval (i.e., flows whose stage exceeded the gravel-sand contact in the bank profile) while overall, open-water flows during 2012 to 2013 were greater. The main distinction between the two time periods however, is the nature of the ice-breakup; whereas the winter 2011 to 2012 had a thermal breakup of the ice cover, the winter 2012 to 2013 had a dynamic breakup of the ice cover that preceded a peak flow event whose magnitude was between the 20- to 50-yr recurrence interval. Figure 4-3 shows the flow record during the spring ice breakups.

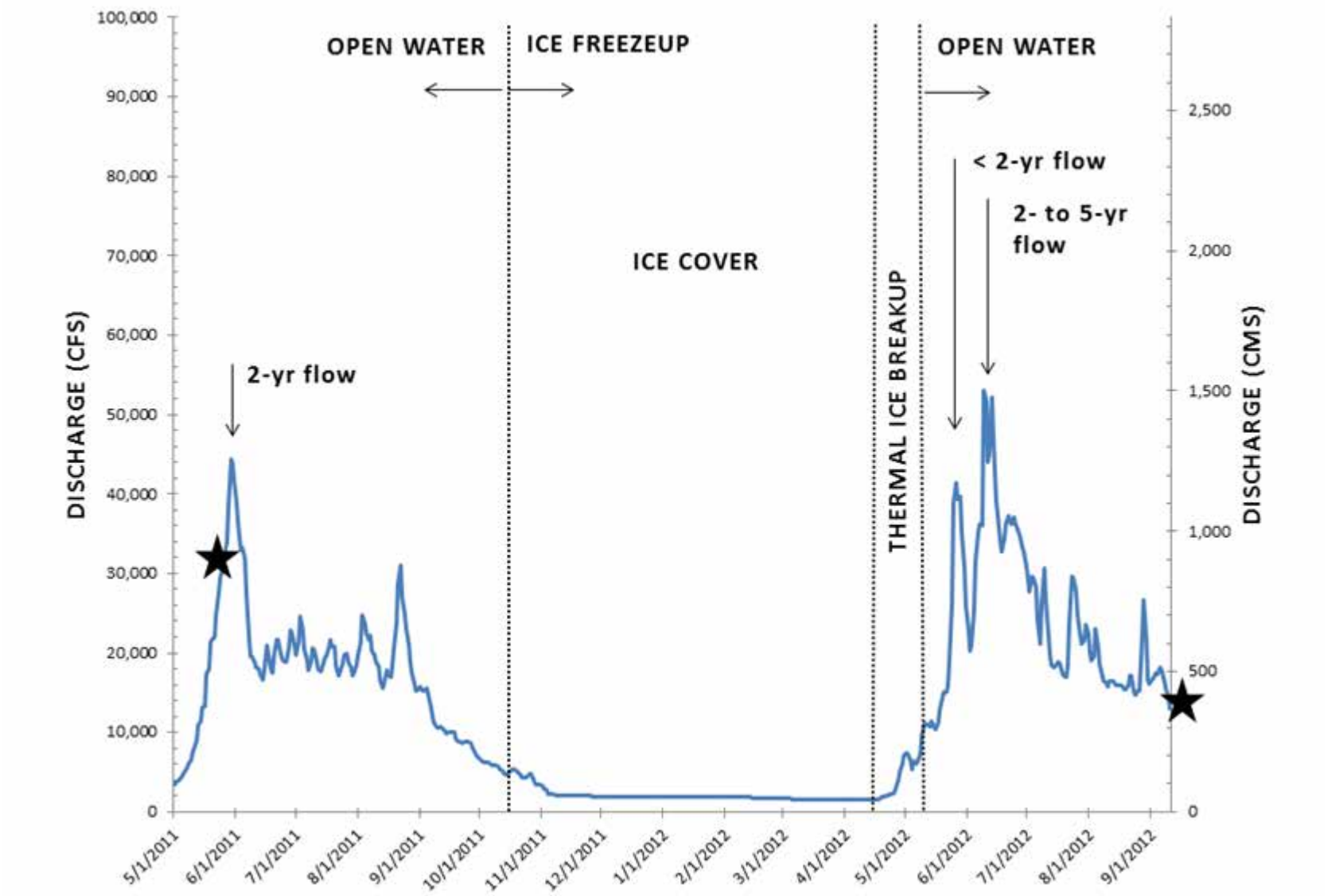

Figure 4-1. Mean daily discharge between 2011 and 2012 aerial imagery flights at Gold Creek gage. The black stars represent date of aerial flight.

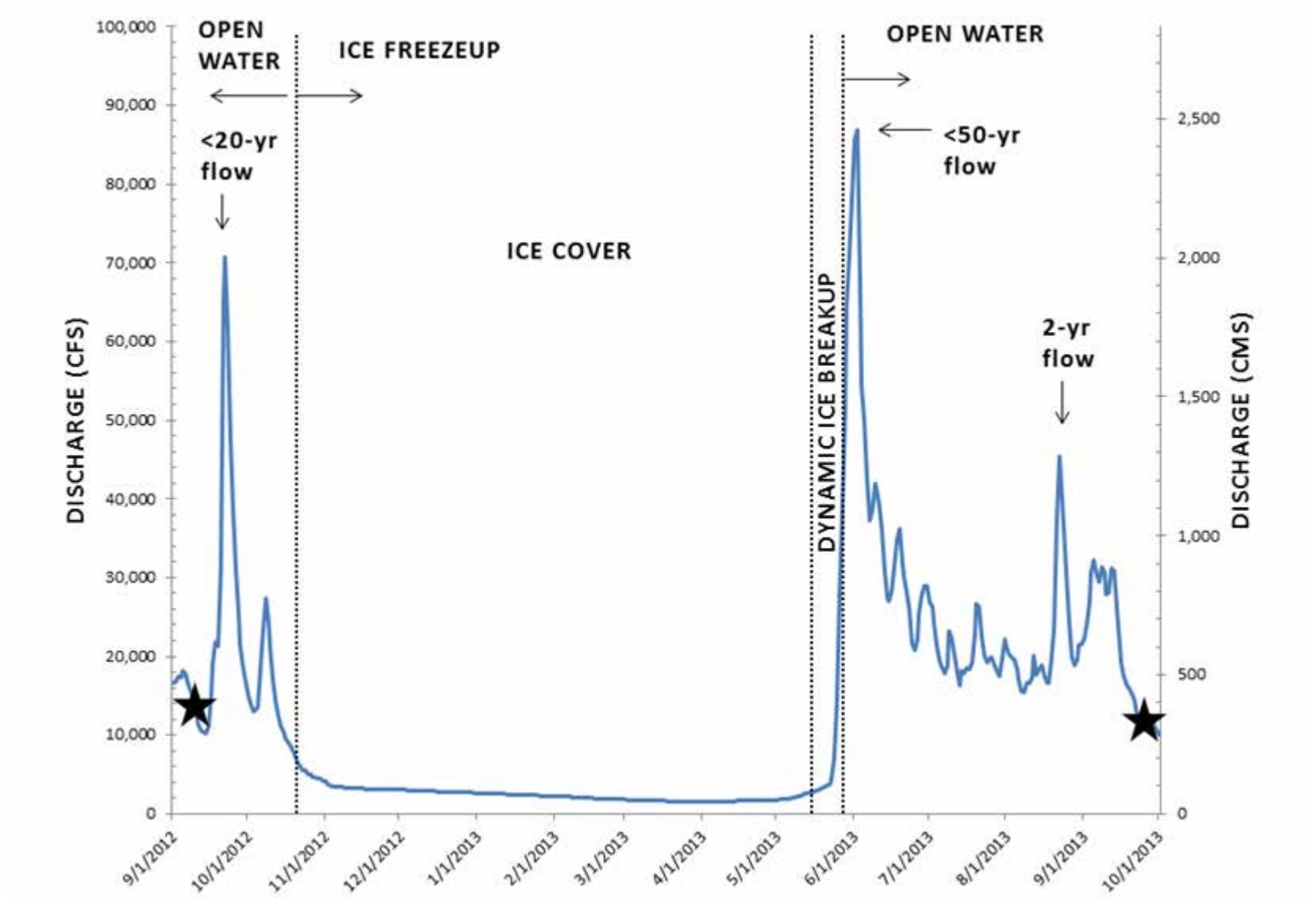

Figure 4-2. Mean daily discharge between 2012 and 2013 aerial imagery flights at Gold Creek gage. The black stars represent date of aerial flight.

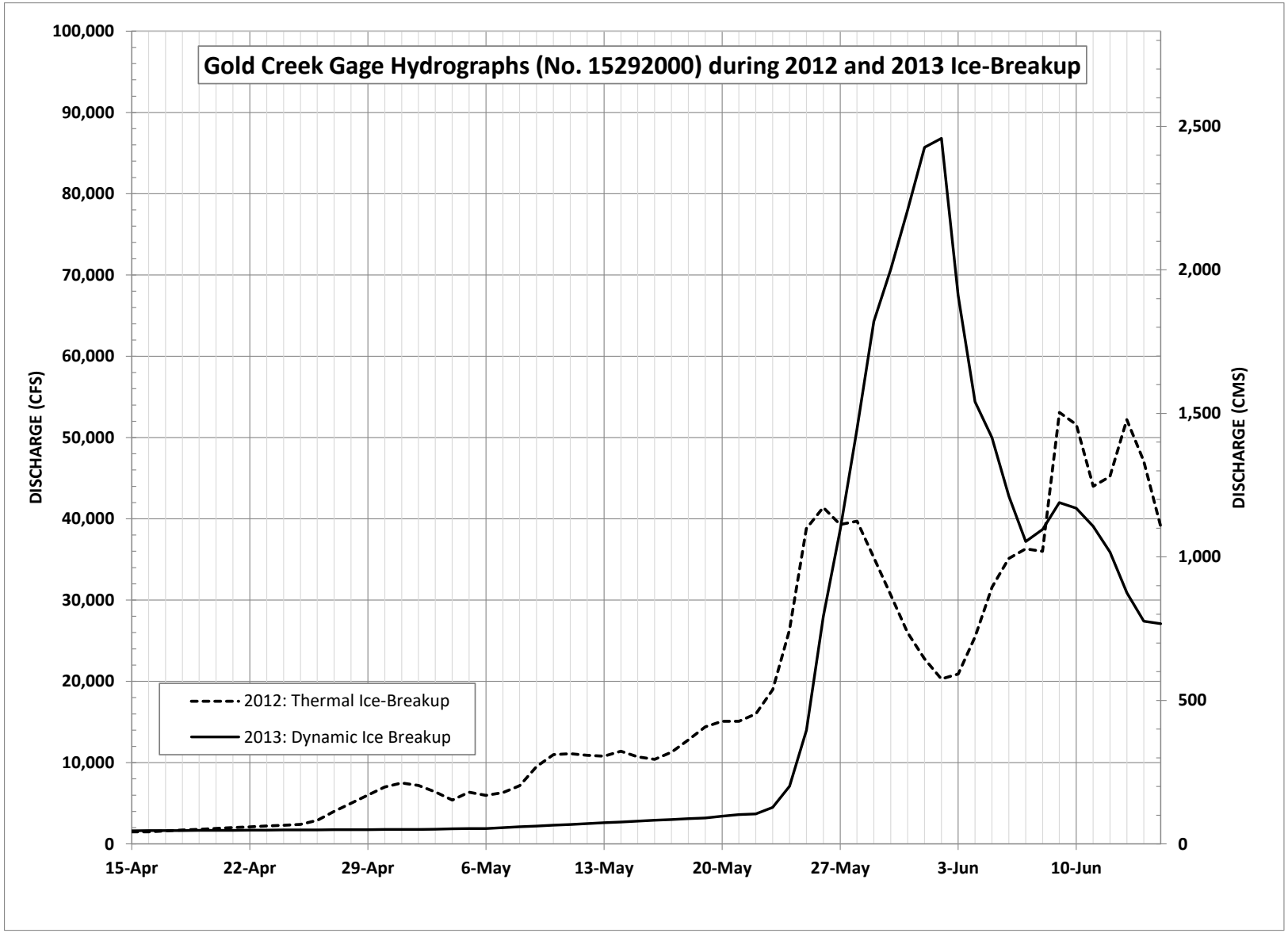

Figure 4-3. Mean daily discharge at Gold Creek gage during 2012 and 2013 ice-breakup.

4.2.1.3 *Analytical Process*

The analytical processes involved determining changes in the bank location, which in turn entailed evaluating changes in the location of bank vegetation.

The main vegetated features along the banks were delineated using aerial photographs obtained during 2011, 2012 and 2013. For each year, land features were categorized as a vegetated feature with tree stands (i.e., a young, mature, or old floodplain) or a vegetated feature with low-lying vegetation (i.e., vegetated bar) as illustrated in Figure 2-5 (Section 2.2.9). Delineating mature tree stands versus low-lying vegetation did not require significant extra analysis time, but did provide insight into the extent that various geomorphic surfaces were eroded. The shapefiles for each year were overlain to identify channel change. As very thin polygons can form due to slight differences in delineation (stemming from the scale the feature was delineated at [1:1000 to 1:4000] or errors due to the tree canopy or shadows), any polygons less than 930 m^2 (10,000 ft^2) were removed from the analysis. This threshold value was selected as differentiating channel change of a unit of area this small, especially when the polygon was long and thin, was often imperceptible. Additionally, areas of 930 m^2 were often 5 percent or less of the area of mid-channel islands, such that removing them from the analysis would not significantly affect identification of large scale channel change. Lastly, polygons approximately 15 m (50 ft) in width were categorized as "less than 15 m." These polygons often were slivers of land that extended along the banks of most features throughout the reach and were likely due to slight differences in delineation rather than actual channel change.

In the process of ortho-rectifying photographs, some tall objects still had some tilt or displacement. This process could introduce errors when delineating vegetated features in GIS. If these polygons were less than 930 m^2 they would have been removed in the initial processing of

the shapefile. Polygons larger than 930 m^2 that indicated channel change (e.g., 2012 vegetation to 2013 channel, or 2012 trees removed to 2013 low-lying vegetation) were then reviewed to assess whether change did in fact occur or if the polygon was a product of image displacement. If polygons about 15 m or less in width were found to have indicated channel change, they were then flagged. Potential errors due to delineation or feature categorization were also possible with the larger polygons. Therefore, features were identified as "yes" for observed channel change, "no" for no channel change, or "unclear." All locations flagged with observable channel change were reviewed using reconnaissance videos. Thus, the areas of observable channel change provide a minimum value for the total amount of erosion that occurred over the two one-year periods given that areas designated as "unclear" or "less than 15 m" may in fact have eroded but were not included in the total erosion summation. To compare this one-year vegetation change data with the longer-term turnover data developed by Tetra Tech (2014f), polygons within the turnover shapefile between 1951, 1983, and 2012 were summed only for areas greater than 930 m^2 (10,000 ft^2).

Lastly, the polygons identified as "yes" for observed channel change were intersected with Middle River terrace polygons. The terrace polygons were identified as surfaces that were at least 1.5 m above the 100-yr water surface elevation (Tetra Tech, 2015c). Erosion area was then summed into three geomorphic surface categories: low-lying vegetation (i.e., vegetated bars), mature tree stands that did not coincide with a terrace surface (i.e., young, mature, or old floodplain), and mature tree stands that did coincide with terrace surfaces (i.e. terrace surfaces).

4.2.2 *Identify Primary Hydrologic Regime of Erosion*

The helicopter-based videos of the river corridor were assessed to identify under which hydrologic regime channel change occurred. The videos show the Middle Reach during ice freeze-

up and breakup, and during the open-water season. Certain instances of channel change between aerial imagery flights were found to have an indistinguishable time period of channel change. Such instances include changes that were about 15 m or less in width, or were along a continuous bank line with no geometric distinguishers in bank shape (e.g., concave bank remains a concave bank) or no distinguishers in bank composition (e.g. no vegetation indicators between the two periods such as fallen or removed trees). Accordingly, periods of channel change fell into four categories: pre-freeze-up, ice-breakup, ice-breakup through the next imagery flight (i.e., Fall), or unclear. Erosion categorized during an unknown time period could be due to fluvial, ice, or a mixture of both processes.

4.2.3 *Identify Dominant Bank-erosion Processes*

The dominant bank-erosion processes were identified in accordance with the flow conditions (open water, freeze-up, breakup) and extent of lateral erosion, as identified in Section 4.2.2. Two dominant erosion processes, impact of ice rubble and ice floes, and ice induced diversion of waterflow, were also numerically investigated.

Approximate impact stresses were developed for impacting ice rubble and ice floes typical to the Susitna River. For a single, drifting ice floe impacting a bank or bar, the magnitude of stress exerted by the floe can be estimated in approximate terms as:

For a single, drifting ice floe impacting a bank or bar, the magnitude of the impact stress exerted by the floe can be estimated in approximate terms as:

$$\sigma = \frac{(virtual\ mass\ of\ ice\ floe * deceleration) + (water\text{-}pressure\ force)}{bank\ contact\ area}$$

Here, virtual mass of an ice floe can be estimated as

$$virtual\ mass = mass\ of\ ice\ floe + C * mass\ of\ fluid\ displaced\ by\ ice\ floe$$

with,

$$mass\ of\ ice\ floe = floe\ volume * \rho_{ice}$$, and,

$$C = added\ mass\ coefficient$$

Deceleration is estimated as,

$$deceleration = (v_1 - v_2)/\Delta t$$

Also, here, water-pressure force is attributable to water thrust ahead of the ice mass. This force is neglected here, because the ice mass is relatively thin such that water can be readily displaced vertically.

The increment of time associated with ice mass impact is

$$\Delta t = time\ for\ ice\ block\ to\ come\ to\ a\ stop \approx \frac{x}{v_{avg}}$$

With, $x = distance\ for\ ice\ block\ to\ come\ to\ stop$, and $v_{avg} = \frac{v_1+v_2}{2}$

The aforementioned equations are difficult to calculate accurately, for several reasons. Notably, the mass of water displaced by a large floe moving along a relatively shallow river channel is difficult to calculate accurately, and changes with proximity to bank. The added-mass coefficient characterizes the mass of water displaced as an ice floe decelerates on approaching a channel bank. Values of added mass are difficult to determine accurately, and indeed change as the floe approaches close to a bank. Further, floe sizes vary in size and shape. Therefore, as the present effort focuses on an approximate level of force, added mass is neglected. Moreover, the actual contact area is hard to assess.

An upper level of force can be estimated by determining the force required to fail the floe in flexure. Flexural failure estimates the vertical component of ice impact on a bank as:

$$N = V/\cos(\alpha)$$

Here, $V = vertical\ component\ \ of\ floe\ failing\ in\ flexure,$ and, $\alpha = bank\ angle$.

The horizontal component of ice impact on a bank, H, is then estimated as:

$$H = N * \sin(\alpha)$$

To investigate ice-induced diversion of water flow, a two-dimensional hydraulic model (SRH-2D) was developed for approximately 4 km on the Susitna River (RK 210 to RK 206). The goal of the fixed-bed model was to simulate hydraulic characteristics in complex flow patterns in order to quantify flow distribution, lateral feature breach (i.e. overtopping), erosion and deposition based on existing and with-project hydrologic, sedimentologic, and ice-regimes (Tetra Tech, 2015d). This existing model was selected to analyze shear stress distributions and water surface elevations under simulated main channel blockages.

The geometry of the existing model (Tetra Tech, 2015d) was modified to simulate blockage in the main channel from ice and diversion into secondary channels. Open-water hydraulic modeling was performed over a range of typical (10,000 to 21,000 ft^3/s; 283 to 595 m^3/s) and extreme (30,000 and 40,000 ft^3/s; 850 and 1,133 m^3/s) discharges during ice-breakup (Jon Zufelt, HDR Alaska, Inc., personal communication)

4.3 Part 3: Comparison of Erosion Rates

Records of the erosion data along Reaches 6 and 7 were presented in a series of maps. The short-term erosion data (Part 2) were compared to long-term erosion data (Tetra Tech, 2014f). Data from records prior to the present study are herein called historical data.

Additionally, the categories of geomorphic surfaces were assigned to the land delineations for the 2011 through 2013 sequential aerial analyses (Section 4.2.1). For the historical data, terrace surfaces were intersected with the historical turnover data to categorize terrace versus active floodplain surfaces. Areas where part of a channel changed to land (i.e., sediment aggradation and

vegetation establishment) during 1951 to 1983 were categorized as low-lying vegetation (i.e., vegetated bars) for the 1983 to 2012 period. No areas were identified as low-lying vegetation for the period 1951 to 1983, because of the difficulty in adequately categorizing vegetated bars versus other vegetated geomorphic surfaces from the black and white aerial photography.

Values of total erosion, in terms of geomorphic surface area, were tabulated for each time period of analysis: i.e., 1951 to 1983, 1983 to 2012, 2011 to 2012, and 2012 to 2013. Values of total erosion of each time period of analysis were also determined by volume. The area of erosion by geomorphic surface was multiplied by the minimum and maximum height of the respective surface. The minimum volume for each geomorphic surface was summed to generate a minimum sediment volume. The maximum volume for each geomorphic surface was summed to generate a maximum sediment volume.

CHAPTER 5: RESULTS

The results of the field work are presented here in accordance with the three-part approach described in Chapter 4.

5.1 Part 1: Observations and Conceptual Models

5.1.1 *Synthesis of Bank Observations*

Typical photographs of banks along Reaches 6 and 7 are illustrated in Figure 5-1a-f. The following features are evident in the photographs:

a. Broken and sheared roots with a downstream directional bend (Figure 5-1a);

b. Cantilevered bank with thick draped rootmats (Figure 5-1b);

c. Vertical and scalloped bank with little to no root reinforcement (Figure 5-1c);

d. A high, vertical bank with little to no root reinforcement (Figure 5-1d);

e. A high bank with gravel-cobbled paved bank toe and channel bed (Figure 5-1e); and,

f. A low, vegetated, gradual angled bank with a gravel-cobbled bank toe (Figure 5-1f).

These features indicate that a large portion of the banks were undercut and had varying levels of bank protection provided by overhanging bank-top vegetation.

As described in Section 2.2.9, the tops of all banks through Reaches 6 and 7 were vegetated with trees and shrubs, with the exception of very old floodplain surfaces or terraces where the tree vegetation succession has reached a point in the continuum where trees are sparse and have been replaced by low-lying shrubs, grasses, and ostrich ferns. The lower geomorphic surfaces (including young floodplains and mature floodplains) had extensive root mats that when exposed by erosion could hang down over the bank face (as shown in Figure 5-1a,b). Vegetation on older surfaces, including old floodplains and Holocene terraces, did not exhibit the same protective effects as the

lower densely vegetated surfaces as evidenced in Figure 5-1c,d. Continued entrainment by water flow, or contact with ice, of the fine-grain bank layers illustrated in Figure 5-1 may initiate gravitational failure from the sparsely vegetated upper bank.

Banks with extensive rootmats typically had an intact bank toe and a swath (a few meters or less) of roots that extended beyond the bank face itself. This occurrence indicates the fine-grained bank material eroded, yet the more erosion resistant bank properties (surface sediment layer and rootmats from top-of-bank vegetation) limited the erosive processes. The distance from the edge of the roots to the bank face may approximate the extent of lateral retreat of the non-cohesive layers.

Some banks were vegetated and gradually sloping, and did not exhibit any signs of active erosion. These banks occurred where an intact gravel-cobble pavement existed on the bank's gentle slope. These banks also corresponded with the location of older geomorphic surfaces, notably alluvial fans or Holocene-age terrace units as shown in Figure 5-1e. They were less commonly observed on geomorphic surfaces in the hydrologically active zone, though when present were found on the inside of bends or at the downstream end of geomorphic surfaces that were within the backwater zone of a downstream constriction (as shown in Figure 5-1f). The gravel and cobble pavement was compacted into a tight matrix of finer sediment, creating a surface easy to walk upon. Sediment samples taken throughout the river corridor often had to be loosened with a pick axe or screwdriver in order to dislodge the particles.

Almost all banks showed some sign of ice disturbance, including ice-impact tree-scars, splays of cobbles or gravels on top of the floodplain, bent down, cracked, or leaning vegetation, ice-bulldozed vegetation, a gouged bank face, or paved gravel-cobble bank toes. Such pavement is a sign of ice disturbance but results in a more erosion-resistant lower bank. Ice effects, as

expected, were more common and often more damaging to the overbank vegetation on lower geomorphic surfaces including vegetated bars and young floodplains. These lower geomorphic surfaces were often characterized by large swaths of ice-bulldozed vegetation or leaning pole poplars. While, the effects of ice were present on higher surfaces including mature floodplains, old floodplains, and terraces, the effects were less pervasive than on the lower geomorphic surfaces and included tree ice-scars, ice-deposited sediment, or pockets of bent and leaning trees. Despite all banks displaying some sign of ice disturbance, the degree to which ice determined the existing bank form and drove bank retreat was unknown.

Figure 5-1. Common features of bank conditions along Reaches 6 and 7 of the Susitna River: (a) broken and sheared roots with a downstream slant and a gravel-cobble pavement at the bank toe; (b) cantilevered bank with draped rootmats; (c) destabilized older surface and collapsing bank; (d) high, vertical bank with downstream slant to roots; (e) a gravel-cobbled paved bank toe below high terrace surface; (f) a gravel-cobbled paved and vegetated gradual sloping angled bank below active floodplain unit.

5.1.2 *Common Profiles of Eroding Bank*

Common profiles of eroding banks are presented for three categories of geomorphic surfaces:

1. the vegetated bar;
2. active floodplain (young, mature, and sometimes old floodplain units); and,
3. infrequently inundated geomorphic surfaces (old floodplains or terrace surfaces).

The common bank forms are dynamic and may change following the next erosive event(s), but there are persistent observable trends.

Annotated profiles of the most common bank forms for each category of surface are presented in Figure 5-2, Figure 5-3, and Figure 5-4, respectively. The bank profiles include zones of influence for various ice or fluvial processes.

Figure 5-2 illustrates a common bank form of vegetated bar surfaces. The bank has a stable toe that is paved or armored with gravels and cobbles, is gradually sloping, and composed of alders and willows. The vegetation often showed signs of bending or ice-push, yet seemed resilient and able to regrow from an established root network.

Figure 5-3 illustrates common banks on young and mature floodplain surfaces. The presence of extensive exposed root wads of trees slumped over the lower bank were common on the Middle Susitna River; this feature, termed “vegetation rip-rap” by Church and Miles (1982) is common on northern rivers and are considered to increase bank resistance (e.g., Smith 1976). Roots stabilized the upper bank (Simon and Collison 2002; Pollen and Simon, 2005) and buffered the abrasive effects of ice rubble moving along banks. The persistence of exposed and ice-abraded rootmats along the Susitna River, especially along cantilevered banks, illustrates bank-stabilizing effects, including:

1. protecting the bank and adjacent vegetation from extensive scour, and,
2. stabilizing the upper bank from subsequent collapse.

While the prevalence of overhanging vegetated rootmats along the Middle Susitna River indicated that these features persist for some time in stabilizing the bank, and thereby preventing significant lateral retreat, this effect is time-limited. In the short-term, rootmats can be damaged by external forces due to subsequent erosive event(s), likely from the mechanical shearing of ice. However, the main time-limiting factor is the geomorphic succession (Figure 2-5) where the vegetation reaches the end of its life cycle and dies off, such that there is a lack of root reinforcement to the upper bank. Accordingly, the bank profile will again be partially or completely exposed, and therefore become more susceptible to the erosive effects of ice and water flow.

Figure 5-4 illustrates a vertical bank form; a common bank form on older geomorphic surfaces and terrace surfaces where there is little root-reinforcement to the upper bank layer. The bank is particularly susceptible to flowing ice-rubble or entrainment by water flow. In Figure 5-4, note the dry layer of bed material at the bank toe is absent of cobble; this condition could indicate removal of sediment particles by ice, or the coarser surface material could have been buried by a finer grained sediment deposit (possibly sourced from the basal gravel core in the adjacent bank).

Figure 5-2. Schematic of low-gradual sloping bank on vegetated bar observed on the Middle Susitna River. Flow moving from top of photo to bottom of photo.

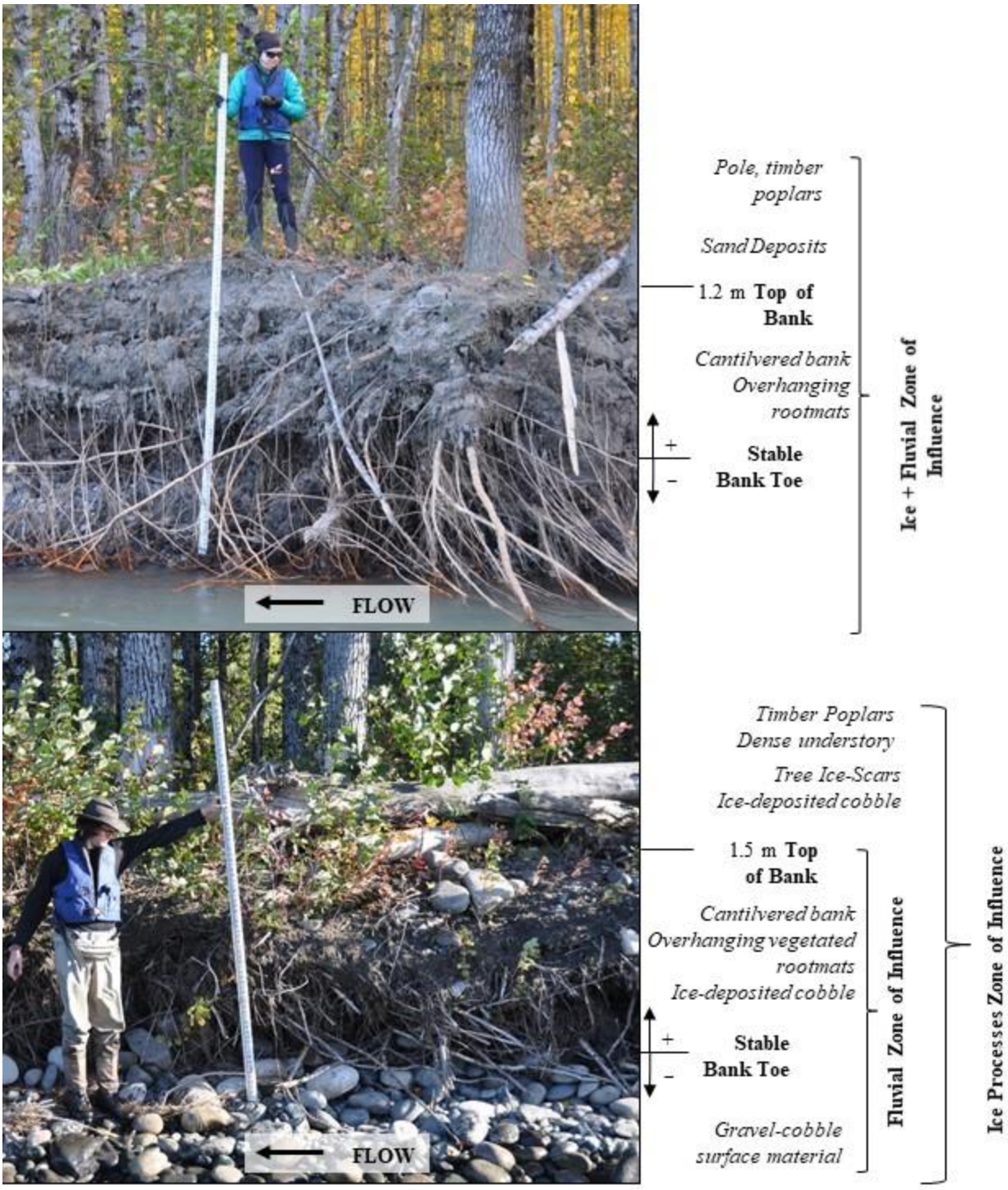

Figure 5-3. Schematic of cantilevered banks on active floodplain surfaces observed on the Middle Susitna River.

Figure 5-4. Schematic of vertical bank on old floodplain/terrace surface observed on the Middle Susitna River.

5.1.3 *Erosional Process Conceptual Models*

The goal of developing erosional process conceptual models is to identify which erosional processes are dominant during the various hydrologic regimes during the year, and which erosional processes may lead to the bank forms and extent of lateral retreat observed along the Middle Susitna River.

It was observed that several erosional processes may occur during the various hydrologic regimes of the Middle Susitna River. In general, the Susitna River appeared to be subject to erosional processes typical of those observed in gravel-bed rivers located in boreal regions. The ensuing discussion elaborates the conceptual models associated with the various erosional processes.

Bank retreat occurs when the stress on the river's banks from applied external forces exceeds the bank's resistive properties. The location, magnitude and duration of applied external force are functions of a suite of variables: regional and local climate, water level, water depths,

velocity, shear stress, presence of in-channel ice, and strength of in-channel ice. Each variable changes through time, but can generally be categorized based on the primary hydrologic regime. A schematic of erosional processes observed to occur along the Susitna River during the primary hydrologic regimes and associated values for discharge, velocity, bank condition, and ice-breakup type is presented in Figure 5-5. Ice-breakup type is used as a proxy term indicating the strength condition of river ice. This figure uses the customary designations for breakup:

1. "Thermal," which indicates ice that has been weakened from solar radiation and rising temperatures; and,
2. "Dynamic," which indicates ice that has maintained strength, is capable of forming in-channel ice jams, and can apply high forces to external objects.

Figure 5-5 presents the range of discharges for each hydrologic regime (as also indicated in Figure 2-4); the solid black line indicates the mean monthly flow while the bounding grey boxes indicate the minimum and maximum monthly flows. Figure 5-5 also presents the general water surface elevations that may occur during each hydrologic regime. Note the presence of an intact ice cover, with a build of frazil underneath and anchor ice on the channel bed during the ice cover period (typically January through April). Blocks and floes of the broken ice cover are illustrated during the Ice-breakup period along with higher discharges that can cause overbank flow in the floodplain. Typical open-water water-surface elevations are less than the active floodplain surface, but may inundate lower vegetated and unvegetated bars. Water-surface elevation is typically low during the ice-freezeup period (except during freezeup jams) and there is a build-up of frazil and bank-attached ice. Velocities for the open-water period were derived from field measurements and a 1-D hydraulic model (Tetra Tech, 2015e) and velocities during the ice-cover were derived from field measurements (HDR Alaska, Inc., 2014b). Velocities for the ice-breakup period encompass

velocities modeled during the open-water period and may reach up to 5 m/s noted in the literature (e.g. Prowse, 1986; Beltaos and Burrel, 2005). Velocities for the ice-freezeup period are based on conjecture and observations, where receding discharge results in low velocities that are typically less than values during the open-water period.

Conceptual models of each of the erosional processes identified in Figure 5-5 are presented in the ensuing sub-sections. As erosional processes involving ice act in conjunction with water flow, making it difficult to differentiate effects due solely to ice or water flow, the combined effects are herein referred to as the "ice-driven regime." The conceptual models are sub-divided based on which influence exerts the driving erosional process; i.e., water flow or ice. The models are used to identify the effects on bank form and lateral bank retreat due to the various erosional processes. Each model is supported by photographs illustrating the effects of the erosional processes on the Middle Susitna River.

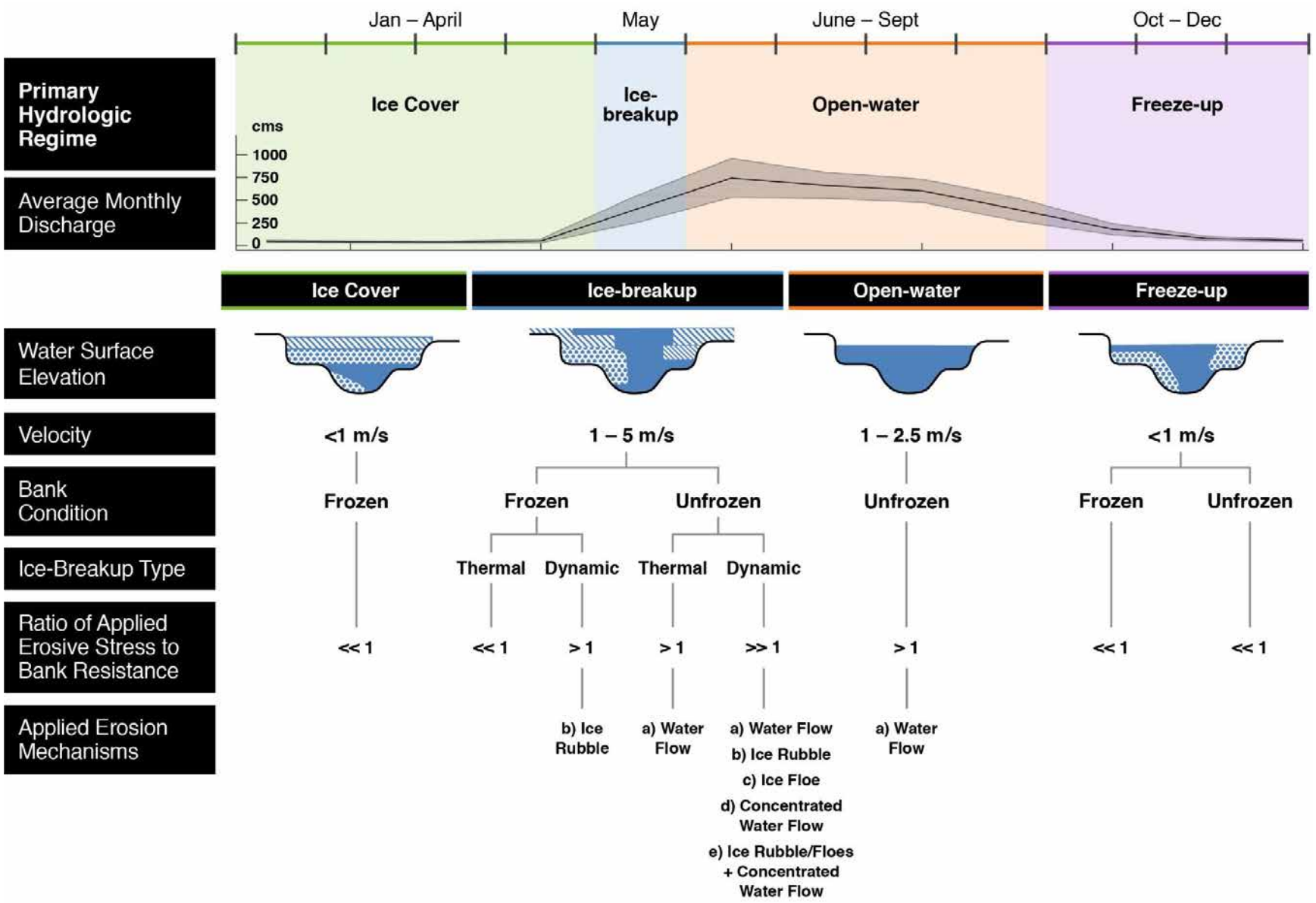

Figure 5-5. Schematic of hydrologic, hydraulic, bank conditions, and applied erosion mechanisms throughout the year.

5.1.3.1 *Water flow (during open-water regime)*

Sometime between May and June, air temperatures and flow rates rise sufficiently for ice to flush from the channel. Bank-erosion processes then are predominantly due to water flow. The open-water regime lasts for approximately 4 to 5 months before the temperatures drop sufficiently for ice to re-appear. Typically, the river begins to freeze-up around mid-October and the ice-driven regime then re-commences.

There are two primary erosive mechanisms due to water flow. The processes are differentiated by whether the shear stress at the bank toe is sufficient to mobilize the sediment grain size along the bank toe. As Thorne (1982) elaborates, significant lateral bank retreat on coarse grained rivers typically occurs when fluvial shear stress at the bank toe is sufficient to mobilize the gravel boundary material which destabilizes the protective armor layer. The following effects on a bank may ensue:

1. gravitational failure of the upper bank;
2. entrainment of all bank material (both fine-grain and lower gravel bank layers); and,
3. lateral bank retreat (shifting bank location from point 1 to point 2 in Figure 5-6)

However, for the Middle Susitna River, incipient motion calculations indicate that fluvial shear stresses (even at the 100-yr recurrence interval) are unable to mobilize the bank toe sediments at many locations that have historically eroded (Tetra Tech, 2015d). The calculations are based on results from a 2D (depth-averaged) numerical model of open-water flows along the river.

If the shear stress at the bank toe were not sufficient to mobilize the gravels and cobbles at the bank toe, then erosion via water flow could only occur when the water-surface elevation is above the basal gravel layer, and in contact with the fine-grained bank material causing “cantilever failure” (e.g., Thorne and Tovey, 1981; Church and Miles, 1982, Collins, 1990). A conceptual

erosion model of this process for the Middle Susitna River is shown in Figure 5-6. The gravel bank layer is typically protected by an armored gravel-cobble surface layer, which in many locations along the study reaches shows signs of ice paving (see Section 5.1.1 *Synthesis of Bank Observations*). When the discharge is greater than the flow required to reach the sand-gravel contact, the following erosion mechanisms may occur:

1. Where bank materials are non-cohesive (sands), flow can entrain bank material and undermine the more cohesive material (silts, clay, and root-reinforced organic material) at the top of the bank;
2. The more cohesive upper bank (due to the presence of silts and clays and "effective" cohesion provided by root reinforcement) slumps over the lower bank; and,
3. Lateral erosion occurs, but the extent of lateral bank retreat is limited due to the protective nature of the root-reinforced upper bank and immobile bank toe (bank location remains approximately around point 1 in Figure 5-6).

The cantilevered bank formation identified in Figure 5-6, at Time 3, is one of the most common bank forms along the Middle Susitna River and is presented in a series of photographs in Figure 5-1a,b (Section 5.1.1) and Figure 5-3 (Section 5.1.2). It is likely that open-water erosional processes contributed to the development of this bank form. However, it is unlikely that open-water erosional processes contribute to large-scale bank retreat. This conjecture is based on an analysis of bank retreat at surveyed cross-sections in Tetra Tech (2015b); from the comparison of 60 cross-sections surveyed in 2012 and 2013 to 2014 LiDAR topography, in which all cross-sections were subjected to a 2-year peak flow where the water-surface elevation is above the basal gravel core and adjacent to the non-cohesive bank sediments and 60 percent of the cross-sections

were subjected to a nearly 50-year peak flow that could inundate the entire bank face, only one location had identifiable, substantial erosion.

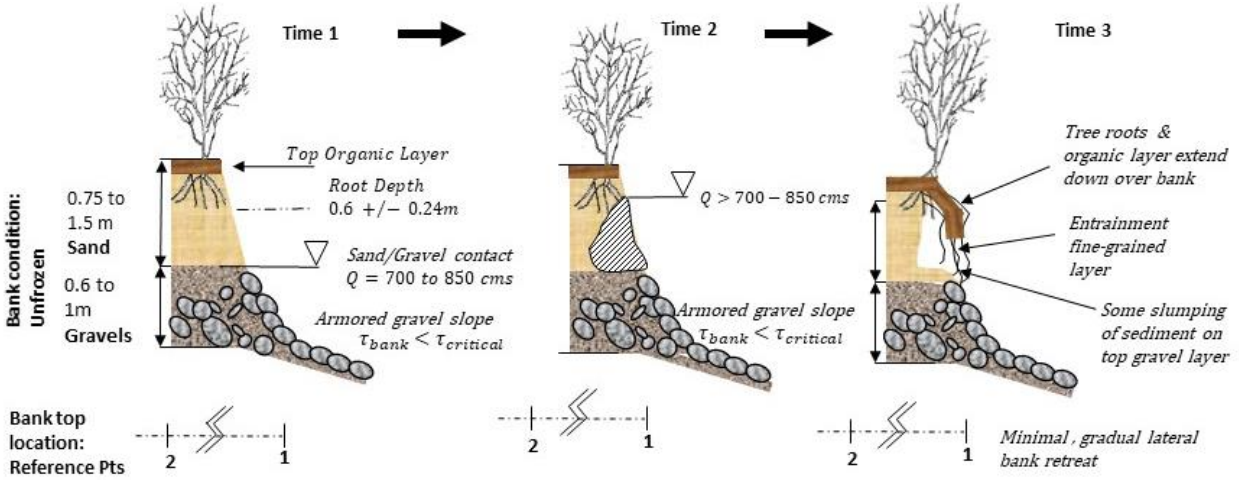

Figure 5-6. Schematic of erosion via waterflow with a stable bank toe.

5.1.3.2 *Ice-Driven Regime*

The manner whereby river ice forms and moves along the river creates additional processes that may drive bank erosion. When ice blocks accumulate or are shoved along a bank, and are directly in contact with a bank, several processes may cause large-scale bank erosion along a root-reinforced cantilever bank:

1. Ice rubble (i.e., small ice blocks typically 10m or less across) may abrade, gouge and remove the bank's protective upper layer of rootmats thereby exposing the bank to subsequent entrainment of fine grained material (Process 1) and remove the surface armor along the bank toe;
2. Ice floes (i.e., large blocks of ice ranging from greater than 10m to over 100m across) allide with banks and ride up onto low islands, bulldozing or completely removing vegetation and gouging into banks (Process 2);

3. Increased velocity of flow may disrupt and remove the armoring pavement of gravel and cobbles at the bank's toe (Process 3); and,
4. A combination ice (Processes 1 and 2) and increased or diverted water flow (Process 3) occur (Process 4).

A fifth process could disrupt the gravel and cobble pavement at the toe of a bank. The process, not directly observed during the field work, involves anchor-ice formation, which may remove gravel and cobbles, thereby exposing the bank's toe to erosion. This process is not explored further in this thesis, because insufficient observations exist of anchor ice along the Middle Susitna River. Further research is needed to investigate this process.

The first four processes are discussed and illustrated below. A caveat is that the extent of gouging of a bank may be mitigated at some locations by the formation of a shear-wall formed when stationary ice rubble flanks a bank. When a shear wall forms, moving ice rubble shears along a face of the shear wall, leaving the bank essentially untouched. A shear wall on the Middle Susitna River is shown in Figure 5-7. When the jam flushes out, remnants of the shear wall may remain, illustrating their protective effects along the bank toe. A possible remnant of a shear wall is shown in Figure 5-8.

Figure 5-7. View upstream of shear wall of ice rubble along the Middle Susitna River near RK 174. Photo was taken by HDR Alaska, Inc., on May 5, 2014.

Figure 5-8. Possible remnant shear wall and ice grounding. The shear wall acts to protect the bank toe. Photo taken by HDR Alaska, Inc. on May 10, 2012.

5.1.3.2.1 **Process 1 – Ice Rubble Gouging River Banks and Vegetation**

Removal of the protective rootmats may be possible through the shearing of ice rubble (i.e. small pieces of the ice cover) along the bank face, as shown in the conceptual model presented in Figure 5-9. If the top of bank were vegetated with exposed rootmats (Figure 5-9a), the removal of organic material may leave either a near vertical bank face that is now exposed, or a less vegetated protected bank that is more vulnerable to entrainment by subsequent flows above the gravel bank toe. Alternatively, if the top of bank were not vegetated, such that there was no protective covering rootmats (Figure 5-9b), the reduced bank resistance may increase the extent of gouging. In some instances, when ice rubble is shearing along the bank toe, there may be removal of the protective gravel-cobble surface layer.

The extent of gouging of the bank is a function of the presence of protective vegetation, ice-strength, and the speed at which ice makes contact with the bank. As shown in Figure 5-9a, where protective top-of-bank vegetation is present, it can shield the bank, limiting the amount of gouging by ice. Subsequent undermining of the bank by ice and gravitational failure of the top of bank vegetation is possible, though is likely limited in lateral extent when the bank is either frozen or unfrozen due to the effective cohesion from vegetation. Ice rubble is shoved downstream, largely tangent to banks, though gouging them when rubble gashes into portions of banks. Rubble impact may be more severe for banks at the head of an island or bar where ice rubble is conveyed directly into the bank. The greater the speed the ice makes contact with the bank, the more force is exerted and the extent of gouging.

Observations along the Middle Susitna River show flow-driven ice rubble and large floes to have sheared along river-bank faces. The result of such shearing is an exposed bank face, sometimes with the remaining root mats scarred, broken, or removed completely. When roots

remained more-or-less intact after contact with moving ice rubble, they were bent in the downstream direction, indicating the general direction of ice rubble motion. The photographs in Figure 5-10a-c show the effects of ice shear along banks of the Susitna River. Figure 5-11 shows localized gouging of a bank that left ridges or scallops in the bank, and likely occurred when the bank was frozen. Approximate magnitudes of stress exerted by ice rubble are presented in Appendix C.

In summary, Process 1 includes the following, observed consequences:

1. Ice-scarred top of-bank vegetation;
2. Removal of vegetation;
3. Gouging of bank material; and,
4. Limited lateral retreat (i.e., the bankline remains approximately at Point 1 in Figure 5-9)

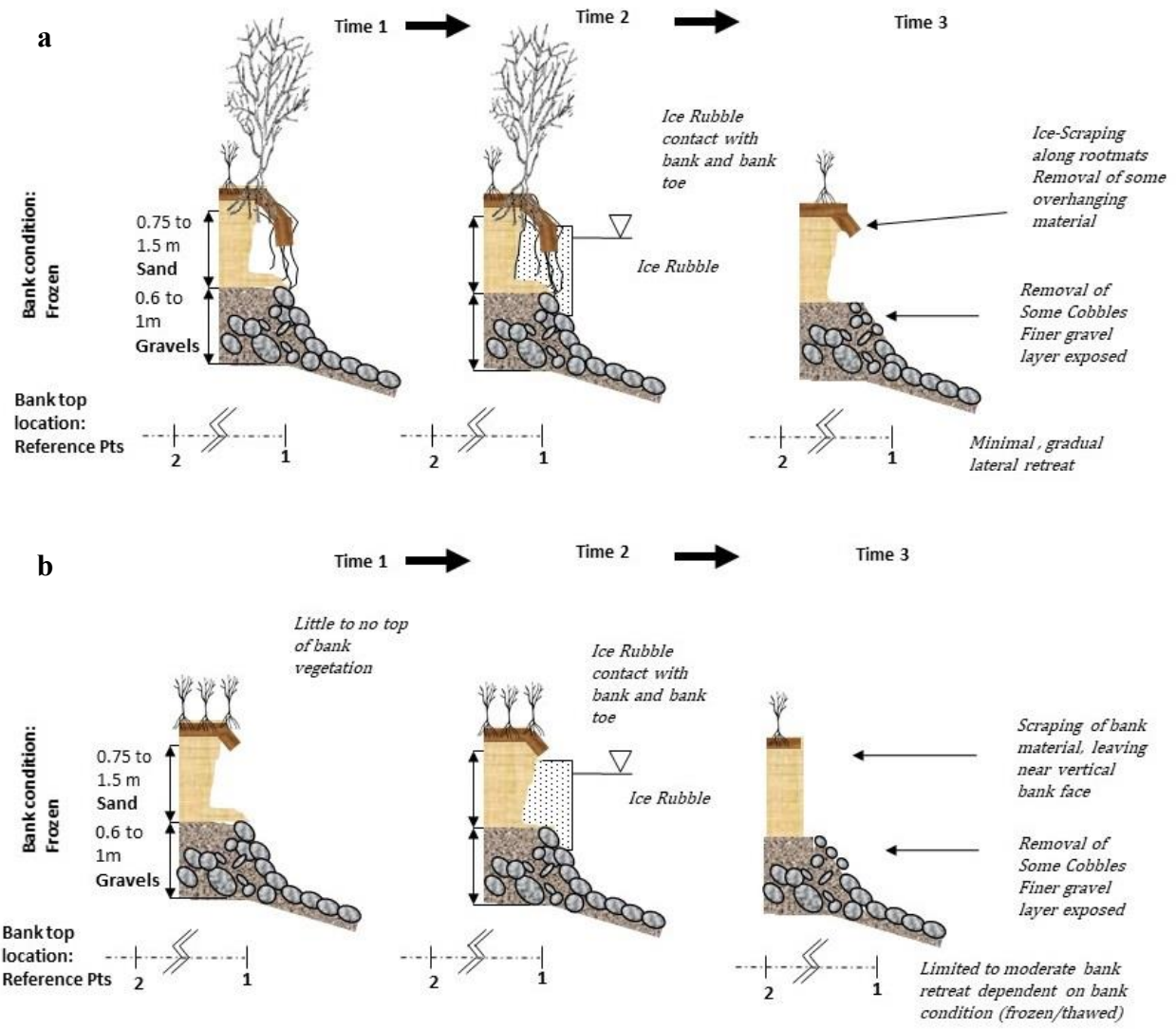

Figure 5-9. Conceptual model of ice rubble shearing along (a) a vegetated top of bank with overhanging top of bank and (b) bank with no to limited top of bank vegetation.

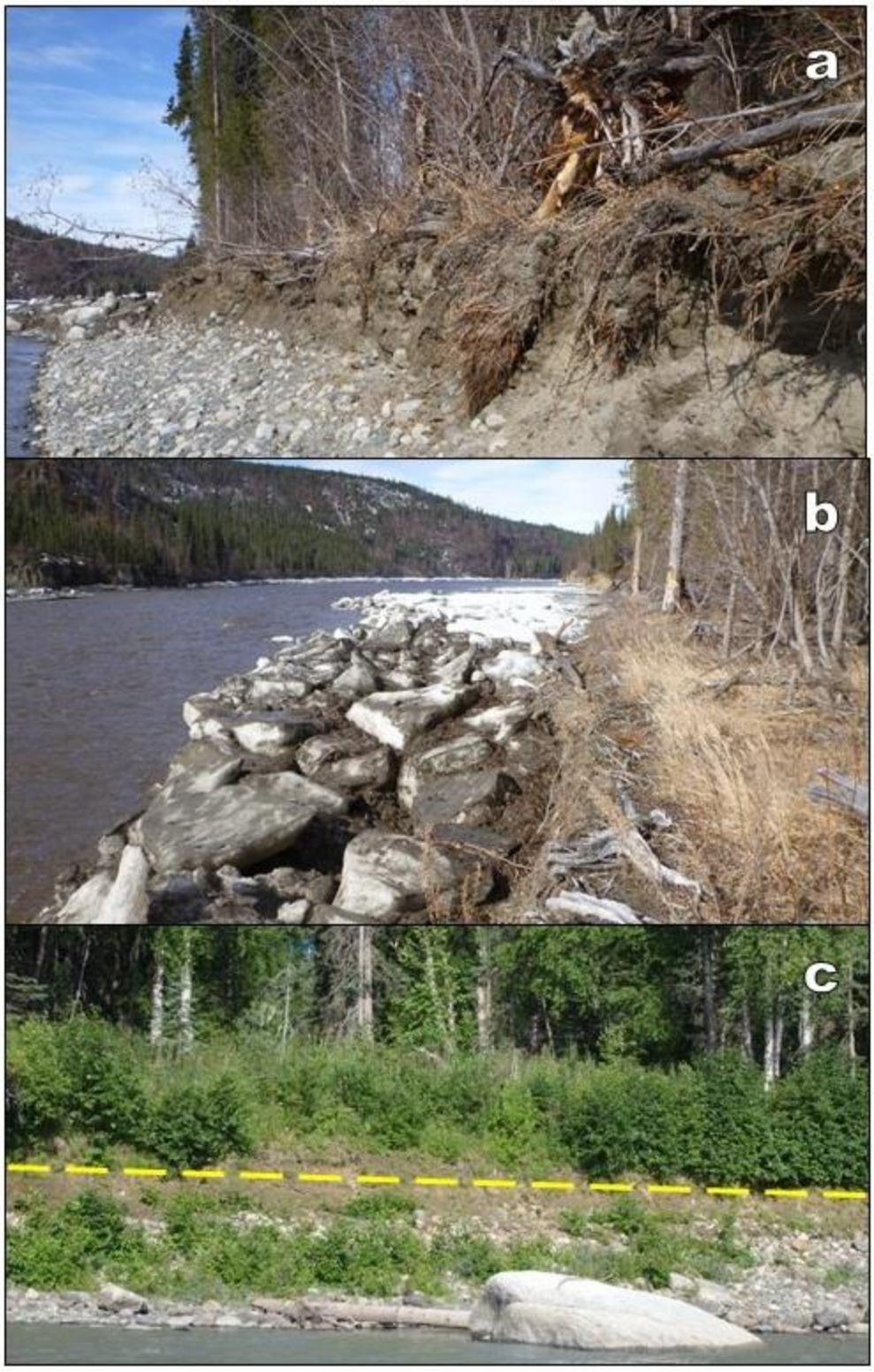

Figure 5-10. Illustrations of ice-block shearing of river banks: (a) and (b) photos taken on May 5, 2012 of ice-block shearing of a mid-channel island at RK 299; and, (c) a photo taken of sheared bank vegetation, on July 24, 2013 at RK 175.

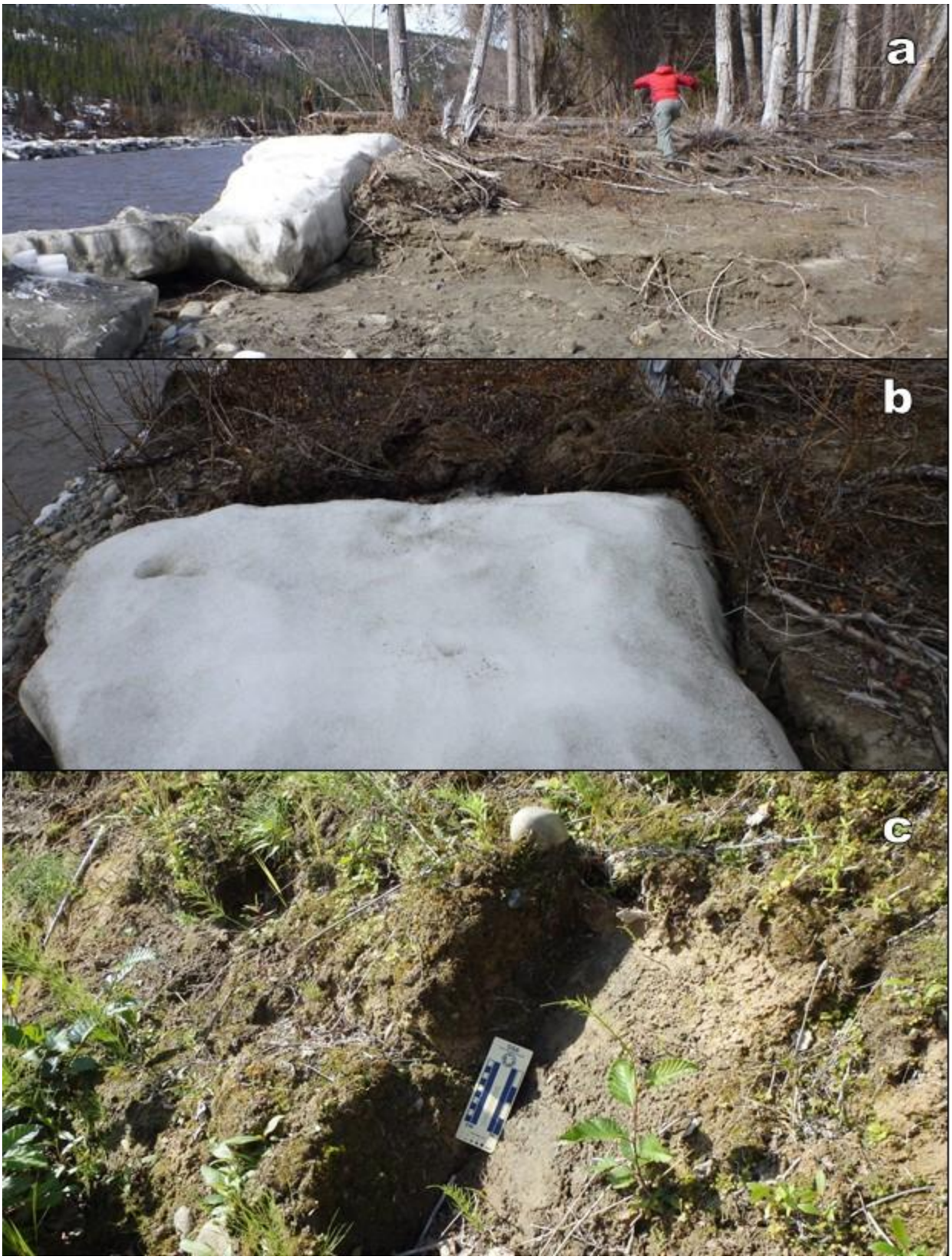

Figure 5-11. Illustrations of ice-block gouging: (a) and (b) are photos taken on May 5, 2012 of head of island at RK 299; and, (c) photo taken on July 23, 2013 of bank at RK 175.

5.1.3.2.2 **Process 2 – Ice Floes Allision of River Banks and Vegetation**

Not only can ice floes remove protective rootmats, but they can significantly shear top-of-bank vegetation. Observations show extensive clearing of vegetation by alliding ice floes; in particular, on lower geomorphic surfaces including vegetated bars and young floodplains. As shown in Figure 5-12, ice floes conveyed by moderate to high water flow are diverted onto low-lying bars thereby ice-bulldozing trees and resetting vegetation to its initial succession. While large swaths of top-of-bank vegetation are removed, some low-lying vegetation may remain or be bent over in the direction of ice floe movement. A field photograph of an ice floe alliding with overbank vegetation is presented in Figure 5-13. Ice floe impact is a function of ice strength, size, and impact velocity. Ice floes that caused minimal damage to overbank vegetation on a mid-channel island in May 2012 (during a mostly thermal ice-breakup year) are shown in Figure 5-14. It is also possible that there may be some degree of ice-ride up from ice rubble and floes along the edges of banks that protect the bank toe such that primarily only the top-of-bank vegetation is affected. Approximate magnitudes of stress exerted by ice floes are presented in Appendix C.

In summary, Process 2 includes the following, observed consequences:

1. Extensive removal of top of bank vegetation; and,
2. Limited lateral retreat (i.e., the bankline remains approximately at Point 1 in Figure 5-12)

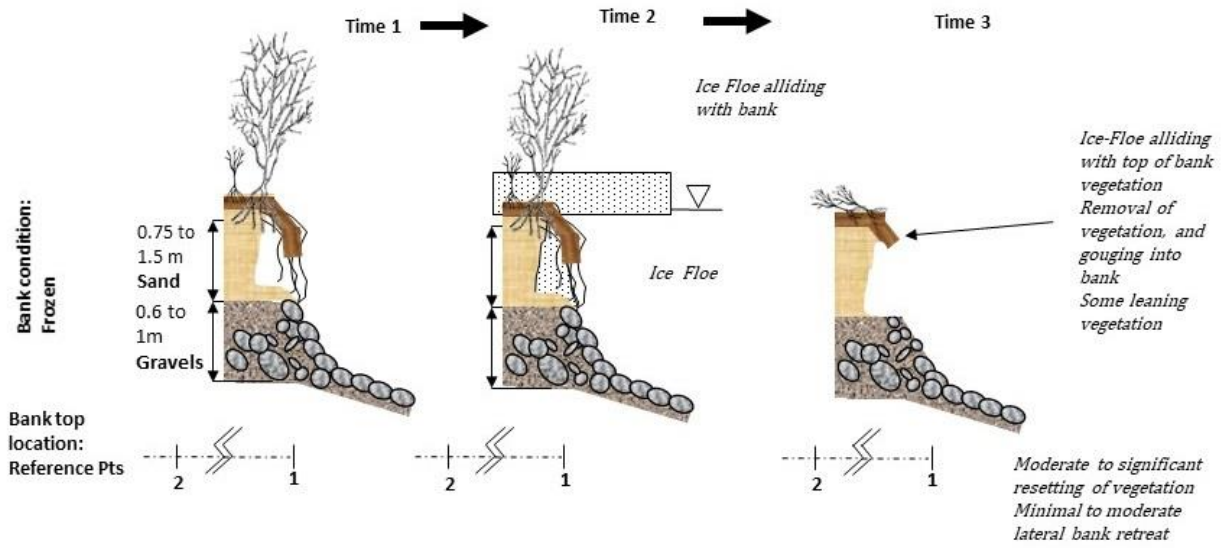

Figure 5-12. Conceptual model of ice floe alliding with bank with top of bank vegetation.

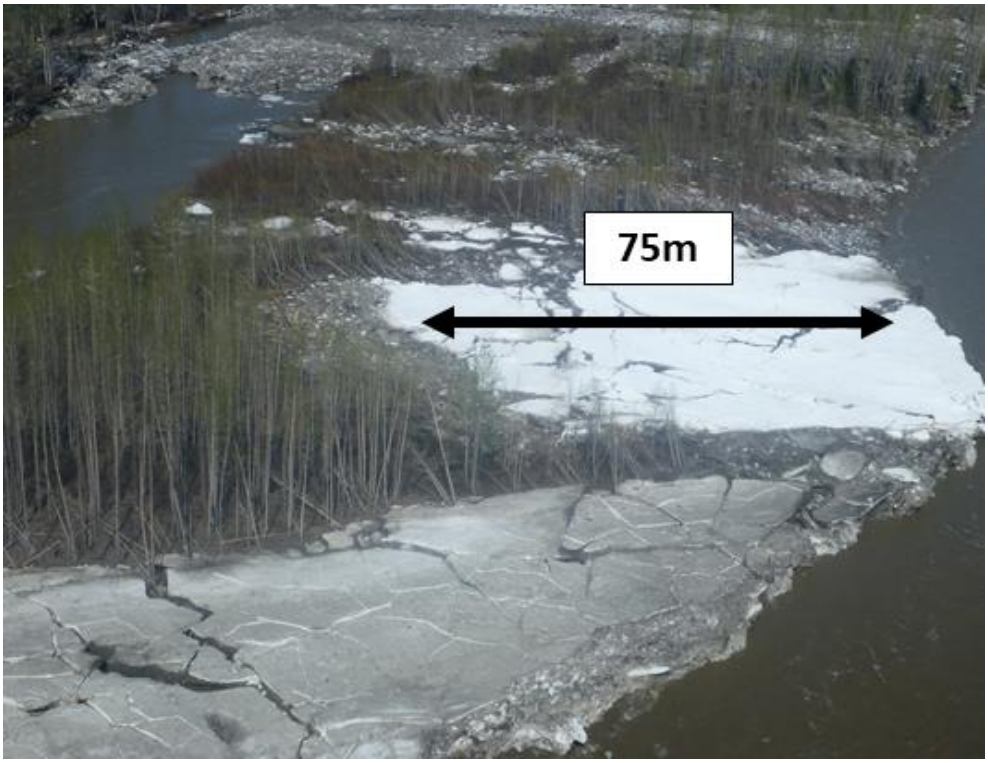

Figure 5-13. Ice floes shoved or alided with a vegetated bar in the Middle Susitna River. This photo was taken May 29, 2013 by HDR Alaska, Inc.

Figure 5-14. Ice floe ride-up on bank in May 9, 2012 causing minimal damage to overbank vegetation. Thise photo was taken by HDR Alaska, Inc.

5.1.3.2.3 **Process 3 – Increased Shear Stress**

Process 3 requires flow-induced shear stress at the base of the bank to increase such that the critical grain shear is exceeded. This process is illustrated in Figure 5-15 and has been documented on the Susitna River by R&M Consultants, Inc in the 1980s and by HDR Alaska, Inc. between 2012-2014. When ice is present, this can occur from concentration of water flow under an ice cover (HDR Alaska, Inc., 2014b), diversion of water flow from an ice jam (R&M Consultants, Inc., 1984), or from the flow surge of an ice-jam break (HDR Alaska,, 2014d). The increased shear stress probably lasts a relatively short period and therefore extensive lateral bank retreat is likely not significant. Typically, this process is limited to locations near or downstream of ice-jams. (See Section 6.1.1 for a more detailed discussion of increased shear stress from diverted water flow on the Middle Susitna River.).

In summary, the main consequences of Process 3 are as follow:

1. Mobilization of gravel and cobbles forming the bank toe pavement;
2. Entrainment of all bank material (both fine-grain and lower gravel bank layers);
3. Undercutting and failure of the vegetated top of bank; and,
4. The limited duration (during a jam) of the event results in limited lateral bank retreat.

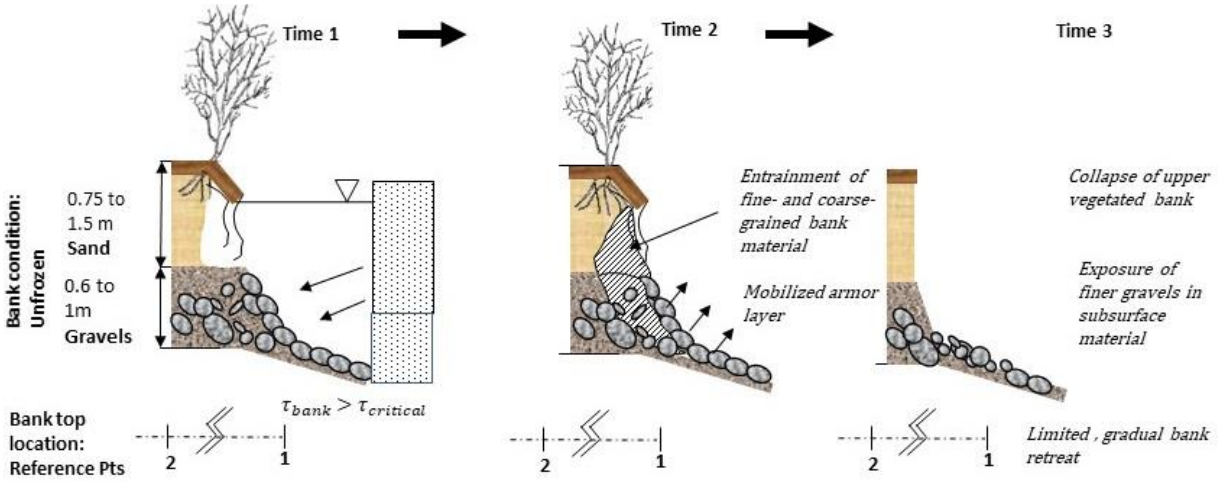

Figure 5-15. Increased shear stress due to diversion of water flow from in-channel ice (shaded blocks at Time 1).

5.1.3.2.4 **Process 4 – Ice Rubble, Floes, and Water Flow**

The combination of Process 1 (ice rubble abrasion), Process 2 (ice floe allision), and 3 (increased shear stress from water flow) result in Process 4, depicted in Figure 5-16a,b. The elevation at which portions of the ice cover are conveyed downstream, results in varying extents of bank erosion and consequent lateral retreat of a bank. Figure 5-16a illustrates the combination of ice rubble and water flow when the water level is below the bank. The overall effects observed are as follows:

1. Mobilization of gravel and cobbles forming the protective pavement at the bank toe;
2. Entrainment of all bank material (both fine-grain and lower gravel bank layers);

3. Slumping of the vegetated top of a bank or gravitational failure of the top of a weakly vegetated bank; and,
4. Moderate lateral bank retreat (from point 1 to point 2 in Figure 5-16a)

If the water surface elevation were equal to or above the floodplain height, as shown in Figure 5-16b, then ice rubble was conveyed above the bank and typically impacted trees and vegetation. The ice rubble conveyed by water flow or shoved by other rubble can push over trees and mow over lower lying vegetation, thereby removing the exposed rootmats on the bank face. When coupled with increased fluvial shear stress at the bank toe, this process can cause substantial bank erosion. Overall the main effects observed may be summarized as follow:

1. Mobilization of gravel and cobbles forming the protective pavement at the bank toe;
2. Entrainment of all bank material (both fine-grain and lower gravel bank layers);
3. Ice-bulldozed vegetation;
4. Ice gouging of bank and floodplain material; all leading to
5. Significant lateral bank retreat (from point 1 to point 3 in Figure 5-16b)

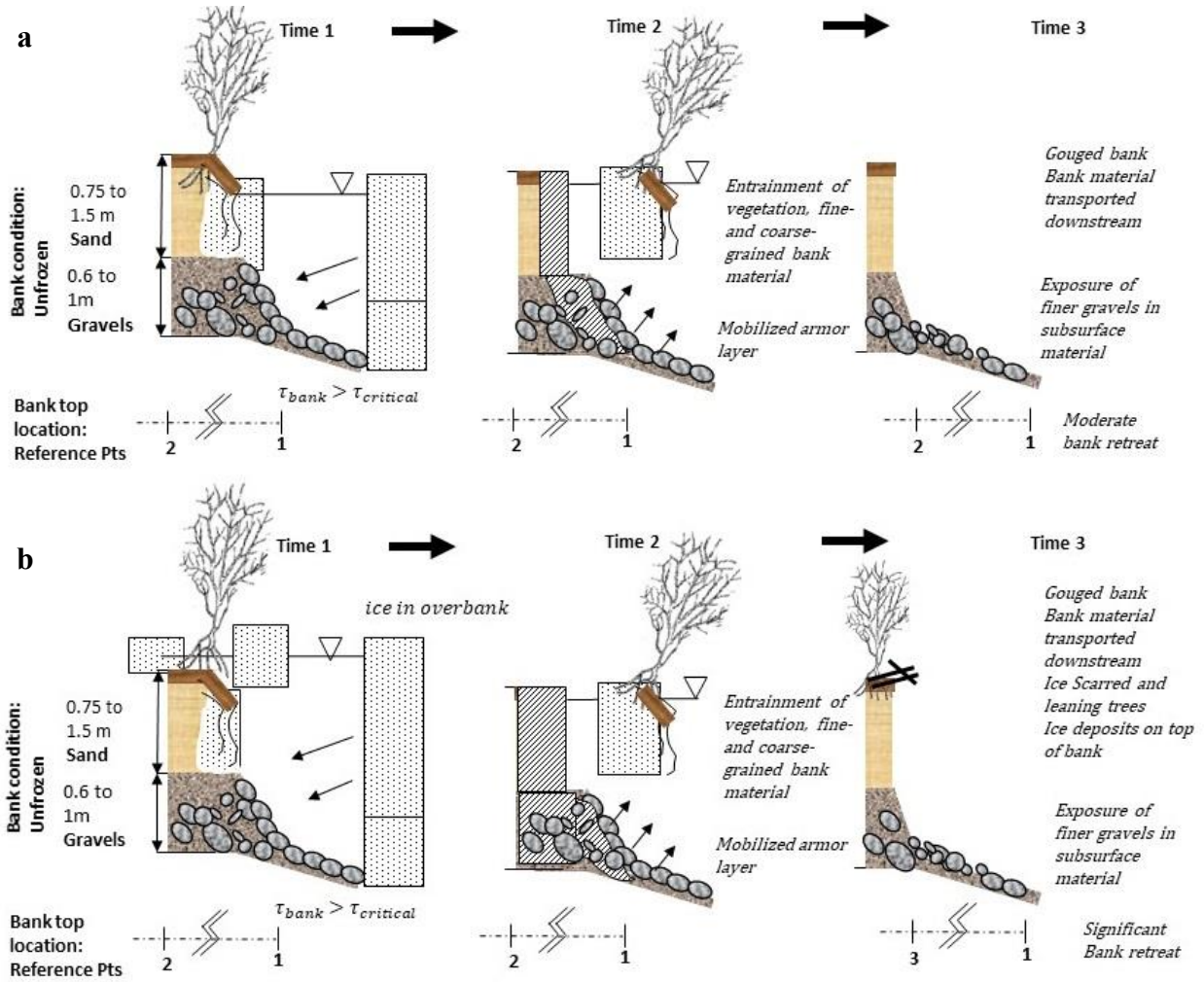

Figure 5-16. Increased shear stress at base of bank coupled with ice rubble. (a) water surface elevation is equal to or less than the bank height; (b) water surface elevation is above bank height transporting ice rubble onto floodplain surface.

Flows conveying ice rubble above a bank may cause substantial clearing of vegetation, as indeed was observed. Figure 5-17 shows a portion of the ice cover, about 100 m in length, that plowed into the overbank during rising flows in late May, 2013, knocking down trees and clearing low-lying vegetation. While tree stands composed of pole poplars were plowed over, the erosive event did not move the channel boundary or bankline.

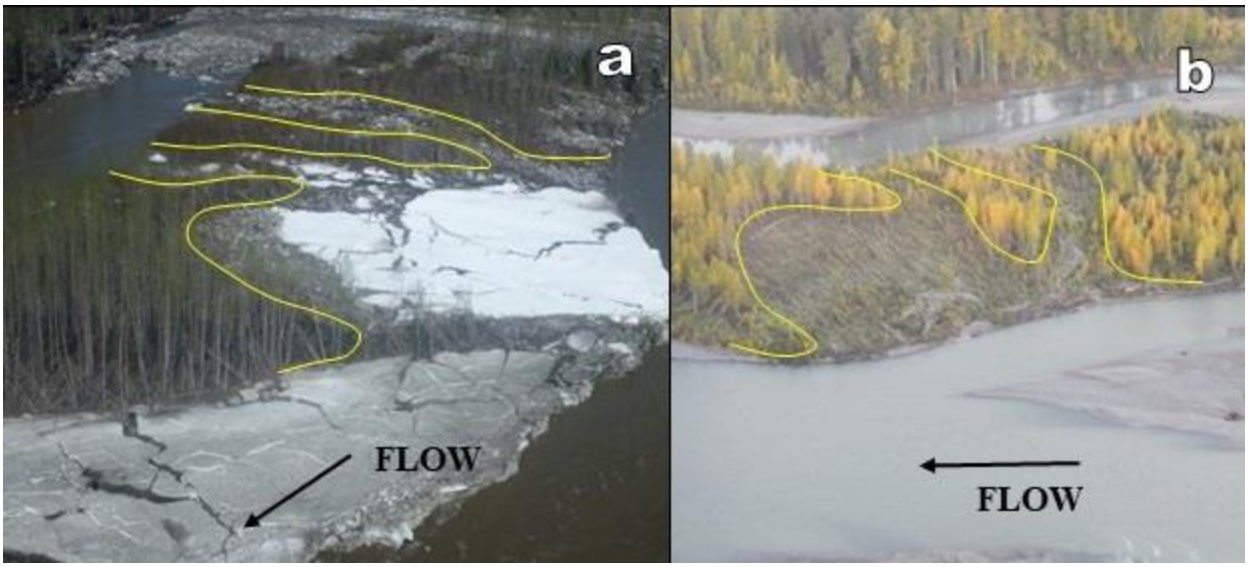

Figure 5-17. Photos of vegetation removal (yellow line delineate areas) by ice-floe impact with a low island (vegetated bar and young floodplain): (a) ice cover shearing vegetation on a mid-channel island at PRM 135.3, taken on May 29, 2013; and, (b) sheared vegetation viewed at the same location on September 19, 2013.

The erosive combination of water flow and ice rubble was observed to differ spatially along the Middle Susitna River. The combination depended on several factors:

1. The near-by occurrence of ice jamming;
2. The breakup of a major upstream ice-jam; and,
3. The magnitude of water flow, and amount and piece size of ice rubble, diverted over low islands, vegetated bars and floodplain regions.

While not captured in photographs during the present study, these processes led to high water flow and ice rubble that eroded 75 meters into the head of the island shown in Figure 5-18.

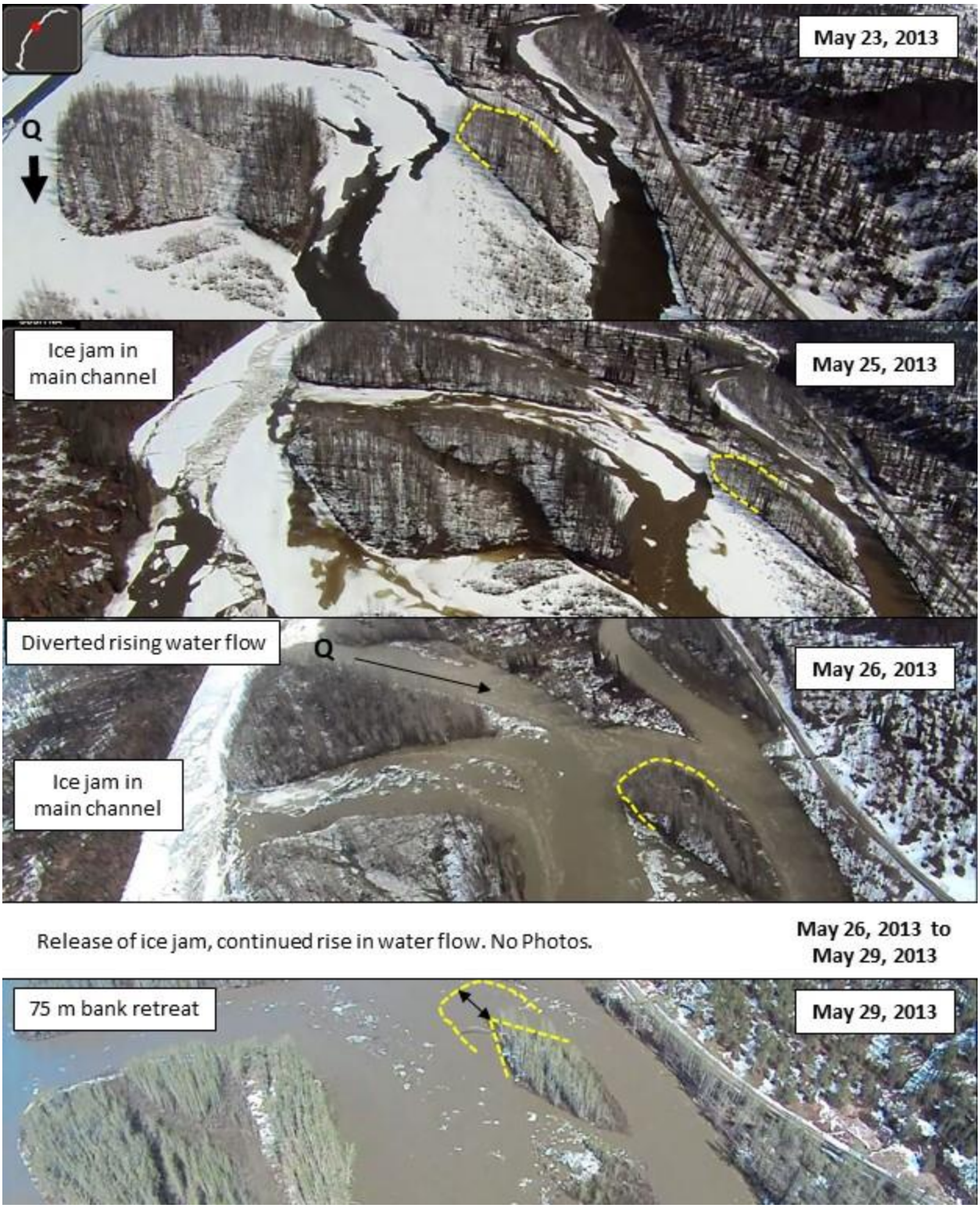

Figure 5-18. Screenshots of videos from aerial reconnaissance flight in secondary channel at RK 212 (Reach 6) during dynamic ice-breakup in May 2013.

5.2 Part 2: Erosion Analysis

5.2.1 *Sequential Aerial Photography Analysis*

Erosion data measured between the periods 2011-2012 and 2012-2013 are presented in Table 5-1. This erosion data includes areas of erosion that could definitively be categorized as eroding between the aerial photography flights. Delineation errors caused by the tree canopy or shadows (see Section 4.2.1.2) meant that some areas could not be adequately verified as actual erosion locations. However, it is possible that areas not categorized as definitive erosion, actually did erode. Nonetheless, it did reveal large-scale channel changes and provided trends of channel change over different years. Therefore, the erosion in Table 5-1, provides a lower bound for the total erosion that occurred.

Table 5-2 summarizes channel change over each one-year period by geomorphic reach. Two types of channel change are distinguished:

1. **Erosion** - i.e., conversion from vegetated bar or floodplain to un-vegetated channel. Areas categorized as eroded indicate vegetation removal and retreat of the vegetated bank line. An example of an area that eroded is presented in Figure 5-19; and,
2. **Vegetation reset** – i.e., the area of mature vegetation on a vegetated bar or floodplain that is converted to low-lying vegetation. Areas categorized as vegetation reset indicate vegetation was bulldozed or reset to its initial succession phase while the bank line location was unchanged. An example of an area that only experienced a reset of the vegetation is presented in Figure 5-20.

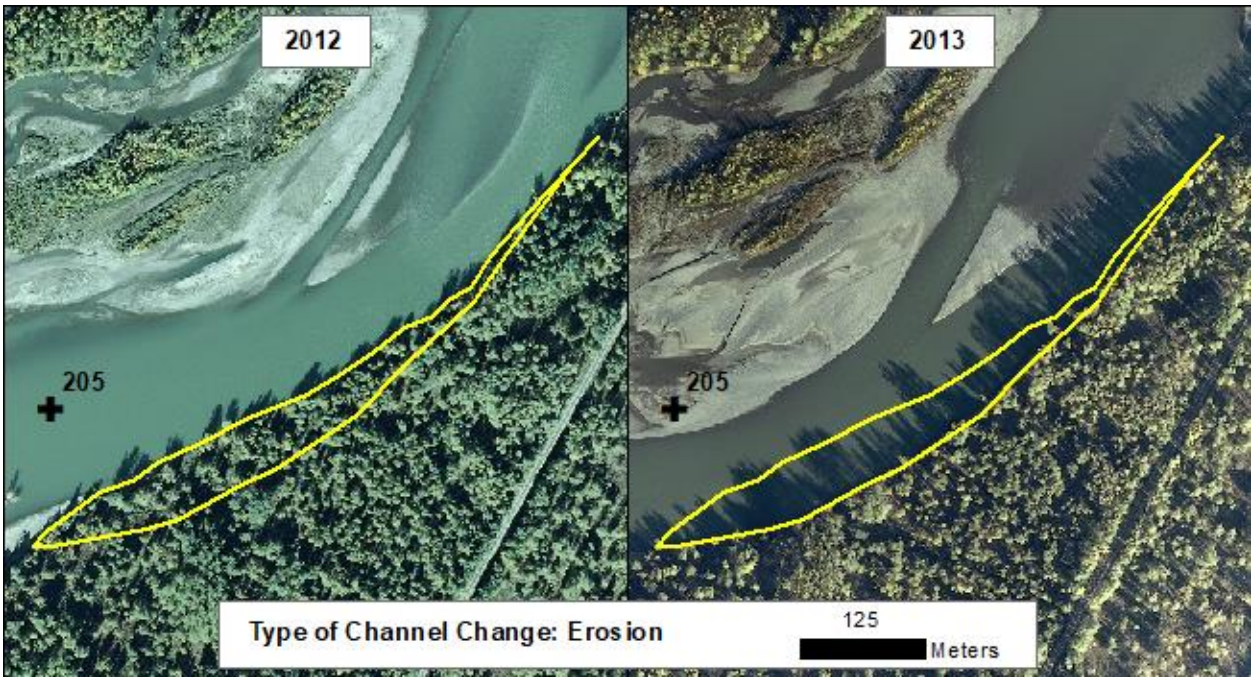

Figure 5-19. Example of channel change categorized as "erosion" at RK 205.

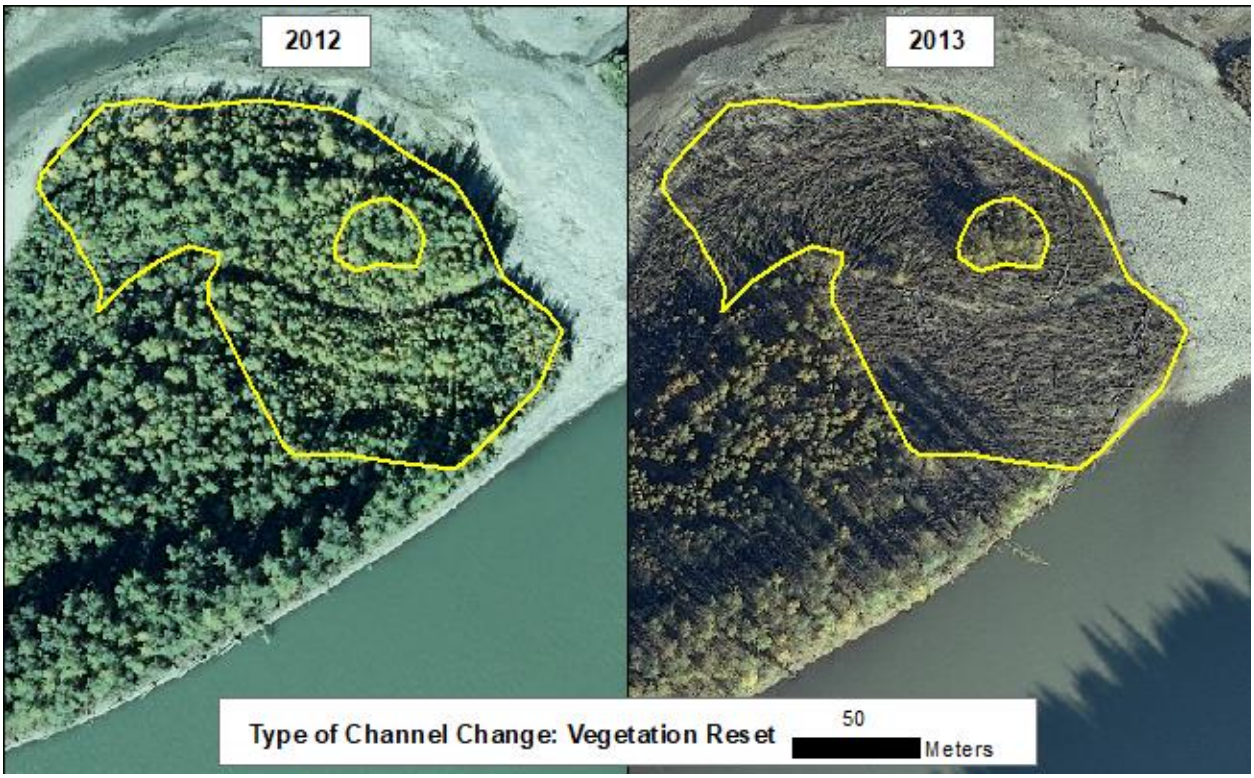

Figure 5-20. Example of channel changed categorized as "Vegetation Reset" at RK 217.

Linking eroded areas to types of geomorphic surfaces provides a means for relating erosion extent to varying degrees of bank resistance; where bank resistance is based on bank height, sediment composition and vegetation. It also provides quantifiable evidence for what geomorphic surfaces, and thereby types of bank profiles, may be more susceptible to erosion. From 2012 to 2013, 75 percent of the erosion in Reach 6 was characterized as mature-tree stands, of which 36 percent were active floodplain surfaces and 39 percent were categorized as terrace surfaces. The remaining 25 percent of eroded area was low-lying vegetation (i.e., vegetated bars). Conversely in Reach 7, about 24 percent of the erosion was characterized as mature tree stands (where 20 percent were active floodplain surfaces and 4 percent were categorized as terrace surfaces) and 76 percent were low-lying vegetation. The total amount and percent of erosion per reach categorized by geomorphic surface is presented in Figure 5-21. All of the vegetation that was reset to its initial succession state occurred on vegetated bar surfaces.

From 2011 to 2012, erosion only occurred in Reach 6. Of the eroded area, 69 percent was categorized as active floodplain while 31 percent was categorized as terrace surfaces.

Table 5-1. Total valley bottom land area, total eroded area, and erosion rates for Reaches 6 and 7 over four time periods.

Time Period	Valley Bottom Land Area (m^2)	Total Eroded Area (m^2)	Eroded Percent of Total Valley Bottom Land Area	Erosion (m^2/km)	Average Lateral Erosion per km (m)
		Reach 6			
2011-2012	14,694,600	6,500	0.04%	200	0.2
2012-2013	14,694,600	158,100	1.1%	5,700	5.7
		Reach 7			
2011-2012	9,978,800	0	0.0%	0	0.0
2012-2013	9,978,800	33,900	0.3%	1,400	1.4

Note:
1. All values are rounded to the nearest hundred
2. Valley Bottom Land Area is determined from the 2012 land area for both 2011-2012 and 2012-2013.
3. Data sources for valley bottom land area can be found within Tetra Tech (2014f)

Table 5-2. Area of erosion and vegetation removal for two one-year periods.

Type of Channel Change	Type of Ice Breakup Year	
	Thermal (2011-2012)	Dynamic (2012-2013)
	Reach 6	
Erosion (m^2)	6,500	158,100
Vegetation Reset (m^2)	0	141,000
	Reach 7	
Erosion (m^2)	0	33,900
Vegetation Reset (m^2)	0	0

Note: All values are rounded to the nearest hundred

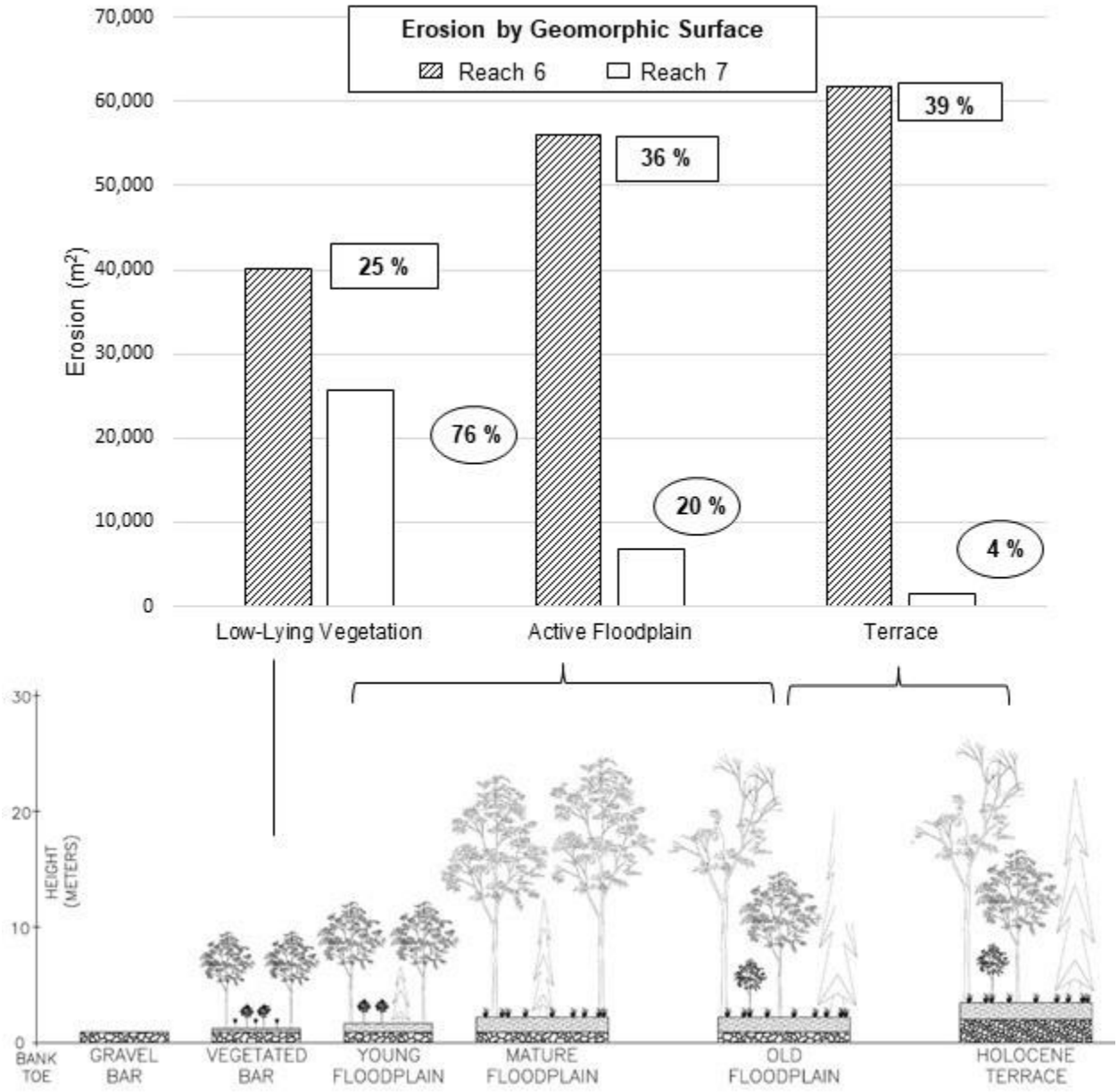

Figure 5-21. Total erosion between 2012-2013 by geomorphic surface for Reach 6 and 7.

5.2.2 *Identification of Primary Hydrologic Regime of Erosion*

Identification of the primary hydrologic regime for the measured erosion was subdivided by each one-year sequential analysis. Only four locations eroded between 2011 and 2012, whereas 63 locations eroded between 2012 and 2013. Each erosion area is shown in a series of maps in Section 5.2.2.1 (2011 through 2012) and Section 5.2.2.2 (2012 through 2013) and colored according to the respective time period of erosion.

5.2.2.1 *2011 through 2012: Thermal Ice-Breakup*

From 2011-2012, no large-scale bank erosion and retreat occurred in Reach 7. Only four locations of erosion and retreat were identified in Reach 6. The locations that experienced bank retreat were along the sides of mid-channel islands or bank-attached floodplain units. Bank retreat did not exceed 10 m. Due to the nature of channel change, the time period for the identified erosion could not be distinguished from the reconnaissance videos or photographs. The locations of erosion between 2011 through 2012 are shown in Figure 5-22.

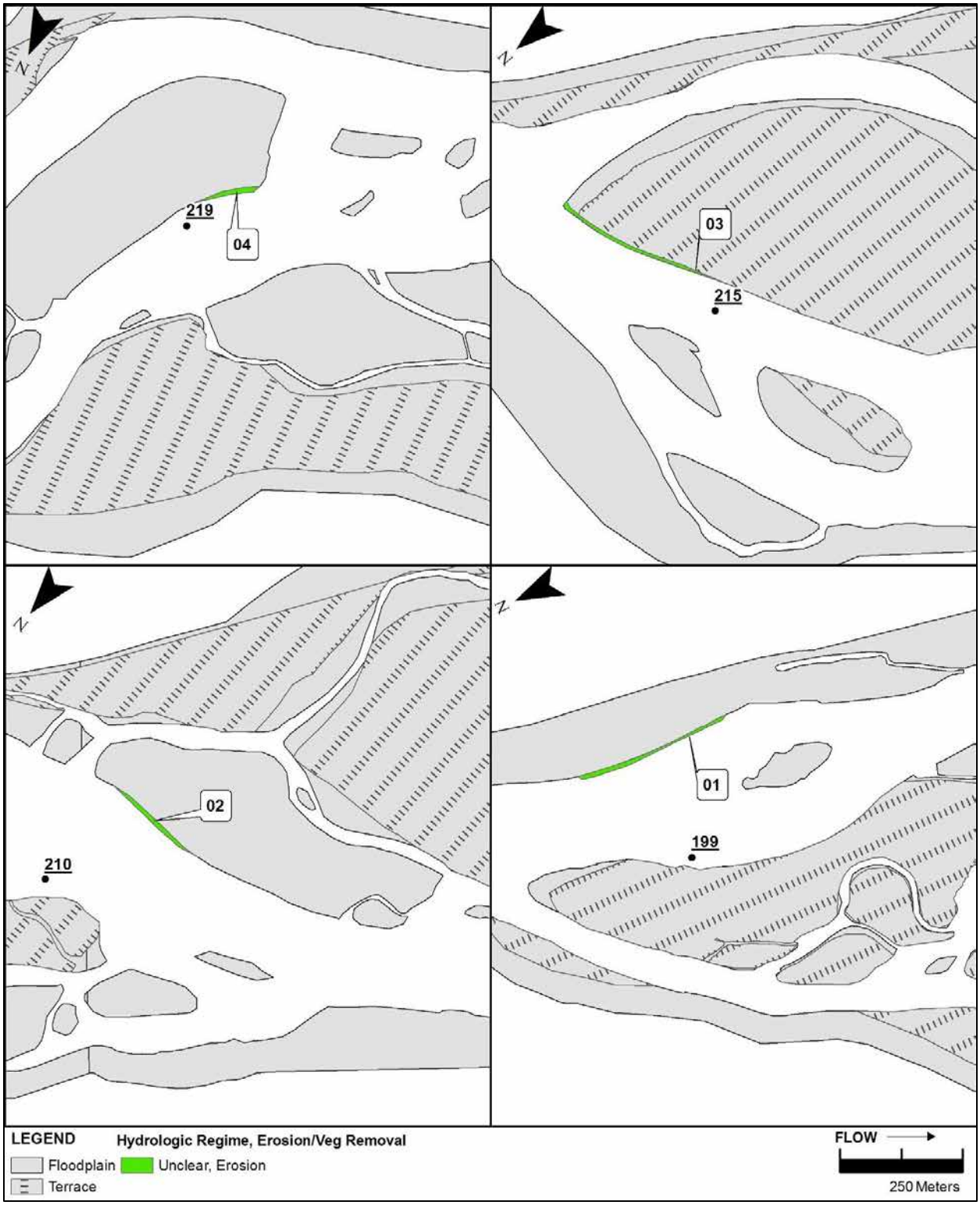

Figure 5-22. Erosion locations (green) between 2011 to 2012 in Reach 6, categorized by primary hydrologic regime. The timing of erosion for all erosion locations was unclear.

5.2.2.2 *2012 through 2013: Dynamic Ice-Breakup*

Table 5-3 summarizes the timing and likely erosion regime (i.e. fluvial or ice-related) for the total extent of erosion occurring between 2012 and 2013. Examples for categorizing erosion into particular hydrologic regimes are presented in a series of figures described below. Erosion locations are first shown in 2012 and 2013 aerial photographs, followed by screenshots of the locations taken from the aerial reconnaissance flight videos. Figure 5-23 and Figure 5-24 provide an example for categorizing an erosion location as "fall through pre-freezeup (Fluvial).". Figure 5-25 and Figure 5-26 provide an example for categorizing an erosion location as "ice-breakup (Ice/Fluvial)". Figure 5-27 through Figure 5-29 provide an example for categorizing an erosion location as "Ice-breakup through Fall (Ice/Fluvial)".

Each area of erosion is illustrated in Figure 5-30 through Figure 5-32 for Reach 6. Areas of erosion are illustrated in Figure 5-33 and Figure 5-34 for Reach 7. The maps include a numeric identifier for each location of erosion by Reach. Reach 6 has identifiers, labeled 1 through 50, and Reach 7 has identifiers labeled 1 through 13. Areas of erosion are colored according to the time period of erosion: "fall through pre-freezeup" is illustrated using a solid blue, "ice-breakup" is illustrated using a solid red, "ice-breakup through fall" is illustrated using a solid purple, and "unclear" is illustrated using a solid green. Mature vegetated land features that converted to low-lying vegetation (i.e. vegetation reset) are illustrated using a hashed fill. As conversion of mature vegetated land features to low-lying vegetation only occurred during the ice-breakup period, the hash is colored red.

Table 5-3. Total Erosion from 2012-2013 (dynamic ice breakup year) categorized by time period of erosion.

Time, Regime (Duration of Period)	Reach 6	Reach 7
	Percent of Total Erosion from 2012-2013	
Fall through Pre-freezeup, (~30 days)	3%	0%
Ice Breakup, Ice/Fluvial, (~5 days)	41%	7%
Ice Breakup Through Fall, Ice/Fluvial (~150 days)	20%	46%
Unclear	36%	46%

For both reaches, the majority of erosion can be described as ice-driven. Approximately one-third of erosion for Reach 6, and approximately one-half of erosion for Reach 7, were unable to be attributed to a particular time period and associated hydrologic regime. In Reach 6, only 3 percent of the eroded area (corresponding to one location; Location No. 29) could be attributed solely to fluvial processes (i.e., occurring pre-freeze up during the open-water season). Given the hydrologic record during the fall of 2012 prior to freezeup, it is likely that this bank eroded during the nearly 20-year flow event in late September. In Reach 7, no areas of erosion could be attributed solely to fluvial processes.

In Reach 6, about 40 percent of the erosion occurred in the ice-breakup window (May 25, 2013 – May 29, 2013). Another 20 percent, categorized as "Ice-breakup through fall", occurred sometime between the onset of ice-break up (May 25, 2013) and when the next imagery set was flown (September 2013). These locations were categorized within this larger time frame because the reconnaissance videos and photographs did not provide sufficient evidence that the location eroded during a specific event (i.e., only during breakup). Some of the videos taken during ice breakup viewed the locations via oblique angles of observation, thus hampering definitive categorization of erosion during ice breakup. Additionally, erosion at these locations was likely exacerbated by the subsequent high-flow event (nearly 50-year event) following breakup.

However, review of the videos and photographs indicated that, for many of the locations that eroded during the ice-breakup to fall period, erosion was likely initiated during ice-breakup; this included erosion location numbers 17, 18, 19, and 20 as shown in Figure 5-27. This conclusion was determined based on the aerial flight images and on-the-ground photographs (Figure 5-29) whereby trees were significantly ice-scarred and leaning over, and lateral bank retreat was significant, ranging from 10 to 30 m.

In Reach 7, about 7 percent of the eroded area occurred during ice breakup. As the nature of erosion at most locations within Reach 7 involved the shearing of floodplain material from along the side of mid-channel islands or bank attached floodplain units, rather than significant bank retreat from the head of an island (as was the case for many erosion locations in Reach 6), it was often difficult to discern when the erosion occurred. Nearly half of the erosion was categorized within the "Ice breakup through fall" period. Like Reach 6, many of these locations appeared to start eroding during ice-breakup, evidenced by adjacent ice-jams and ice-rubble moving across the erosion locations, but its exact timing was unclear.

Figure 5-23. Erosion Location No. 29 in 2012 and 2013 aerial photographs. Note the shape of the bankline change from a convex to a concave shape.

Figure 5-24. Screenshot of Reach 6 Erosion Location 29 from aerial reconnaissance video flown October 26, 2012 during freeze-up. Yellow dash line identifies bankline that is concave in shape. This location is categorized as eroding during the fall through pre-freezeup time period (i.e., fluvial erosion processes).

Figure 5-25. Erosion Location No. 22a (low-lying vegetation), No. 22b (mature vegetation), and No. 23 in 2012 and 2013 aerial photography.

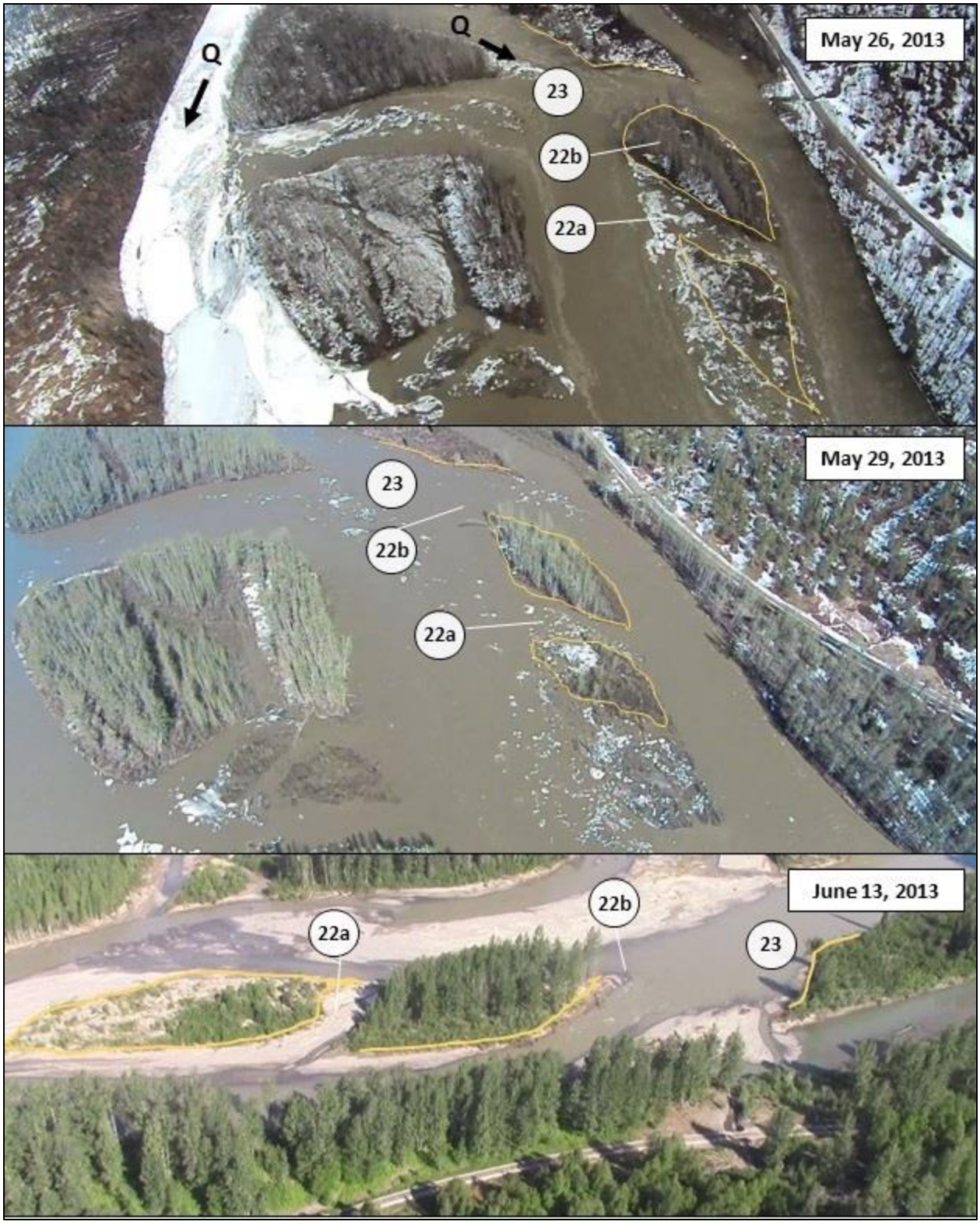

Figure 5-26. Screenshot of Reach 6 Erosion Locations No. 22 and 23 taken during ice-breakup (May 26 and May 29) and post high open-water flow (June 13). All locations were categorized as eroding during the ice-breakup period (i.e., ice/fluvial erosion processes).

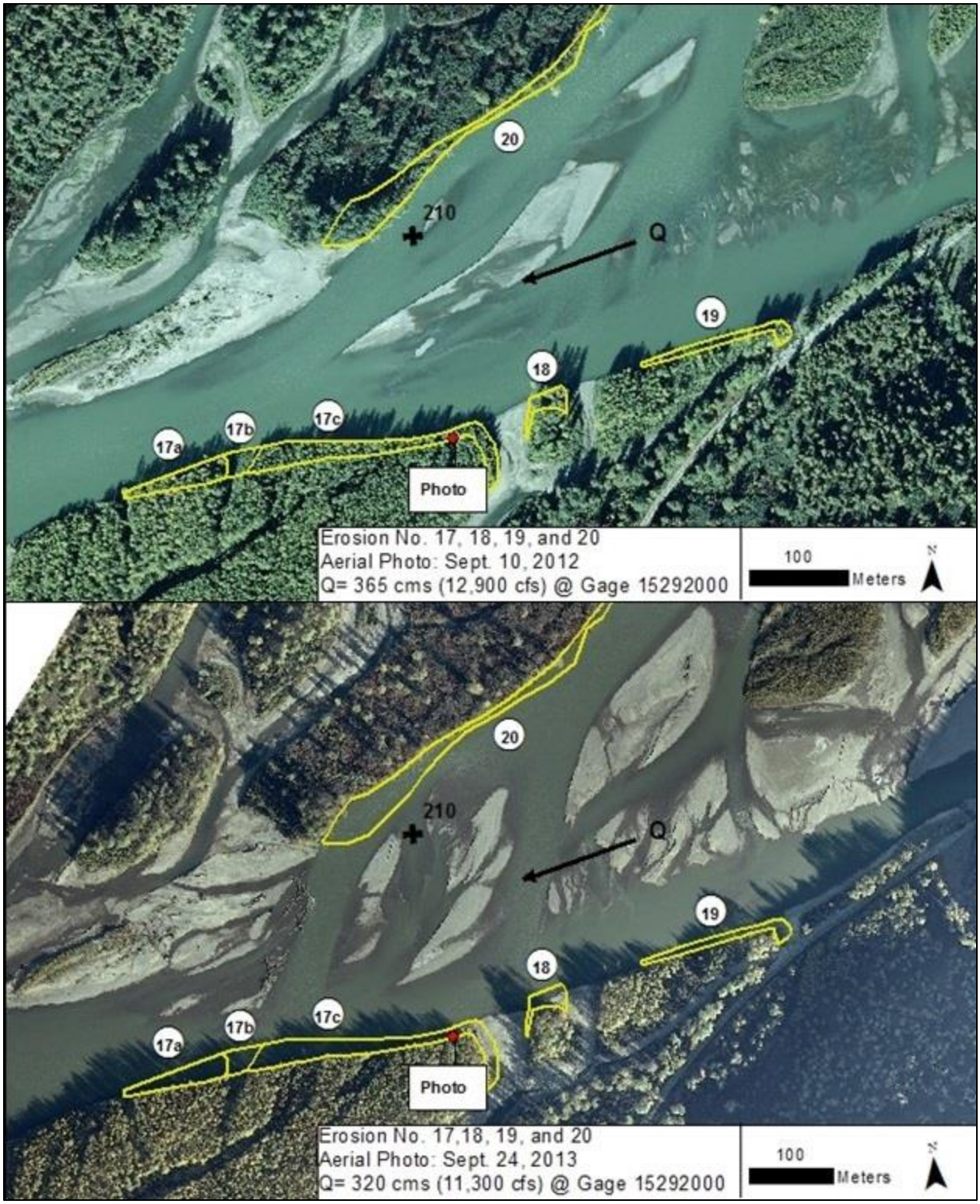

Figure 5-27. Reach 6, Erosion Location No. 17 through No. 20, in 2012 and 2013 aerial photography.

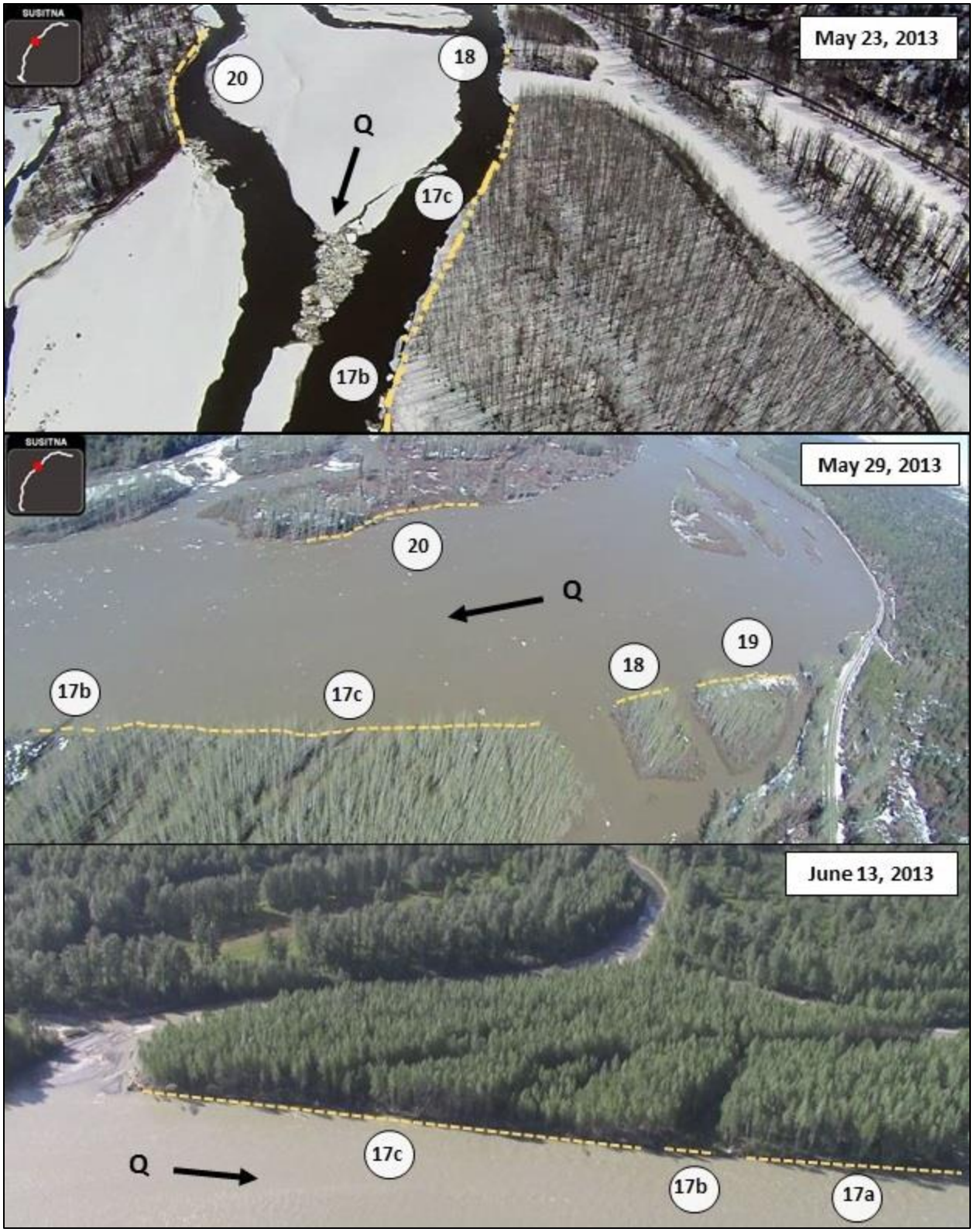

Figure 5-28. Screenshot of Erosion Locations. No. 17-20 from aerial reconnaissance videos taken during ice-breakup (May 23 and May 29) and post high open-water flow (June 13). Locations categorized as eroding during the ice-breakup through open-water period (i.e., ice/fluvial erosive processes).

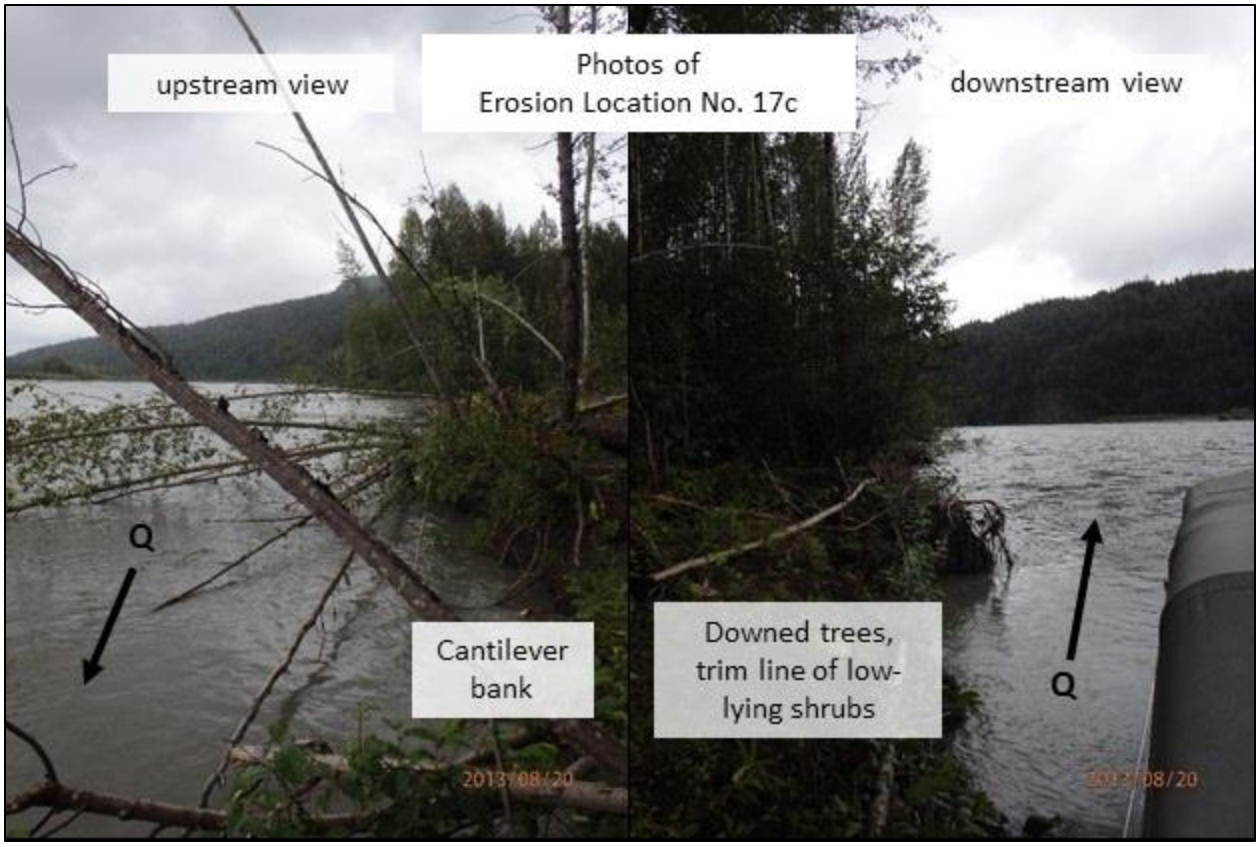

Figure 5-29. Ground observations of Erosion Location No. 17c. Location noted as "Photo" in aerial view of area in Figure 5-27.

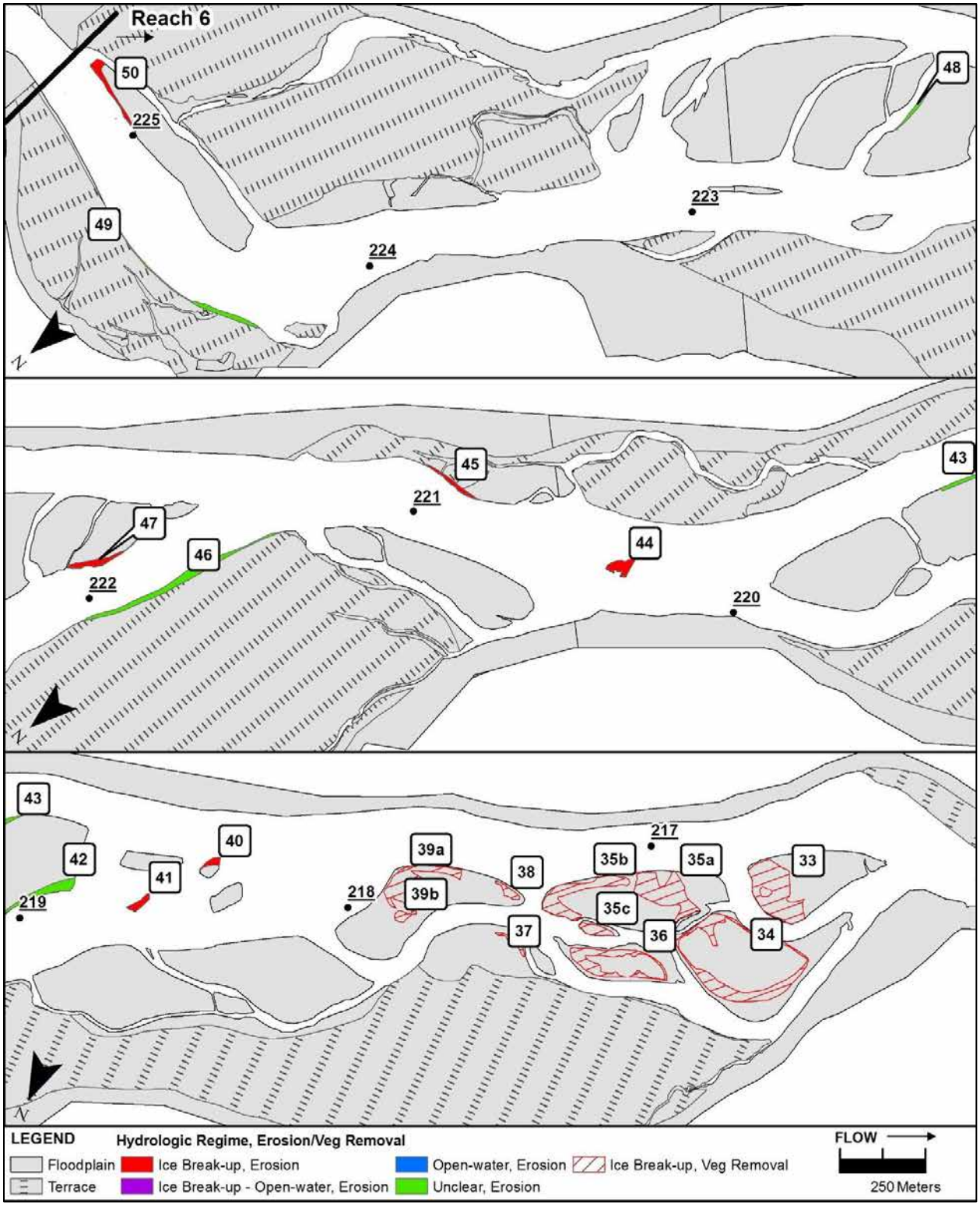

Figure 5-30. Erosion locations and vegetation removal/reset between 2012 to 2013 for Reach 6 RK 225 to RK 216, categorized in terms of primary hydrologic regime (the various colors).

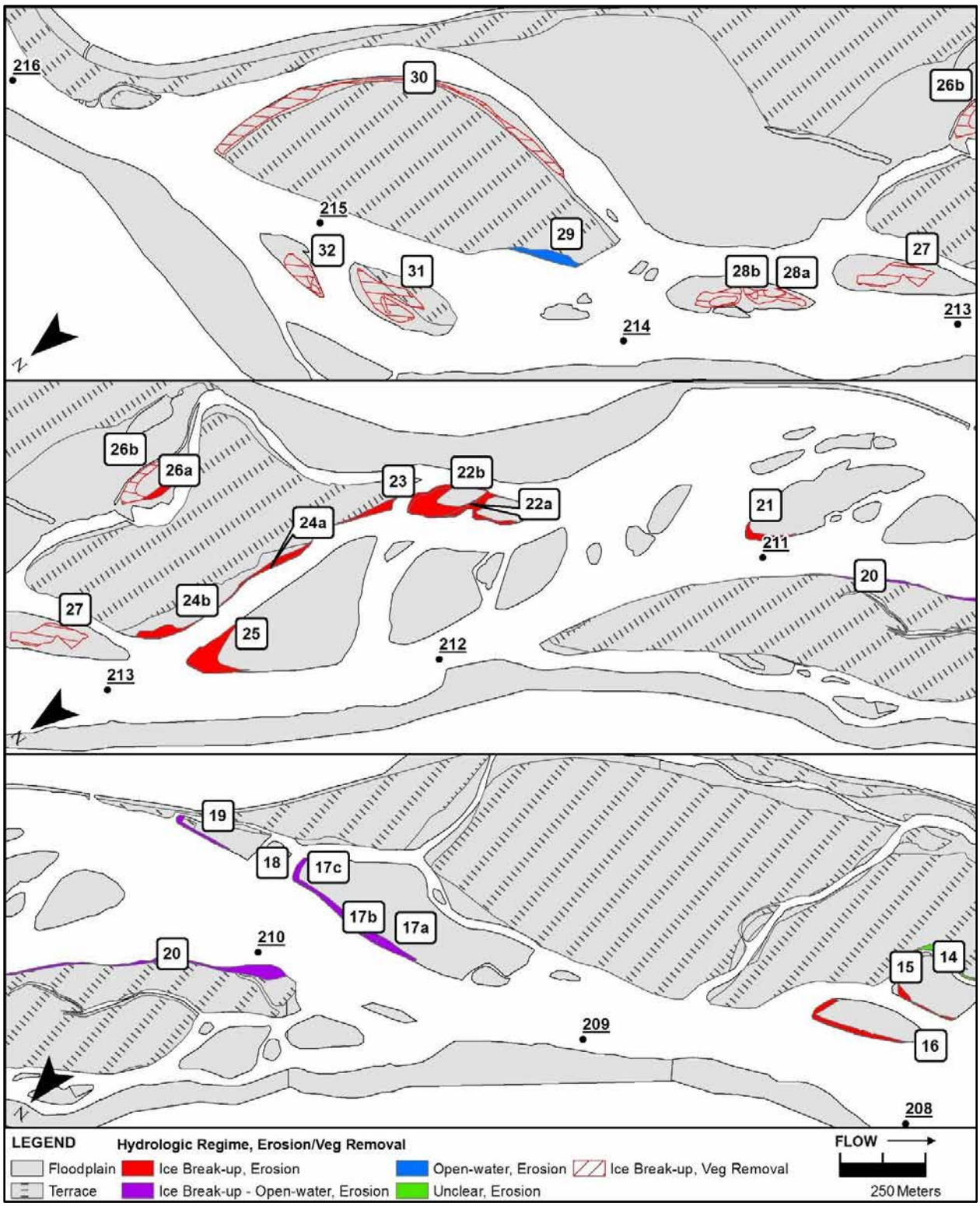

Figure 5-31. Erosion locations and vegetation removal/reset between 2012 to 2013 for Reach 6 RK 216 through RK 208, categorized in terms of primary hydrologic regime.

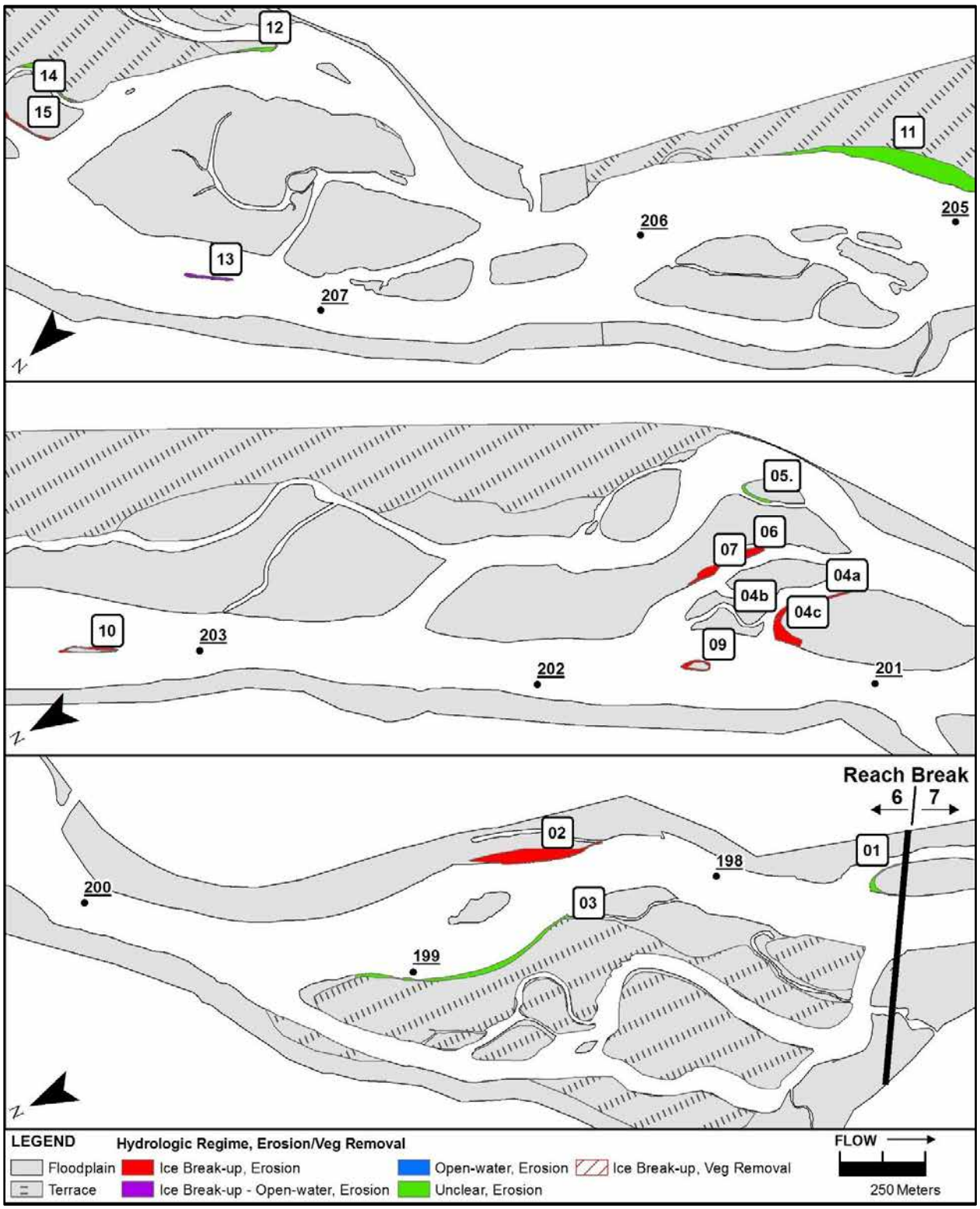

Figure 5-32. Erosion locations and vegetation removal/reset between 2012 to 2013 for Reach 6 RK 208 through RK 19, categorized in terms of primary hydrologic regime.

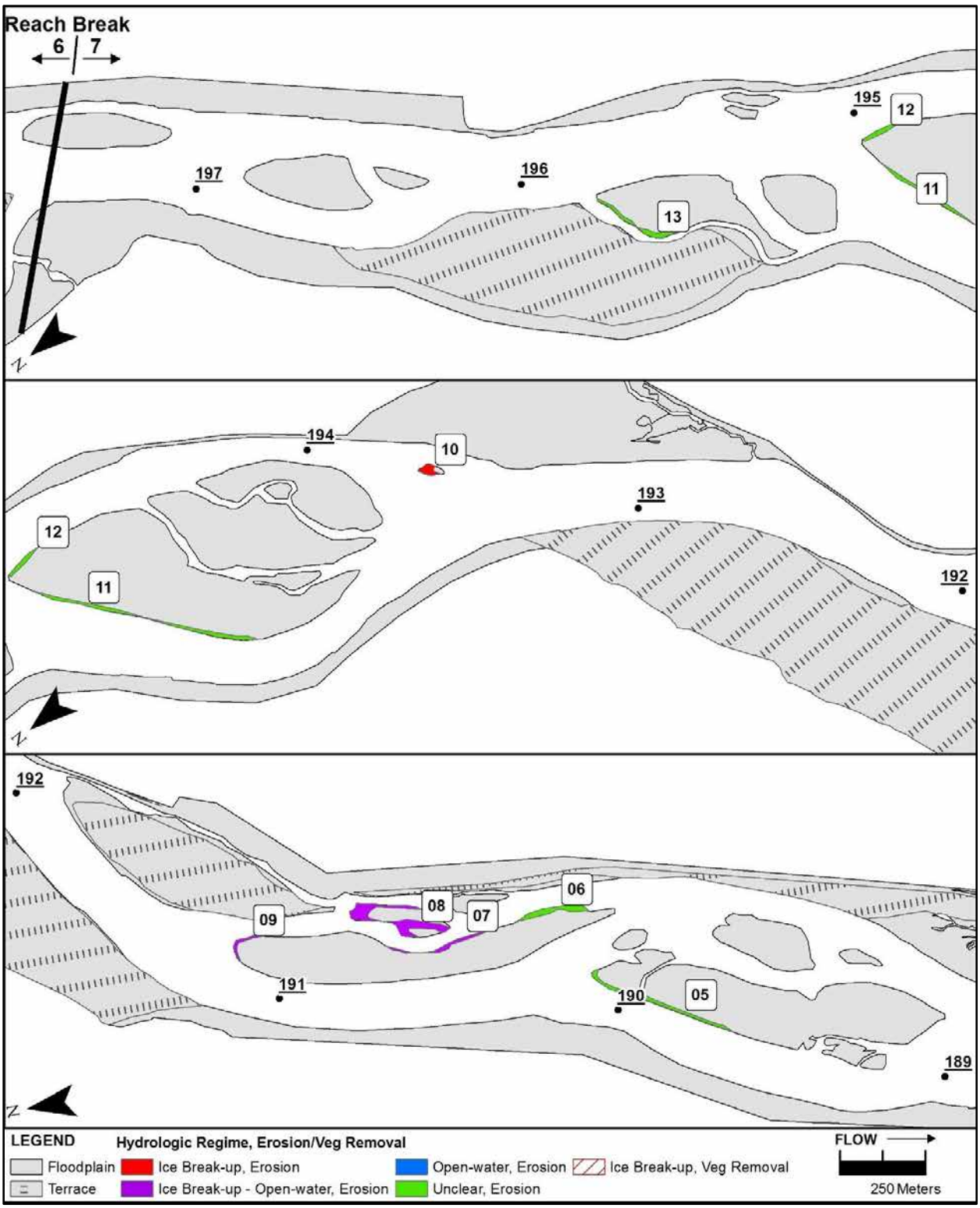

Figure 5-33. Erosion locations and vegetation removal/reset between 2012 to 2013 for Reach 7 RK 197 through RK 189, categorized in terms of primary hydrologic regime.

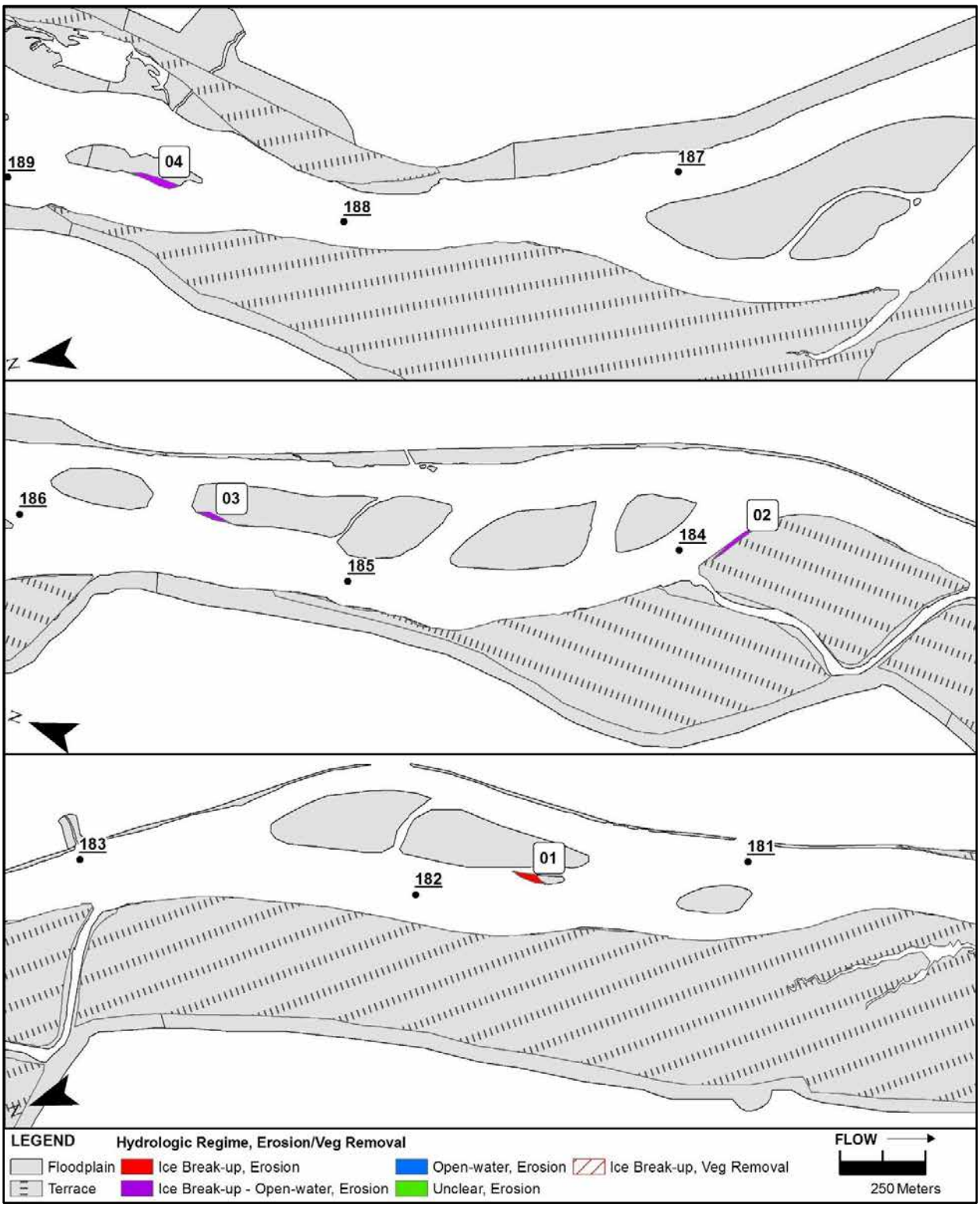

Figure 5-34. Erosion locations and vegetation removal/reset between 2012 to 2013 for Reach 7 RK 189 through RK 180, categorized in terms of primary hydrologic regime.

5.2.3 *Dominant Erosive Processes*

Overall, a majority of erosion in the two geomorphic reaches (61 percent of erosion in Reach 6 and 53 percent of erosion in Reach 7), and all vegetation scour, occurred predominantly during ice breakup or during both ice breakup and the open-water regime immediately after ice breakup. Thus, the dominant erosive processes were present during the ice-driven hydrologic regime (Section 5.1.3).

The extent of lateral bank retreat ranged from 10 m to 75 m, and up to 700 m in the streamwise direction. The aerial reconnaissance videos indicate that relatively large ice floes floating above the active floodplain height were responsible for clearing large swaths of trees on mid-channel islands and bank adjacent floodplains (see Appendix B for aerial images of each erosion location during ice-break up). Low-lying vegetated bars and younger floodplains in the main channel experienced significant bull-dozing by both ice rubble and ice floes. Bulldozing also occurred on vegetated bars and active floodplain units in secondary channels. The erosion areas in secondary channels coincided with main channel ice jams that diverted water into the multi-channel complex formed of low islands and bank-attached floodplain units. The extent of erosion on active floodplain surfaces in secondary channels indicates that ice-blocks were likely necessary to bulldoze the heavily vegetated surfaces. Signs of ice-scared trees and mowed over vegetation are apparent in the reconnaissance videos flown June 13 after ice-breakup. It appears that a large amount of erosion that occurred during the ice-breakup period occurred sometime on or after May 26, when large ice jams were known to have collapsed on the rising limb of a near 50-yr open water peak flow.

To investigate the erosive potential of ice-rubble and ice floes flowing into or adjacent to banks (Processes 1 and 2), the stress associated with ice-blocks alliding into banks were estimated.

The results are summarized in the following sub-section (Section 5.2.1.1). Shear stresses were easily high enough to move the gravel and cobbles that paved and armored the bank toe. Small ice blocks may be responsible for local gouging but limited lateral bank retreat. Large ice floes are capable of causing high stresses on banks, and are more likely to cause significant bank erosion.

Given that there was a nearly 20-yr flow event following the 2012 aerial photography, yet only 3 percent of the erosion of Reach 6 and no erosion in Reach 7 was attributed to open water erosion between 2012-2013, large open-water peak events appear to be incapable of driving significant large-scale bank retreat. It is likely that many locations that were classified as eroding during the time period, "unclear," actually eroded from a mix of ice and fluvial processes during ice breakup. This conclusion is corroborated by previous incipient motion analyses of the gravel and cobble channel bed and bank toe (Tetra Tech, 2015d).

However, the role of ice in increasing flow-induced shear stress (Process 3) is presently unknown. To explore this process, a 2D numerical model simulating fluvial shear stresses from diversion of main channel flow (due to hypothetical ice-jams) was run over a series of ice-breakup discharges. The goal was to identify if the diversion of main channel flow (without ice) into both a wide and narrow secondary channel would be capable of mobilizing the bank toe. The results are summarized in Section 5.2.1.2. While, diversion of water flow alone did not mobilize the bank toe at locations known to have eroded, insights into the degradation and aggradation nature of ice-jam induced flooding, emerged. The 2D modeling is elaborated in Appendix D, while modeling results are elaborated in Section 5.2.1.2 below.

5.2.3.1 *Numerical Investigation of Impacting Ice Rubble and Floes*

As described in Section 5.2.1, the impact of ice rubble and floes on against and over the bank caused significant gouging of banks, shearing of vegetation, and lateral bank erosion. This

process was well-documented in site visit photographs (see Appendix B), but had not yet been quantified. A numerical investigation into the approximation of possible impact stresses exerted by ice rubble and ice floes was performed for sizes typical of the Middle Susitna River. The investigation is elaborated in Appendix C; a summary of the results from the analysis follow.

The impact stress of a small ice block (i.e. less than 10 m across) is high enough to entrain large cobbles (e.g. greater than 100 Pa when moving at 1 m/s), shear cohesive bank material, or gouge into a bank. However, the stress is often comparable to or less than the resistant strength of tree-root reinforced bank soil (i.e. less than 12 KPa). If the ice block impacts a root-reinforced bank, roots may fail at smaller contact areas, leading to localized erosion, but may not fail at larger contact areas. Additionally, the presence of ice rubble may create shear-walls (Figure 5-7) that in turn protect the bank from significant gouging or lateral retreat.

In contrast to ice rubble impact, typical ice floes (e.g. 100 m^3 and greater), moving at 3 m/s or more, well exceed resistant strengths of tree-root reinforced bank soil, and are much more capable of large-scale clearing of vegetation and bank erosion (shown in Figure 6-2). Small and medium size ice floes shoved or allided into and on top of banks were observed in many field photographs during ice-breakup (Appendix B) and are more likely to cause moderate to significant bank erosion.

The upper limit of force impact by an ice floe upon a bank force is the force required to break the ice floe. Most ice blocks and floes were observed to be mostly intact during ice-breakup but contained flexural failure ridges. This observation indicates that the contact stress between the ice floe was less than crushing strength of river ice at the time of ice-cover breakup (say, about 1,000 kPa), but reached the horizontal stress limit for an ice floe that failed in flexure (e.g. 300 to 500 kPa).

5.2.3.2 *Numerical Investigation of Ice-Induced Diversion of Water Flow*

The erosion analysis in Part 2 (Section 5.2) identified a combination of ice and fluvial processes responsible for the majority of large-scale erosion. Screenshots taken from the aerial reconnaissance flight videos (Appendix B) indicate many locations that eroded during ice breakup, or between ice-breakup and fall, were adjacent to main channel ice-jams. Therefore, these bank sites were subject to ice-induced diversion of flow, and concentration of rising water flow into secondary channels.

Though previous numerical modeling on the Susitna River indicated fluvial shear stresses were unable to mobilize the bank toe, at even the highest open-water flows (Tetra Tech, 2015d), the consequences of an increase in shear stresses associated with ice-induced concentration or diversion of flow had not yet been investigated.

This study evaluated the increase in fluvial shear stress resulting from concentration of flow diverted by an ice jam (Ice-Driven Regime Process 3, Section 5.1.3.2.3). The analysis evaluated fluvial shear stress only. No ice-modeling was performed as part of this analysis. Open-water hydraulic modeling was performed using a 2D depth-averaged numerical model for two different geometric scenarios:

1. Blockage in the main channel whereby flow is diverted into a wide secondary channel; and,
2. Blockage in the main channel whereby flow is diverted into a narrow secondary channel.

The methods, results, and discussion for this analysis are provided in Appendix D. The primary insights from the analyses are presented below.

While shear stress at known erosion locations between 2012 to 2013 increased due to the concentration of flow diverted at lower flows, compared to higher open-water flows, it was still

not sufficient to mobilize the sediment grain size at the bank toe. This finding indicates that the diversion of water flow alone is likely not sufficient to cause significant lateral bank retreat. It certainly is possible that increased discharge could cause erosion at or above the gravel/sand interface. It is also important to note that some, though few, locations that eroded between 2012 to 2013, did have shear stress at the bank toe greater than the critical threshold to mobilize the bank toe material; these locations were upstream of a constriction (17a and 17b in Figure D-3).

Shear stress maps of each modeling scenario compared to existing conditions revealed trends of locations that were more or less prone to erosion. Diversion of flow into both the wide and secondary channels resulted in overtopping of the adjacent floodplain surface. As expected, the magnitude of overtopping was more pronounced for the flow diversion into the narrow secondary channel. In both scenarios increased shear stresses were observed at two types of locations while decreased shear stress was observed at one. The main trends are as follow:

1. In existing secondary channels, the increased shear stress is sufficient to mobilize the channel bed material,
2. Increased shear stress at the downstream end of depressions or overflow channels on the floodplain surface; and,
3. Decreased shear stress upstream of the ice jam owing to a local reduction in water surface slope.

Each of these locations are labeled with a numeric identifier (i.e. 1, 2, or 3) in the shear stress difference mapping in Figure 5-36. Shear stress difference mapping for the range of modeled flows is included in Appendix D. Note there is fluctuation of shear stress values in the wide secondary channel, just upstream of the convergence of another small channel; this is illustrated in Figure

5-35 and Figure 5-36. This pattern could be due to model instability or it could be instability due to near-critical flow conditions.

.

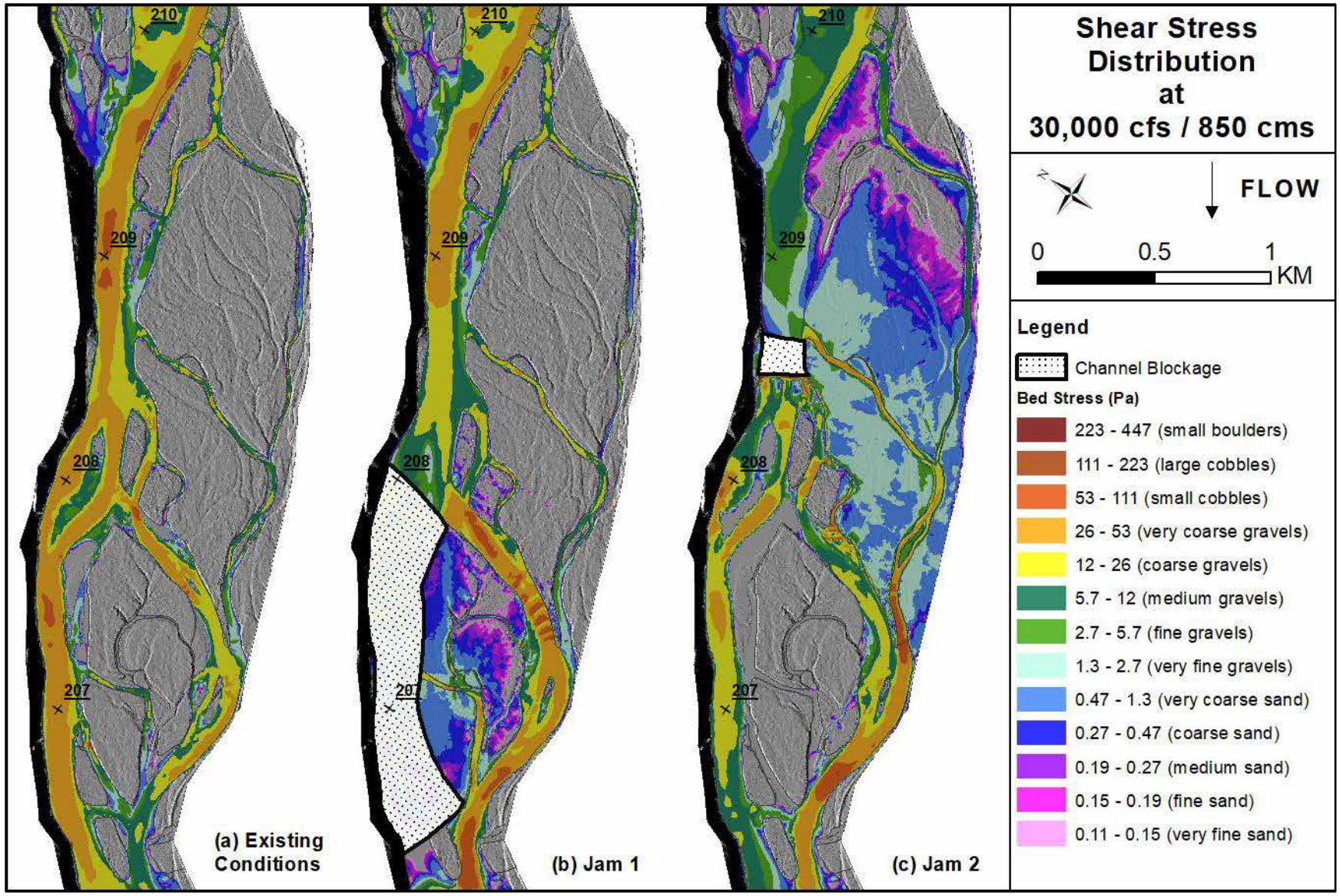

Figure 5-35. Shear stress difference mapping for two scenarios of flow diversion into secondary channels compared to existing condition.

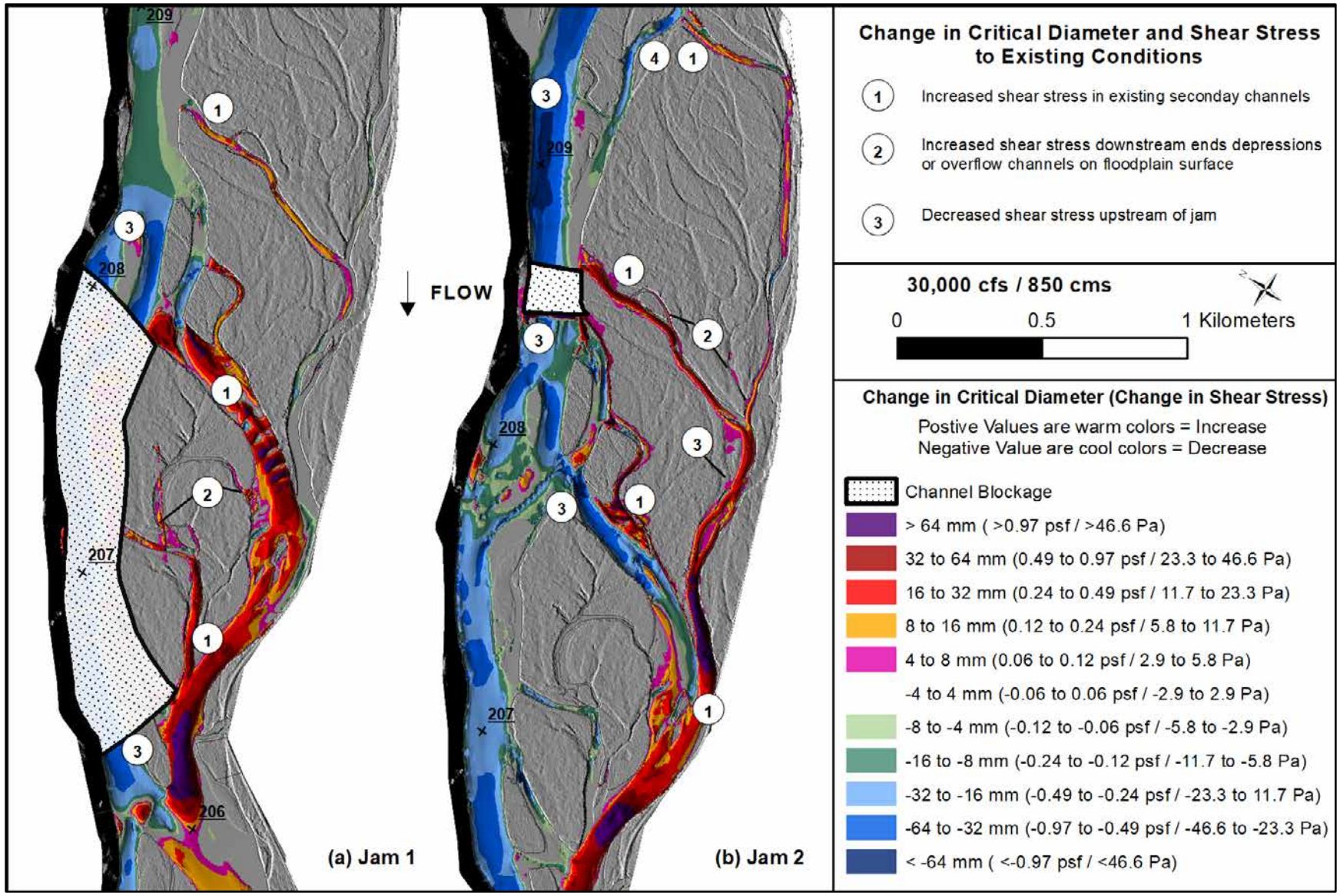

Figure 5-36. Change in critical diameter and shear stress from two channel blockages compared to existing conditions.

5.3 Part 3: Comparison of Erosion Rates

5.3.1 *Synthesis of Historical Erosion*

To visually identify locations of bank erosion that occurred since 1951, and to assess reach-wide erosion trends, the historical erosion locations and locations of actively eroding banks were mapped for Reaches 6 and 7. The maps are presented in Figure 5-37 through Figure 5-39. Historical erosion locations were derived from channel-turnover data summarized in Tetra Tech (2014f). The turnover data identify long-term changes in channel and floodplain (i.e., vegetated land units) between three sets of aerial photography flown in 1951, 1983, and 2012. In Figure 5-37 through Figure 5-39, the areas that converted from channel to land (owing to sediment aggradation and vegetation establishment) between 1951 and 1983 are colored dark green, whereas areas of conversion between 1983 and 2012 are colored light green. Similarly, areas that converted from land to channel (due to bank erosion) between 1951 and 1983 are colored dark blue, whereas erosion areas between 1983 and 2012 are colored light blue. Actively eroding banks were identified in the field during the summer of 2013 and are noted as bold black lines with black hash marks along the banks; banks were often characterized as actively eroding in accordance with their cantilever bank form or gouged bank faces with knocked over trees and exposed bank material. To identify whether ice-blocks were conveyed on the top of banks and across the floodplain, which can provide clues to erosive mechanisms at historic erosion locations, the locations of ice scars on trees were also compiled in the mapping, and illustrated as white circles with black dots.

As the historical mapping in Figure 5-37 through Figure 5-42 illustrates, locations of erosion between 1951 and 1983 tended to also erode during the 1983-2012 period. The majority of the banks that have historically eroded also align closely to banks field-identified as eroding in 2013, indicating that signs of erosion persist. While many of these locations were in areas prone

to erosion, on the outside of bends (e.g., locations RK 221, RK 210, RK 207 left bank) or upstream of constrictions (e.g., RK 222, RK 210, RK 188), some locations were in stable, well-vegetated areas, on the inside of bends (e.g., RK 225 [formation of side channel in 1951 that has since vegetated], RK 215, RK 199, RK 190) or at the heads of islands where flow diverges (e.g., RK 218.8, RK 202.5, RK 201.8).

The turnover data identify large-scale changes in channel or land features (i.e., multiple meters in lateral bank retreat), while field identification of eroding banks may capture erosion locations with less than multiple meters of bank retreat. Some banks identified as currently eroding, typically due to their cantilevered nature or exposed root mats and bank face, did not align with any erosion between 1951 to 2013 (e.g., RK 219.5 right bank, RK 219-RK 217 left bank, RK 200-199 left bank, and a majority of Reach 7). This finding indicates two possibilities:

1. There was some local erosion and lateral bank retreat, however significant lateral bank retreat (i.e. more than a few meters) did not occur such that it was captured in the historical sequential aerial photography analysis; or
2. there was some local erosion and no lateral bank retreat (i.e. only entrainment of the fine-grained non-cohesive bank layers and slumping of the vegetated upper bank).

The widespread evidence of ice disturbance on vegetation indicates that ice-blocks and floes had accumulated to form ramps onto the bank or had been shoved over the bank top during ice-breakup flooding. Yet, significant lateral bank retreat did not occur at every ice-scar location. In fact, many ice-scars were observed in areas where little to no erosion had occurred. High-stage ice events that caused ice floes to scar vegetation may not have generated enough energy to erode banks, the banks could have been frozen when ice came in contact with the bank thereby limiting the magnitude of lateral bank retreat, or, the water stage may have been higher than the bank height

such that ice blocks were conveyed above the bank face with sufficient force to scar trees or reset vegetation without interacting with the bank.

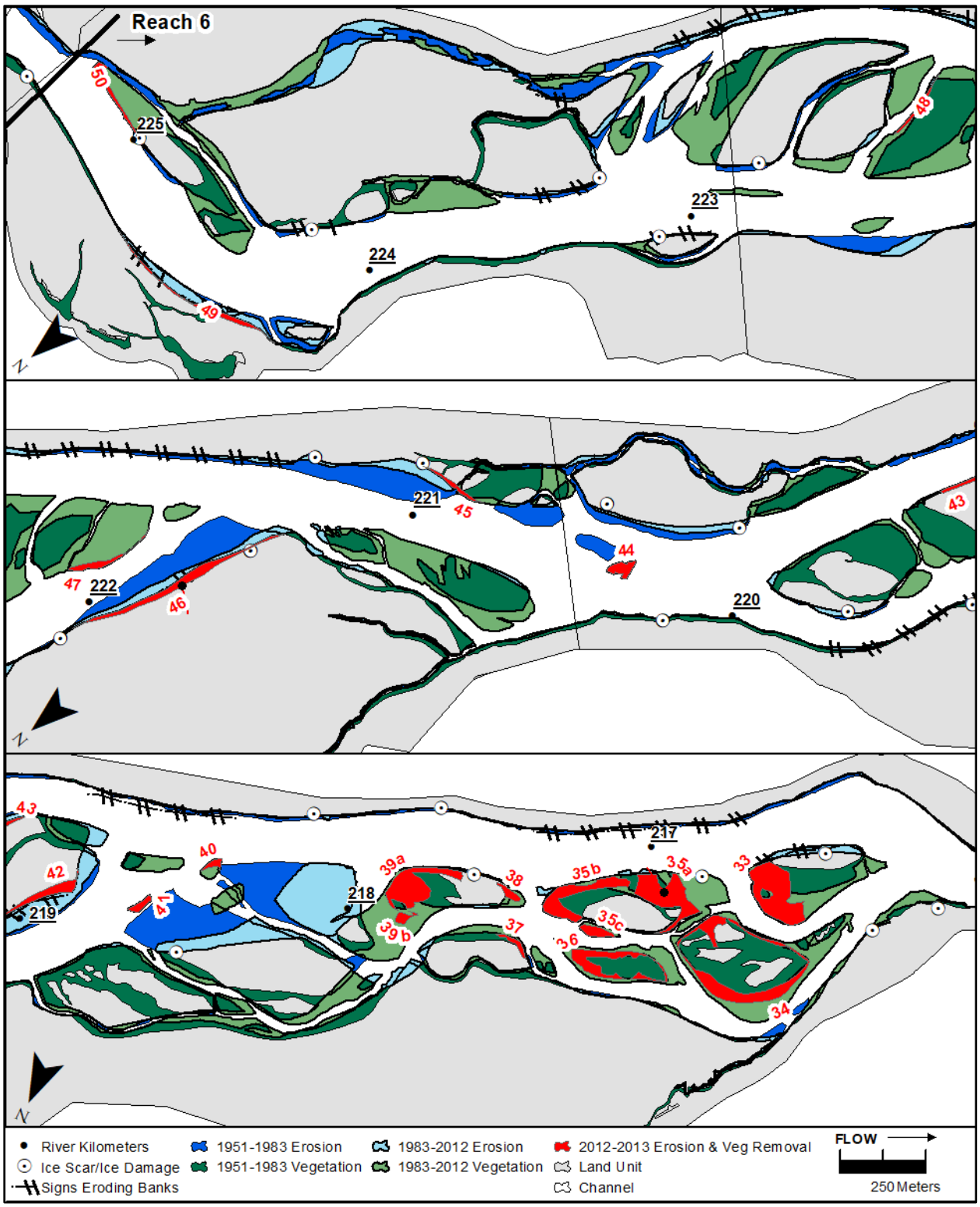

Figure 5-37. Long-term and short-term turnover mapping for Reach 6 RK 225 - RK 217. The red numbers indicate erosion locations between 2012 and 2013 (Section 5.2.2)

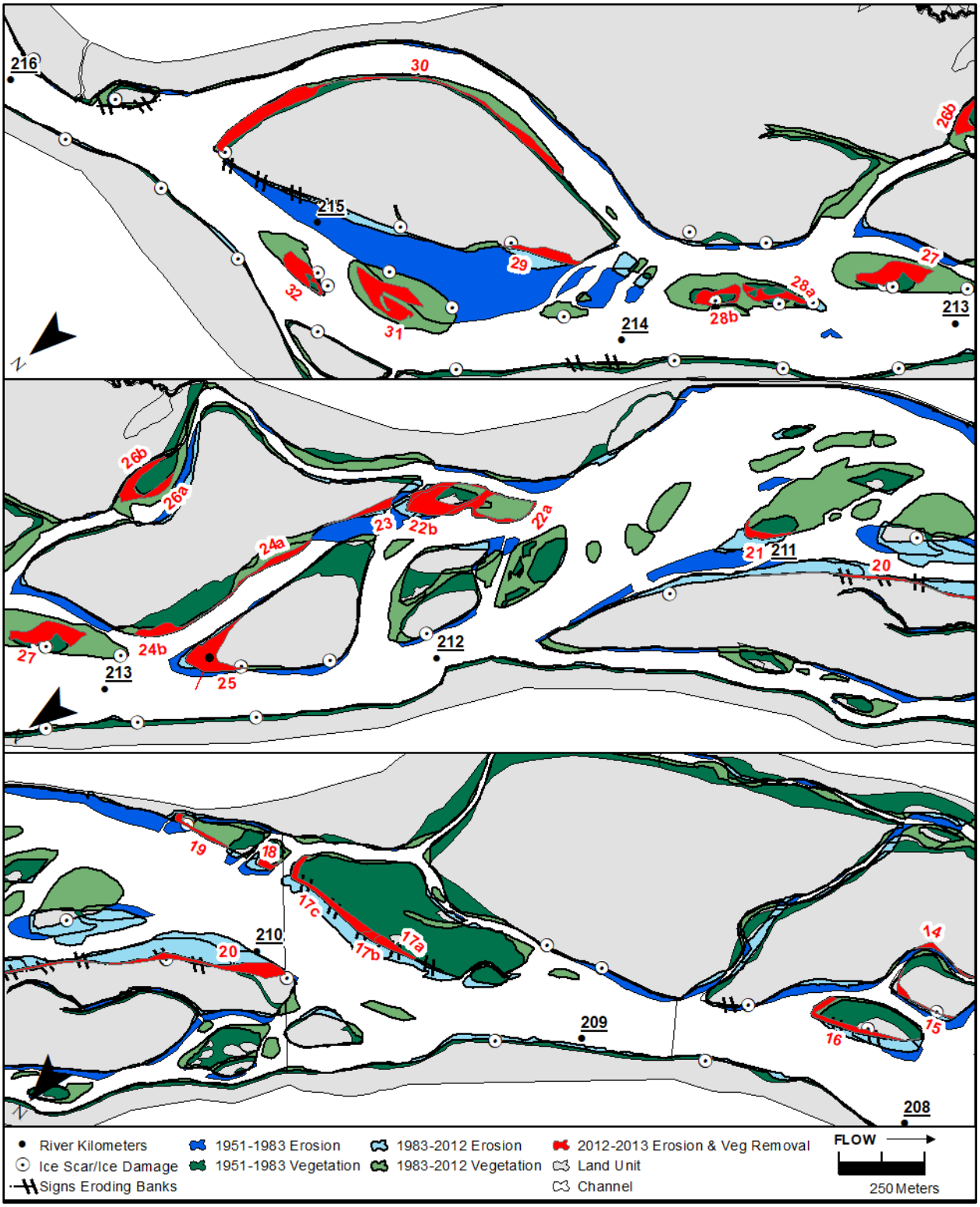

Figure 5-38. Long-term and short-term turnover mapping for Reach 6 RK 216 - RK 208. The red numbers indicate erosion locations between 2012 and 2013 (Section 5.2.2).

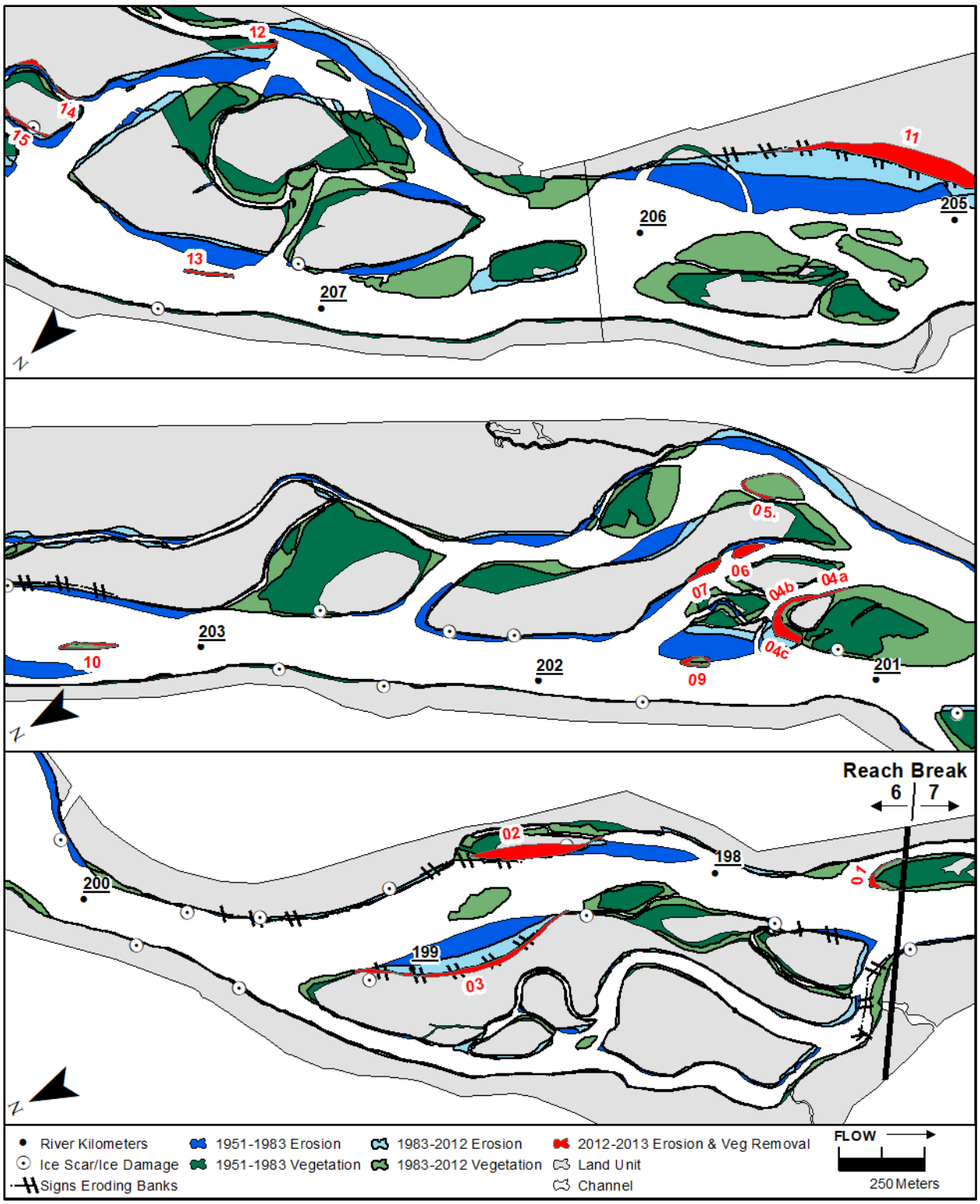

Figure 5-39. Long-term and short-term turnover mapping for Reach 6 RK 208 - RK 198. The red numbers indicate erosion locations between 2012 and 2013 (Section 5.2.2)

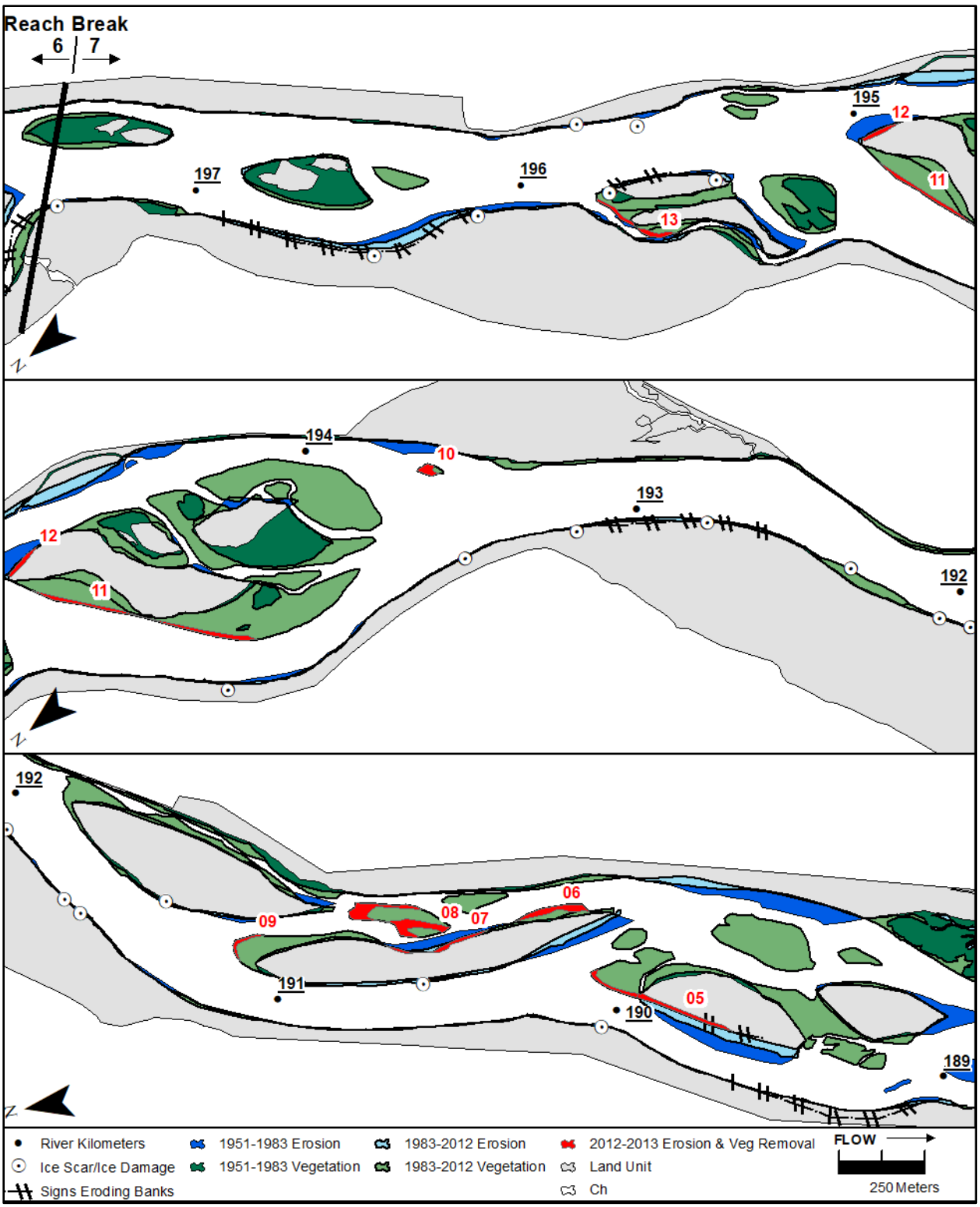

Figure 5-40. Long-term and short-term turnover mapping for Reach 7 RK 198 - RK 189. The red numbers indicate erosion locations between 2012 and 2013 (Section 5.2.2)

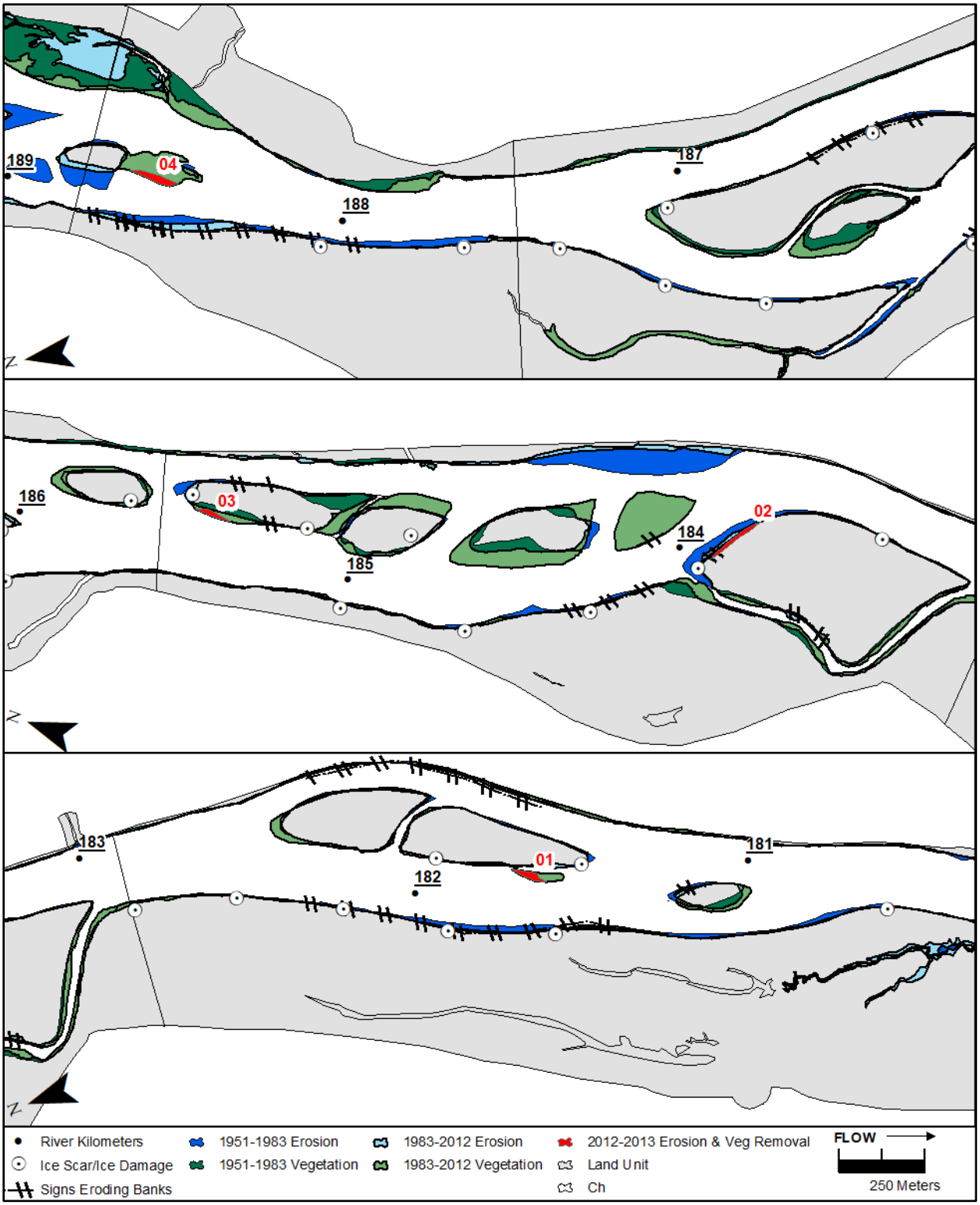

Figure 5-41. Long-term and short-term turnover mapping for Reach 7 RK 189 - RK 181. The red numbers indicate erosion locations between 2012 and 2013 (Section 5.2.2)

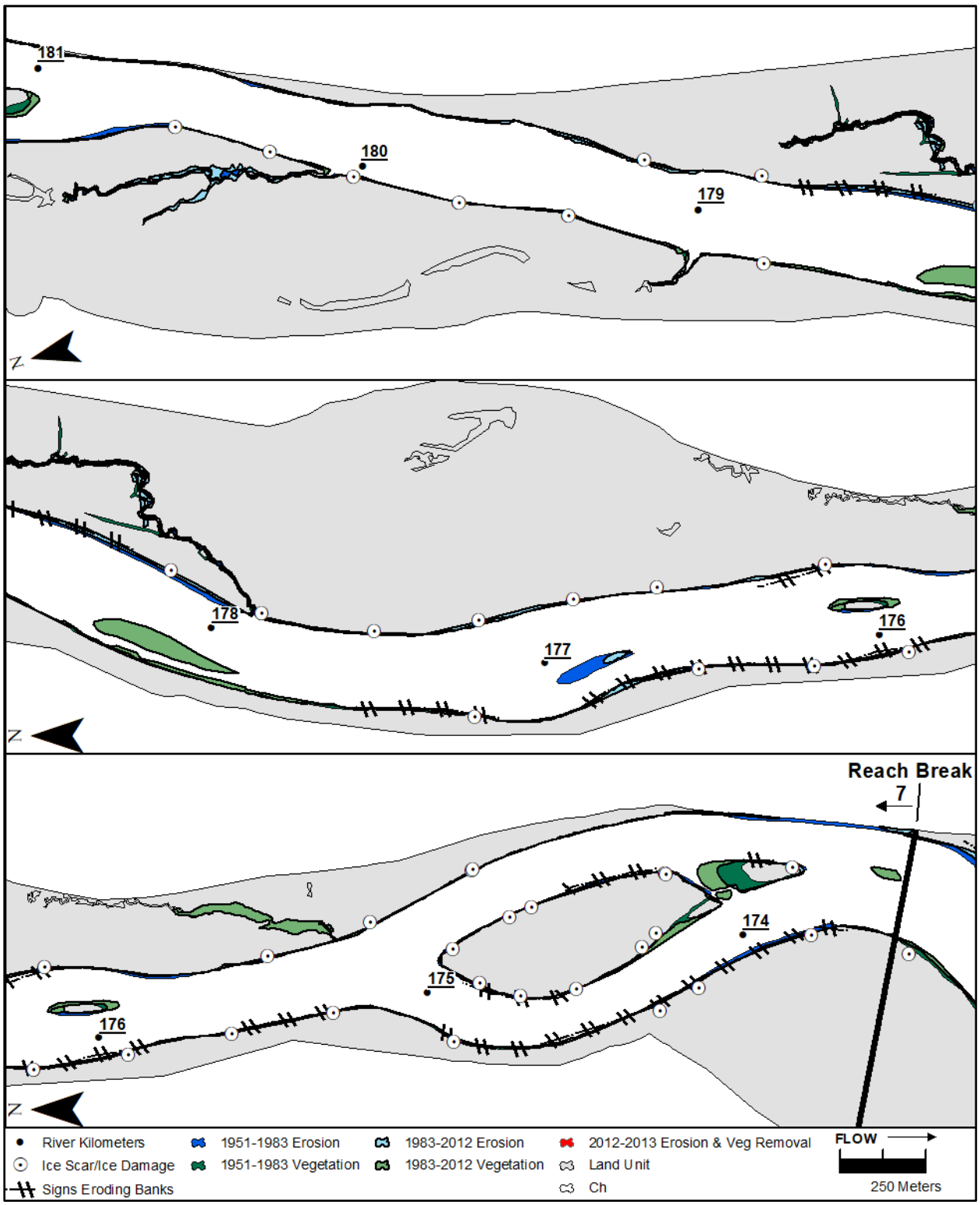

Figure 5-42. Long-term and short-term turnover mapping for Reach 7 RK 181 - RK 174. The red numbers indicate erosion locations between 2012 and 2013 (Section 5.2.2)

5.3.2 *Comparison of Long-term and Short-term Erosion Rates*

Erosion data for the current short-term erosion analysis (Section 5.2.1) and long-term analysis (Tetra Tech, 2014f) are compiled in Table 5-4. For both geomorphic reaches, erosion during 2012-2013 was nearly 4 to 8 times the historical erosion rates, while erosion during 2011-2012 was minimal. Total erosion during 2012-2013 ranged from 10 to 30 percent of the total amount of historical erosion. Between 2011-2012 erosion rates and total erosion were small fractions of historic rates of erosion. These rates indicate that large-scale erosion is episodic.

The amount of low-lying vegetation converted to channel in Reach 6 between 2012 and 2013, indicates that more erosion could have occurred between the sequences of historical aerial photographs that cover two approximately 30-year periods. However, it would not be accounted for if vegetation established sometime before the next set of aerials was collected. Therefore, these long-term erosion values are minimum values for the total area of land converted to channel.

Table 5-4. Total area of valley bottom-land, total eroded area, and erosion rates for Reaches 6 and 7 over four time periods.

Time Period	Valley Bottom Land Area (m^2)	Total Eroded Area (m^2)	Eroded Percent of Total Valley Bottom Land Area	Erosion (m^2/km)	Erosion Rate (m^2/km/yr)	Erosion (m/y)	Eroded percent of 1951-1983 Erosion	Eroded percent of 1983-2012 Erosion
Reach 6								
1951-1983	13,306,400	1,192,800	9.0%	42,800	1,300	1.3		
1983-2012	13,844,000	538,700	3.9%	19,300	700	0.7		
2011-2012	14,694,600	6,500	0.04%	200	200	0.2	0.5%	1.2%
2012-2013	14,694,600	158,100	1.1%	5,700	5,700	5.7	13.3%	29.3%
Reach 7								
1951-1983	9,471,200	318,200	3.4%	13,300	400	0.4		
1983-2012	9,418,000	151,100	1.6%	6,300	200	0.2		
2011-2012	9,978,800	0	0.0%	0	0	0.0	0.0%	0.0%
2012-2013	9,978,800	33,900	0.3%	1,400	1,400	1.4	10.7%	22.4%

Note:
1. All values are rounded to the nearest hundred
2. Valley Bottom Land Area is determined from the land area from 1951 for 1951-1983, from 1983 for 1983-2012, and 2012 for both 2011-2012 and 2012-2013
3. Data sources for valley bottom land area and historical erosion rates can be found within Tetra Tech (2014f)

5.3.3 *Comparison of Long-term and Short-term Eroded Surfaces*

Generally, there are similar trends in the magnitude of erosion for the three categories of geomorphic surfaces over the various time periods for each geomorphic reach. In Reach 6, excluding erosion that occurred between 2011 to 2012, the erosion of terrace surfaces (i.e., high banks with minimal upper bank root-reinforcement, Figure 5-4 in Section 5.1.2) was 40 to 50 percent of the total erosion during each time period. In Reach 7, 40 to 50 percent of the historical erosion also corresponded to terrace surfaces. Between the time periods that vegetated bar surfaces were linked to erosion data (i.e. 1983-2012 and 2012-2013), erosion of vegetated bars composed nearly 25 percent of the total erosion while the active floodplain surfaces composed 25 to 33 percent of total erosion. The anomaly to this trend was in Reach 7; between 2012 to 2013, only 4 percent of the total eroded area corresponded to terrace surfaces and 76 percent corresponded to

vegetated bars. Notably, for both reaches, excluding the period 2011 to 2012, approximately 75 percent of the total erosion was either on higher geomorphic surfaces or on vegetated bars, while approximately 25 percent of total erosion was on active floodplain surfaces. This finding indicates that most erosion is on surfaces with less relative root reinforcement than the more active floodplains surfaces; for the terrace surfaces, root reinforcement, if present, is higher on the bank and less able to form "vegetation rip-rap" while vegetated bars are typically low enough in the channel to be overridden by ice, thereby negating protective qualities provided by root reinforcement.

Table 5-5. Percent short-term and long-term erosion that eroded from terrace surfaces, active floodplain surfaces, and low-lying vegetation.

Time Period	Total Eroded Area (m^2)	Percent Erosion of Terrace Surfaces[1]	Percent Erosion of Active Floodplain Surfaces[2]	Percent Erosion of Low-lying vegetation[3]
		MR-6		
1951-1983	1,192,200	45%	55%	n/a
1983-2012	538,400	53%	26%	22%
2011-2012	6,500	31%	69%	0%
2012-2013	158,000	39%	35%	25%
		MR-7		
1951-1983	318,000	41%	59%	n/a
1983-2012	151,000	53%	20%	27%
2011-2012	0	0%	0%	0%
2012-2013	33,900	4%	20%	76%

Note:

1 Terrace surfaces were defined as land units within the valley bottom that were 1.5m higher than the 100-year water-surface elevation (Tetra Tech , 2015c).

2 Active floodplain surfaces were defined as land units within the valley bottom that were vegetated with mature tree-stands. For the 2011-2012 and 2012-2013 periods this was determined during the sequential aerial photography analysis. This constituted all of the area that was not terrace surfaces between 1951-1983 as there was no reliable method to determine what were mature tree stands or low-lying vegetation. For the 1983-2012 period this was determined by subtracting the total area of low-lying vegetation from the total area that eroded that was not a terrace surface.

3 For the periods 2011-2012 and 2012-2013, low-lying vegetation was determined during the sequential aerial photography analysis. For the period 1983-2012, low lying vegetation that eroded was determined as the amount of vegetation that established between 1951-1983 and subsequently eroded during 1983-2012.

Table 5-6. Range of erosion volumes for Reaches 6 and 7 over four time-periods by geomorphic surface.

Time Period	Terrace		Active Floodplain		Vegetated Bars	
	Min Surface Ht (m)	Max Surface Ht (m)	Min Surface Ht (m)	Max Surface Ht (m)	Min Surface Ht (m)	Max Surface Ht (m)
	1.75	2.8	1.35	2.5	0.9	1.6
	Volume (m^3)					
	Reach 6					
1951-1983	945,520	1,512,833	880,069	1,629,757	n/a	n/a
1983-2012	494,980	791,968	187,069	346,424	105,287	187,176
2011-2012	3,500	5,600	6,075	11,250	0	0
2012-2013	108,150	173,040	75,600	140,000	36,180	64,320
	Reach 7					
1951-1983	229,790	367,663	252,034	466,729	n/a	n/a
1983-2012	140,595	224,952	40,994	75,914	36,265	64,471
2011-2012	0	0	0	0	0	0
2012-2013	2,625	4,200	9,180	17,000	23,040	40,960

Table 5-7. Range of erosion volumes for Reaches 6 and 7 over four time-periods.

Time Period	Total Volume (m^3)	
	Minimum[1]	Maximum[2]
	Reach 6	
1951-1983	1,825,589	3,142,589
1983-2012	787,335	1,325,567
2011-2012	9,575	16,850
2012-2013	219,930	377,360
	Reach 7	
1951-1983	481,823	834,393
1983-2012	217,854	365,337
2011-2012	0	0
2012-2013	34,845	62,160

Note:

1 Minimum erosion volume determined by summing minimum volume for each geomorphic surface in Table 5-6.

2 Maximum erosion volume determined by summing maximum volume for each geomorphic surface in Table 5-6.

CHAPTER 6: DISCUSSION

This chapter discusses and further explains several aspects of the results presented in Chapter 5. Discussed first are the main findings from the bank-erosion analysis and identification of the dominant bank-erosion processes. Also included is a discussion of the numerical investigation into ice-induced flow diversion and its consequences for bank erosion. Bank-erosion mechanisms and the effects of bank erosion on the fluvial morphology of the Middle Susitna River are considered. Lastly, rates of channel change are discussed by geomorphic reach, by general frequency, and compared to other river systems.

6.1 Erosive Processes

6.1.1 *Erosion Analysis and Processes*

Relatively minor bank erosion occurred between the 2011 and 2012 aerial-photography flights. Only four locations were identified, and all of them were located in Reach 6. The locations of bank retreat were along the sides of mid-channel islands or bank-attached floodplain units and did not exceed 10 m. Nearly 75 percent of the eroded area corresponded to active floodplain surfaces while the remaining 25 percent corresponded to terrace surfaces. The timing of erosion within the year could not be determined.

For both geomorphic reaches, channel change that occurred between the 2012 and 2013 aerial imagery flights ranged from 10 to 30 percent of channel change that occurred in the approximate 30-year periods between 1951 to 1983 and 1983 to 2012. More than half of the total erosion corresponded to, or was initiated during the ice-driven regime. The dominant erosive processes, as described in Section 5.1.3.2, were ice rubble abrasion, ice-floe impact; and the combination of ice and concentrated water flow. Parsing out the localized effect of each process

at each location site was not possible. The extent of lateral bank retreat greater than 10 m, and up to 700 m in the streamwise direction, very likely indicates the combined action of ice rubble and floes with water flow (Process 4). Given the rather high erosion thresholds throughout the Middle Susitna River, high erosive stress is necessary to overcome the bank resistance; evidenced by the, paved cobble and gravel bed material, vegetated banks, and modest rates of historical channel change. Sufficient water levels are necessary to convey ice rubble above the bank to bull-doze vegetation, and sufficient water velocities are necessary to drive ice rubble into and adjacent to banks.

Review of the reconnaissance videos over the series of days that spanned a particularly dynamic ice-break up yielded illustrative clues of these dominant erosive processes. Screenshots from the aerial reconnaissance videos of each erosion site are compiled in Appendix B; ice jams are visible in many of the images.

During the 2013 ice breakup, flow diversion into side channels and sloughs, even when occurring at lower discharges, caused side channels to be inundated up to the vegetation line. If bank-attached ice had already been dislodged and transported downstream, this process exposed bank material to erosion. Figure 6-1 provides a series of photos illustrating the development of a flow diversion immediately upstream of an ice jam.

While both year-long periods (2011 to 2012 and 2012 to 2013) experienced large open-water events, the reset of vegetation to its initial succession only occurred during the dynamic ice-break year (2012-2013). Locations of greatest re-set and removal of vegetation were, as expected, adjacent to ice jam locations, where the effects of flooding and release of ice floes from a jam were the most severe. Ice rubble and floes transported overbank often sheared low-lying vegetation, bending, breaking, and removing previously established plant communities. This process occurred

throughout the Middle River and was especially evident on lower, younger floodplain surfaces as well as the periphery of more mature, older floodplains. All locations where vegetation was reset occurred during the ice-breakup window due to overbank flow transporting ice rubble and floes (Figure 6-2). In most instances, individual blocks of ice rubble or floes had collided with vegetation above ground such that root systems did not protect vegetation against impact. Some geomorphic surfaces, with young low-lying shrubs and limited older growth, were found to have extensive root systems beneath the surface; this indicated the surface was older than the size of the above-ground vegetation may indicate (Kevin Featherston, R2 Resources; personal communication) and is consistent with ice-scouring of lower geomorphic surfaces in other boreal rivers (Scrimgeour et al., 1994; Uunila and Church, 2015). In these instances, ice continually sheared vegetation above the ground, yet did not completely remove the plant community, allowing the vegetation to regrow in the following seasons. Roots were observed to be very effective at anchoring the sediments.

The lack of vegetation reset in Reach 7 compared to that in Reach 6 (Table 5-2) was due to several factors, notably:

1. Limited ice-jamming within the latter reach; and,
2. The limited extent of lower, younger floodplain surfaces in Reach 7 compared to Reach 6.

It appears that removal of bank material at the heads of islands and along bank faces, slightly widened the heads of some secondary channels. This effect, coupled with ice-scour may keep secondary channels connected to the primary channel(s) by limiting vegetation colonization.

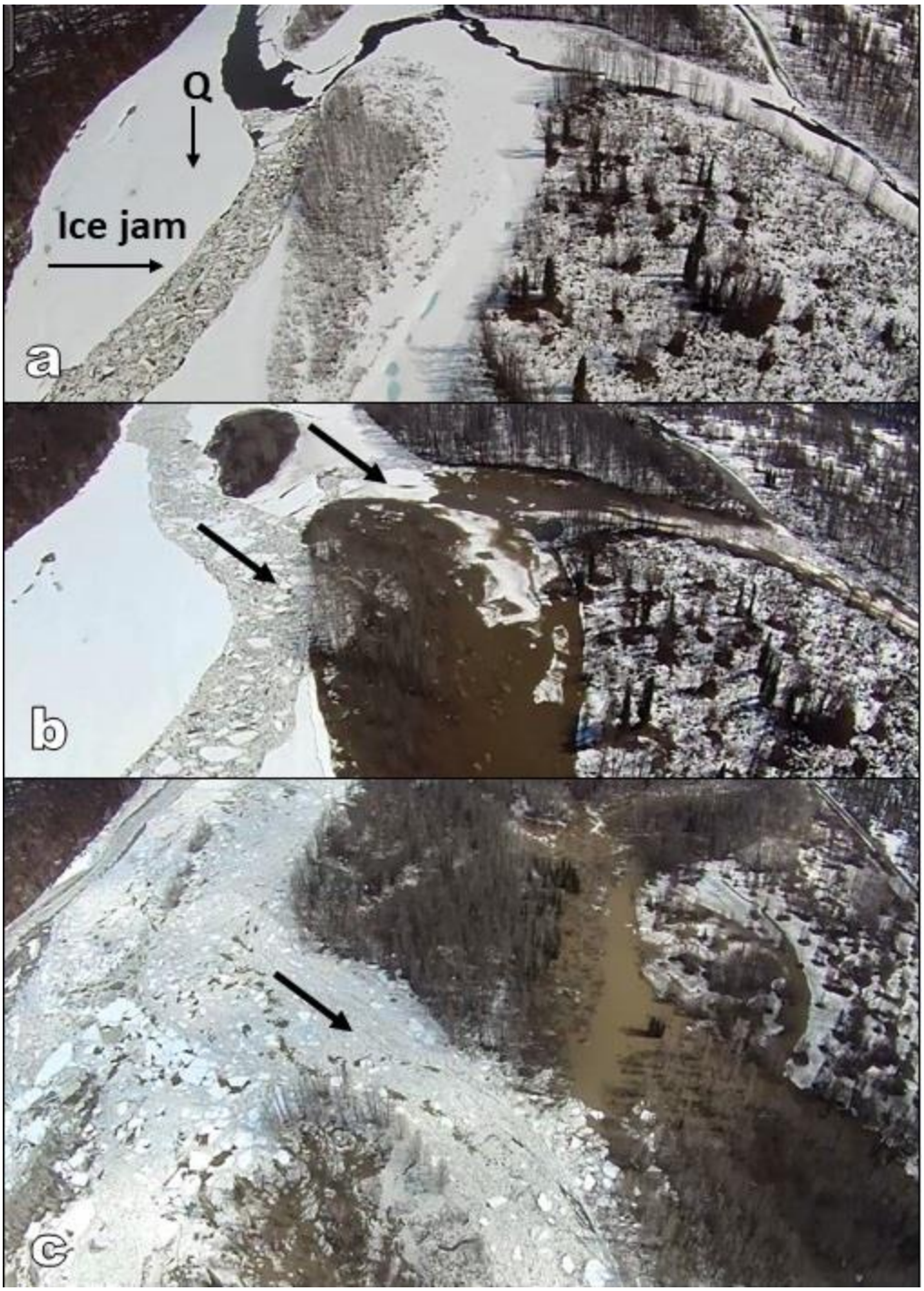

Figure 6-1. Series of screenshots from aerial reconnaissance of ice-break at RK 213. Black arrows indicate direction of flow. (a) Photo taken on May 23, 2013, with ice jam in main channel; (b) photo taken on May 25, 2013 with ice-induced diversion of flow into side channel; and, (c) photo taken on May 26, 2013 illustrating diversion of ice blocks into side channel.

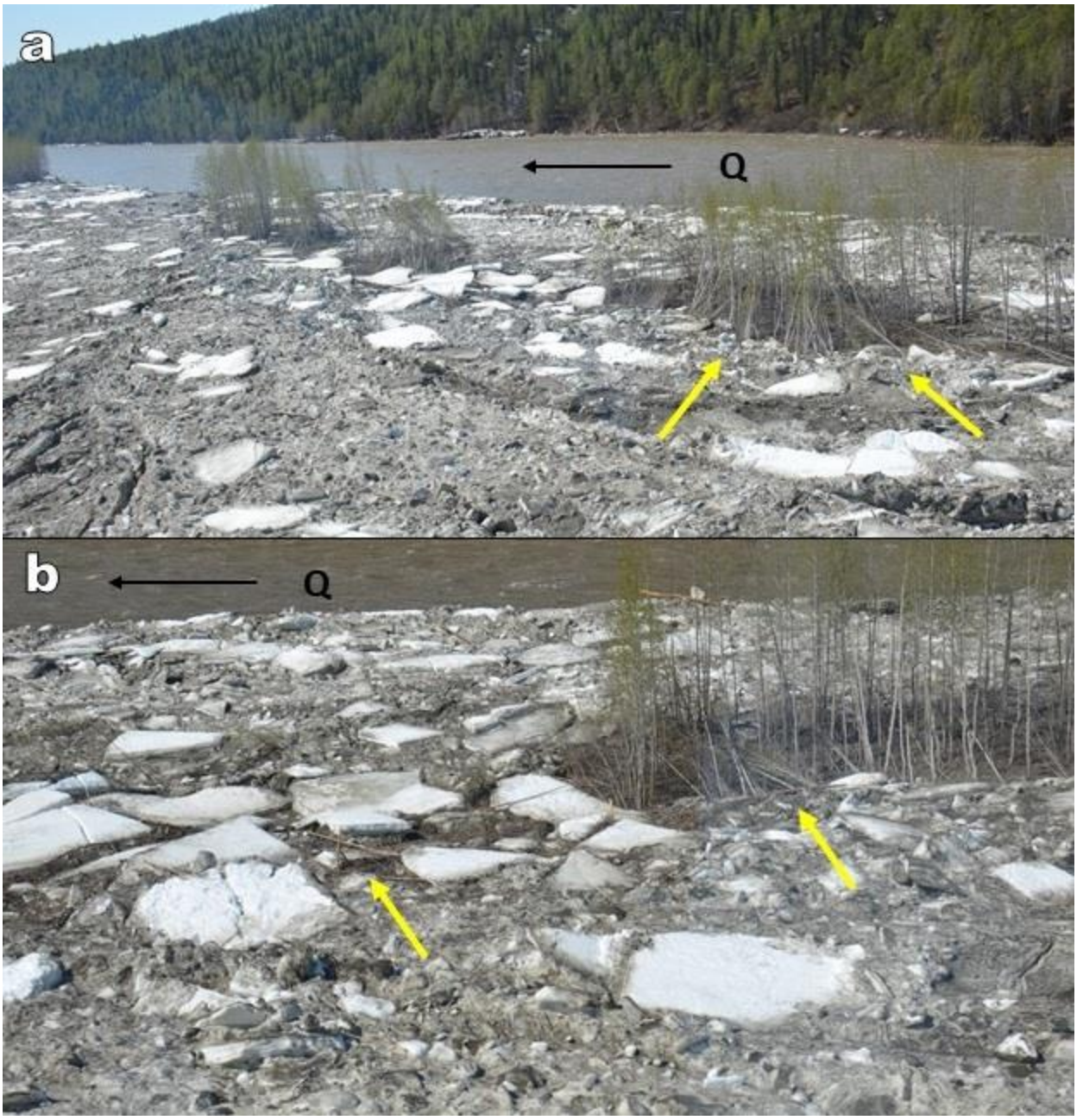

Figure 6-2. Ice jam released ice blocks shearing across island surface. Yellow arrows pointing to knocked over trees and trees transported on ice floes. Trees are approximately 10 to 20m tall. The photos were taken on May 29, 2013 near RK 214 on the Susitna River: (a) view downstream at RK 214, (b) view towards right bank at RK 214.

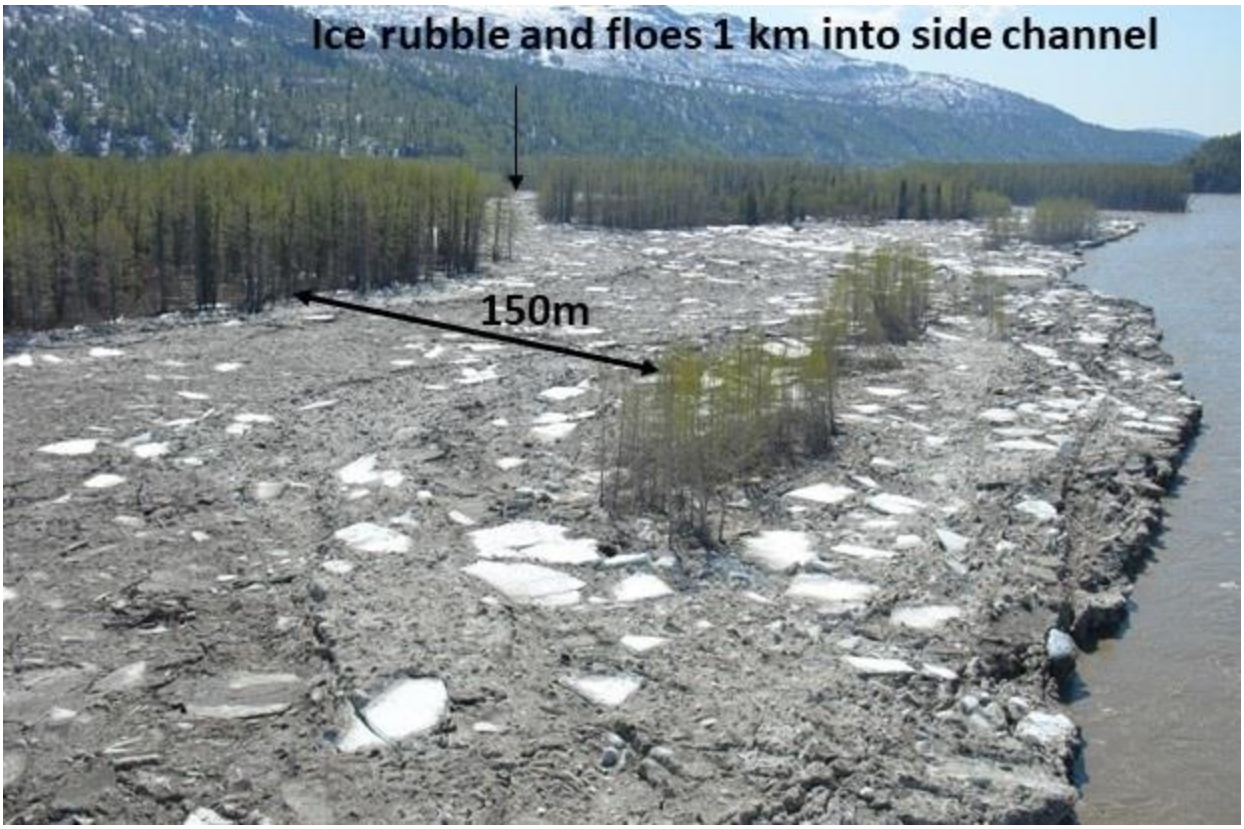

Figure 6-3. Expanse of ice rubble and ice floes grounded in side channel complex near RK 214. Photo taken on May 29, 2013. Arrow points to distance down side channel with considerable ice-rubble and local site of erosion and vegetation reset from ice.

6.1.2 *Numerical Investigation of Ice-Induced Diversion of Water Flow*

Ice-induced diversion of flow has been observed on other northern rivers. Notably, Zablinksky et al. (2002) found ice-induced concentration of flow on the Missouri River to exacerbate local bed and bank scour near the concentrations. Whereas the findings reported by Zablinksky et al. (2002) were for concentration of flow around bars and islands in the Missouri's main channel, the concentration of flow into secondary channels, or onto adjacent floodplain units, can have a similar scour effect. Observations on the Milk River (located in southern Alberta and northern Montana) indicated that channels blocked by ice create sufficient stage and hydraulic gradient to scour deeply (up to multiple meters) into the adjacent floodplain. In this regard, Smith

and Pearce (2002) report how re-routed water flowed across a floodplain and converged at the downstream end of a floodplain unit. The converged water created a waterfall, and associated plunge pool, eroded into the sandy overbank material and initiated an erosion head-cut that progressed along the channel.

As discussed in Section 5.2.1.2, three trends for flow-related, shear-stress redistribution were identified from the numerical investigation into ice-induced diversion of water flow on the Susitna River:

1. In existing secondary channels, the increased shear stress was sufficient to mobilize the channel bed material;
2. The shear stress increased at the downstream end of depressions or overflow channels on the floodplain surface; and,
3. Shear stress decreased upstream of the ice jam owing to a local reduction in water-surface slope.

The occurrence of increased shear stress at the downstream ends of depressions concurs with observations of gully erosion across meander lobes on the Milk River from ice-induced flow diversion (Smith and Pearce, 2002). Additionally, this same finding emerges for overflow channels on the floodplain surface. These two regions correspond somewhat to the waterfall, plunge pool, and subsequent head-cutting observed for the Milk River (Smith and Pearce, 2002), although plunge pools are much less likely to form on the armored-bed of Middle Susitna River; and indeed have not been observed in the river. Instead, for the Middle Susitna River, observations show the formation of incisions along the floodplain surface. The incisions were more pronounced at regions of flow convergence, and likely propagated upstream when the ground was unfrozen.

When the ground was frozen, flow-induced shear stress likely could not exceed the bank's capacity to resist erosion by water shear.

Decreased shear stress upstream of ice-jams is a common feature of ice jam processes and may even lead to short-term aggradation along a channel or floodplain surface. The choking and backwater effect of ice jams reduces the energy gradient thereby limiting the energy available for sediment transport or bed and bank erosion (Zabilanksy et al., 2002). A reduced channel conveyance capacity can cause local aggradation under the ice cover and short-term bar development that may be swept downstream during breakup or subsequent higher open-water flows (Zabilanksy et al., 2002). Backwater effects from ice jams can also lead to sediment aggradation on the floodplain. On the Susitna River, sands stored in the channel during freeze-up were noted to be remobilized during the ice-breakup period and can be deposited in the overbank from ice-induced flooding (Figure 6-4).

The numerical modeling revealed preferential pathways for flow and, thereby, areas prone to erosion that when coupled with ice, could combine to cause large-scale channel change. Within the model domain, there were 11 locations that eroded during the period 2012 to 2013. Shear stress at each of these locations was evaluated under existing conditions and under the flow diversion scenarios (see Appendix D, Figure D-2 through D-4). While diverted flow did not mobilize sediment at the bank toe at locations that were not already above the critical threshold, it is possible that water surges more typical of ice-jam breaks can be sufficient to mobilize bed and bank material. Such surges increase the hydrodynamic load on downstream ice covers or ice jams. Observations from the literature indicate that surges released from ice-jam breaks have reached velocities up to 5 m/s (Beltaos and Burrell, 2005) creating sufficient shear stress to easily erode channel banks. In consequence, the bed can become armored with coarser particles, as was

observed once the surges had passed. While such stage increases were not directly observed in the study reaches, there is evidence that surges occur along the Middle Susitna River. For example, large and rapid stage increases recorded at the USGS Gold Creek gage, and the prevalence of armored coarser particles at various sites, indicate the occurrence of ice-jam released surges.

It is also possible that different jam locations than those modeled, especially local jams in closer proximity to the known erosion locations, could cause a concentrated lower flow to exceed the critical grain size threshold. Figure 5-35 and Figure 5-36 (Section 5.2.1.2) present an example of locations with mobilized grain size increases of 16 mm to 32 mm or more.

Additionally, water-surface profiles measured over 488 m (1,600 ft) from before and during the location of a major ice jam on the Middle Susitna River, revealed an increase in water surface slope from 0.0019 to 0.0033 once the channel was jammed with ice; local stages on the Susitna River were found to increase by nearly 1 m over 24 hours (R&M Consultants, Inc., 1984). As this ice jam began to grow from accumulated ice rubble discharging from Devils Canyon, building pressure was noted in the jam. At some critical pressure, a chain reaction of collisions caused portions of the ice cover to collapse-thicken and consolidate (a usual thickening mechanism for jams) and then fail simultaneously and completely. The thickening and consolidation events occurred periodically over a 4-hour observation period and appeared to be controlled by the volume of incoming ice. The consolidation events caused downstream surge waves which were able to break up all the downstream shore-fast ice into 9 m-wide and 1 m-thick ice blocks and shove them onto nearby gravel bars. This process may contribute to the extensive paving observed along the Susitna River. If the gravel bars were vegetated, this likely would cause significant shearing or complete removal of the vegetation.

Figure 6-4. Sand aggradation from ice-induced flooding in Focus Area 128 during 2014 ice-breakup. Sand deposited on ice-cover which subsequently melted. (Photo courtesy of Jon Zufelt, HDR Alaska, Inc.).

6.2 Erosion Resistance Properties

As mentioned in Chapter 5, three variables were found to increase the erosion resistance of banks:

1. Gravel-cobble pavement at bank toe;
2. Root-reinforced top of bank; and,
3. The presence of bank-attached ice or a protective shear-wall of ice rubble.

The presence of a gravel-cobble pavement significantly reduces erosion driven by toe scour, but gravel and cobbles were found dispersed over other parts of the river channel and floodplain. Though some locations along the river corridor were mobilized by fluvial shear stress (Appendix D), such mobilization did not occur along the entire reach. Ice floes and large ice blocks can shove and deposit large cobbles and boulders along bank toes, effectively coarsening the bank

toe sediment gradation. The presence of large ice blocks along the bank toe applies large forces on the bed helping to pave the bed-material and increasing the shear forces necessary for mobilization. In a laboratory study, Ettema and Kennedy (1982) found ice ride-up to be preceded by ice slab accumulations over armor boulders; the accumulation acts to protect the armor boulders from subsequent ice impact. Coarse cobble-boulder pavements have been found to be erosion-resistant. Mackay and MacKay (1977) speculated that some pavements may remain stable for at least a century before the original boulders in the pavement are plucked and eventually replaced.

Quantifying erosion by geomorphic surface infers types of surfaces that are more or less susceptible to erosive processes. As elaborated in Section 5.3.3, active floodplain surfaces comprised approximately one-quarter of the total erosion in both geomorphic reaches, as opposed to the remaining three quarters of erosion corresponding to vegetated bar or terrace surfaces. It is the active floodplain surfaces (young floodplains, mature floodplains, and some old floodplains), that are composed of thick root-reinforced top of bank layers (Figure 5-1a,b). The flexible and resilient roots are effective deflectors from flowing ice and slump over the bank after entrainment of the sandy middle bank layers, providing "vegetated rip-rap" to the cantilevered bank (Figure 5-3).

Though not as long-lasting as cobble-gravel pavements or vegetation rip-rip, the presence of bank-attached ice was observed to limit the time banks are subjected to the abrasive effects of water flow and ice-rubble. When ice-protected, banks can remain stable while flows are confined to the river's main channel, and jam formation diverts water and ice-rubble over a floodplain. Not until the bank-ice is dislodged will the bank be exposed to external erosive mechanisms. To be kept in mind is that the dislodgement of bank-attached ice can itself remove or pluck vegetation

from a bank (Zabilansky et al. 2002). The resulting exposed band of bank soil can be susceptible to erosion.

6.3 Morphology and Ice Processes

Certain channel morphologies trigger ice-jam formation. These features include sharp bends or flow expansion areas (e.g., Gerard, 1989; Beltaos, 1995). Channel constrictions and expansions are common throughout the Middle Susitna River. Ice accumulation as local jams was commonly observed in the wider valley bottom regions of the two reaches. The presence of multiple side-channels and low-elevation morphologic features relate to jam formation, being consequent to jam formation and, in turn, promoting the formation and longevity of ice jams. Secondary channels, also common in the wider valley bottom regions, enabled water to divert around a jam, thereby reducing the hydrodynamic pressure that would otherwise increase until the jam broke.

Bypass channels which occur as side channels, side sloughs, or shallow depressions in the floodplain, are common throughout the Middle Susitna River. The similarity of geomorphic surfaces and vegetation succession on the upstream and downstream sides of the bypass channels, suggest that the channels were formed by erosion. An example of a bypass channel is shown in Figure 6-5. Note, that the entrance of this bypass channel is oriented perpendicular to the typical flow path. Though the bypass channel was at its current geometry before diversion of ice-blocks that are shown in shown in Figure 6-5a, the image indicates that diverted flow from the main channel causes relatively high ice and hydraulic forces along banks of bypass channels. The bypass channel was present and un-vegetated in 1983 and 1951 aerial photography indicating the formation of the feature occurred prior to earliest data collection effort.

Bypass channels may persist for decades without forming a continuous channel across the overbank surface. Overbank depressions and flow paths are illustrated in Figure 6-6 and Figure 6-7. Figure 6-6 shows an aerial view of a geomorphic surface with bypass channels present in 1951, 1983, and 2012 aerial photography. Figure 6-7 shows an on-the-ground photo of one of the bypass channels; ice-scars on trees and bedded down vegetation are visible.

Like for other enlarged channels in boreal environments, it is unclear whether the current morphologic configuration was developed by other environmental processes and permits diffusion of ice-induced flow through bypass channels that are marked by ice signatures, or, whether ice processes eroded the surfaces to create these features. It is clear however, that ice is an agent in enlarging some secondary channels and was observed to cause the formation of at least one new channel.

Observations reported during the 1976 ice-breakup just downstream of the Gold Creek Bridge (RK 225) describe large ice-jam in the main channel that diverted flowed into an adjacent bypass channel and dissected the existing (old) floodplain to form what is now Slough 11 (Schoch 1984). Schoch (1984) notes that, since 1976, multiple, smaller ice jams have enlarged the slough. Delineated channel and land features in the area of the slough are illustrated in Figure 6-8.

Creation of new bypass channels may be more likely on older surfaces, not only because of their prevalence through the river corridor, occupying more than one-half of the non-channel valley bottom area, but also due to lower tree density and therefore lower hydraulic roughness. These surfaces may also be particularly susceptible to incision from ice-induced overbank flow (Section 6.1.2). Spatially, this process predominantly occurs upstream of major constrictions. The constrictions control the depositional, wider valley bottom reaches, where a suite of geomorphic

surfaces and channel types are found. Terraces, also found within these multi-channel sub-reaches, indicate the multi-channel depositional reaches have been present for hundreds of years.

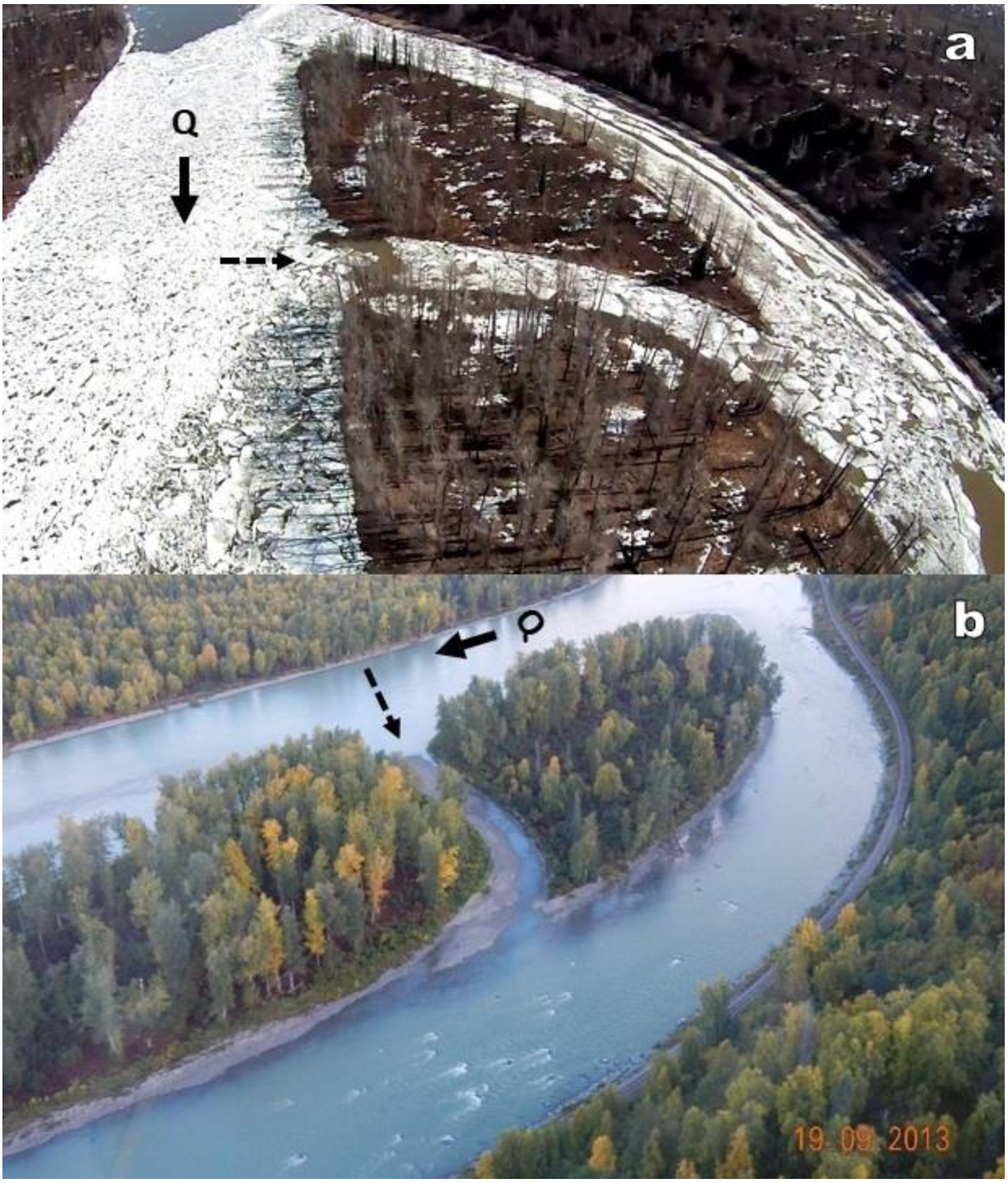

Figure 6-5. A local ice jam in a split-channel section near RK 182 backs up water and ice diverting ice blocks into a bypass channel (noted by black-dashed line). Photo (a) is screenshot from a helicopter reconnaissance flight on May 25, 2013. Photo (b) taken on September 19, 2013.

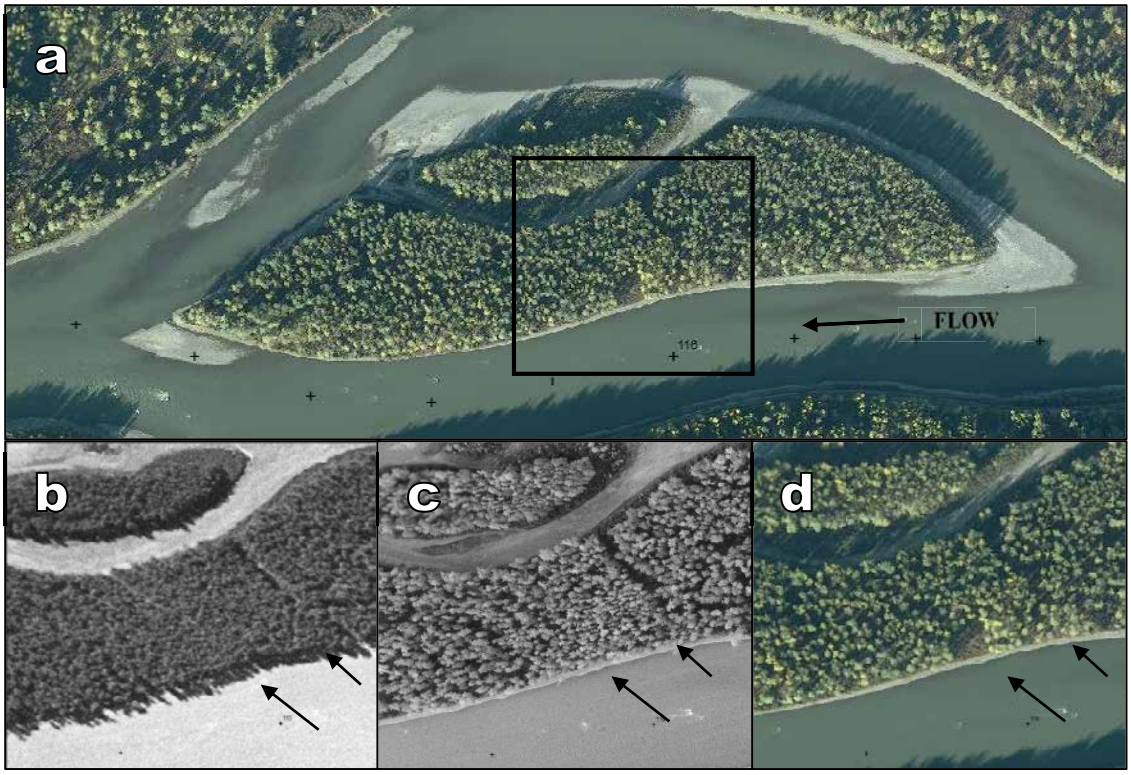

Figure 6-6. Location of overbank flow channels near RK 187: (a) identifies the area of interest by a black box, (b) illustrates the chute channels in 1950s aerial photography; (c) 1983 aerial photography; and, (d) 2013 aerial photography.

Figure 6-7. View down chute channel at RK 187 (shown by black arrows in Figure 6-6) with broken down vegetation and ice scars on trees up to 2m above ground level.

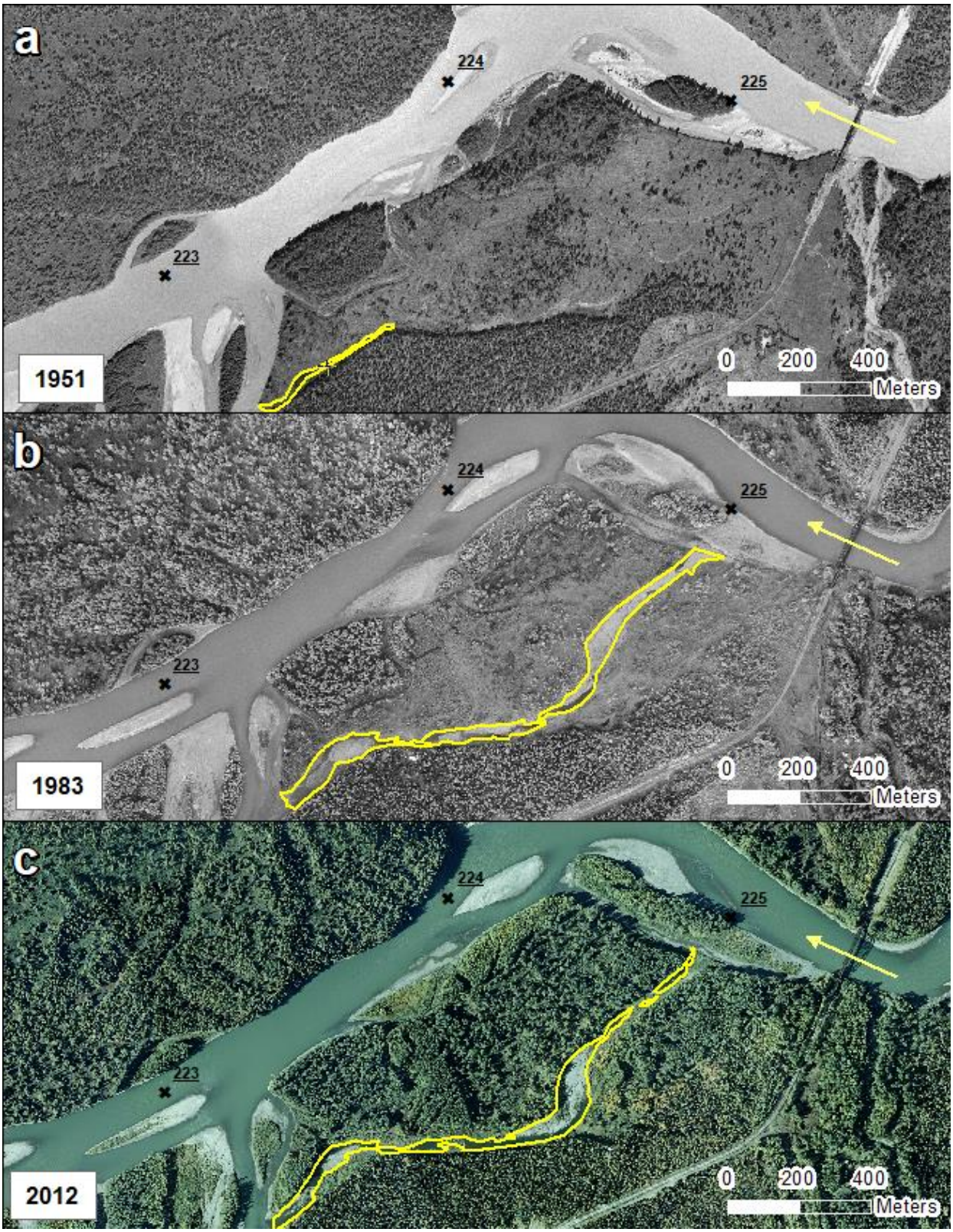

Figure 6-8. (a) Slough 11 illustrated by yellow delineation at RK 225 to RK 223 in 1951 aerial photography, (b) 1983 aerial photography, and (c) 2012 aerial photography. Yellow arrow indicates direction of flow.

6.4 Rates of Channel Change

6.4.1 *Rates of Channel Change by Geomorphic Reach*

For any time period, Reach 7 had less of its total valley bottom area (by percentage) eroded in comparison to Reach 6. Thus, a major finding of this study is that bank erosion occurred less in predominantly single-channel meandering reaches than in predominantly multi-channel reaches. As the study reach is oriented in a west-southwest direction, it is possible that local temperature gradients and insolation may have caused Reach 7 to begin thawing and breaking up before ice floes from upstream begin moving downstream. The simpler geomorphic nature of Reach 7, may also limit the magnitude and extent of ice jam formation in this reach.

Overall channel gradient and valley-bottom width are distinct variables for each geomorphic reach, and may aggravate ice-induced erosion. As elaborated below, thicker ice covers, combined with preferential ice jam development, compounds the local effects of ice-induced bank erosion in Reach 6 versus Reach 7.

The impact of ice processes is in part controlled by channel morphology and especially channel gradient. During freeze-up when channel resistance to flow depth increases, the consequent increase in hydraulic gradient caused an increase in the hydraulic thickening of the ice cover, thereby requiring a larger volume of ice in order for the ice cover to progress upstream. The increase in hydraulic gradient from Reach 7 upstream to Reach 6 led to a thicker ice cover during the winter of 2012/2013, whose major thicknesses ranged from 0.5-1.0 m to 0.7 to 1.4 m; exceptionally thicker accumulations occurred at some congestion locations along the river, but not in Reaches 6 and 7.

Channel sites less prone to ice-jam formation, coincided with reduced bank erosion. Straight reaches tend to breakup first (as also noted by Beltaos, 2007), limiting the amount of jams

that form, break, and re-form. This was observed along Reach 7, which thus experienced less erosion than did Reach 6, which had more sub-reaches with multiple channels. Ice jam locations on the Susitna River are consistent with locations identified in the literature (e.g., as described in the leading reference, Beltaos, 1995).

6.4.2 *General Frequency of Dominant Erosive Events*

The results of this study indicate that large-scale erosion (i.e. greater than 10 m), occurs due to a combination of ice and water flow from episodic dynamic ice breakup events in the spring. The combined probability of regional weather patterns, basin snow conditions, and in-channel ice-conditions (including factors such as ice jam locations and ice-strength) that can generate a reach-wide dynamic ice-breakup is low, as evidenced by the long-term rates of erosion along the Middle Susitna River.

However, estimating the frequency and behavior of ice jam floods differs from open-water floods in that they cannot simply be estimated from knowledge of floods at other locations on the river (Beltaos, 1995). The formation of ice jams is often site-specific, dependent on discharge (some jams may form at lower discharges but not at higher dischargers, or vs. versa), and not consistent year-to-year (Jon Zufelt, HDR, Alaka Inc., personal communication). Additionally, using spikes in water levels at gaging stations to develop recurrence intervals for jam events, could only be used to estimate frequency within the vicinity of the gaging station; even large jam events would not be captured by the stage gage if the jam formed or broke more than a few kilometers from the gaging station.

Future considerations for developing recurrence intervals for dynamic ice-breakup events may include dating ice-scars throughout the study reaches, as outlined in Boucher (2008) and Boucher et al. (2012). Other methods may parallel what is being done for estimating the recurrence

of ice-thrust events against dams and spillways, with some modifications. The latter approach includes developing a recurrence curve for ice thickness at specific sites. Ice thickness is estimated using accumulated degree-days of freezing. Simplified recurrence curves for dynamic breakups of the ice cover is then approximated with temperature data; if temperature rise is in excess of a critical rate for temperature rise, dynamic ice-breakups are assumed to occur. Temperature data are often used from the closest weather station. In reality, variations in the rate of temperature rise may differ through the river corridor leading to complex scenarios of dynamic ice breakups in some locations but not in others. However, a long temperature record that matches the length of the flow record, and at multiple locations along the study reach, does not exist for the Susitna River. Yet, the simplified temperature approach may provide a decent first approximation to the frequency of dynamic ice-breakup events.

6.4.3 *Comparison with Other River Systems*

A general comparison of rates of erosion on the Susitna River with rates at other river systems with a similar channel classification is possible. Albeit approximate, the comparison enables the rates of erosion on the Susitna River to be put into a broader context.

Lagasse et al. (2004) documented, for open-water flows, the rate and extent of channel migration for a range of different river systems using time-sequential aerial photography. Specifically, the apex of meander bends was monitored through time and converted into erosion rates by channel width per year. Rivers analyzed as part of the Lagasse et al. (2004) study were predominantly single channel as categorized according to Brice (1975). The channel system that most resembled the Susitna River (C sites from Lagasse et al. [2004]) had a mean migration rate of 0.032 channel widths per year, or approximately 1 channel width in 30-years.

In comparison, along the Middle Susitna River, the extent and rates of erosion between 1951 to 1983 and 1983 to 2012 for Reaches 6 and 7 were much less. Erosion rates in Reach 6 were 0.0038 (1951 to 1983) and 0.0021 (1983 to 2012). Erosion rates in Reach 7 were 0.0018 (1951 to 1983) and 0.001 (1983 to 2012). The erosion rates developed for the Susitna River using reach-average data ranged from 8 to 31 times less than comparable sites from Lagasse et al. (2004).

To better compare rates of erosion on the Susitna River to erosion rates from the rivers monitored in Lagasse et al. (2004), the apex of channel bend migration was also measured for 22 sites on the Susitna River. Apex channel migration ranged from 0.0008 to 0.009 with an average of 0.003 channel widths per year. This results in erosion rates 11.5 times less than comparable sites from Lagasse et al. (2004).

The lower rates of bank erosion along the Middle Susitna River, being a factor of 10 less than comparable channel systems, indicate a rather stable river system. Low rates of erosion have also been observed in other boreal rivers (Scott, 1978). Rates on the Sagavanirktok River, Alaska (Brice, 1971) and rivers in the Canadian Arctic (Lewis and McDonald, 1973) were surprisingly low on the reach-scale though significant local lateral retreat did occur. Brice (1971) also indicated that the planform of the Sagavanirktok River was similar over a 20-year period; consistent with planform observations on the Susitna River. Scott (1978) suggests that the overall low long-term rates of erosion, described by Brice (1971) and Lewis and McDonald (1973), may be due to the timing of erosion; whereby most erosion occurs in small increments during the spring breakup flooding. The results described herein for the Susitna River, indicate that the timing of erosion also occurs during breakup flooding but more likely occurs in large increments rather infrequently.

These comparisons are made with caution, as direct comparisons between river systems are not possible. For example, the rivers described by Brice (1971) and Lewis and McDonald

(1973) are inset within permafrost terrain, a condition not present in the study reaches of the Susitna River. However, the analysis and comparison of erosion rates in northern environments does necessitate further study, as a changing climate may affect key erosional processes and have implications for downstream changes in sediment and flow supply (McNamara and Kane, 2009).

It is possible that lower rates of geomorphic change on the Susitna River are due to the changed hydrologic and sedimentologic regimes following the Little Ice Age. The Little Ice Age, which reworked alluvial and glacial material along the Middle Susitna River, left coarser sediment material that contemporary flows are insufficient to mobilize on a relatively frequent basis. Hence, the Middle Susitna River could be a non-regime channel whereby geomorphic change predominantly occurs in the wider valley bottom regions upstream of constrictions where there is aggradation of sand-size and finer sediments that can be reworked under the contemporary hydrologic conditions.

Yet the findings that ice-induced processes appear to be dominant in causing large-scale channel changes suggest that the current hydrologic regime is capable of reworking channel material, but only under specific conditions; i.e., during dynamic ice-breakup conditions which requires a rather cold winter followed by rapid warming that is able to maintain the strength of in-channel ice blocks and sufficiently raise water flows to cause ice jamming. This insight offers another explanation as to the low rates of channel change: the conditions required to cause a dynamic breakup occur rather infrequently.

Low rates of channel change may likely be a product of both the above explanations: the Little Ice Age left a coarser lag deposit and the current hydrologic regime is largely only able to exceed the threshold for sediment mobilization (and subsequent bank erosion driven by toe scour and ice-abrasion) under specific hydrologic and climatic conditions that occur rather infrequently.

CHAPTER 7: CONCLUSIONS AND RECOMMENDATIONS

This thesis quantified the extent erosion is driven by ice-processes on a large, free-flowing, coarse-bed river. The study illuminated processes causing bank erosion yet also identified critical areas for further research. Study conclusions are organized by the respective study questions in Section 7.1. Recommendations for future research are discussed in Section 7.2.

7.1 Conclusions

1. *When, annually, does the most bank erosion occur (i.e., during the open-water season or when ice is in the channel)?*

The location and extent of bank erosion was determined using sequential aerial photography which captured a thermal and dynamic ice-breakup. Land features were categorized based on type of geomorphic surface, such that varying bank properties could be linked to total erosion. Intermittent site visits flown between the aerial photography datasets were used to identify the timing of erosion within the year (i.e. during the open-water period, ice-breakup period, or a combination of the two). The analysis found the majority of bank-erosion occurs or is initiated when ice is in the channel, during a dynamic ice breakup. This condition may persist for only a few days in several years. This conclusion is supplemented by numerical modeling indicating fluvial bed shear stresses are insufficient to mobilize the bank toe material in many areas along the study reach (Section 2.8 and Section 5.2.1.2).

2. *What processes drive bank erosion along the boreal Middle Susitna River?*

Bank erosion processes were characterized into time periods within the year and summarized by conceptual erosion models (Section 5.1.3). Based on the erosion analysis in question 1,

observational evidence (5.2.1), and quantification of open-water shear stresses (5.2.1.2), the dominant erosion processes were ice-induced flow diversion of water flow and ice floes. Ice-induced erosion processes affect banks and vegetation through shearing, gouging, and stripping. Blocks of ice rubble moving abrasively along vegetated banks, shear bank material and vegetation leaving vertically exposed banks with ice-scarred intact vegetation. However, when the ice is in the form of rubble comprising relatively small blocks (e.g., less than about 2 m in width), the rubble forms a protective shear-wall barrier that causes moving ice not to directly impact the river's banks. Individual large ice floes gouge into banks leaving distinct ridges in the bank material. In particular, ice-floe impact was most pronounced at banks not aligned with the approach flow. While shear stress generated by ice-blocks can be quite high, the effects are often localized.

Vegetated bars and terrace surfaces were the most susceptible to bank erosion by impacting ice floes (Section 5.3.3). Given their relative low elevation in the channel, vegetated bars are subjected more frequently to the effects of ice. Ice rubble collides with vegetation above ground, such that root systems do not protect vegetation against impact. However, bulldozing of low-lying vegetation does not necessarily cause erosion but will cause the vegetation succession to reset. During the dynamic ice-breakup event in 2013, ice reset the vegetation succession on large swaths of mid-channel vegetated bars but did not significantly modify the bankline. Terrace surfaces, slightly higher in elevation than the active floodplain units, and typically vegetated by decadent or minimal top of bank vegetation, more often displayed vertical bank profiles due to the lack of protection from overhanging rootmats.

However, ice exerts both erosive and protective effects on bank erosion. The effects depend on the relative size and velocity of ice moving along a channel. This study found overhanging rootmats, gravel-cobble pavements, and bank-attached ice or ice shear-walls to limit bank erosion.

Erosion on active floodplain surfaces with protective rootmats and gravel-cobble bank toe pavements, was approximately 25 percent of total erosion from both long-term and short-term erosion analyses.

3. *What extent, and why, do erosional processes vary along the study reach?*

Wider sub-reaches with multiple channels were more prone to ice-jamming and subsequent diversion of flow and ice rubble, causing lateral bank retreat. More bank retreat in wider sub-reaches was also due to the increased presence of vegetated bars, active floodplain and terraces surfaces that form in the wider depositional sub-reaches. The wider sub-reaches persist through time and are controlled by geologic and geomorphic constrictions. Additionally, the most vulnerable banks potentially subject to ice erosion are banks aligned somewhat transversely to the main channel, which are more prevalent in the multi-channel Reach 6. Such banks occur at the upstream end of bars and islands, and are especially prone to impact by relatively large ice floes conveyed by water flow. Consequently, bank erosion occurred less in predominantly single-channel reaches than in the predominantly multi-channel reaches.

4. *How do short-term rates compare to long rates of erosion and how do these rates compare to other gravel-bed channels?*

The relative magnitudes of short-term erosion compared to long-term erosion (Section 5.3.2) indicates that large-scale erosion is episodic. Episodic bank erosion is substantiated by the finding that the majority of large-scale bank erosion evaluated over two distinct ice breakup regimes and open-water flows was found to occur or initiate during a dynamic ice-breakup (Section 5.2.1). Dynamic ice breakups may persist for only a few days in several years. and may

help explain why rates of erosion are relatively low in comparison to other rivers (Section 6.4.3). However, low long-term rates of erosion may also be due to erosion-resistance properties of ice and vegetation (Section 6.2). A protective effect from ice includes the formation of gravel-cobble pavements at bank toes. Additionally, protective effects from vegetation include root-reinforced top of bank layers that slump over cantilevered banks effectively providing vegetated rip-rap to an exposed bank face.

7.2 Recommendations for Further Research

Whether ice-processes are responsible for maintaining and forming channel morphology on the Susitna River, is a complex issue. Consequently, scope exists for considerable further research. Fluvial numerical modeling indicates steady-state water flow, in an unblocked or blocked channel (Section 6.1.2), may not be sufficient to mobilize the channel bed and bank material. Yet flow diversion from numerical modeling does suggest erosion prone locations that coupled with ice-rubble and ice floes could cause incision or gouging of the floodplain surfaces. Observations indicate ice-induced diversion of flow and ice rubble can cause formation of secondary channels (Section 6.3). There is a need for a similitude analysis that helps to place the influences in a rational framework regarding channel size and type, ice-piece size, and flow conditions at the time of ice-cover breakup.

In a recent study, Beltaos (2018) and Beltaos et al. (2018), quantified the magnitude of ice-jam release waves, or "javes" on the Athabasca River; even at a moderate discharge, associated water velocities from the jave were equal or greater than velocities during the open-water period at higher discharges. While ice-induced flow diversion may not be sufficient alone to mobilize the bank toe or channel bed on the Susitna River, "javes" could contribute to bed and bank

mobilization and subsequent lateral erosion. An observational and numerical study of "javes" on the Susitna River would be useful for further characterizing possible erosional processes.

Given that the majority of channel-change is driven episodically by a combination of ice and water flow, and the effective discharge of surface building sediment (i.e. gravel), is between the 20- to 50-year peak flow, it is possible that flows of moderate magnitude and frequency, as suggested by Wolman and Miller (1960), may not be the most effective in forming or maintaining the planform and geometry of the channel. This exception to the typical fluvial model has been proposed for other rivers in northern environments (Walker and Hudson, 2003; Kane, 2012). The further study of hydraulic geometry relations on the Susitna River would provide a meaningful contribution to the role of ice and channel form in the growing research of gravel-bed rivers in boreal regions; it may also illuminate whether the current channel form was enlarged by ice or is a relic from an earlier hydrologic and sedimentologic regime.

Regardless, if dynamic ice-breakups are responsible for driving large-scale bank erosion under the current hydrologic and sedimentologic regime, further research regarding the frequency at which these occur, and how these events may be modified due to climate change, is fundamental for predicting the occurrence and maintenance of side channels and side sloughs that are preferential for aquatic habitat.

REFERENCES

ABR, Inc., 2014. Initial Study Report, Part A: Sections 1-6, 8-10, Riparian Vegetation Study Downstream of the Proposed Susitna-Watana Dam, Study Plan Section 11.6. Susitna-Watana Hydroelectric Project, FERC No. P-14241 Filing: June 3, 2014. Prepared for Alaska Energy Authority, Anchorage, Alaska. http://www.susitna-watanahydro.org/wp-content/uploads/2014/05/11.6_RIP_ISR_PartA.pdf

Abramov, R.V., 1957. Nishi vytaivaniya [Thaw-out niches]. *Priroda,* 46(7), pp.112-113.

Alaska Energy Authority (AEA), 2012. Revised Study Plan. Susitna-Watana Hydroelectric Project, FERC Project No. 14241 Submittal: December 14, 2012. http://www.susitna-watanahydro.org/study-plan.

Alaska Power Authority, (APA) 1984. Draft Environmental Impact Statement. Susitna Hydroelectric Project, FERC Project No. 7114 – Alaska. Volume 1 – Volume 7. May 1984. ARLIS document number "APA 1653" at http://www.arlis.org/susitnadocfinder/.

Arctic Environmental Information and Data Center, 1984a. Assessment of the Effects of With-Project Instream Temperatures on Susitna River Ice Processes in the Devil Canyon to Talkeetna Reach. Susitna Hydroelectric Project, FERC Project No. 7114. Submitted to Harza-Ebasco Susitna Joint Venture. Prepared for the Alaska Power Authority. ARLIS document number "SUS 438" at http://www.arlis.org/susitnadocfinder/.

Arctic Environmental Information and Data Center, 1984b. Susitna River Ice Study: 1982-1983. Susitna Hydroelectric Project, FERC Project No. 7114. Under Contract to Harza-Ebasco Susitna Joint Venture. Prepared for Alaska Power Authority. ARLIS document number "APA 472" at http://www.arlis.org/susitnadocfinder/.

Ashton, G.D., 1986. *River and lake ice engineering*, Water Resources Publications, Littleton, Co., U.S.A.

Ashton, W.S., Bredthauer, S.R., 1986. Riverbank Erosion Processes on the Yukon River at Galena, Alaska. In: Proceedings, Cold Regions Hydrology Symposium, Fairbanks Alaska, American Water Resources Association, pp.415-423

Bätz, N., Colombini, P., Cherubini, P., Lane, S.N., 2016. Groundwater controls on biogeomorphic succession and river channel morphodynamics. *Journal of Geophysical Research: Earth Surface*, 121(10), pp.1763–1785.

Beltaos, S., 1995. *River ice jams*, Water Resources Publications, Highlands Ranch, Co., U.S.A.

Beltaos, S., 2018. Erosion potential of dynamic ice breakup in Lower Athabasca River. Part II: Field data analysis and interpretation. *Cold Regions Science and Technology*, 148, pp.77–87.

Beltaos, S., Carter, T., Rowsell, R., Depalma, S, 2018. Erosion potential of dynamic ice breakup in Lower Athabasca River. Part I: Field measurements and initial quantification. *Cold Regions Science and Technology*, 149, pp.16–28.

Beltaos, S., Burrell, B.C., 2005. Field measurements of ice-jam-release surges. *Canadian Journal of Civil Engineering*, 32(4), pp.699–711.

Beltaos, S., 2007. The role of waves in ice-jam flooding of the Peace-Athabasca Delta. *Hydrological Processes*, 21(19), pp.2548–2559.

Best, H., McNamara, J.P., Liberty, L., 2005. Association of ice and river channel morphology determined using ground-penetrating radar in the Kuparuk River, Alaska, Arctic. *Arctic, Antarctic, and Alpine Research*, 37(2), pp.157-162.

Boucher, É., 2008. Analyse hydro-climatique et géomorphologique des déglacements mécaniques de la rivière Necopastic au Québec nordique. Department of Geography, Laval University, Québec, Canada. 153 pp.

Boucher, E., Bégin, Y., and Arseneault, D., 2009. Impacts of recurring ice jams on channel geometry and geomorphology in a small high-boreal watershed. *Geomorphology*, 108(3), pp. 273-281.

Boucher, E., Bégin, Y., Arseneault, D., and Taha, B.M.J., 2012. Long-term and large-scale river-ice processes in cold-region watersheds. In: Church, M., Biron, P., Roy., A (Eds.), *Gravel-Bed Rivers: Processes, Tools, Environments*, John Wiley & Sons, Ltd, Chichester, West Susswex, UK, pp.546-554.

Bray, D.I., 1982. Regime Equations for Gravel-Bed Rivers. In: Hey, R.D, Bathurst, J.C., Thorne, C.R. (Eds), *Gravel-bed Rivers: fluvial processes, engineering, and management,* John Wiley & Sons.

Brice, J.C., 1971. Measurement of lateral erosion at proposed river crossing sites of the Alaska pipeline. U.S. Geologic Survey, Water Resources, Alaska District.

Bunte, K., Abt, S.R., 2001. Sampling Surface and Subsurface Particle-Size Distributions in Wadable Gravel- and Cobble-Bed Streams for Analyses in Sediment Transport, Hydraulics, and Streambed Monitoring. U.S. Dept. of Agriculture, Forest Service, Rocky Mountain Research Station, Fort Collins, Co., U.S.A.

Calkin, P.E., Wiles, G.C., Barclay, D.J., 2001. Holocene coastal glaciation of Alaska. *Quaternary Science Reviews*, 20(1), pp.449-461.

Church, M., Miles, M.J., 1982. Discussion on Processes and mechanisms of bank erosion. In: Hey, R.D, Bathurst, J.C., Thorne, C.R. (Eds), *Gravel-bed Rivers: fluvial processes, engineering, and management,* John Wiley & Sons.

Church M., Slaymaker O., 1989. Disequilibrium of Holocene sediment yield in glaciated British Columbia. *Nature*, 337(6206), pp.452-454.

Collins, C.M. 1990. Morphometric Analyses of Recent Channel Changes on the Tanana River in the Vicinity of Fairbanks, Alaska. USA Cold Regions Research and Engineering Laboratory, CRREL Special Report 90-4.

Curran, J.H., McTeague, M.L., 2011. Geomorphology and Bank Erosion of the Matanuska River, Southcentral Alaska. U.S. Geological Survey Scientific Investigations Report 2011-5214, 52 p.

Czudek, T., Demek, J., 1970. Thermokarst in Siberia and its influence on the development of lowland relief. *Quaternary Research*, 1, pp.103-120.

Dupre, W.R., Thompson, R., 1979. The Yukon Delta: A model for deltaic sedimentation in an ice-dominated environment. *11th Annual Offshore Technology Conf.,* pp. 657-664.

Ettema, R., 2002. Review of Alluvial-channel Responses to River Ice. *Journal of Cold Regions Engineering*,16(4), pp.191-217.

Ettema, R., Kempema, E., 2012. River-Ice Effects on Gravel-Bed Channels. In: Church, M., Biron, P., Roy., A (Eds.), *Gravel-Bed Rivers: Processes, Tools, Environments*, John Wiley & Sons, Ltd, Chichester, West Susswex, UK, pp.525-540.

Ettema, R., Kennedy, J.F., 1982. Ice Study for the Port of Nome, Alaska. Iowa Institute of Hydraulic Research. IIHR Limited Distribution Report No. 101.

Ferrick, M.G., Gatto, L.W., Grant, S.A., 2005. Soil Freeze-Thaw Effects on Bank Erosion and Stability: Connecticut River Field Site, Norwich, Vermont. USA Cold Regions Research and Engineering Laboratory, CRREL Special Report 89-12.

Fischenich, J.C., Allen, H., 2000. Stream Management. U.S. Army Engineer Research and Development Center, Environmental Laboratory, SR-W-001.

Gerard, R., 1989. Hydroelectric Power Development and the Ice Regime of Inland Waters: A Northern Community Perspective. Surface Water Division National Hydrology Research Institute Environment Canada, Saskatoon, Saskatchewan.

Gurnell, A.M., Petts, G.E. 2002. Island-dominated landscapes of large floodplain rivers, a European perspective. *Freshwater Biology*, 47(4), pp.581-600.

HDR Alaska, Inc., 2014a. Initial Study Report, Part A: Sections 1-6, 8-10, Ice Processes in the Susitna River Study, Study Plan Section 7.6. Susitna-Watana Hydroelectric Project, FERC No. P-14241 Filing: June 3, 2014. Prepared for Alaska Energy Authority, Anchorage, Alaska. http://www.susitna-watanahydro.org/wp-content/uploads/2014/05/07.6_ICE_ISR_PartA_1_of_2.pdf

HDR Alaska, Inc., 2014b. 2013 Ice Field Measurements. Appendix B to Initial Study Report, Part A: Sections 1-6, 8-10, Ice Processes in the Susitna River Study, Study Plan Section 7.6. Susitna-Watana Hydroelectric Project, FERC No. P-14241 Filing: June 3, 2014. Prepared for Alaska Energy Authority, Anchorage, Alaska. http://www.susitna-watanahydro.org/wp-content/uploads/2014/05/07.6_ICE_ISR_PartA_2_of_2_Apps.pdf

HDR Alaska, Inc., 2014c. White Paper: Review and Compilation of Existing Cold Regions Hydropower Project Operations and Effects. Appendix C to Initial Study Report Part C:Executive Summary and Section 7. Susitna-Watana Hydroelectric Project, FERC No. P-14241 Filing: June 3, 2014. Prepared for Alaska Energy Authority, Anchorage, Alaska. http://www.susitna-watanahydro.org/wp-content/uploads/2014/06/07.6_ICE_ISR_PartC.pdf

HDR Alaska, Inc., 2014d. Detailed Ice Observations, October 2013 – May 2014. Ice Processes in the Susitna River, Study 7.6. Susitna-Watana Hydroelectric Project, FERC No. P-14241 Filing: September 17, 2014; Technical Memorandum. Prepared for Alaska Energy Authority, Anchorage, Alaska. 71 p. http://www.susitna-watanahydro.org/wp-content/uploads/2014/09/07.6_ICE_TechMemo_2014_0916.pdf

HDR Alaska, Inc., 2015. 2014-2015 Study Implementation Report, Ice Processes in the Susitna River, Study 7.6. Susitna-Watana Hydroelectric Project, FERC No. P-14241 Filing: November 9, 2015. Prepared for Alaska Energy Authority, Anchorage, Alaska. http://www.susitna-watanahydro.org/wp-content/uploads/2015/11/07.6_ICE_SIR.pdf

Hooke, J.M., 1979. An Analysis of the Processes of River Bank Erosion. *Journal of Hydrology*, 42, pp.39-62.

Kellerhals, R., and Church, M., 1980. Comments on "Effect of channel enlargement by river processes on bankfull discharge in Alberta, Canada" by D.G. Smith. *Water Resources Research,* 16(6), pp.1131-1134.

Kindle, E.M., 1918. Notes on sedimentation in the Mackenzie River Basin. *Journal of Geology*, 26, pp.341-360.

Lagasse, P.F, Zevenbergen, L.W., Spitz, W.J., Thorne, C.R., Ayres Associates, Inc., 2004. Methodology for Predicting Channel Migration. Prepared for National Cooperative Highway Research Program. Washington, DC: The National Academies Press. https://doi.org/10.17226/23352.

Lawson, D.E., United States Army Corps of Engineers, Alaska District, Cold Regions Research Engineering Laboratory, 1983. Erosion of perennially frozen streambanks. CRREL Special Report 83-29.

Lawson, D.E., Chacho, E.F., Jr., Brockett, B.E., Wuebben, J.L., Collins, C.M., Arcone, S.A., Delaney, A.J., and Cold Regions Research Engineering Laboratory, 1986. Morphology, hydraulics and sediment transport of an ice-covered river: Field Techniques and initial data. CRREL Special Report 86-11.

Lewis, C.P., McDonald, B.C., 1973. Rivers of the Yukon north slope. In: Fluvial processes and sedimentation: Proc. Hydrology Symposium no. *9*, Univ. of Alberta, Edmonton, pp.251-271.

Luckman, B.H., 2000. The Little Ice Age in the Canadian Rockies. *Geomorphology*, 32(3), pp.357-384.

Marusenko, Y. I., 1956. The Action of Ice on River Banks. *Priroda*, 12, pp.91-93. *In Russian.*

MacKay, D.K., Sherstone, D.A., Arnold, K.C., 1974. Channel ice effects and surface water velocities from aerial photography of Mackenzie River breakup. In: Hydrological Aspects of Northern Pipeline Development. Environmental Social Committee, Northern Pipelines, Task Force on Northern Oil Development, Report No. 74-12, pp.71-107.

Mackay, J.R., MacKay, D.K., 1977. The stability of ice-push features, Mackenzie River, Canada. *Canadian Journal of Earth Sciences*, 14(10), pp.2213-2225.

McNamara, J.P., 2012. Is there a Northern Signature on Fluvial Form? In: Church, M., Biron, P., Roy., A (Eds.), *Gravel-Bed Rivers: Processes, Tools, Environments*, John Wiley & Sons, Ltd, Chichester, West Susswex, UK, pp.541-545.

McNamara, J.P., Kane, D.L, 2009. The impact of a shrinking cryosphere on the form of arctic alluvial channels. *Hydrological Processes*, 23(1), pp159-168.

Michel, B., 1971. Winter Regime of Rivers and Lakes. Cold Regions Science and Engineering Monograph III-B1a.

Miles, M., 1976. An Investigation of Riverbank and Coastal Erosion, Banks Island, District of Franklin. Geological Survey of Canada, Paper no. 76-1A, 1976, pp.195-200.

Millar, R.G., 2000. Influence of bank vegetation on alluvial channel patterns. *Water Resources Research*, 36(4), pp.1109-1118.

Nanson, G.C., Hickin, E.J., 1986. A statistical analysis of bank erosion and channel migration in western Canada. *Geological Society of America Bulletin,* 97, pp.497-504.

Niehus, C.A., 2002. Evaluation of Factors Affection Ice Forces at Selected Bridges in South Dakota. U.S. Geological Survey Water Resources Investigations Report 02-4158. https://pubs.usgs.gov/wri/wri024158/wri024158_files/wri024158.pdf

Oatley, J. A., 2002. Ice, bedload transport, and channel morphology on the upper Kuparuk River. Master thesis. University of Alaska Fairbanks, 92 pp.

Outhet, D.N. 1974. Progress Report on Bank Erosion Studies in the Mackenzie River Delta, N.W.T. In: Hydrological Aspects of Northern Pipeline Development. Environmental Social Committee, Northern Pipelines, Task Force on Northern Oil Development, Report No. 74-12.

Pollen, N., Simon, A., 2005. Estimating the mechanical effects of riparian vegetation on stream bank stability using a fiber bundle model. *Water Resources Research*, 41(7).

Prowse, T.D., 1986. Ice jam characteristics, Liard-Mackenzie rivers confluence. *Canadian Journal of Civil Engineering*, 13(6), 653-665.

Prowse, T.D., 2001. River-Ice Ecology. I: Hydrologic, Geomorphic, and Water-Quality Aspects. *Journal of Cold Regions Engineering*, 15(1), pp.1-16.

Prowse, T.D. Culp, J.M., 2003. Ice breakup: a neglected factor in river ecology. *Canadian Journal of Civil Engineering*, 30(1), pp.128–144.

R&M Consultants, Inc., 1981. Ice Observations 1980-1981. Susitna Hydroelectric Project. Under Contract to Harza-Ebasco Susitna Joint Venture. Prepared for Acres American Incorporated. ARLIS document number APA 32 at http://www.arlis.org/susitnadocfinder/.

R&M Consultants, Inc., 1984. Susitna River Ice Study: 1982-1983. Under Contract to Harza-Ebasco Susitna Joint Venture. Prepared for Alaska Power Authority. Final Report. Document No. APA 472 at http://www.arlis.org/susitnadocfinder/.

R2, 2014. Riparian Instream Flow Groundwater/Surface Water Study. Susitna-Watana Hydroelectric Project, FERC No. P-14241 Filing: September 30, 2017; Technical Memorandum. Prepared for Alaska Energy Authority, Anchorage, Alaska. 58 p. http://www.susitna-watanahydro.org/wp-content/uploads/2014/09/07.5_GW_GWS_T5_TM_Riparian_Final_Draft_20140926.pdf

Reyes, A.V., Luckman, H.H., Smith, D.J., Clague, J.J., and Van Dorp, R.D., 2006. Tree ring dates for the maximum Little Ice Age advance for Kaskawulsh Glacier, St. Elias Mountains, Canada. *Arctic*, 59 (1), pp.14-20.

Ritchie, W. and H.J. Walker. 1974. Riverbank forms of the Colville River delta. In: Reed Jr., J.C., Sater, J.E. (Eds), *The Coast and Shelf of the Beaufort Sea*, Arctic Institute of North America, Washington, D.C., pp. 545-562.

Schiechtl, H., 1980. *Bioengineering for Land Reclamation and Conservation*. The University Alberta Press, Edmonton, Canada.

Schumm, S.A., 2005. *River Variability and Complexity*. Cambridge Univ. Press. Cambridge, U.K., 220 p.

Scrimgeour, G.J., Prowse, T.D., Culp, J.M., Chambers, P.A., 1994. Ecological effects of river ice break-up: a review and perspective. *Freshwater Biology*, 32, pp.261-275.

Scott, K.M. 1978. Effects of Permafrost on Stream Channel Behavior in Arctic Alaska. Geological Survey Professional Paper 1068.

Simon A, Collison A.J.C, 2002. Quantifying the mechanical and hydrologic effects of riparian vegetation on streambank stability. *Earth Surface Processes and Landforms*, 27(5), pp.527-546.

Smith, D.G., 1976. Effect of vegetation on lateral migration of anastomosed channels of a glacier meltwater river. *Geological Society of America Bulletin*, 87(6), pp.857-860.

Smith, D.G., 1979. Effects of channel enlargement by river ice processes on bankfull discharge in Alberta, Canada. *Water Resources Research*, 15(2), pp.469-475.

Smith, D.G., 1980. River ice processes: thresholds and geomorphic effects in northern and mountain rivers. In: Coates, D.R., Vitek, J.D. (Eds), *Thresholds in Geomorphology*, George Alleen and Unwin, London, pp.323-345.

Smith, D.G, Pearce, C.M., 2002. Ice jam-caused fluvial gullies and scour holes on northern river flood plans. *Geomorphology* 42(1), pp.85-95.

Sutherland, A.J., 1987. Static armor layers by selective erosion. In: Thorne, C.R., Bathurst, J.C., Hey, R.D. (Eds), *Sediment Transport in Gravel-Bed Rivers*, John Wiley, Chichester, pp.243-267

Tetra Tech. 2013a. Stream Flow Assessment. Susitna-Watana Hydrolectric Project, FERC No. P-14241. Prepared for Alaska Energy Authority, Anchorage, Alaska. 103 p. http://www.susitna-watanahydro.org/wp-content/uploads/2013/03/SuWa-2012-StreamFlow.pdf

Tetra Tech 2013b. Mapping of Aquatic Macrohabitat Types at Selected Sites in the Middle and Lower Susitna River Segments from 1980s and 2012 Aerials. Susitna-Watana Hydroelectric Project, FERC No. P-14241. Prepared for Alaska Energy Authority, Anchorage, Alaska. 91 p. http://www.susitna-watanahydro.org/wp-content/uploads/2013/03/DRAFT_SuWa-2012-Geomorph-Mapping-TM-03152013.pdf

Tetra Tech. 2014a. Winter Sampling of Main Channel Bed Material. Susitna-Watana Hydroelectric Project, FERC No. P-14241 Filing: September 26, 2014; Technical Memorandum. Prepared for Alaska Energy Authority, Anchorage, Alaska. 68 p. http://www.susitna-watanahydro.org/wp-content/uploads/2014/09/06.6_FGM_2014_Winter_Bed_Material_Sampling_TM_complete.pdf

Tetra Tech, 2014b. 2014 Update of Sediment Transport Relationships and a Revised Sediment Balance for the Middle and Lower Susitna River Segments. Susitna-Watana Hydroelectric Project, FERC No. P-14241 Filing: September 17, 2014. Prepared for Alaska Energy Authority, Anchorage, Alaska. 83 p. http://www.susitna-watanahydro.org/wp-content/uploads/2014/09/06.5_GEO_2014_Sediment_TM-and-Appendices.pdf

Tetra Tech, 2014c. Assessment of the Potential for Changes in Sediment Delivery to Watana Reservoir Due to Glacial Surges. Susitna-Watana Hydroelectric Project, FERC No. P-14241 Filing: November 14, 2014; Technical Memorandum. Prepared for Alaska Energy Authority, Anchorage, Alaska. 21 p. http://www.susitna-watanahydro.org/wp-content/uploads/2014/11/6.5_GEO_2014_Glacial_Surge_TM.pdf

Tetra Tech, 2014d. Study Component 3 – Initial Effective Discharge Analysis for the Mainstem Susitna River and Tributaries. Appendix B to the Geomorphology Study (6.5) Initial Study Report. Susitna-Watana Hydroelectric Project, FERC No. P-14241 Filing: June 3, 2014. Prepared for Alaska Energy Authority, Anchorage, Alaska. http://www.susitna-watanahydro.org/wp-content/uploads/2014/05/06.5_GEO_ISR_PartA_3_of_3_Apps.pdf

Tetra Tech, 2014e. Susitna River Historical Cross Section Comparison. Susitna-Watana Hydroelectric Project, FERC No. P-14241 Filing: September 17, 2014; Technical Memorandum. Prepared for Alaska Energy Authority, Anchorage, Alaska. 53 p. http://www.susitna-watanahydro.org/wp-content/uploads/2014/09/06.5_GEO_2014_Historical_Cross-Section-and-Appendix.pdf

Tetra Tech, 2014f. Mapping of Geomorphic Features and Turnover within the Middle and Lower Susitna River Segments from 1950s, 1980s, and Current Aerials. Susitna-Watana Hydrolectric Project, FERC No. P-14241 Filing: September 26, 2014; Technical Memorandum. Prepared for Alaska Energy Authority, Anchorage, Alaska. http://www.susitna-watanahydro.org/wp-content/uploads/2014/09/06.5_GEO_2014_GeomFeat_Turnover_TM.pdf

Tetra Tech, 2014g. Geomorphology Study, Study Plan Section 6.5, Initial Study Report, Part A: Sections 1-6, 8-10. Susitna-Watana Hydroelectric Project, FERC No. P-14241 Filing: June 3, 2014. Prepared for Alaska Energy Authority, Anchorage, Alaska. http://www.susitna-watanahydro.org/wp-content/uploads/2014/05/06.5_GEO_ISR_PartA_1_of_3.pdf

Tetra Tech, 2014h. Initial Study Report, Part A: Sections 1-6, 8-10, Geomorphology Study, Study Plan Section 6.5 Susitna-Watana Hydroelectric Project, FERC No. P-14241 Filing: June 3, 2014. Prepared for Alaska Energy Authority, Anchorage, Alaska. http://www.susitna-watanahydro.org/wp-content/uploads/2014/05/06.5_GEO_ISR_PartA_1_of_3.pdf

Tetra Tech. 2014i. Updated Mapping of Aquatic Macrohabitat Types in the Middle Susitna River Segment from 1980s and Current Aerials. Susitna-Watana Hydrolectric Project, FERC No. P-14241 Filing: September 26, 2014; Technical Memorandum. Prepared for Alaska Energy Authority, Anchorage, Alaska. http://www.susitna-watanahydro.org/wp-content/uploads/2014/09/06.5_GEO_2014_Updated_AqMacrohabitat_Mapping_TM1.pdf

Tetra Tech, 2015a. Geomorphic Reach Delineation and Characterization, Upper, Middle, and Lower Susitna River Segments – 2015 Update Technical Memorandum. Attachment 1 to 06.05 Geomorphology Study 2014-2015 Study Implementation Report. Susitna-Watana Hydroelectric Project, FERC No. P-14241 Filing: November 2015. Prepared for Alaska Energy Authority, Anchorage, Alaska. 37 p. http://www.susitna-watanahydro.org/wp-content/uploads/2015/10/06.5_GEO_ISR_SIR_Att1_UpdatedReachDelineation.pdf

Tetra Tech, 2015b. 2014-2015 Study Implementation Report, Fluvial Geomorphology Below Watana Dam Study 6.6. Susitna-Watana Hydroelectric Project, FERC No. P-14241 Filing November 9, 2015. Prepared for Alaska Energy Authority, Anchorage, Alaska. http://www.susitna-watanahydro.org/wp-content/uploads/2015/11/06.6_GEOMOD_SIR1.pdf

Tetra Tech, 2015c. 2014-2015 Study Implementation Report, Geomorphology Study, Study Plan Section 6.5. Susitna-Watana Hydroelectric Project, FERC No. P-14241 Filing November 9, 2015. Prepared for Alaska Energy Authority, Anchorage, Alaska. http://www.susitna-watanahydro.org/wp-content/uploads/2015/10/06.5_GEO_ISR_SIR1.pdf

Tetra Tech. 2015d. 2014 Fluvial Geomorphology Model Development. Susitna-Watana Hydroelectric Project, FERC No. P-14241 Filing: November 2015; Study Completion and 2014/2015 Implementation Reports. Attachment 1 to 06.06 Fluvial Geomorphology Modeling below Watana dam 2014-2015 Study Implementation Report. Prepared for Alaska Energy Authority, Anchorage, Alaska. 100 p. http://www.susitna-watanahydro.org/wp-content/uploads/2015/10/06.6_GEOMOD_SIR_Att1_FGMDev.pdf

Tetra Tech, 2015e. 1-D Bed Evolution Model of the Middle and Lower Susitna River: Model Development and Calibration. Susitna-Watana Hydroelectric Project, FERC No. P-14241 Filing: November 2015; Study Completion and 2014/2015 Implementation Reports. Appendix A of Attachment 1 to 06.06 Fluvial Geomorphology Modeling below Watana dam 2014-2015 Study Implementation Report. Prepared for Alaska Energy Authority, Anchorage, Alaska. 87p. http://www.susitna-watanahydro.org/wp-content/uploads/2015/10/06.6_GEOMOD_SIR_Att1_AppA_1D-BEM.pdf

Thorne, C., 1982. Processes and mechanisms of bank erosion. In: Hey, R.D, Bathurst, J.C., Thorne, C.R. (Eds), *Gravel-bed Rivers: fluvial processes, engineering, and management,* John Wiley & Sons.

Thorne, C.R., Tovey, K.N., 1981. Stability of composite river banks. *Earth Surface Processes and Landforms*, 6(5), pp469-484.

United States Army Corps of Engineers, 2016. HEC-RAS River Analysis system Hydraulic Reference Manual, Version 5.0. February. http://www.hec.usace.army.mil/software/hec-ras/documentation/HEC-RAS%205.0%20Reference%20Manual.pdf

Uunila, L.S, 1997. Effects of river ice on bank morphology and riparian vegetation along the Peace River, Clayhurst to Fort Vermilion. *Proceedings of the 9th Workshop on River Ice, Fredericton, New Brunswick, 24-26 September*. Canadian Geophysical Union, pp. 315-334.

Uunila, L., Church, M., 2015. Ice on Peace River: Effects on Bank Morphology and Riparian Vegetation. In: Church, M. (Ed), *The Regulation of Peace River: a Case Study for River Management*, John Wiley & Sons, Ltd., Chichester, West Sussex, UK.

Viereck, L. A., Dyrness, C. T., Batten, A. R., Wenzlick, K.J., 1992. The Alaska Vegetation Classification. General Technical Report PNW-GTR-286. Pacific Northwest Research Station, U.S. Forest Service, Portland, Oregon. 278 p. https://www.fs.fed.us/pnw/publications/pnw_gtr286/

Walker, H.J. and Arnborg, L., 1966. Permafrost and ice-wedge effects on riverbank erosion. In: Permafrost: International Conference, Lafayette, Indiana, Proceedings, National Research Council, Pub. No 1287, pp.164-171.

Walker, J.H., Hudson, P.F., 2003. Hydrologic and geomorphic processes in the Colville River delta, Alaska. *Geomorphology*, 56(3), pp.291–303.

Wentworth, C.K. 1932. Geologic work of ice jams in subarctic rivers. Washington University Studies, St. Louis, 7, pp.49-82.

Wolman, G.M., Miller, J.P., 1960. Magnitude and Frequency of Forces in Geomorphic Processes. *The Journal of Geology,* 68(1), pp.54-74.

Wu, T.H., 2013. Root reinforcement of soil: Review of analytical models, test results, and applications to design. *Canadian Geotechnical Journal,* 50(3), pp.259-274.

Zabilanksy, L.J., Ettema, R.J. Wuebben, J. and Yankielun, N.E., 2002. Survey of River-ice Influences on Channel Bathymetry along the Fort Peck Reach of the Missouri River, Winter 1998-1999. United States Army Corps of Engineers, Cold Regions Research and Engineering Laboratory, Hanover NH, Contract Report.

APPENDIX A: AERIAL PHOTOGRAPHS

LEGEND

500 Meters

2011 Aerial Imagery

June 18 (505 cms) and July 21 (520 cms) for RK 225 to RK 188

May 25 (867 cms) for RK 188 to RK 174

LEGEND

500 Meters

2011 Aerial Imagery

June 18 (505 cms) and July 21 (520 cms) for RK 225 to RK 188

May 25 (867 cms) for RK 188 to RK 174

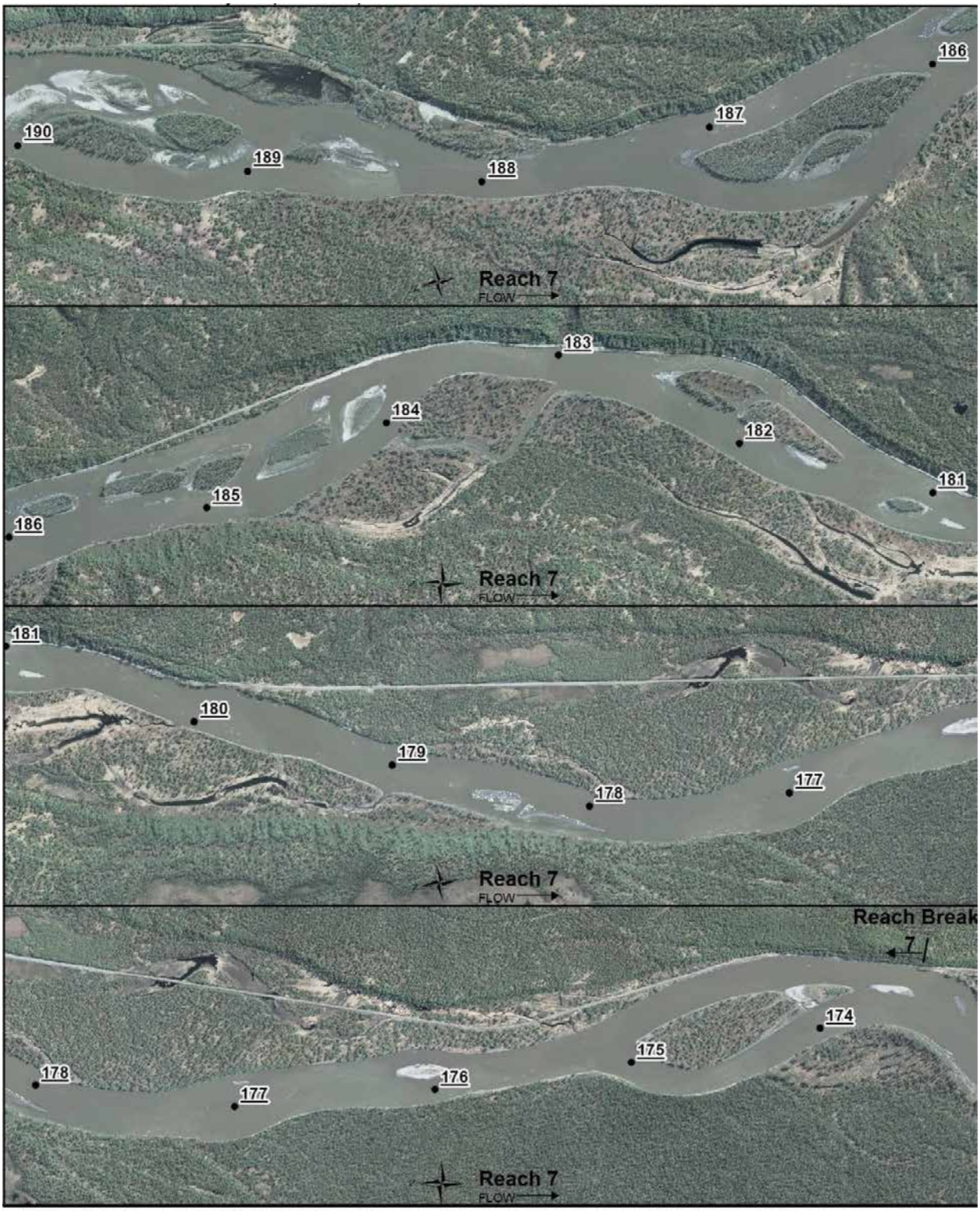

LEGEND

500 Meters

2011 Aerial Imagery

June 18 (505 cms) and July 21 (520 cms) for RK 225 to RK 188

May 25 (867 cms) for RK 188 to RK 174

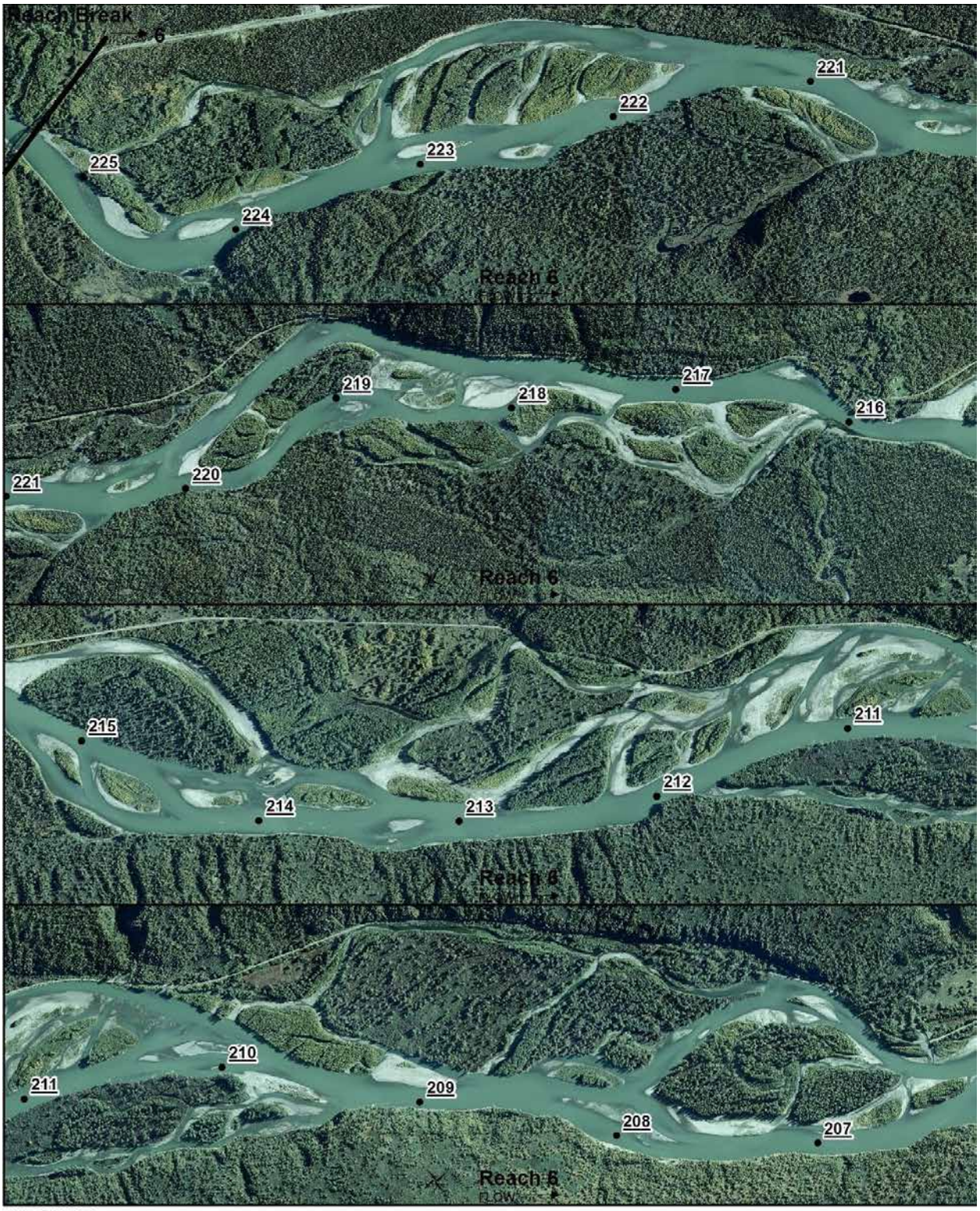
Reach Break
6
1
221
222
223
225
224
Reach 6
219
218
217
216
221
220
Reach 6
215
211
212
214
213
Reach 6
210
211
209
208
207
Reach 6
LEGEND
500
Meters
2012 Aerial Imagery
September 10 (365 cms)


206
205
204
203
202
Reach 6
FLOW
Reach Break
6 7
198
201
202
200
199
Reach 6
FLOW
Reach Break
6 7
195
194
196
197
193
Reach 6
193
192
190
189
191
Reach 6
LEGEND
500
Meters
2012 Aerial Imagery
September 10 (365 cms)


186
187
190
189
188
Reach 7
FLOW
183
184
182
181
185
186
Reach 7
FLOW
181
180
179
177
178
Reach 7
FLOW
Reach Break
7
174
175
178
176
177
Reach 7
FLOW
LEGEND
500
Meters
2012 Aerial Imagery
September 10 (365 cms)

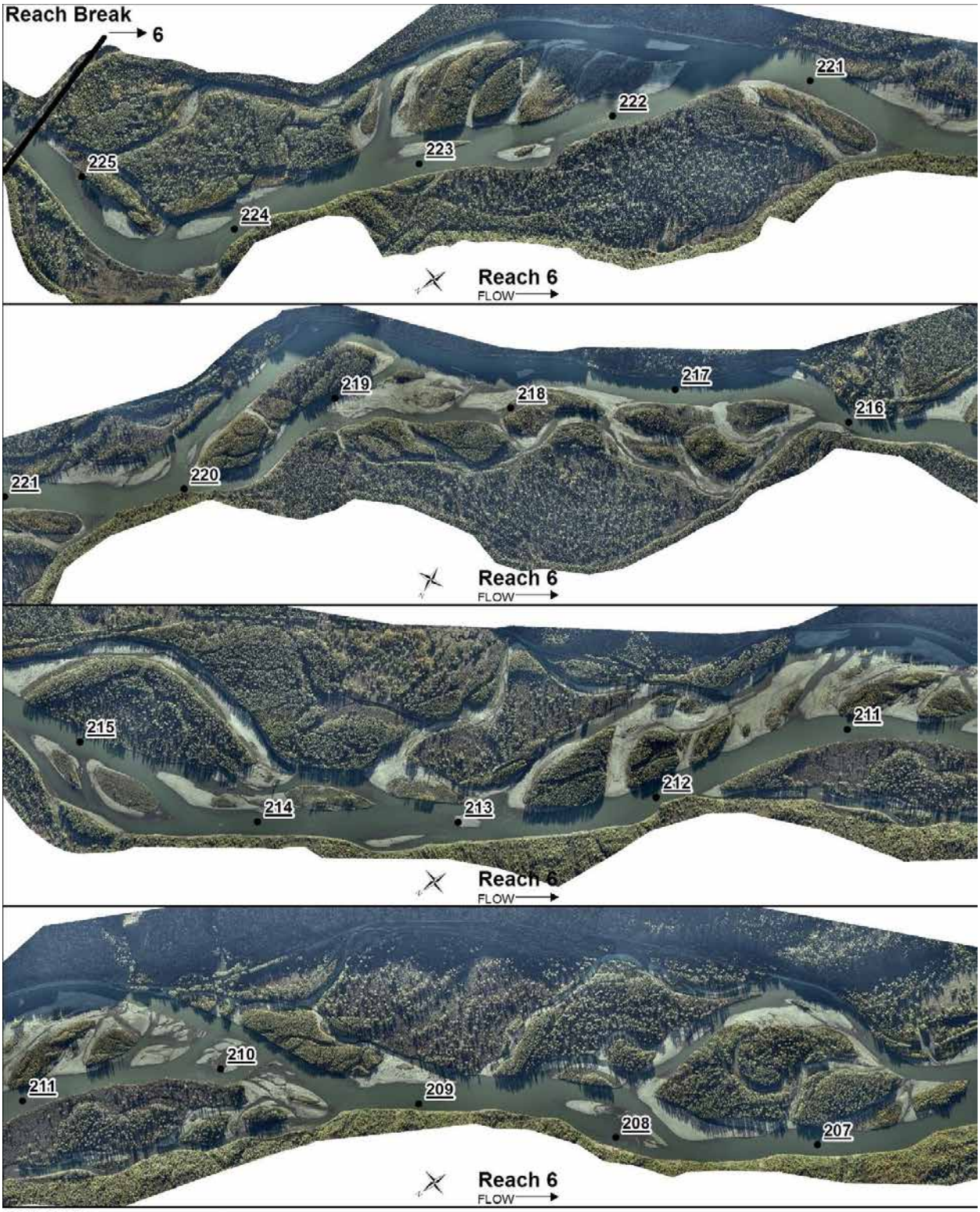
Reach Break
6
225
224
223
222
221
Reach 6
FLOW
221
220
219
218
217
216
Reach 6
FLOW
215
214
213
212
211
Reach 6
FLOW
211
210
209
208
207
Reach 6
FLOW
LEGEND
500
Meters
2013 Aerial Imagery
September 24 (320 cms)

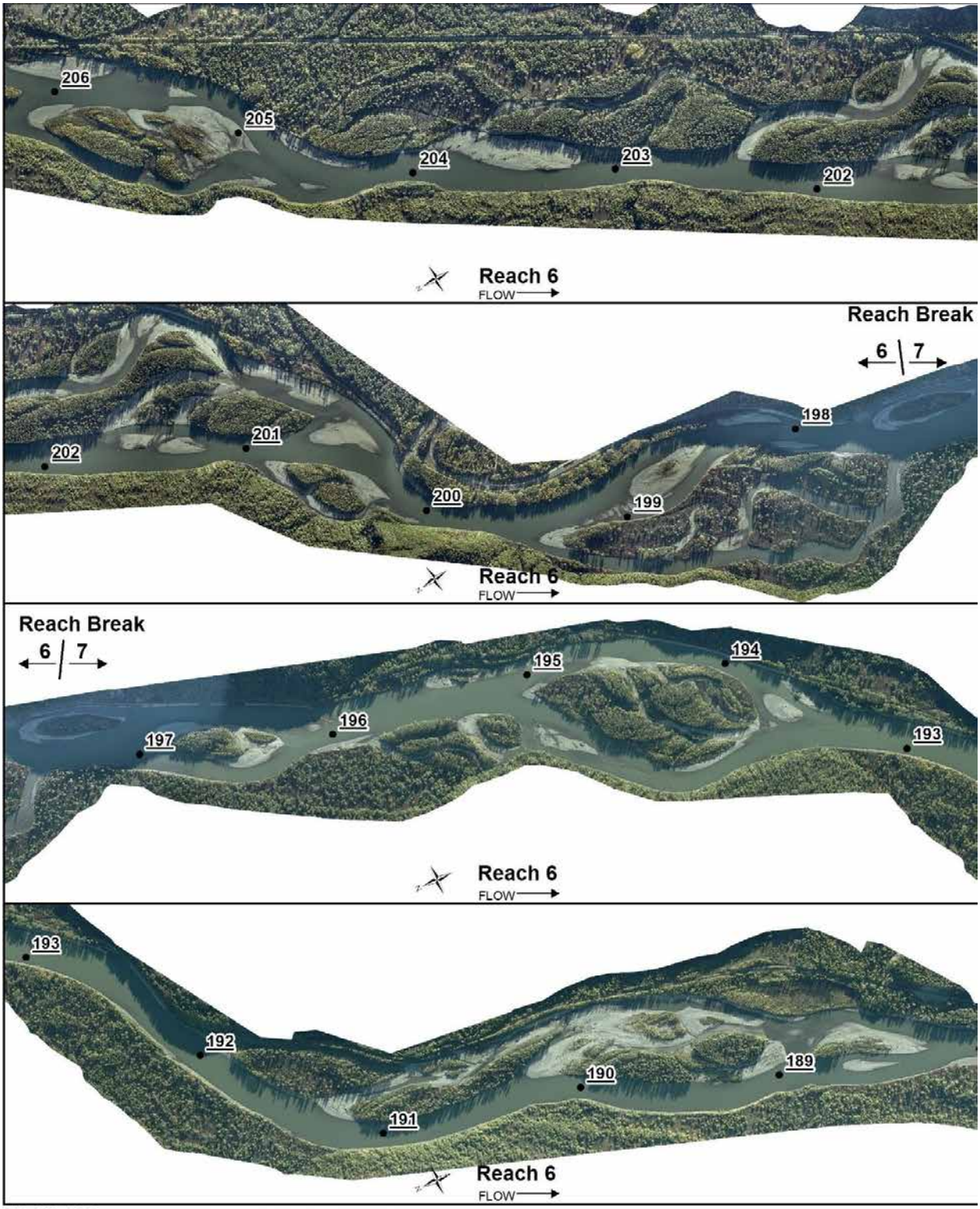
206
205
204
203
202
Reach 6
FLOW
Reach Break
6 | 7
198
201
202
200
199
Reach 6
FLOW
Reach Break
6 | 7
195
194
196
197
193
Reach 6
FLOW
193
192
190
189
191
Reach 6
FLOW
LEGEND
500
Meters
2013 Aerial Imagery
September 24 (320 cms)

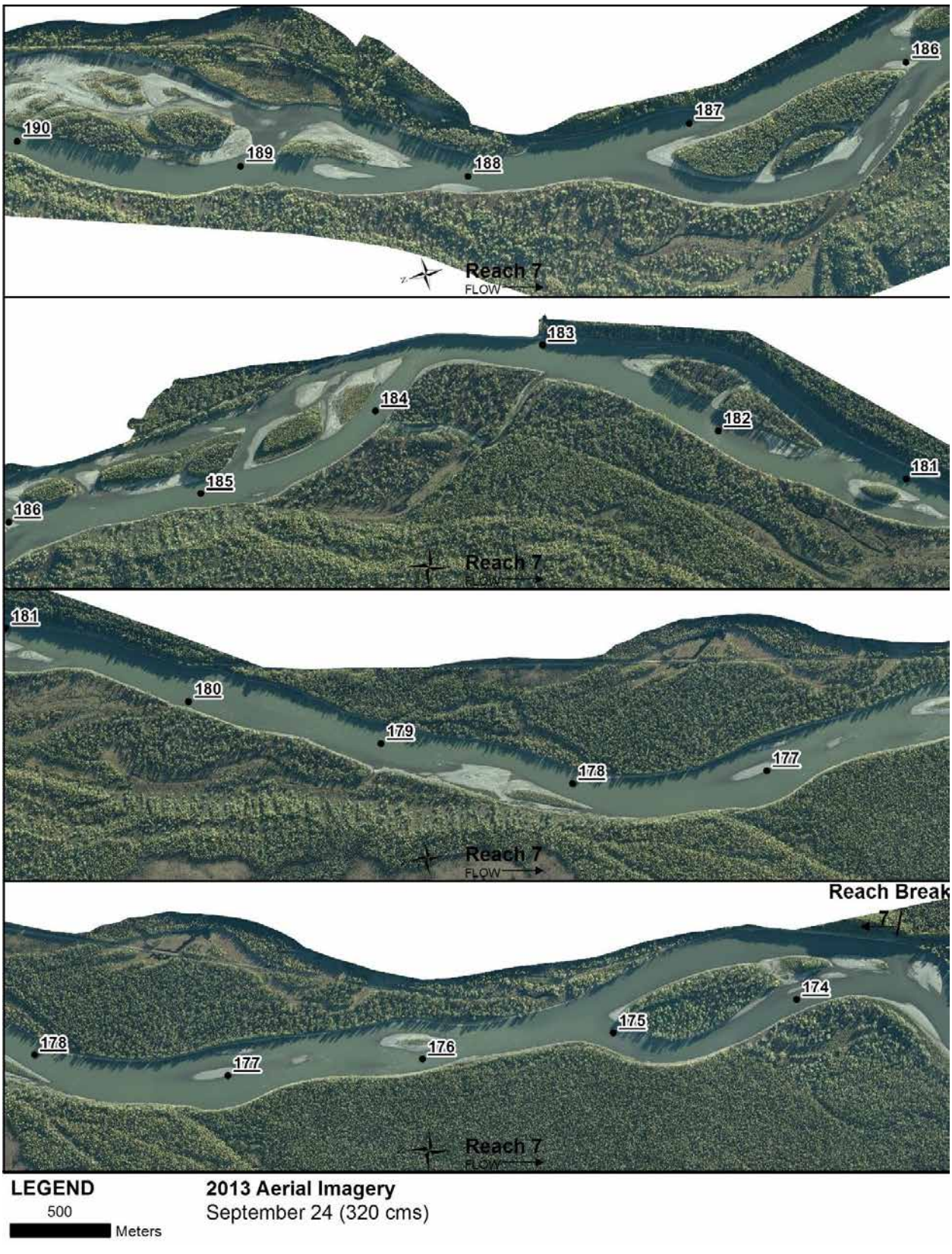
186
187
190
189
188
Reach 7
FLOW
183
184
182
181
185
186
Reach 7
FLOW
181
180
179
178
177
Reach 7
FLOW
Reach Break
7
174
175
178
176
177
Reach 7
FLOW
LEGEND
500
Meters
2013 Aerial Imagery
September 24 (320 cms)

APPENDIX B: 2012-2013 TURNOVER MAPS AND IMAGES BY EROSION LOCATION

B.1 Reach 6

B.1.1 Erosion Location No. 50

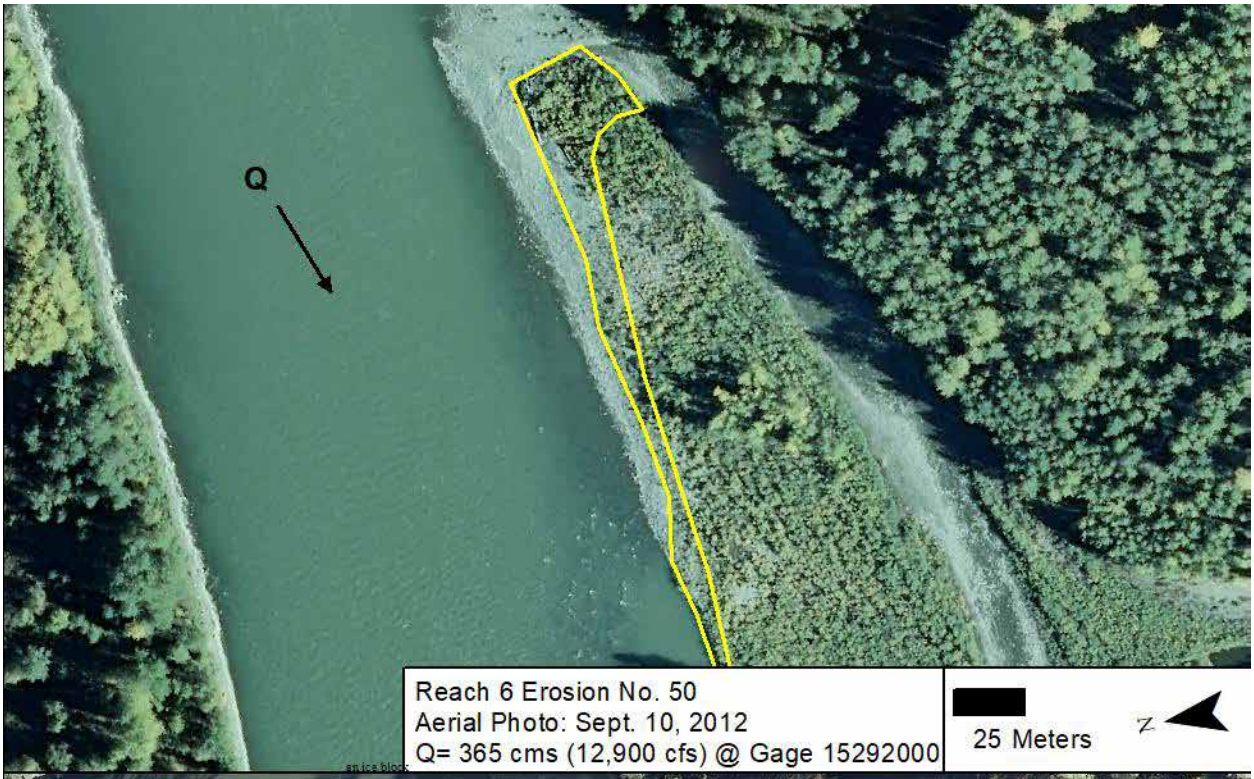

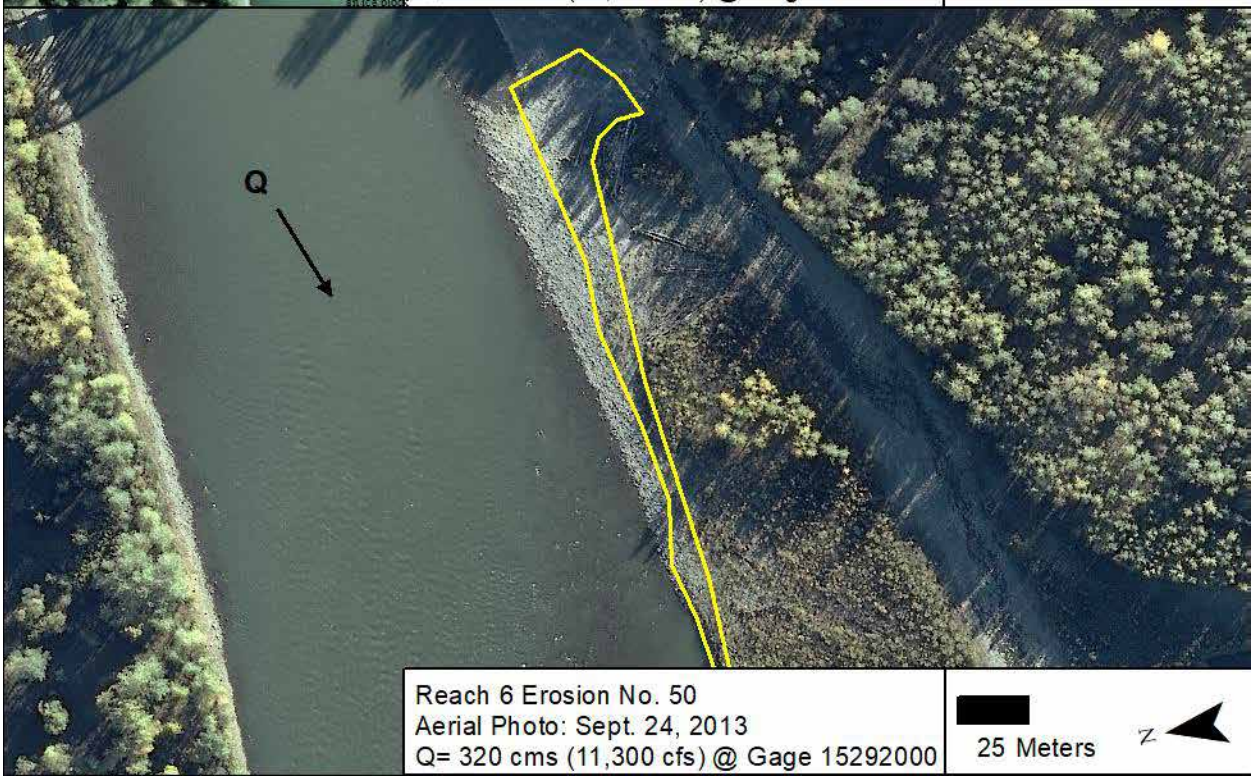

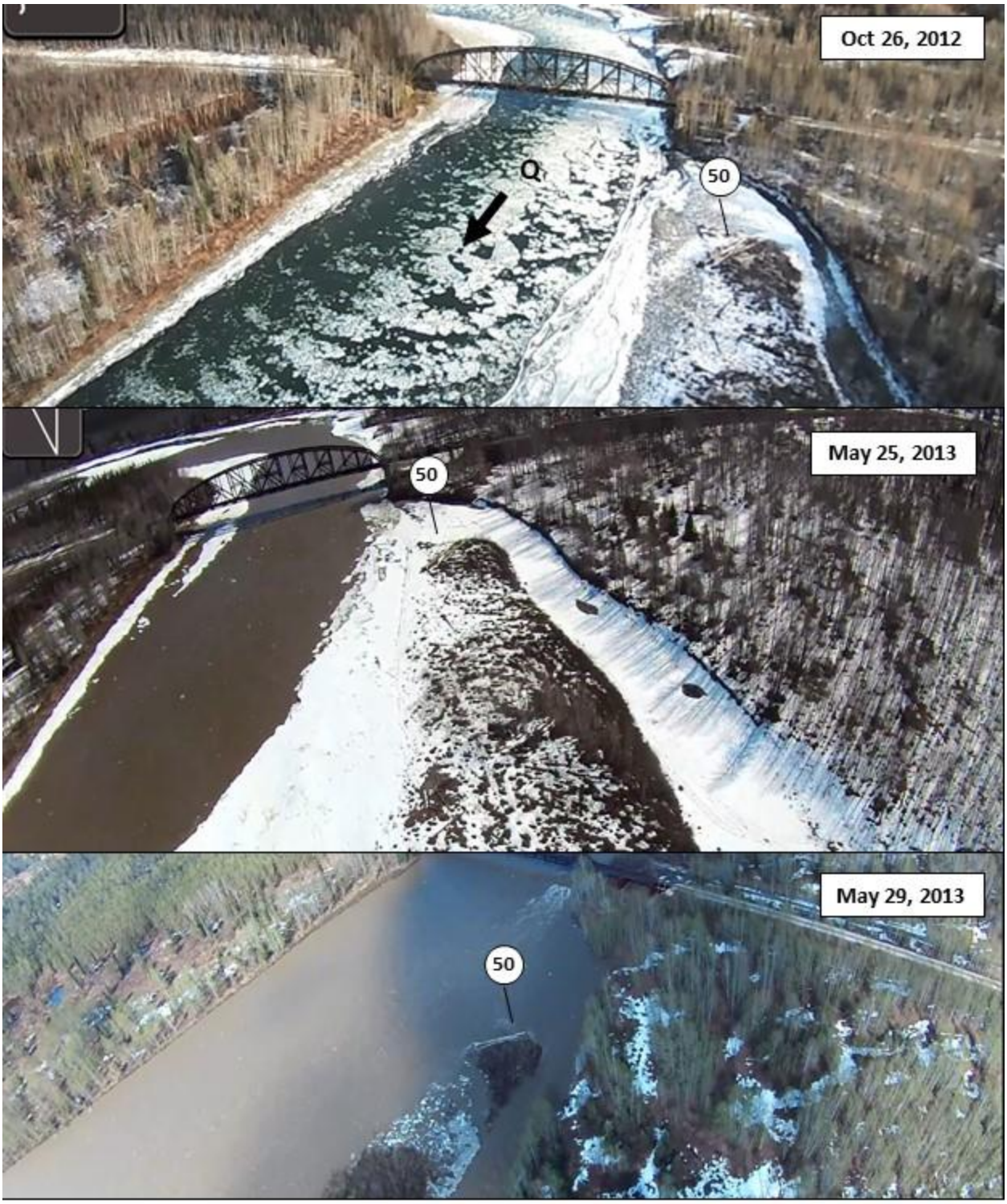
Oct 26, 2012
Q
50
May 25, 2013
50
May 29, 2013
50

B.1.2 Erosion Location No. 49

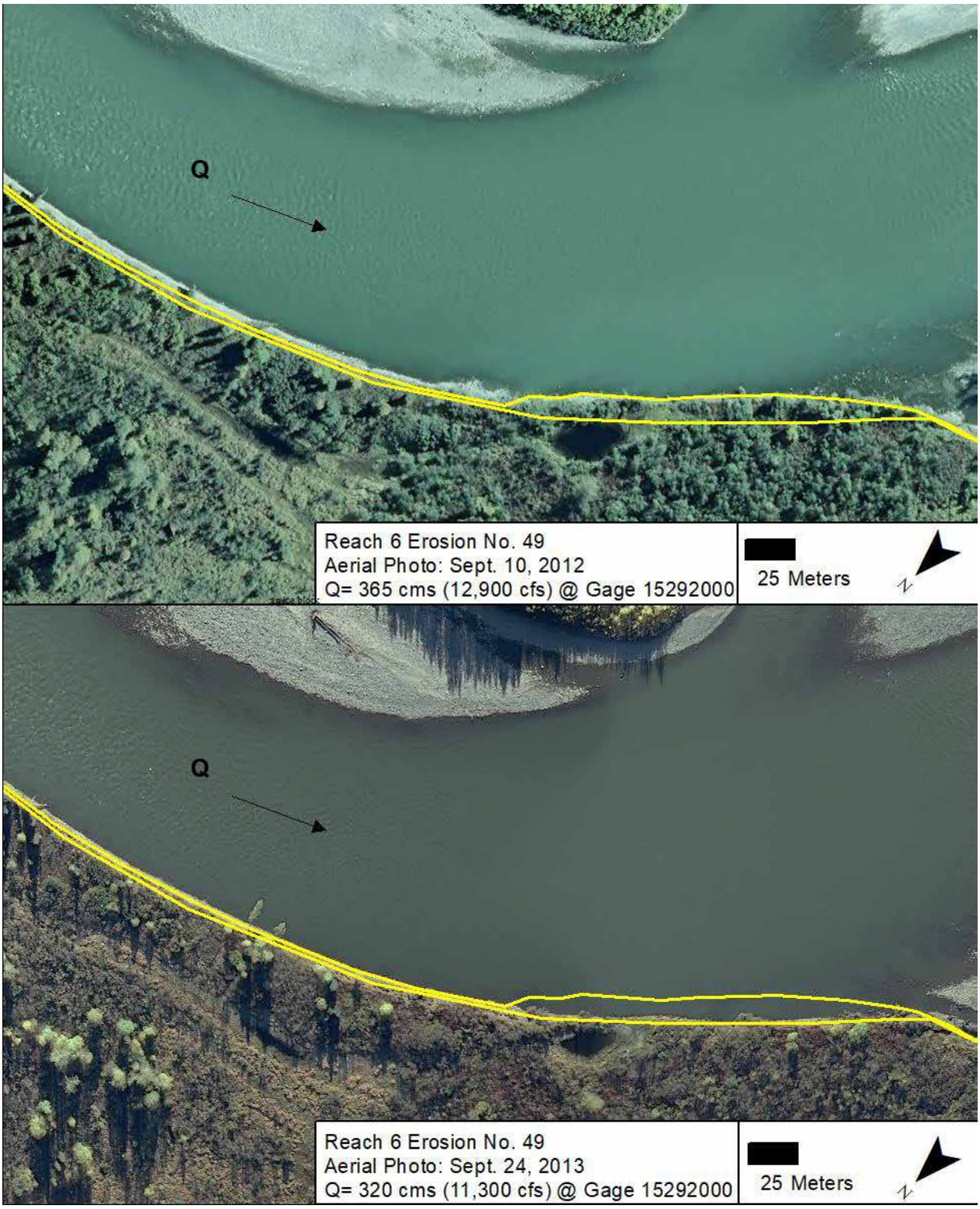


Oct 23, 2012
Q
49
May 26, 2013
49

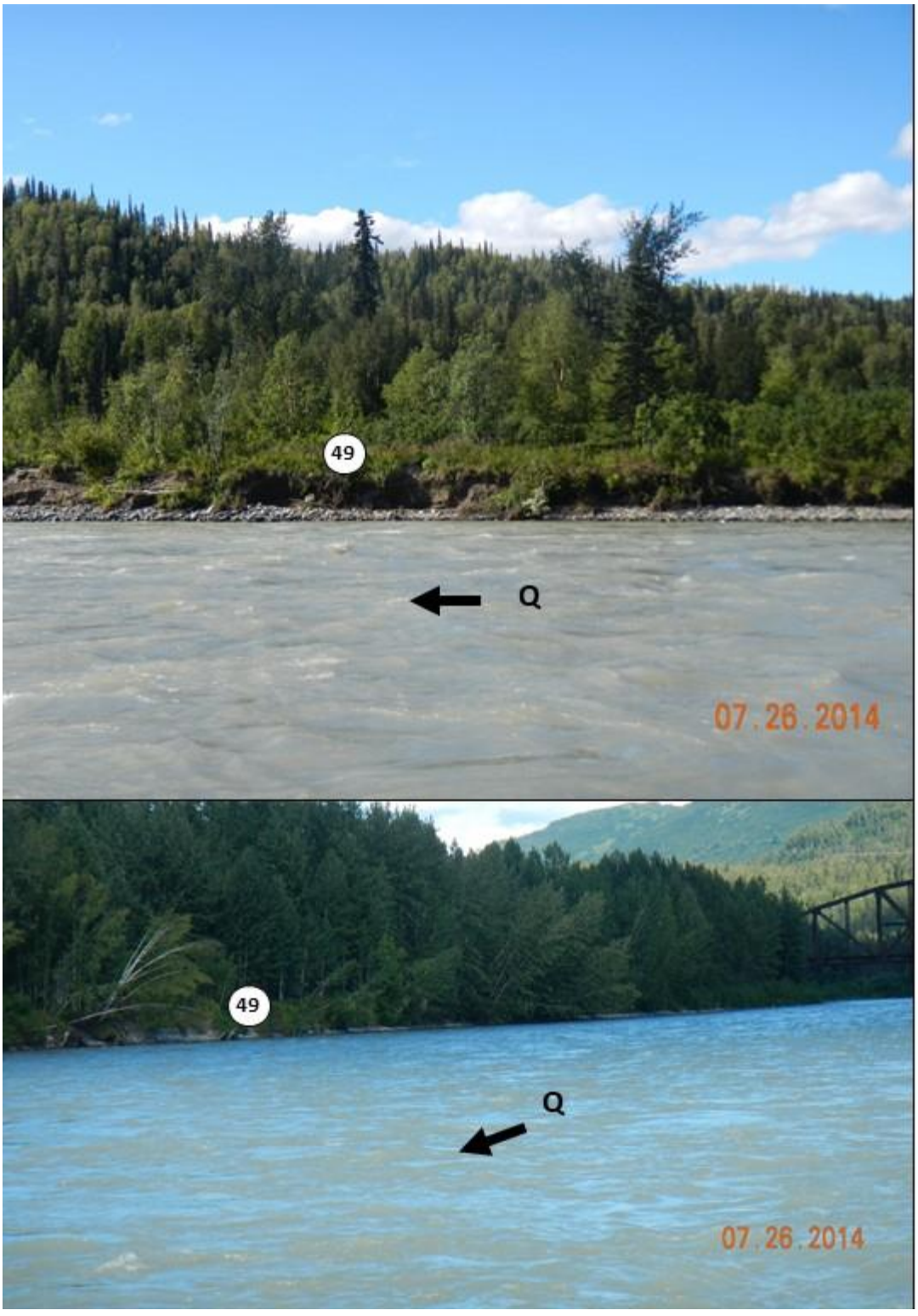
49
Q
07.26.2014
49
Q
07.26.2014

B.1.3 Erosion Location No. 48

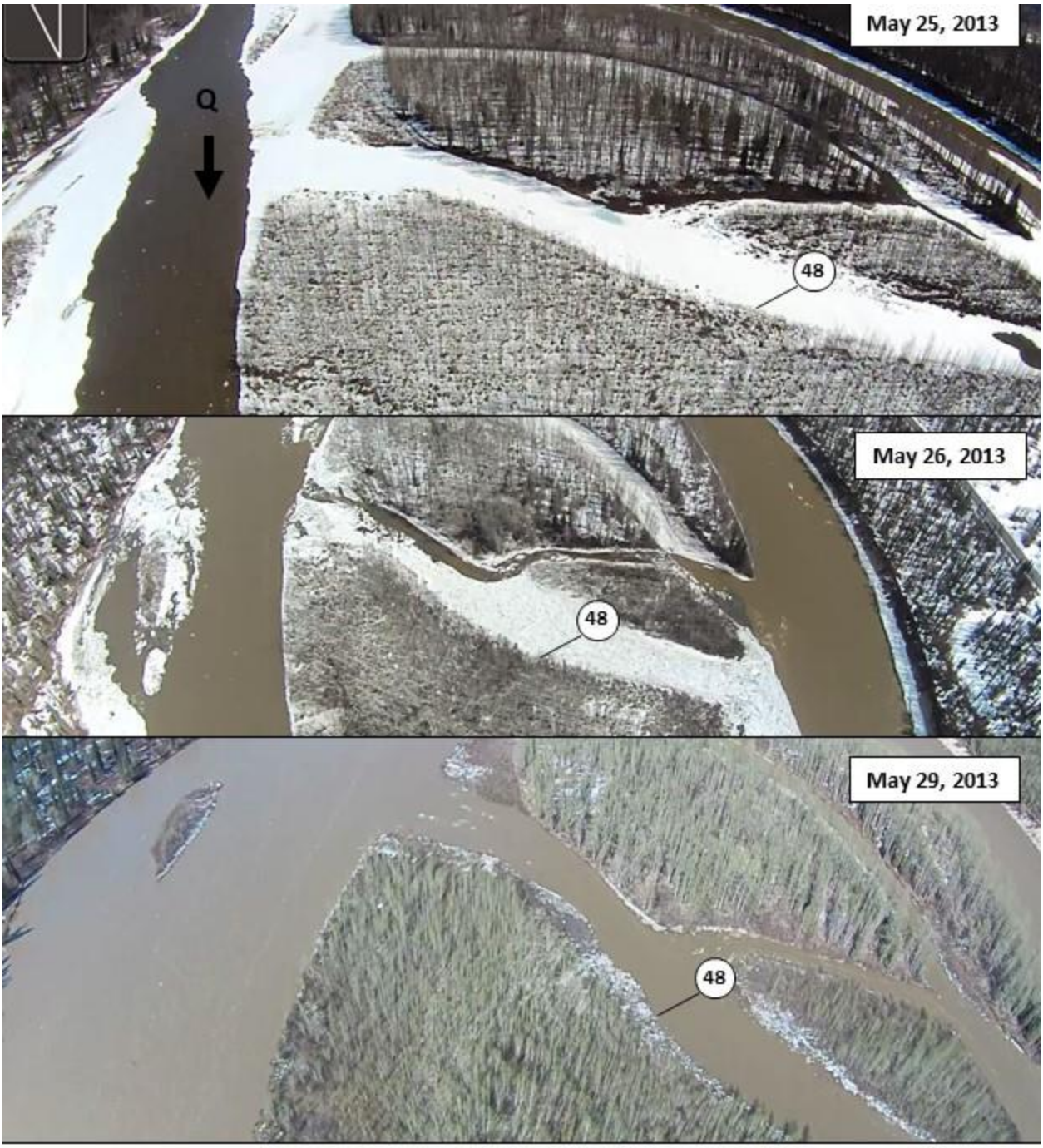
May 25, 2013
Q
48
May 26, 2013
48
May 29, 2013
48

B.1.4 Erosion Location No. 47-46

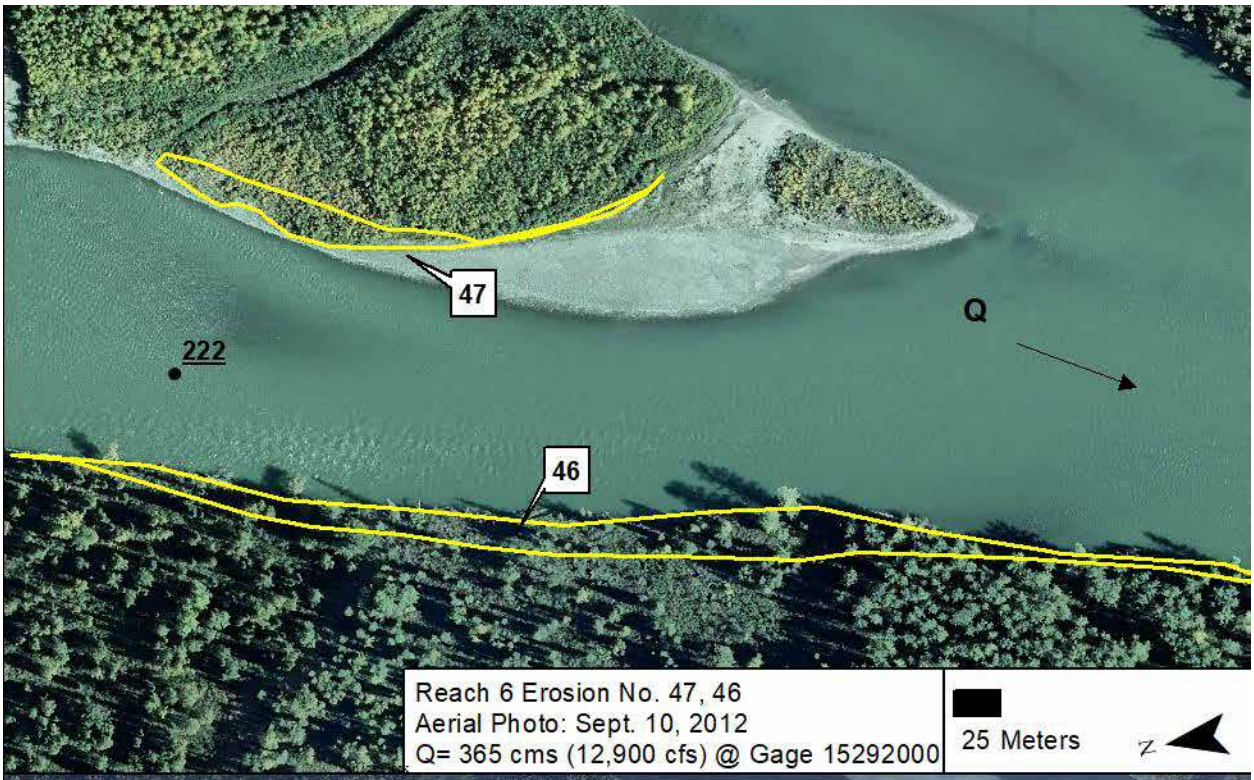

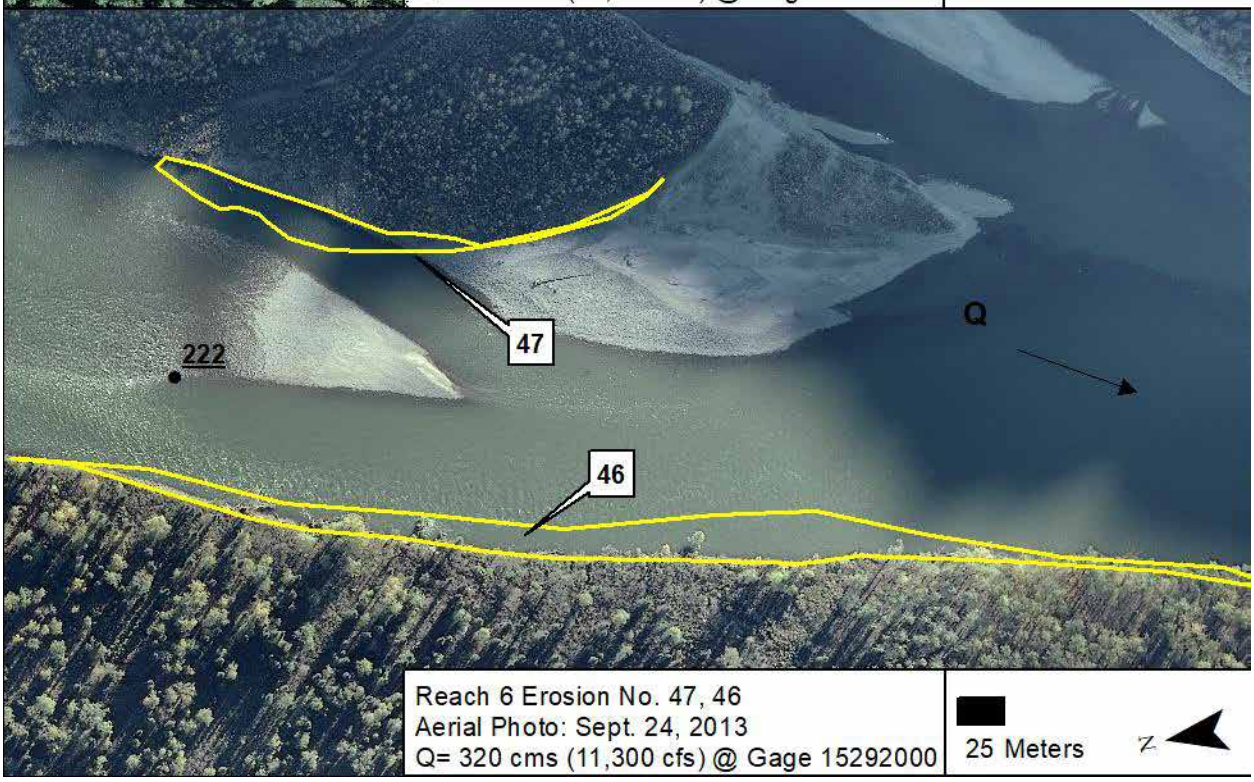

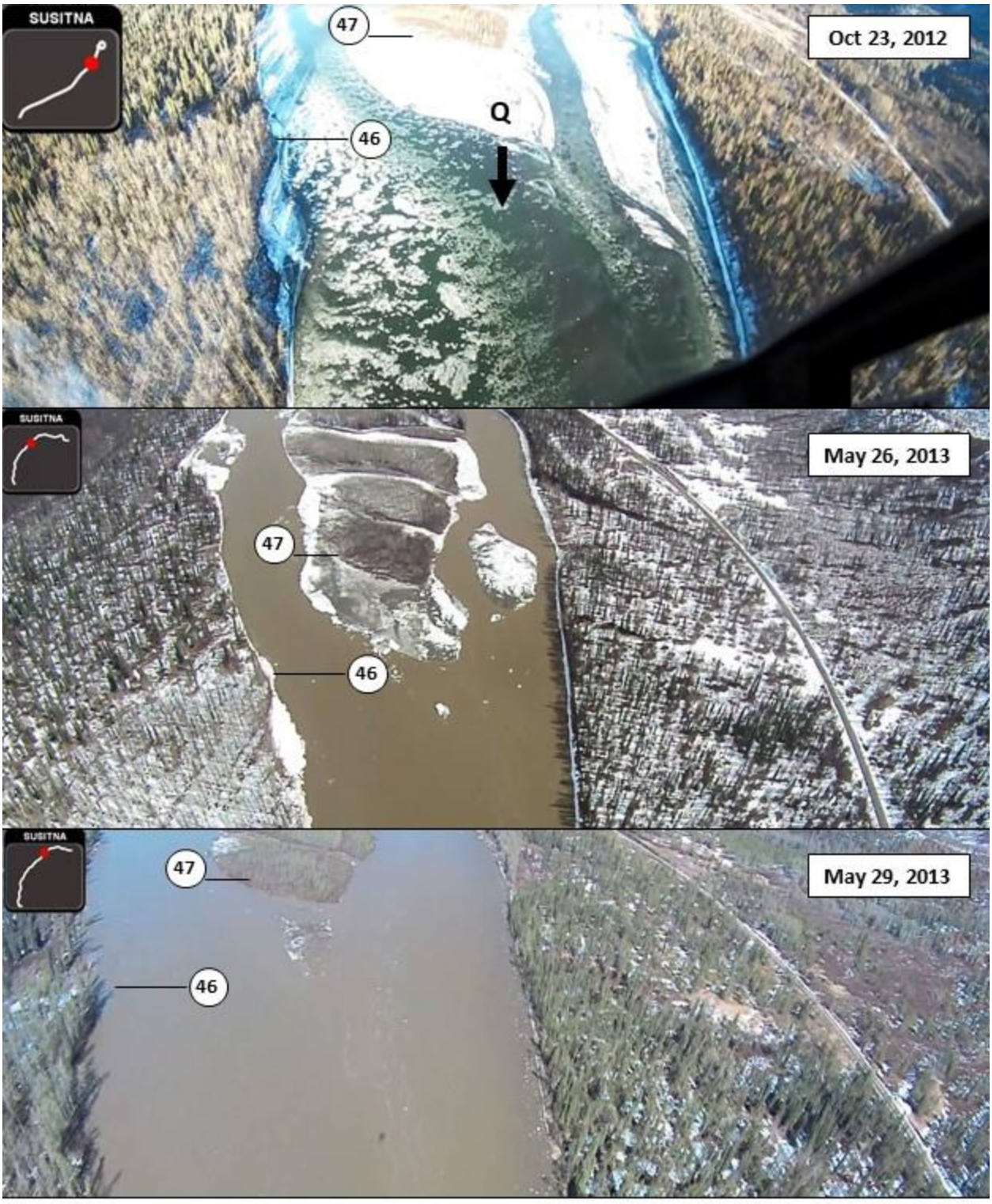
SUSITNA
47
Oct 23, 2012
Q
46
SUSITNA
May 26, 2013
47
46
SUSITNA
47
May 29, 2013
46

B.1.5 Erosion Location No. 45


SUSITNA
Oct 23, 2012
Q
45
SUSITNA
May 26, 2013
45
May 29, 2013
45

B.1.6 Erosion Location No. 44

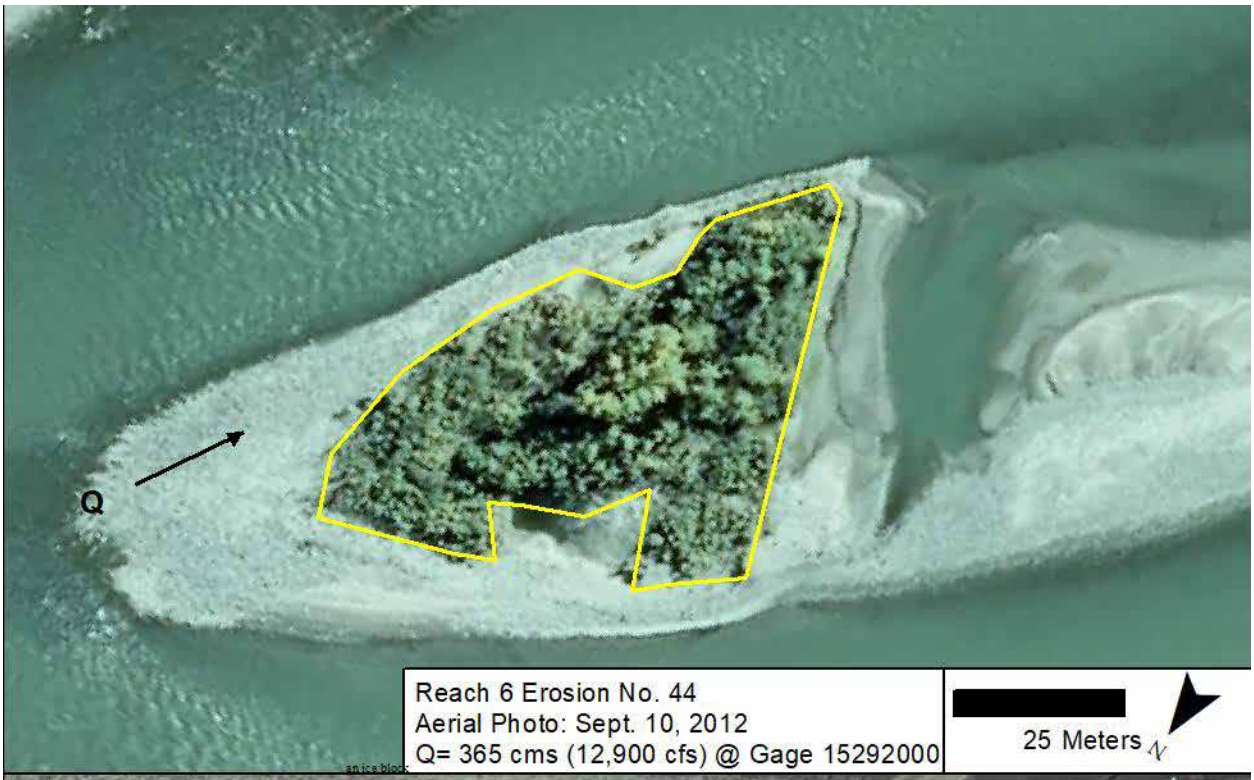

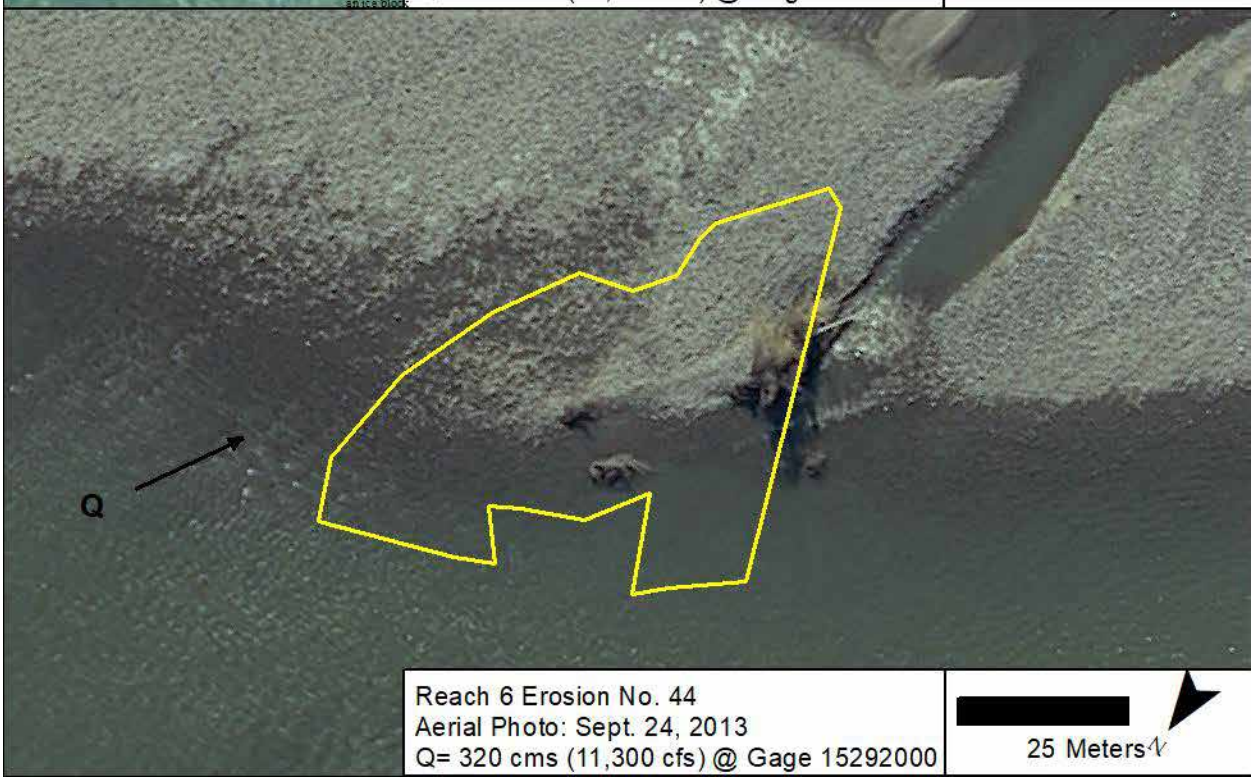

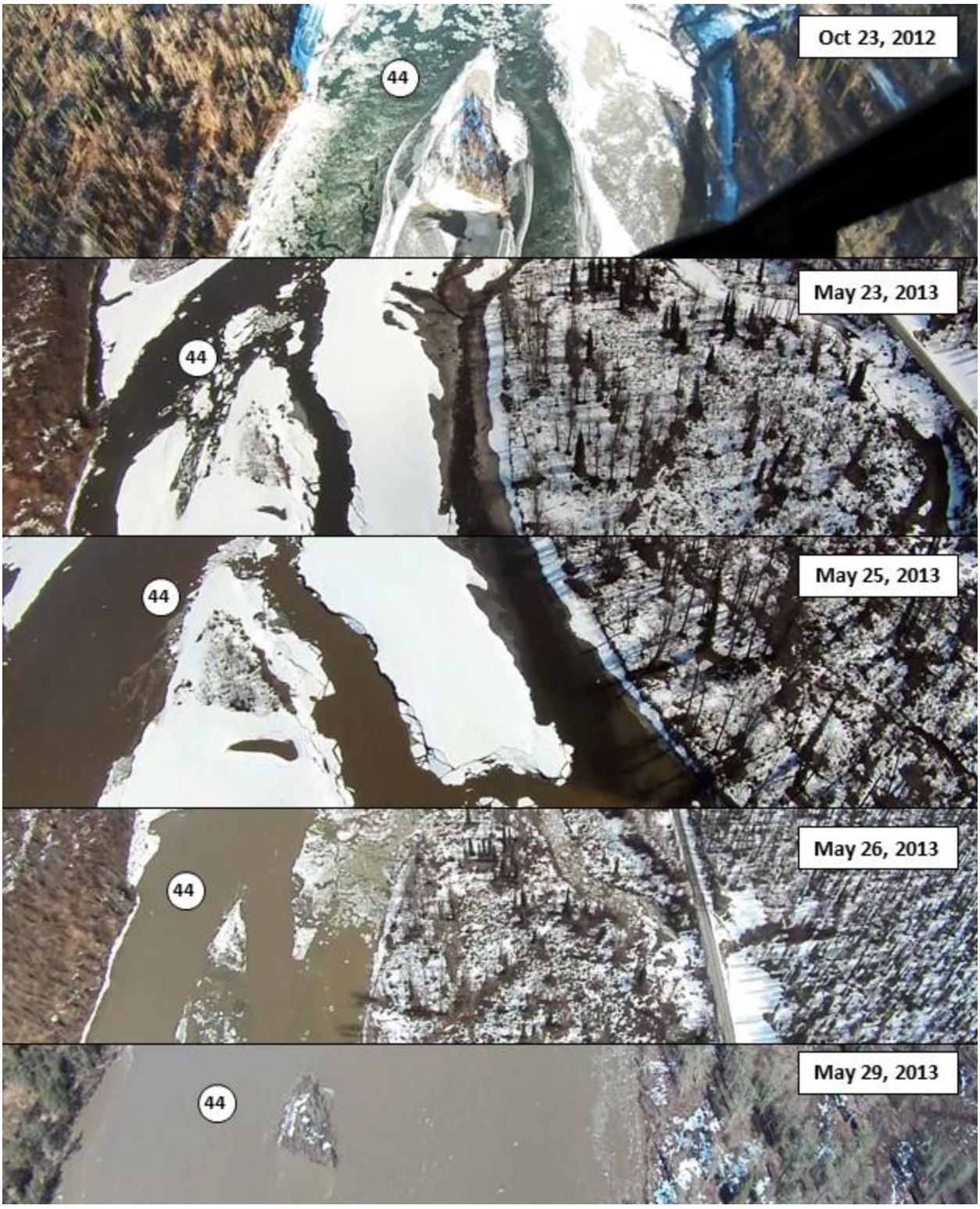
Oct 23, 2012
44
May 23, 2013
44
May 25, 2013
44
May 26, 2013
44
May 29, 2013
44

B.1.7 Erosion Location No. 43

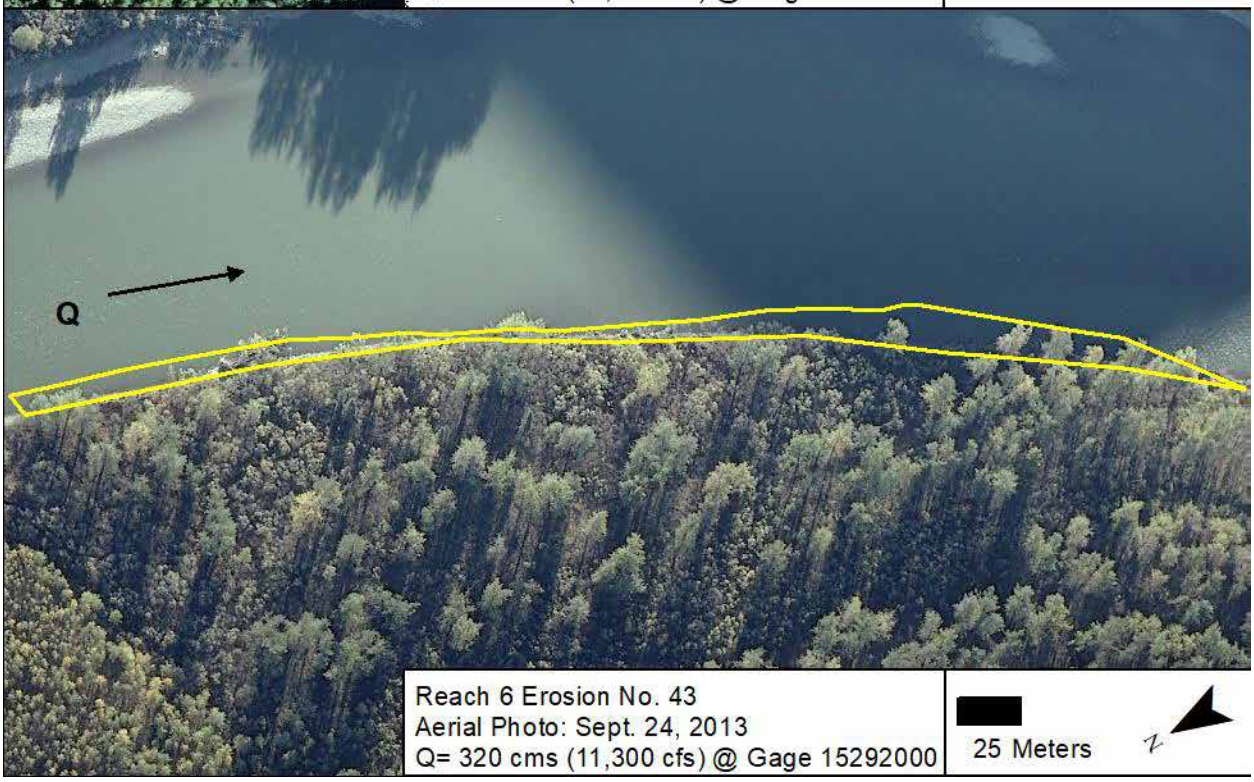

B.1.8 Erosion Location No. 42

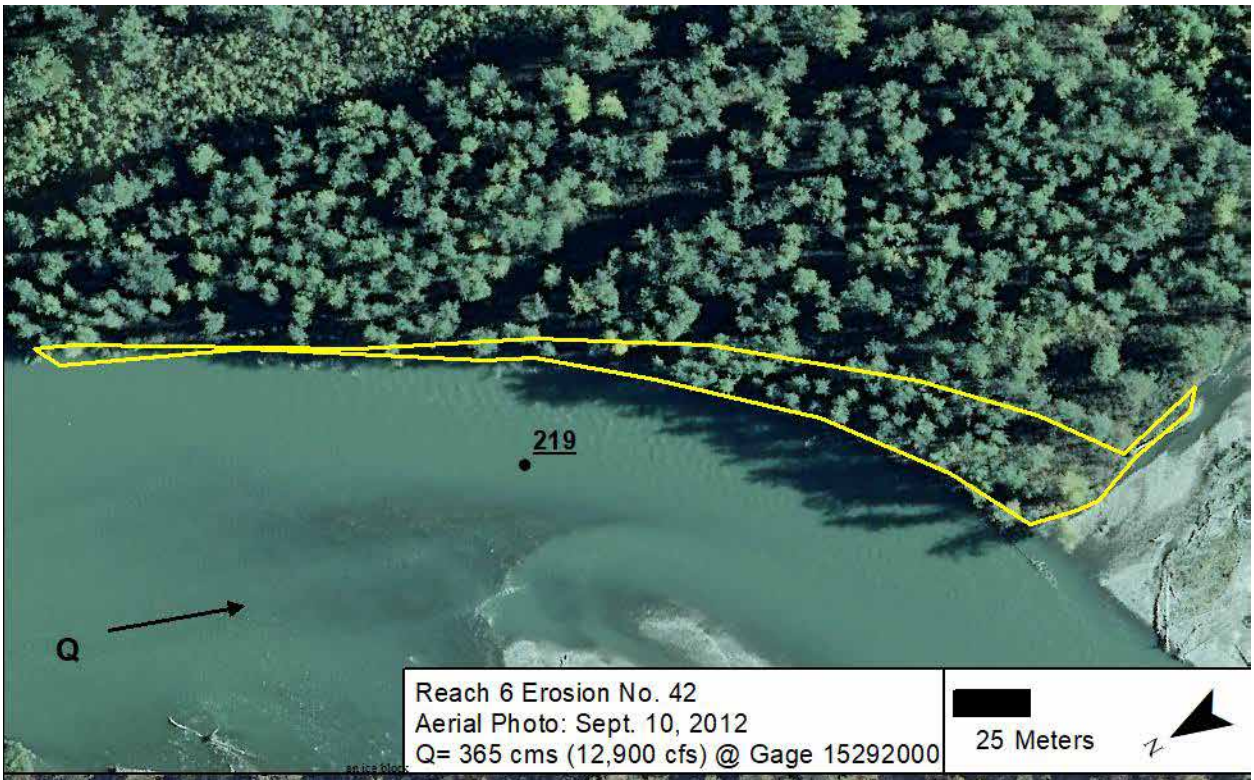

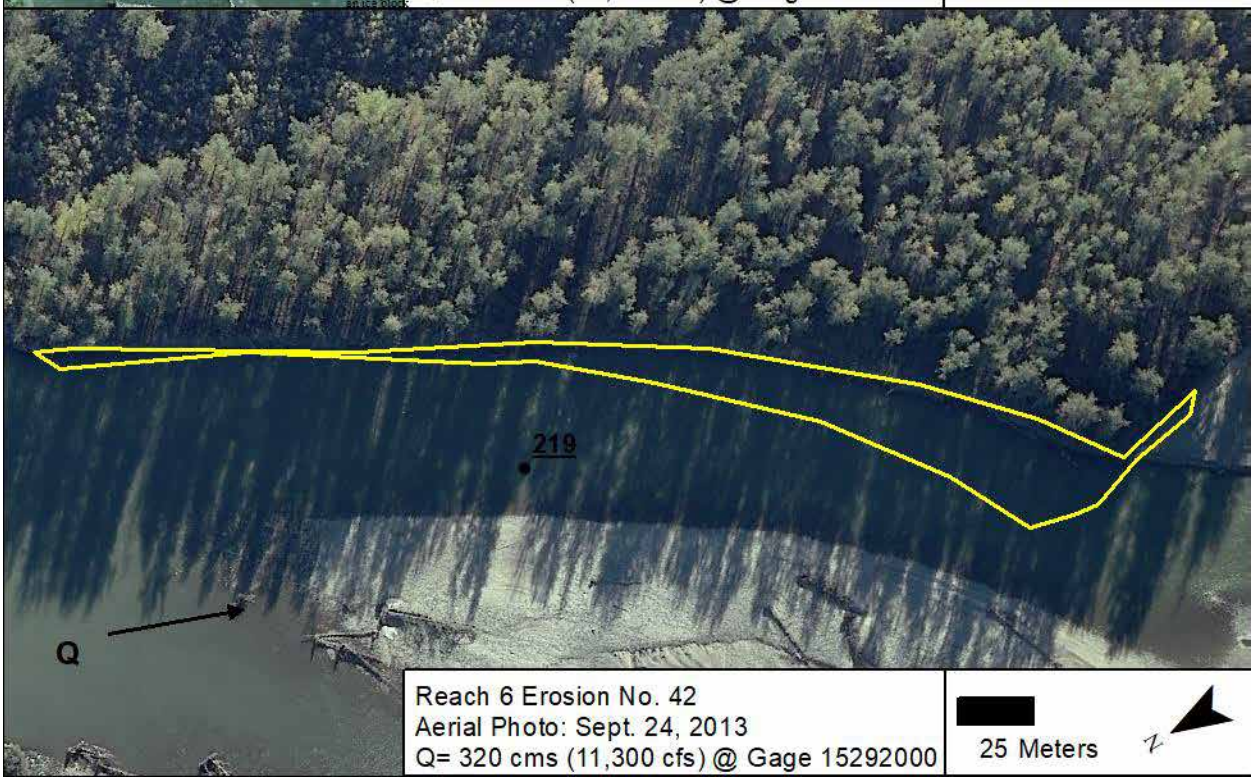

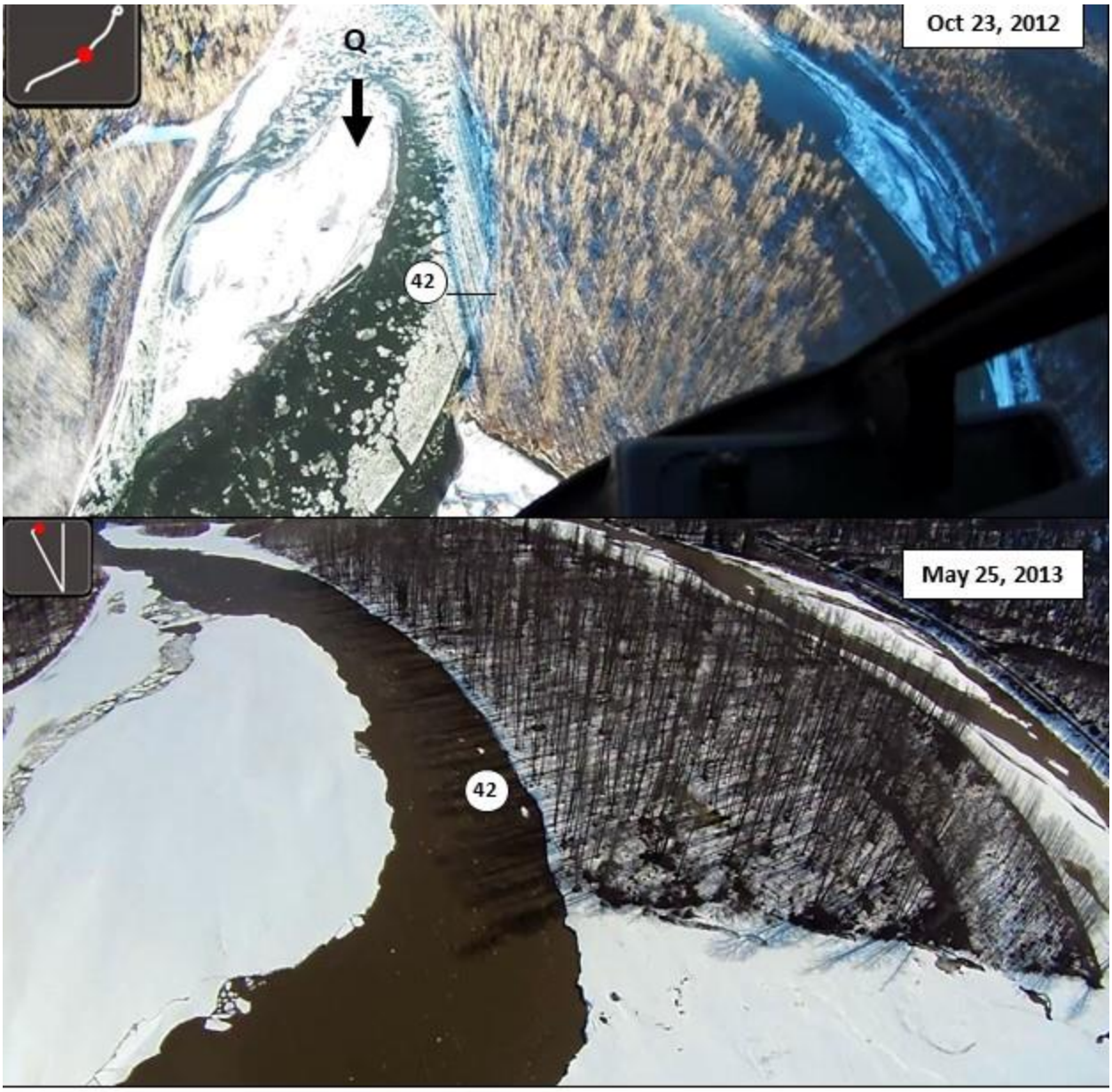
Oct 23, 2012
Q
42
May 25, 2013
42

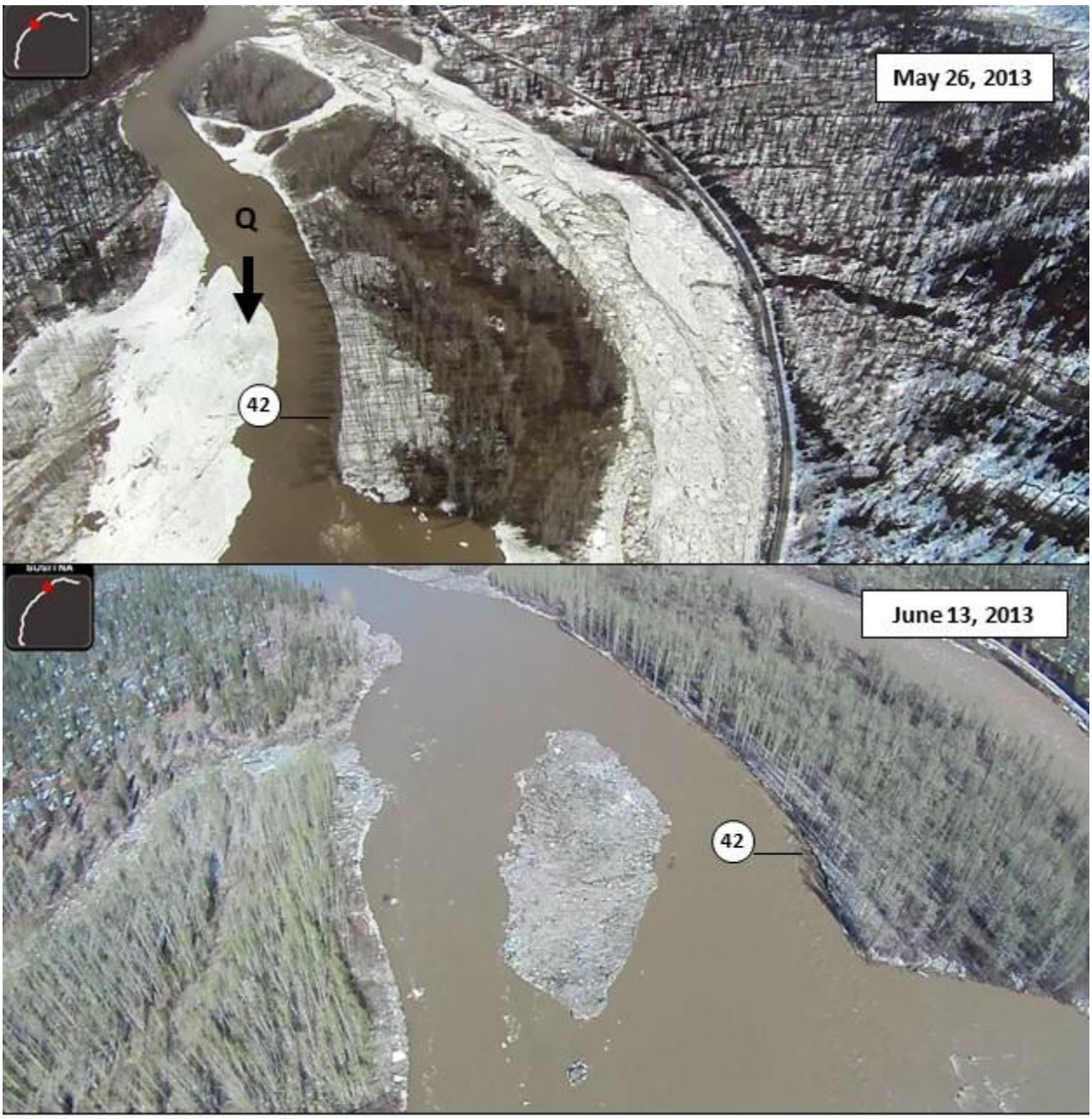
May 26, 2013
Q
42
June 13, 2013
42

B.1.9 Erosion Location No. 41-40

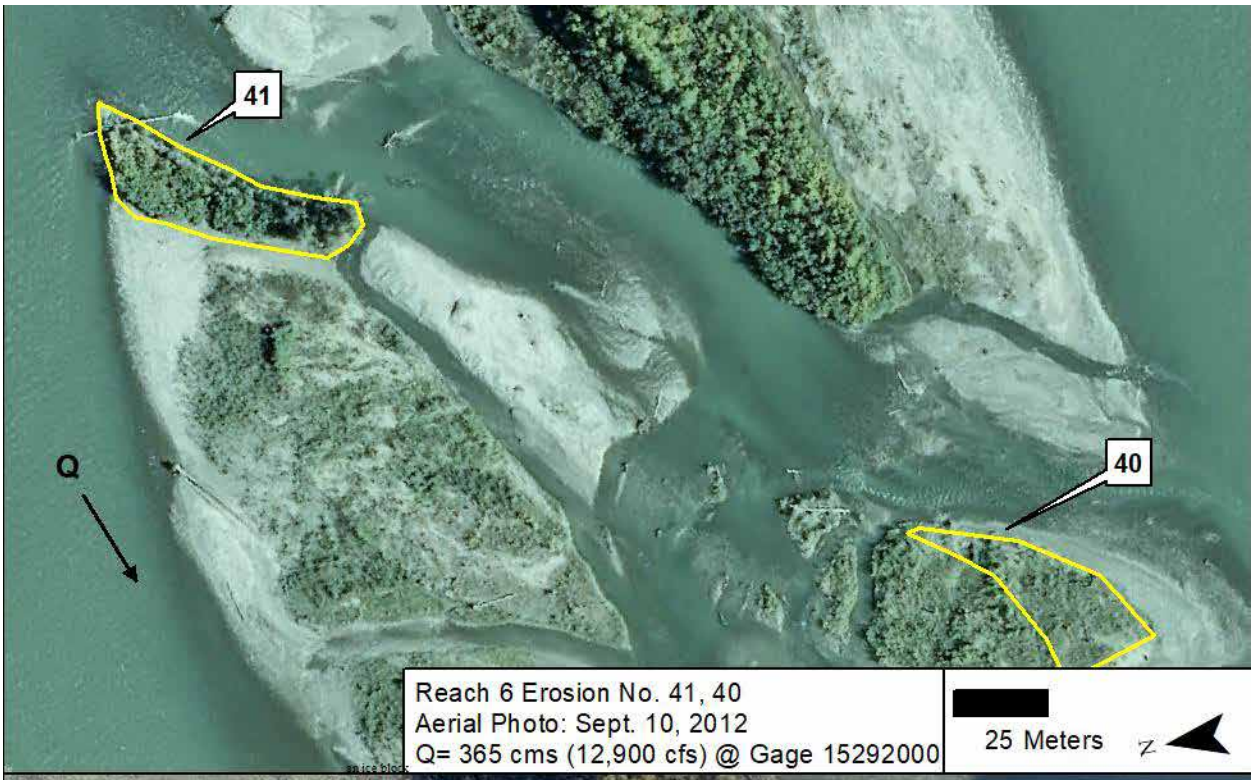

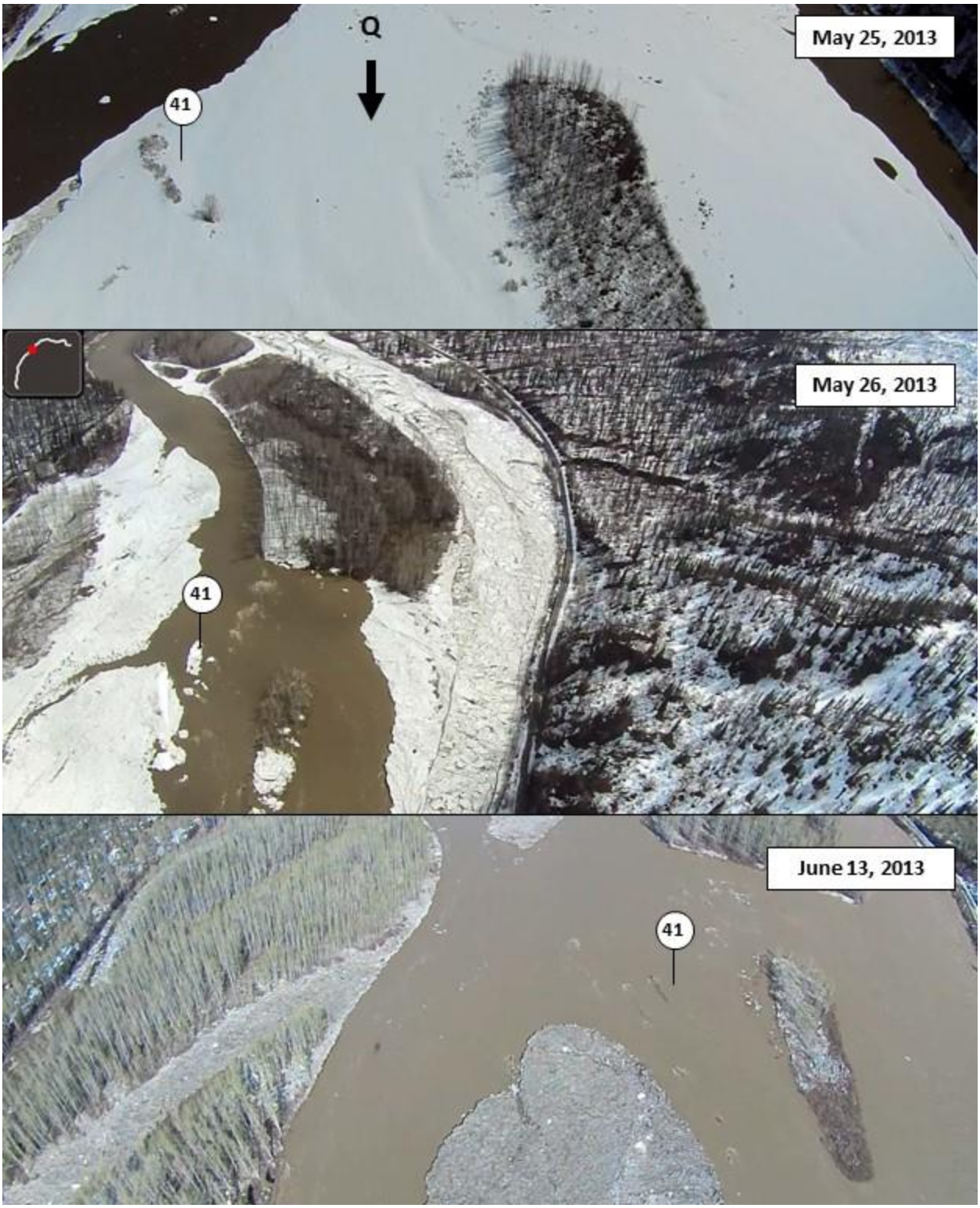
Q
May 25, 2013
41
May 26, 2013
41
June 13, 2013
41

B.1.10 Erosion Location No. 39-37

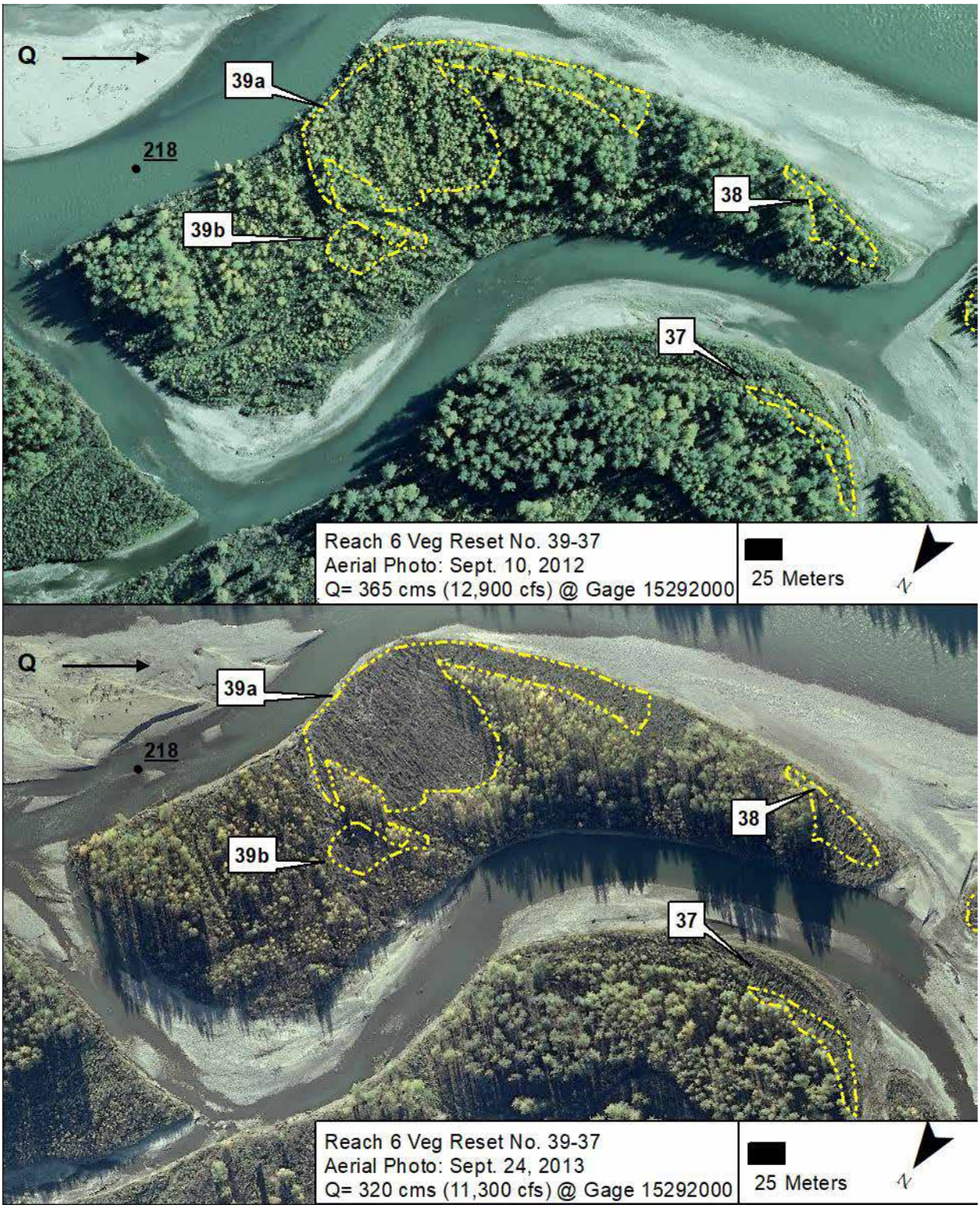


May 23, 2013
39
Q
37
SUSITNA
May 25, 2013
39
38
37


May 29, 2013
39
Q
38
37
June 13, 2013
39
Q
June 13, 2013
39
Q

B.1.11 Erosion Location No. 36-35

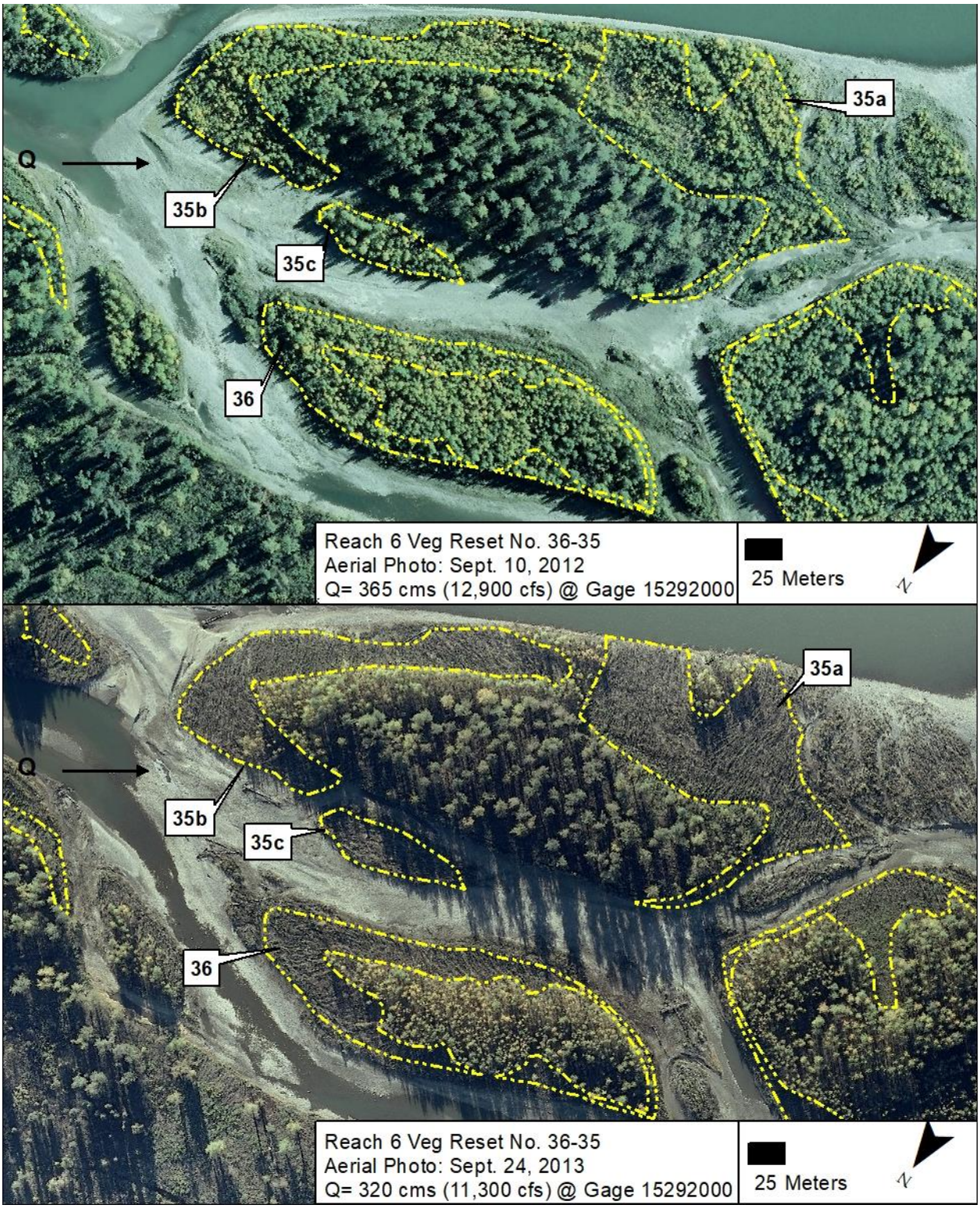

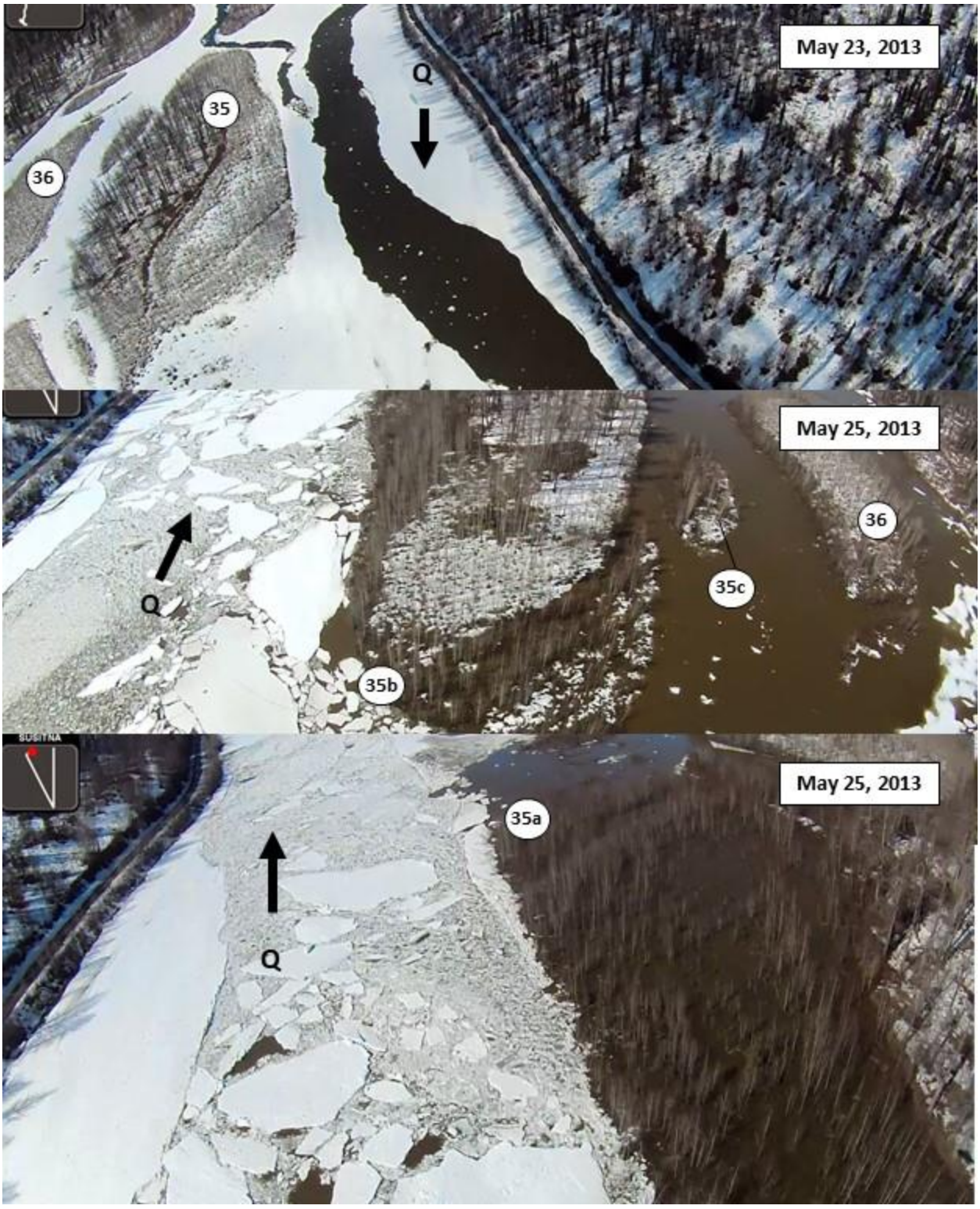
May 23, 2013
Q
35
36
May 25, 2013
Q
36
35c
35b
May 25, 2013
35a
Q

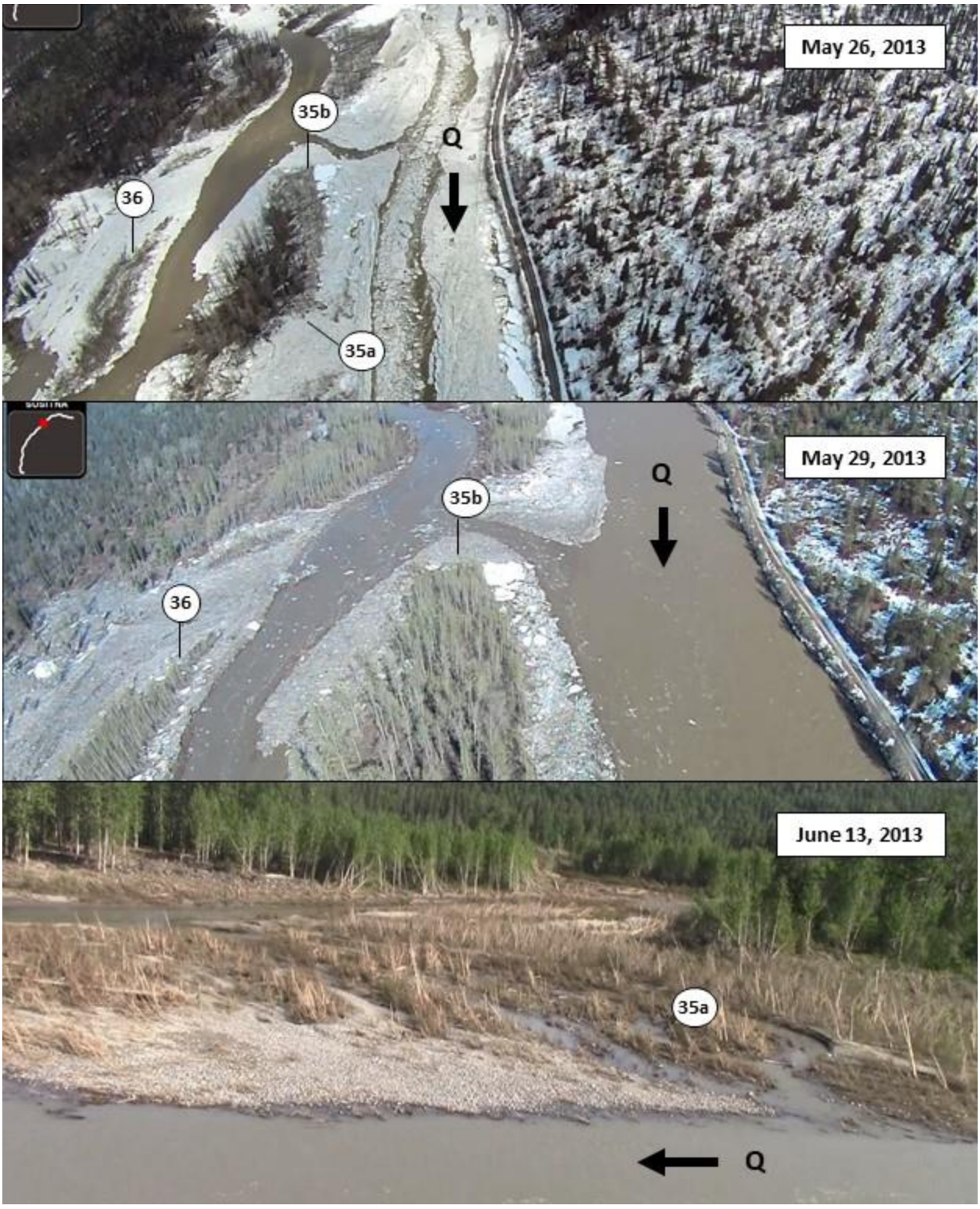
May 26, 2013
35b
Q
36
35a
May 29, 2013
Q
35b
36
June 13, 2013
35a
Q

B.1.12 Erosion Location No. 34-33

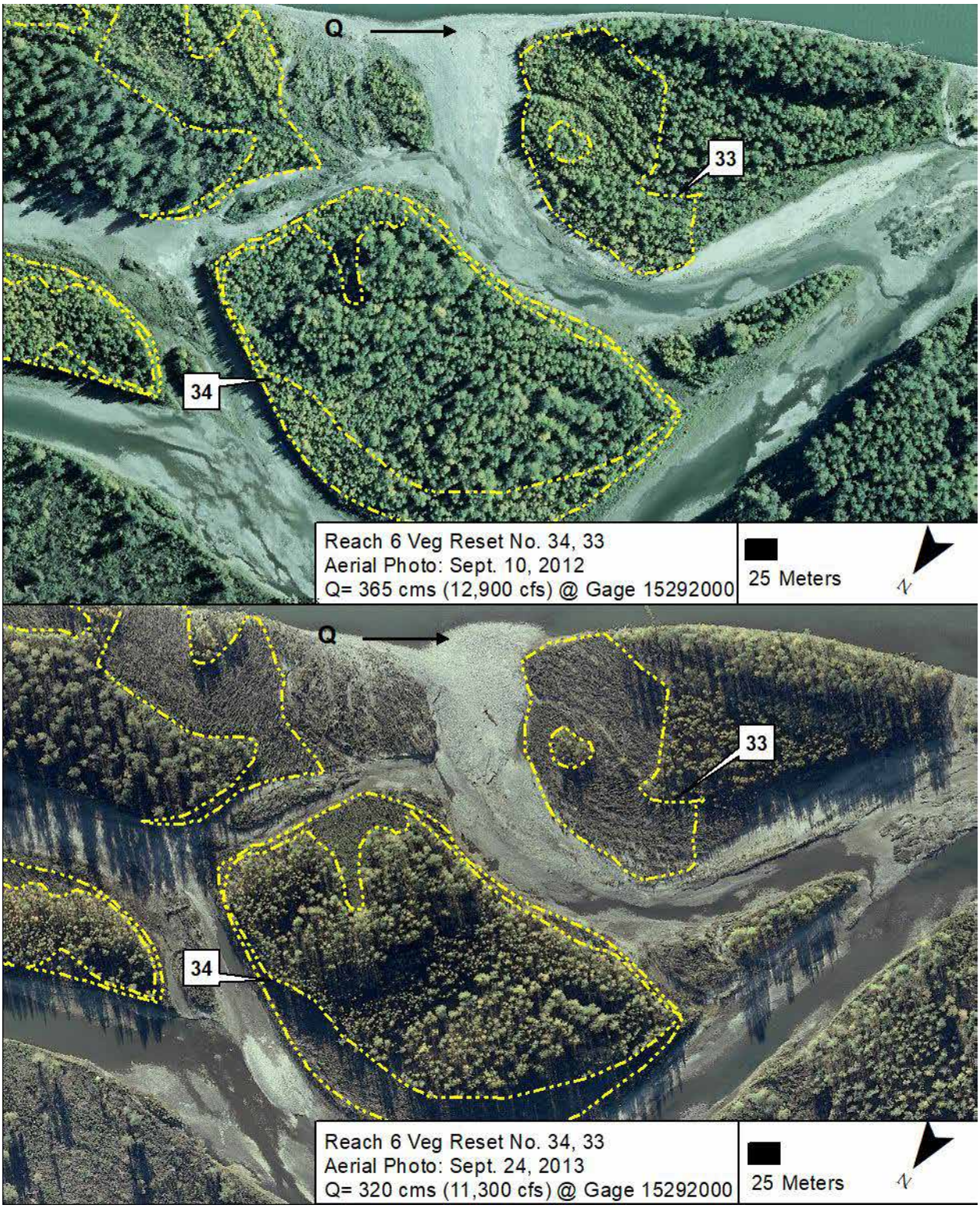

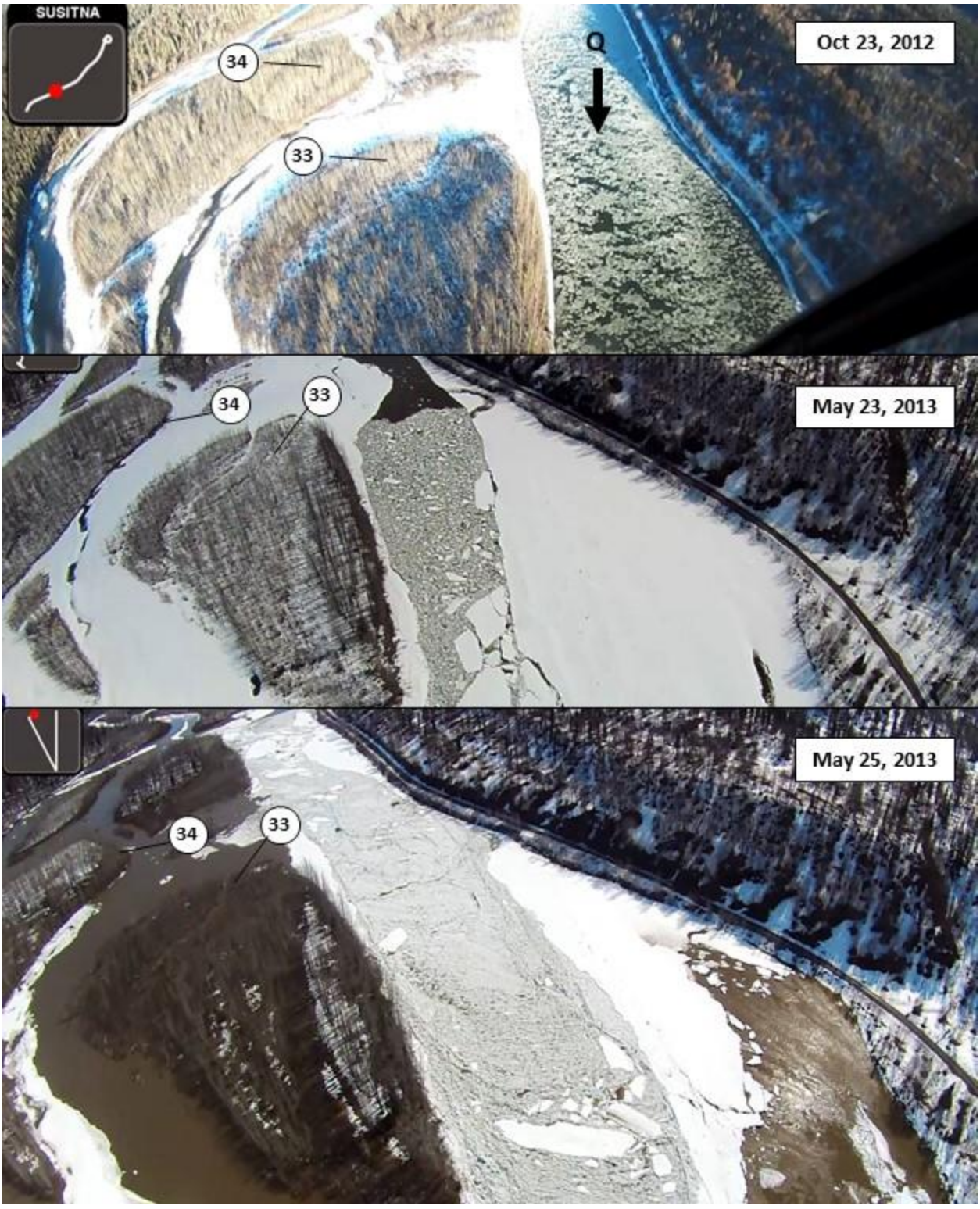
SUSITNA
34
33
Q
Oct 23, 2012
34
33
May 23, 2013
34
33
May 25, 2013

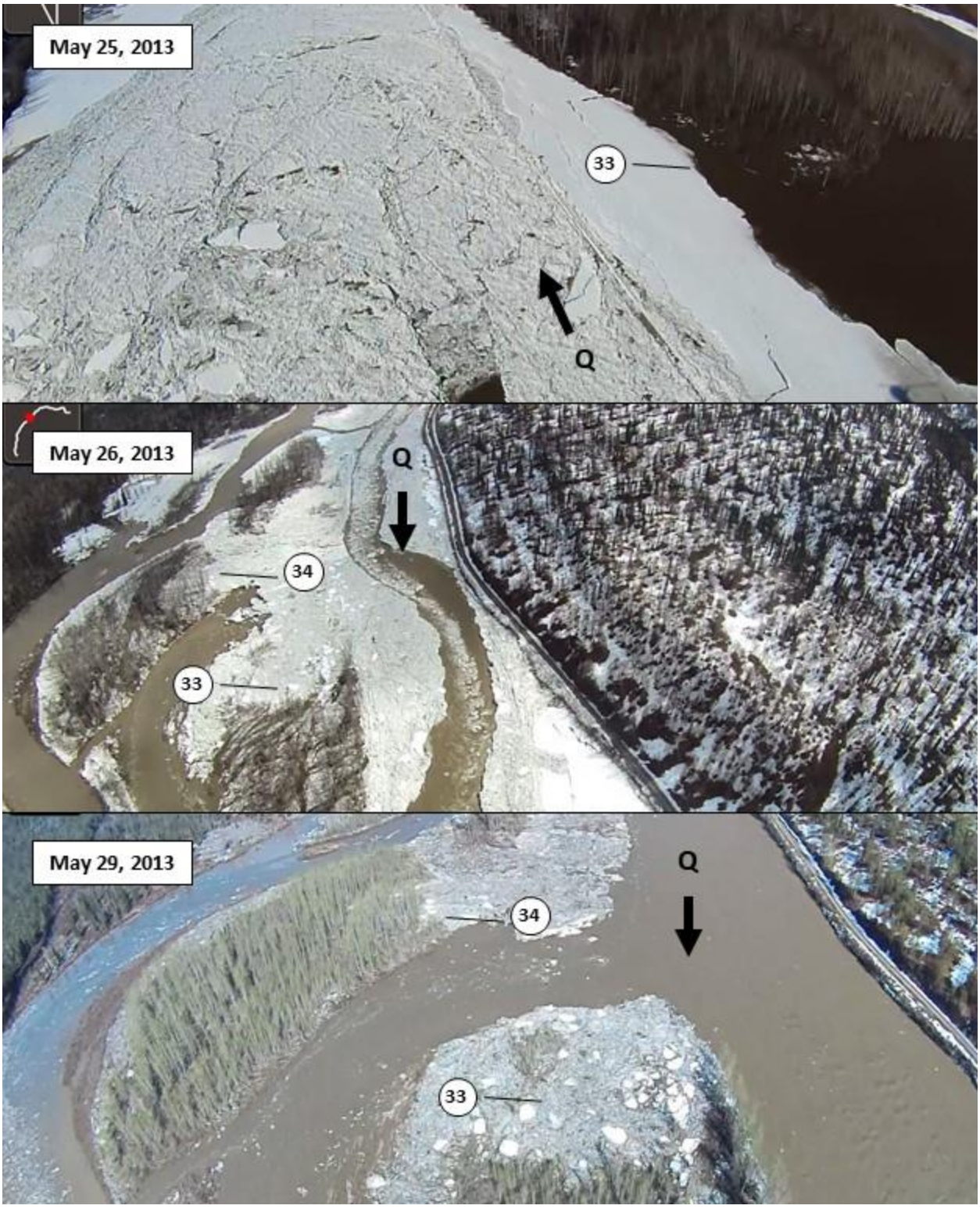
May 25, 2013
33
Q
May 26, 2013
Q
34
33
May 29, 2013
Q
34
33

B.1.13 Erosion Location No. 32-31

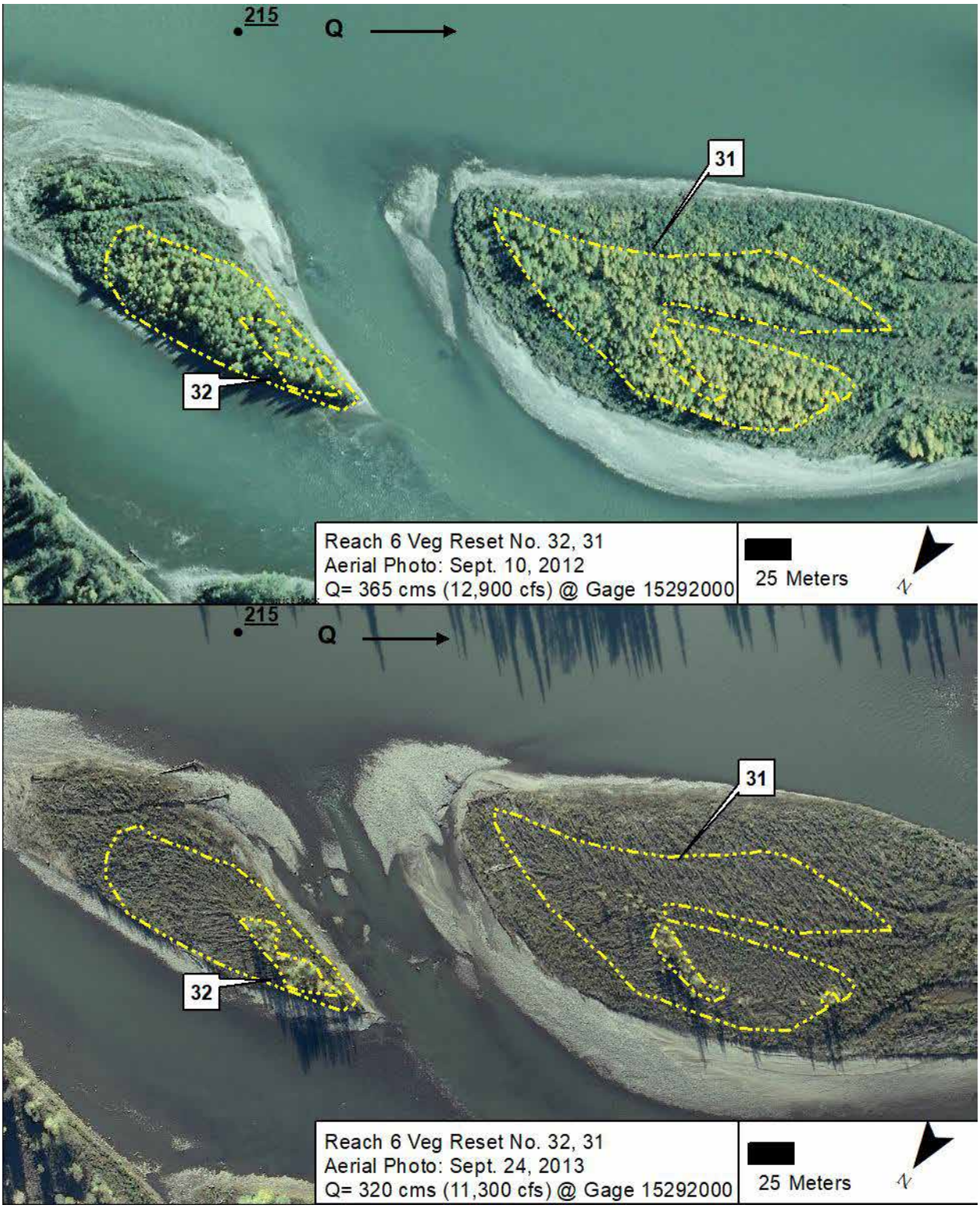

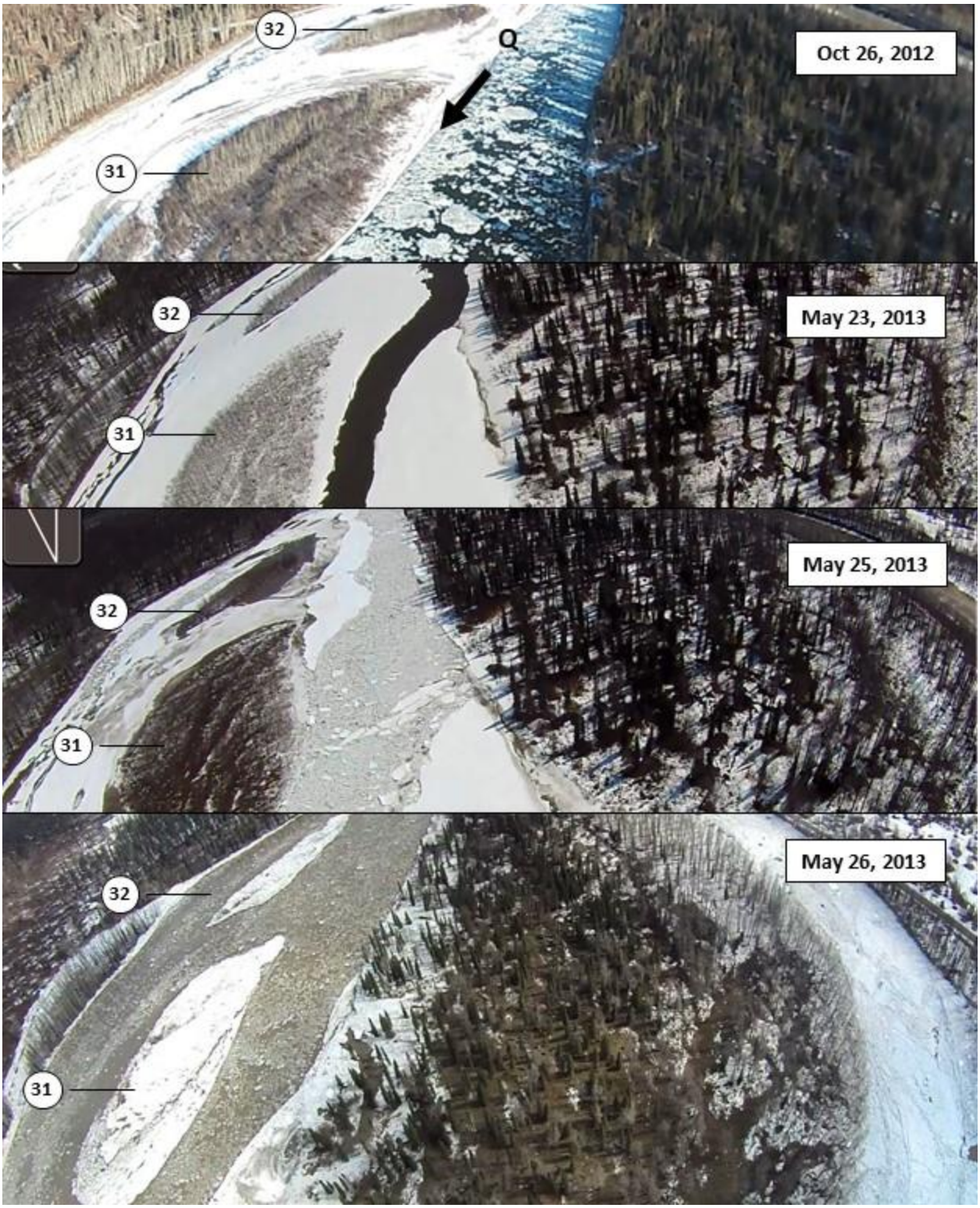
32
Q
Oct 26, 2012
31
32
May 23, 2013
31
May 25, 2013
32
31
May 26, 2013
32
31

B.1.14 Erosion Location No. 30

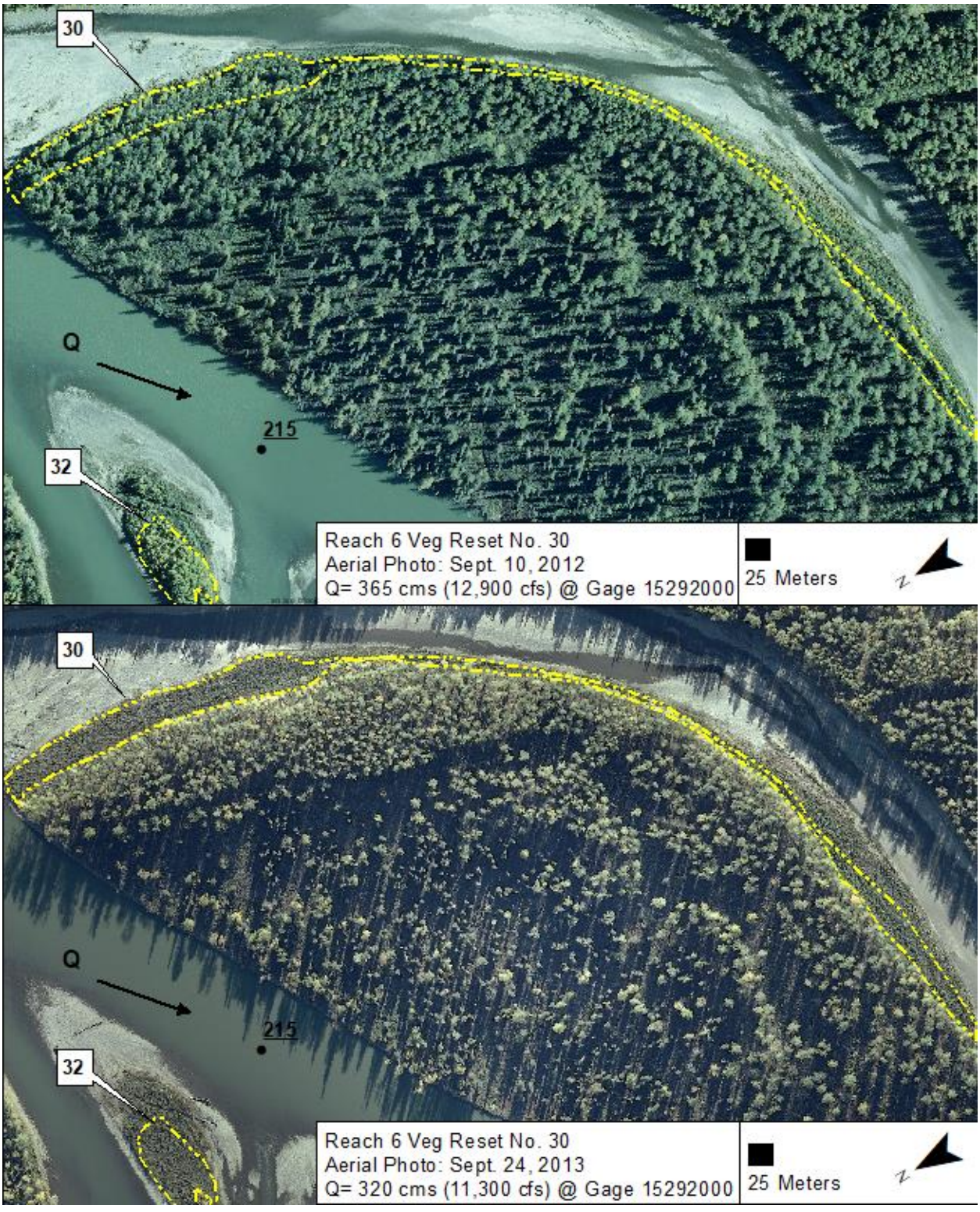


May 26, 2013
30
Q
SUSITNA
May 29, 2013
Q
30
June 13, 2013
30
Q

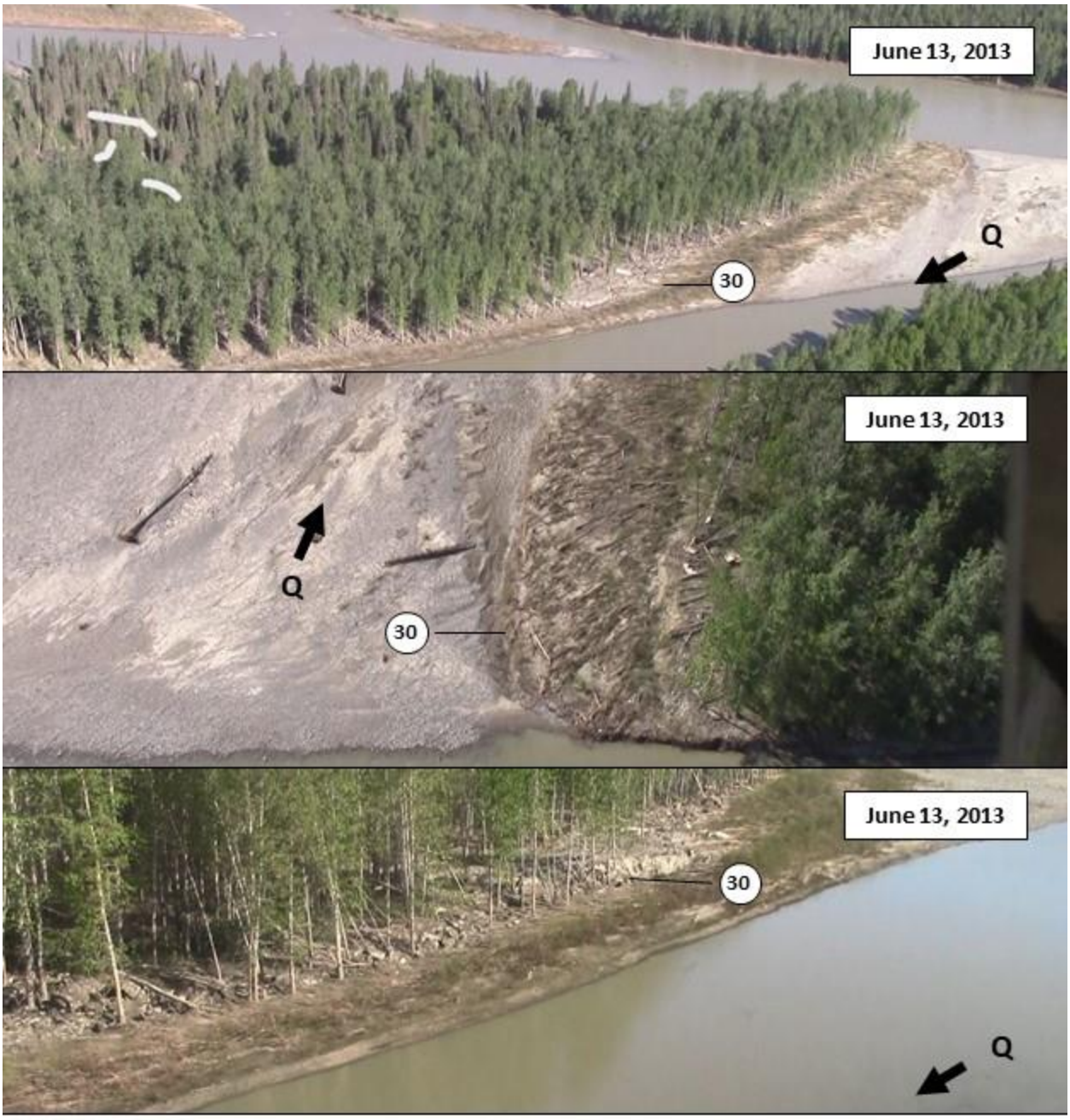
June 13, 2013
Q
30
June 13, 2013
Q
30
June 13, 2013
30
Q


June 13, 2013
30
Q

B.1.15 Erosion Location No. 29

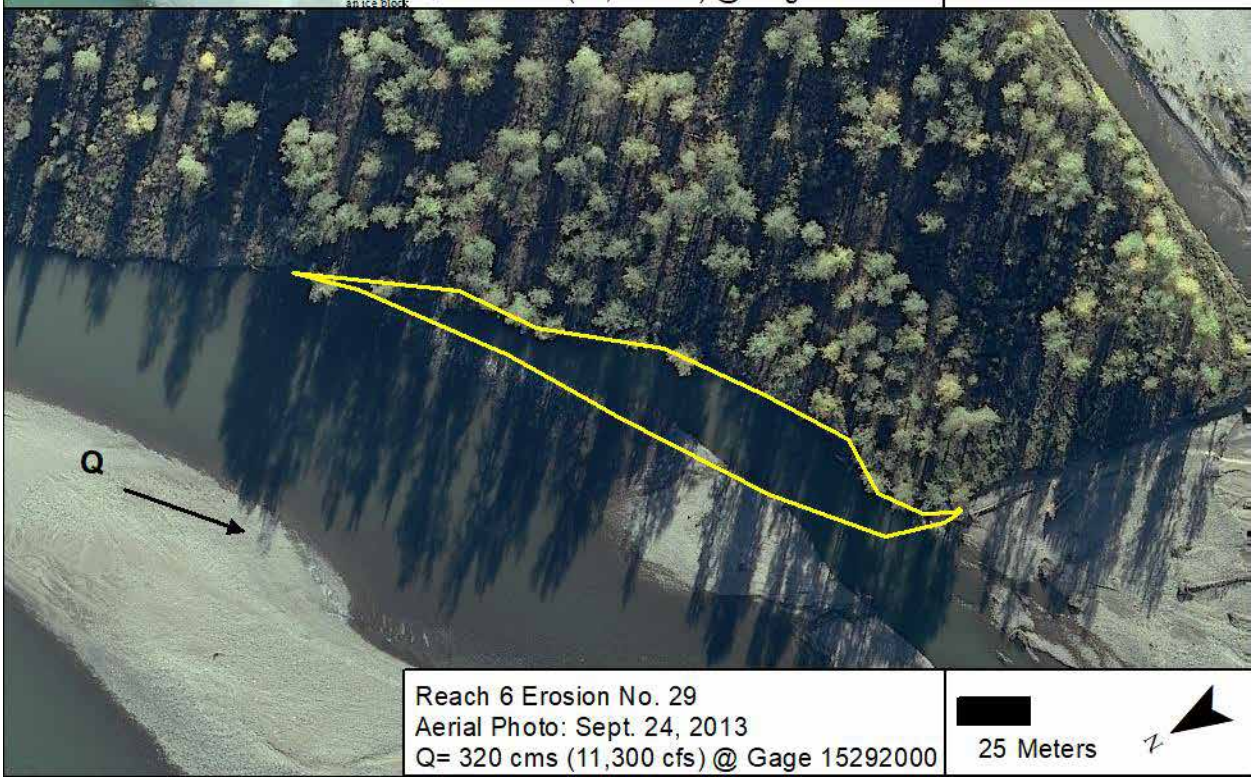


SUSITNA
Q
SUSITNA RIVER MILE: 129.7
LAT: 62.7048
LONG: -149.8405
ALT(FT): 1362
TIME: 14:02:03.59
SUSITNA WATANA
OCT 26 2012

B.1.17 Erosion Location No. 28

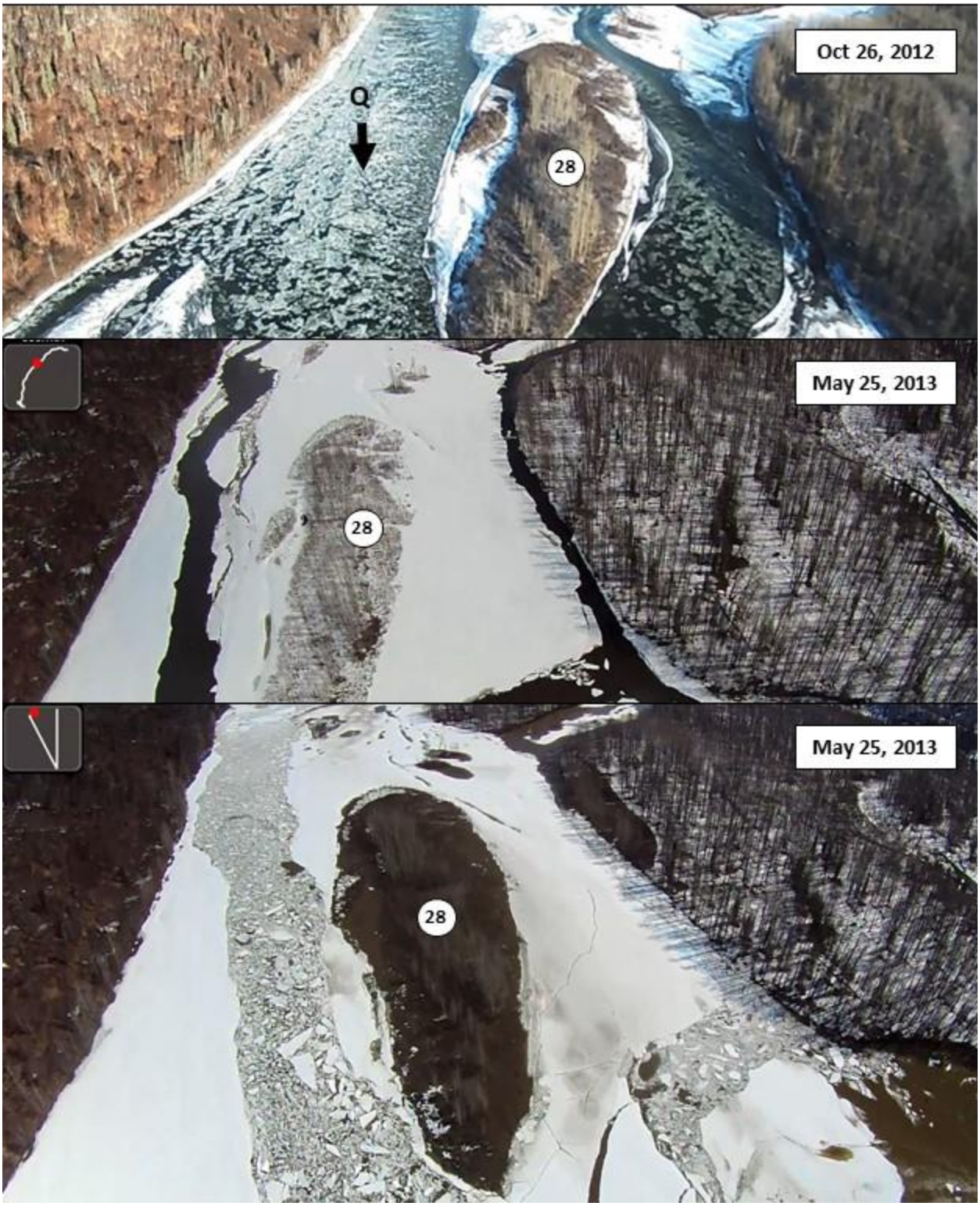
Oct 26, 2012
Q
28
May 25, 2013
28
May 25, 2013
28


May 26, 2013
Q
28
May 29, 2013
28
June 13, 2013
28
Q

B.1.18 Erosion Location No. 27

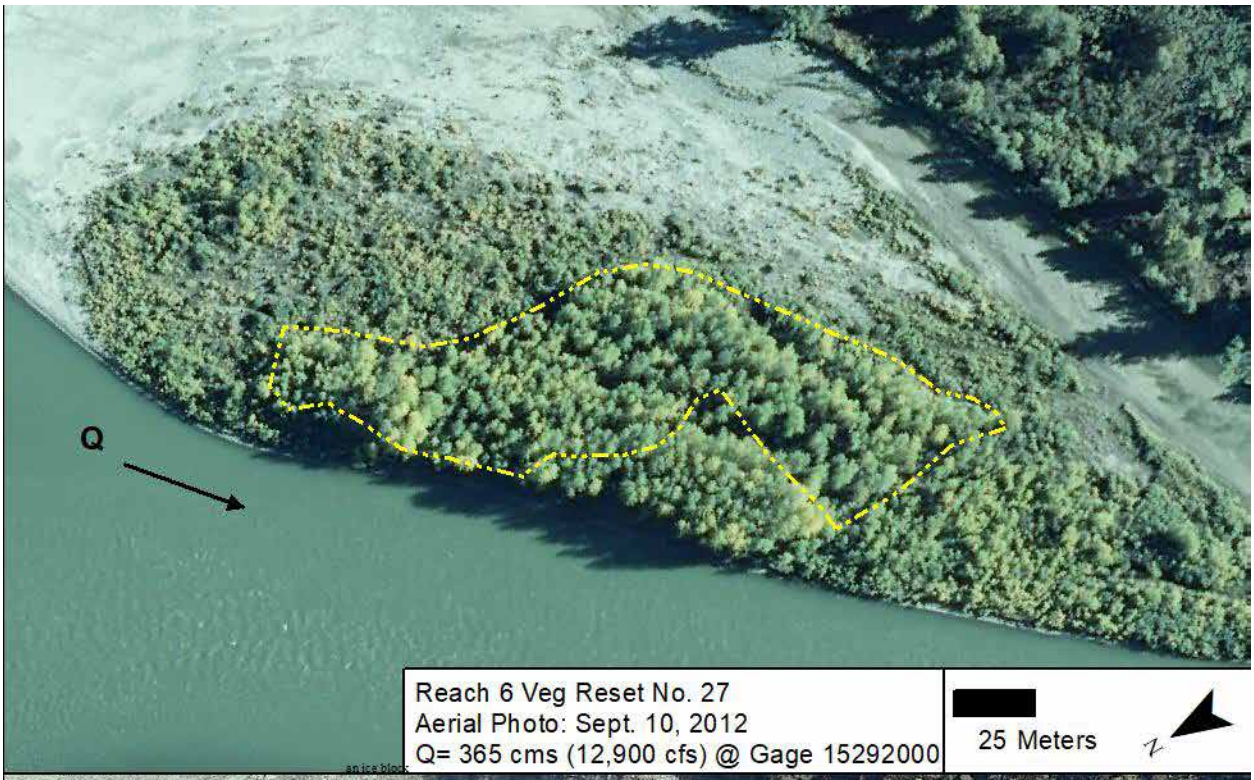


Q
27
May 23, 2013
27
May 25, 2013
27
May 26, 2013
27
Q
June 13, 2013

B.1.19 Erosion Location No. 26

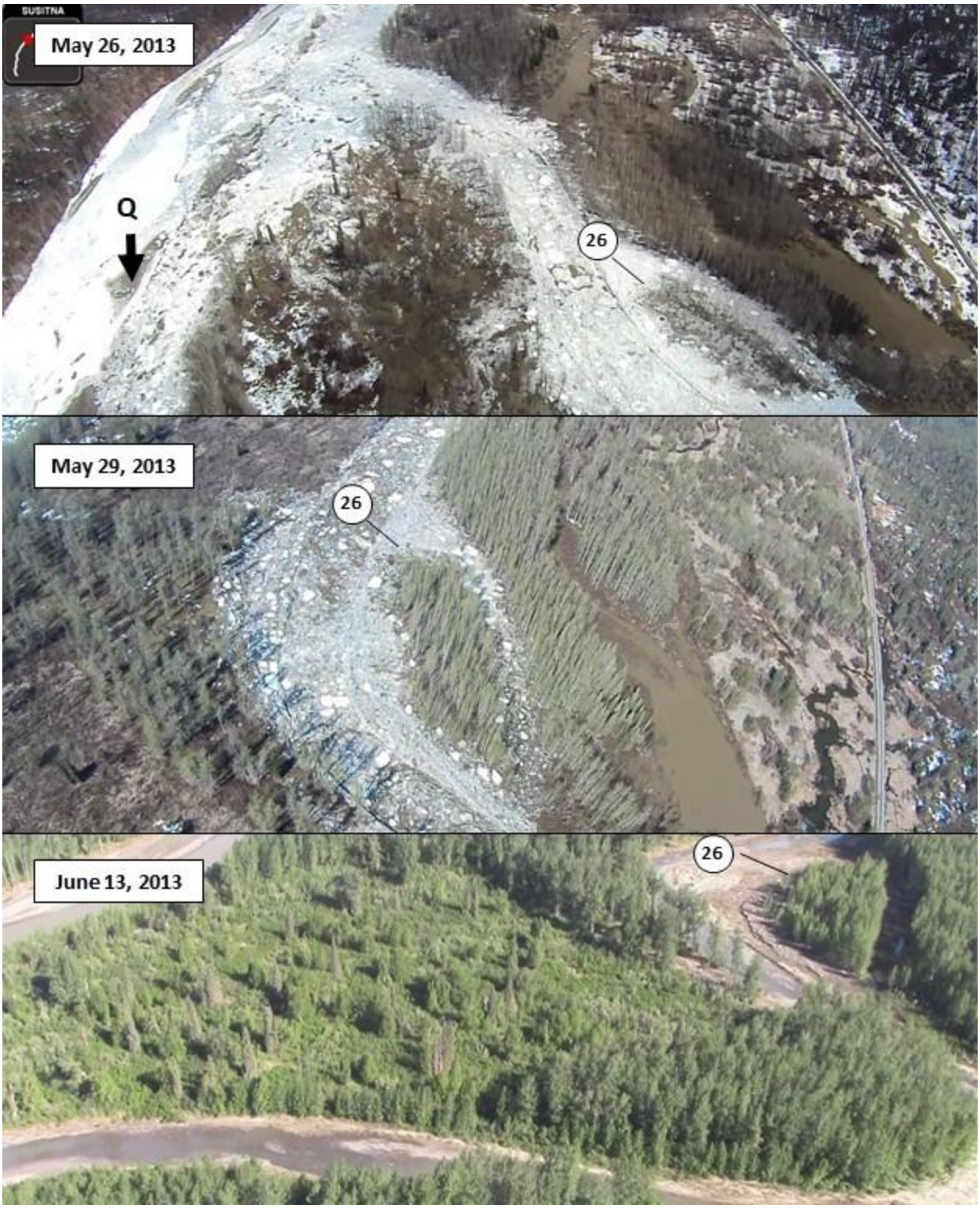
SUSITNA
May 26, 2013
Q
26
May 29, 2013
26
June 13, 2013
26

B.1.20 Erosion Location No. 25-24

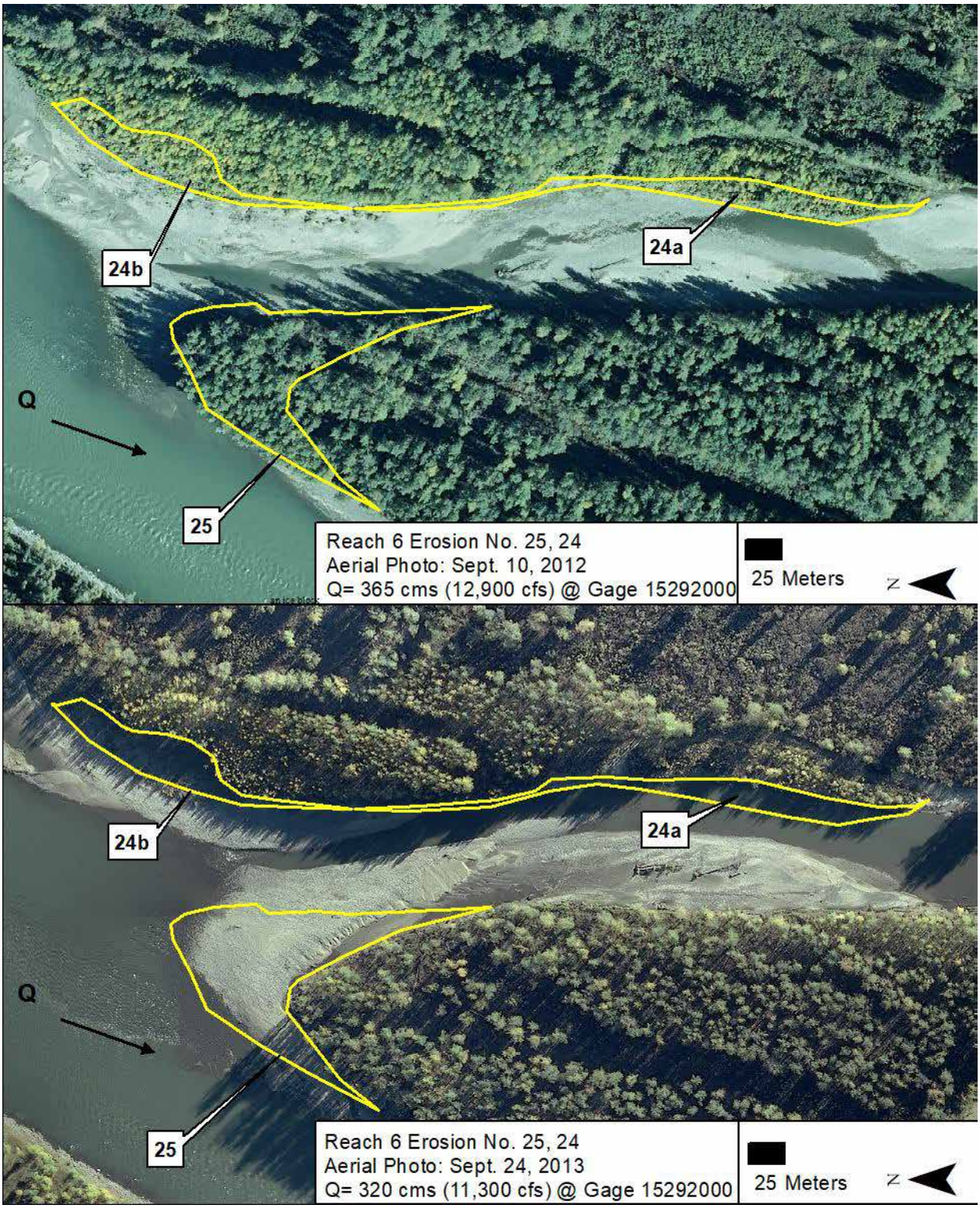

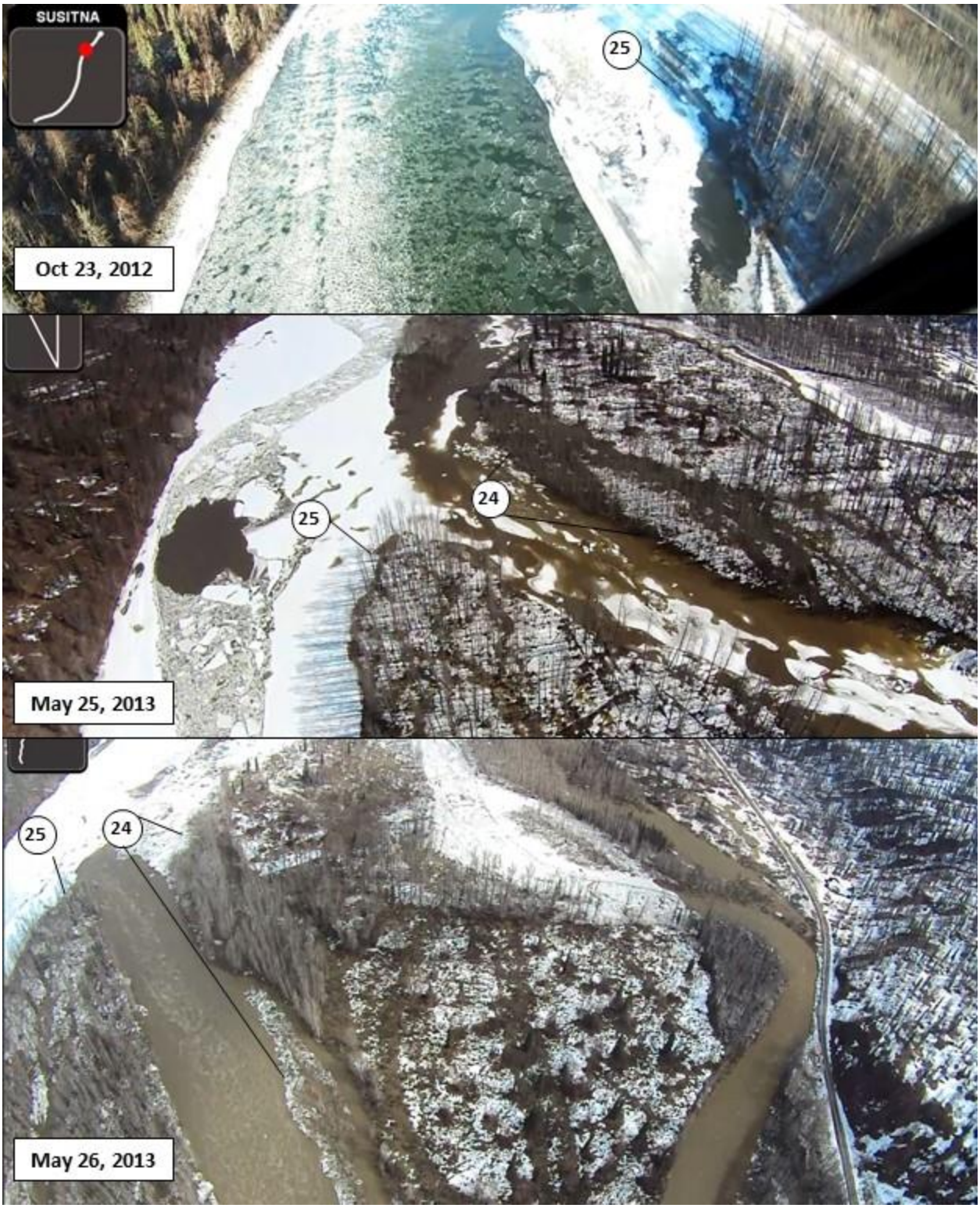
SUSITNA
25
Oct 23, 2012
25
24
May 25, 2013
25
24
May 26, 2013


SUSITNA
May 25, 2013
24b
24a
May 25, 2013
24b
June 13, 2013
24b
June 13, 2013
24a

B.1.21 Erosion Location No. 23- 22

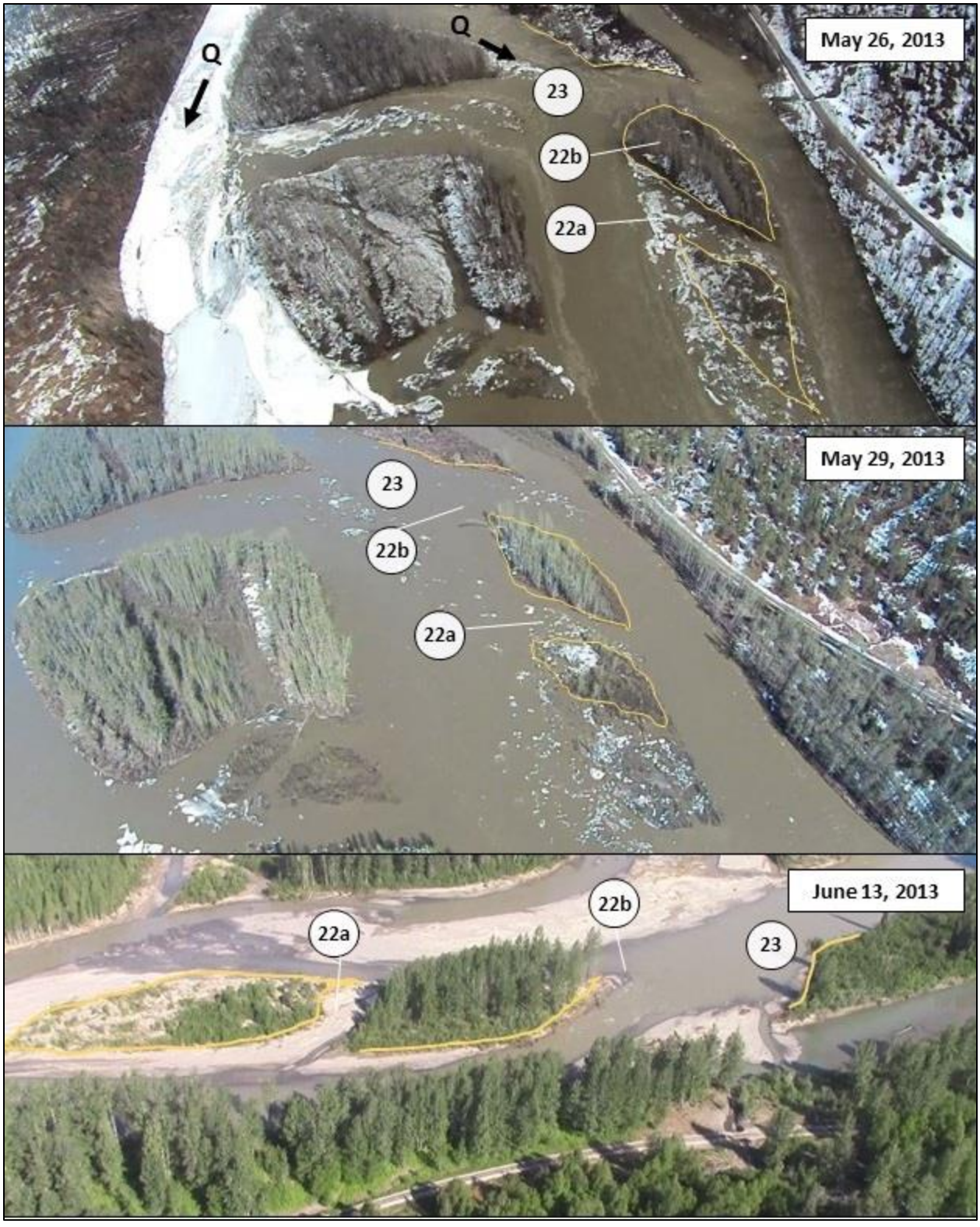
Q
Q
May 26, 2013
23
22b
22a
May 29, 2013
23
22b
22a
June 13, 2013
22a
22b
23

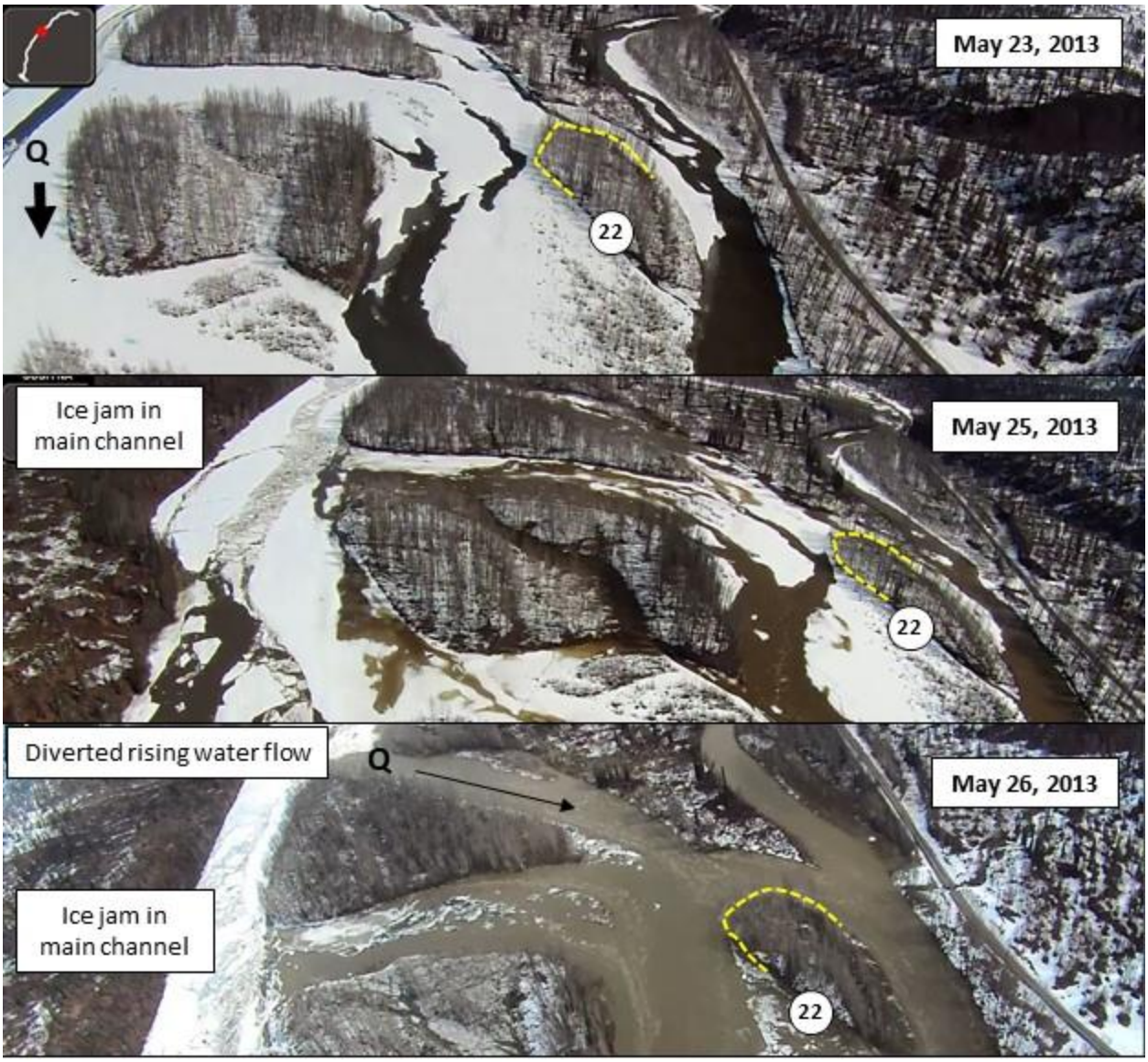

Release of ice jam, continued rise in water flow. No Photos.

May 26, 2013 to
May 29, 2013

B.1.22 Erosion Location No. 21

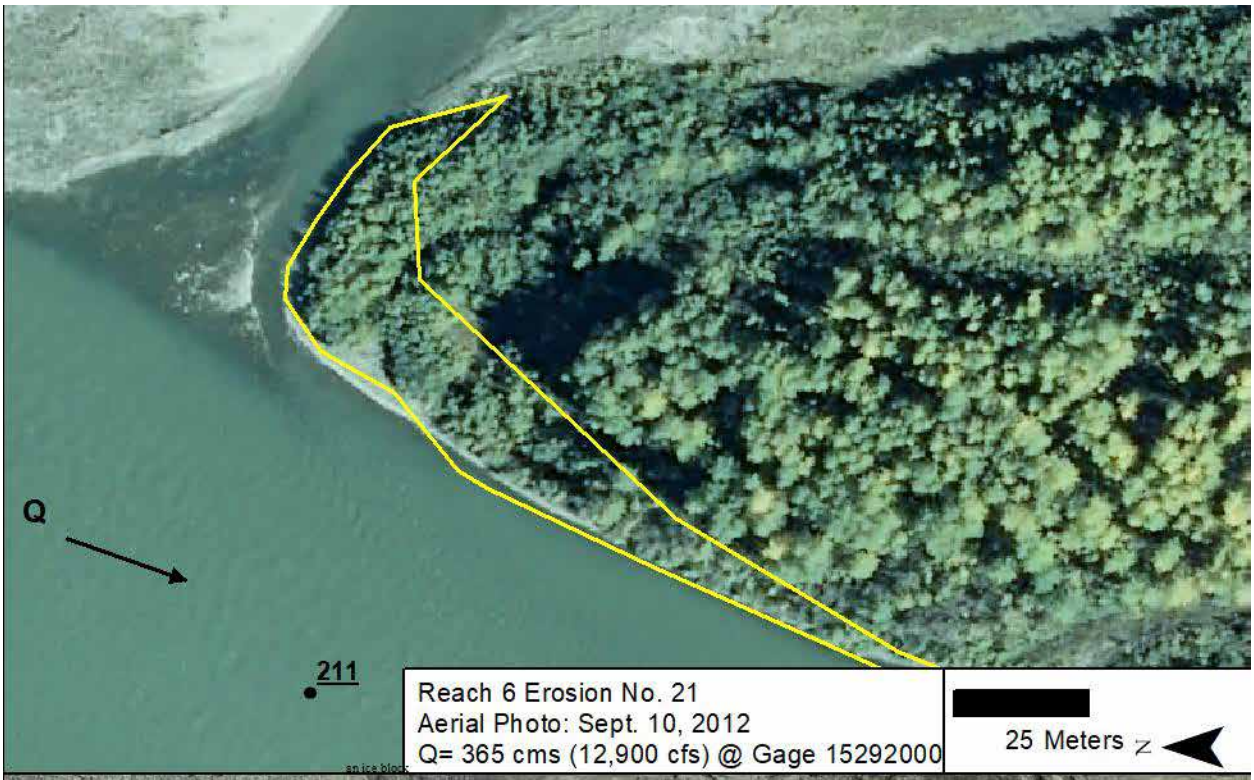

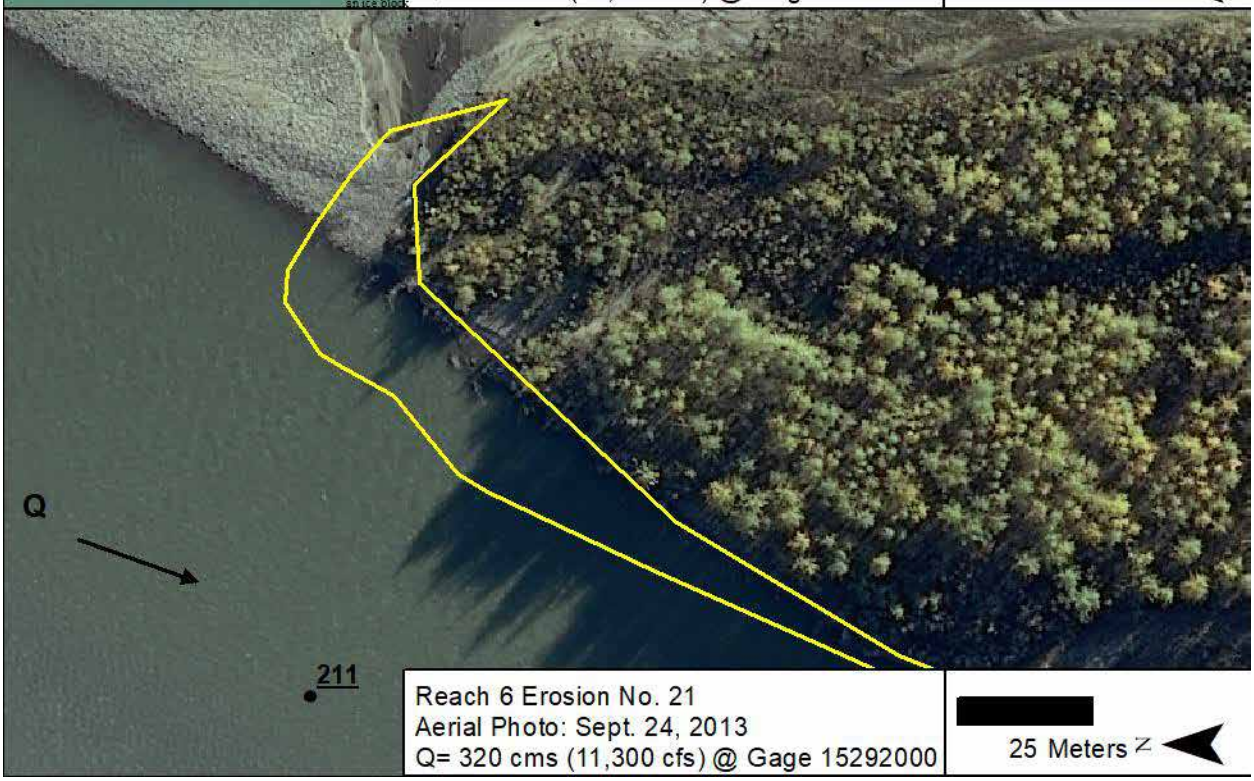

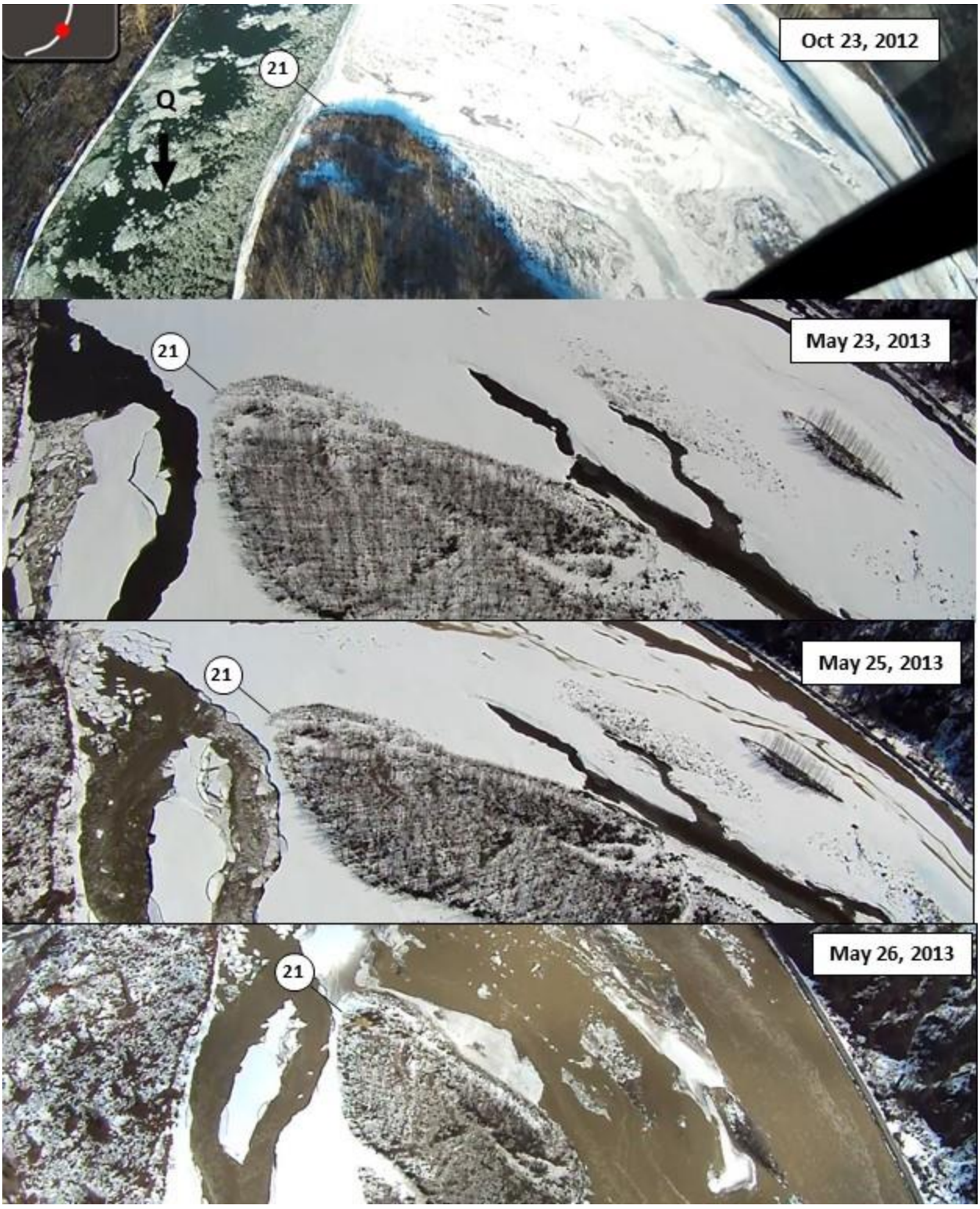
Oct 23, 2012
21
Q
May 23, 2013
21
May 25, 2013
21
May 26, 2013
21

B.1.23 Erosion Location No. 20-17

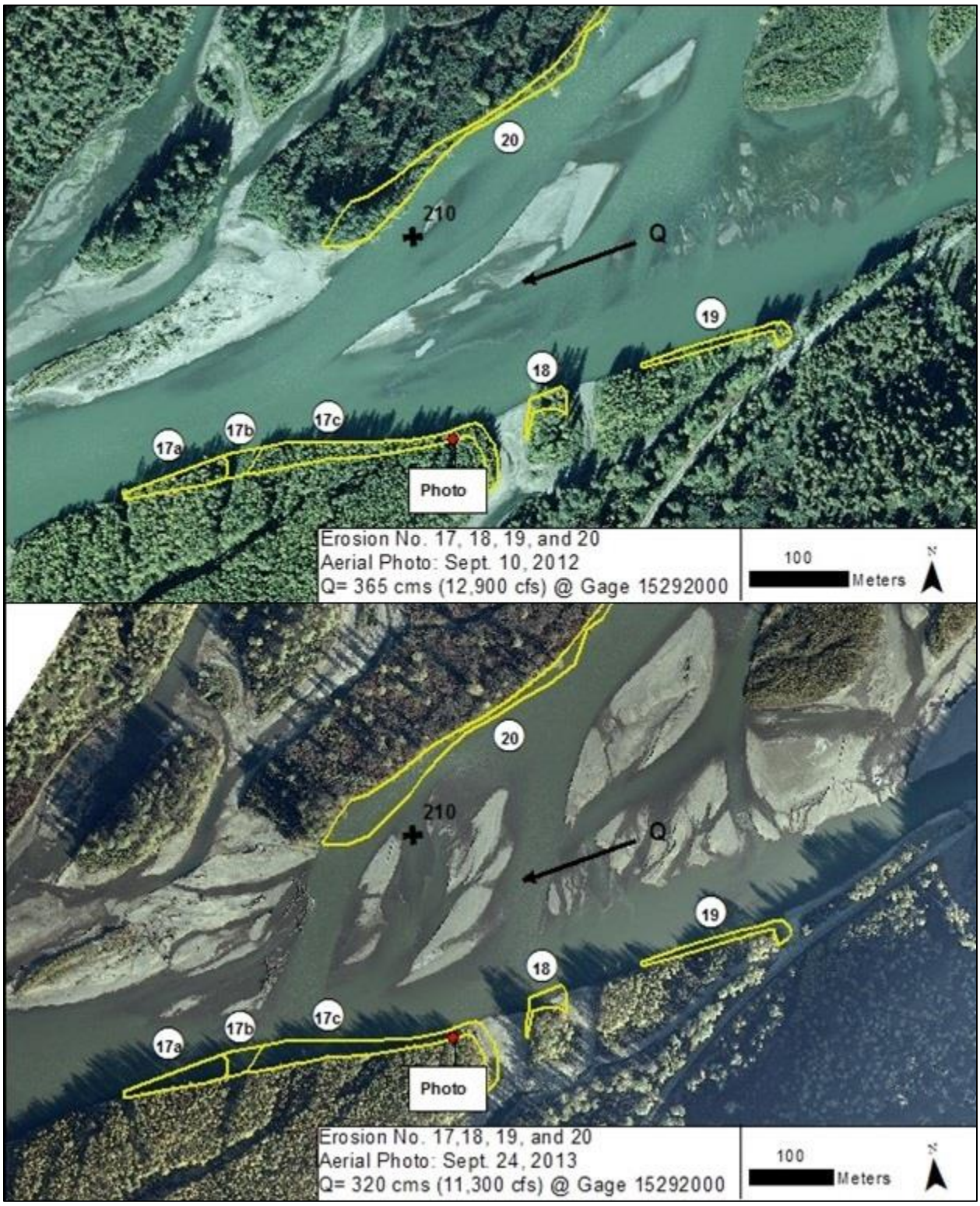

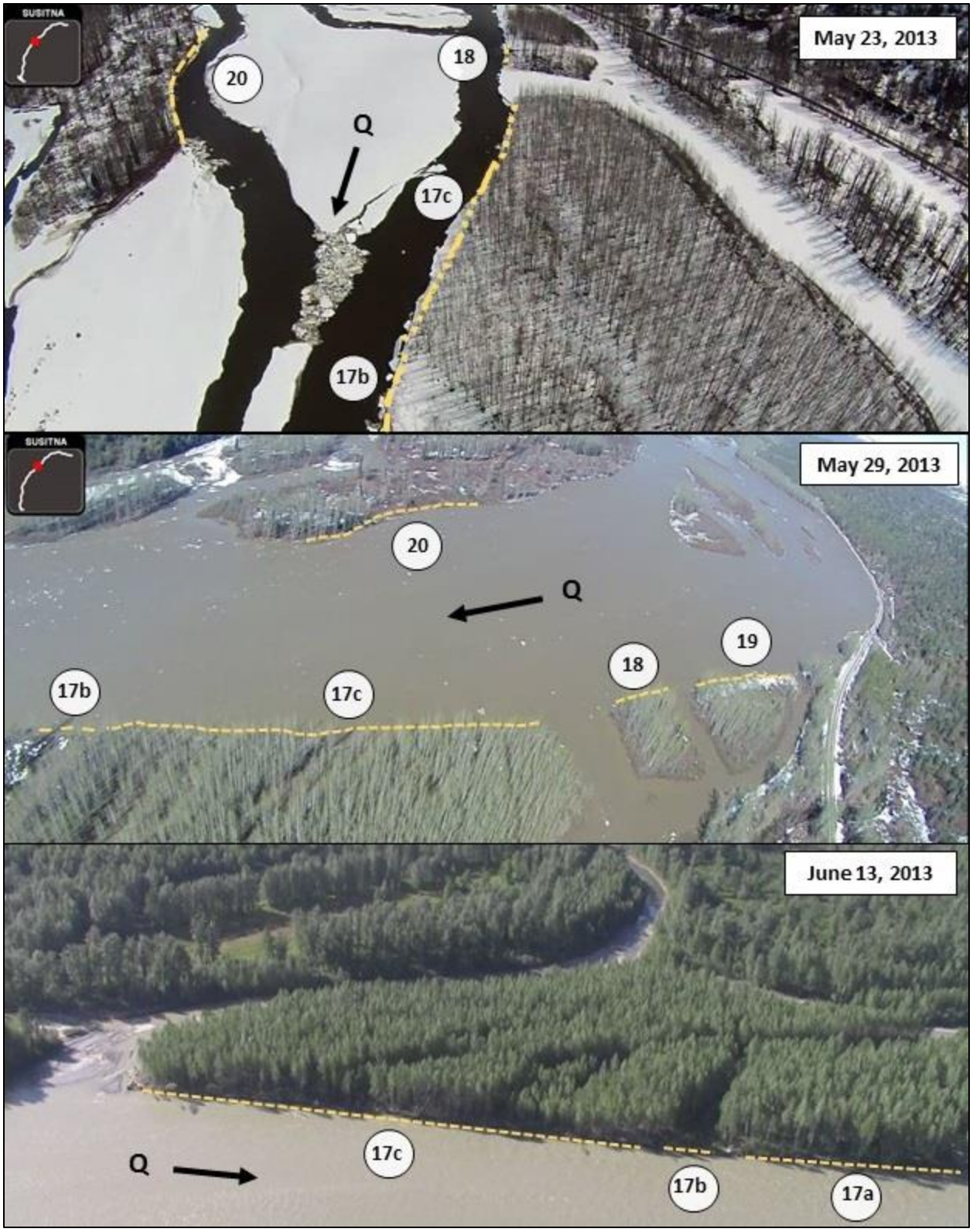
SUSITNA
May 23, 2013
20
18
Q
17c
17b
SUSITNA
May 29, 2013
20
Q
19
18
17b
17c
June 13, 2013
Q
17c
17b
17a

B.1.24 Erosion Location No. 16-14

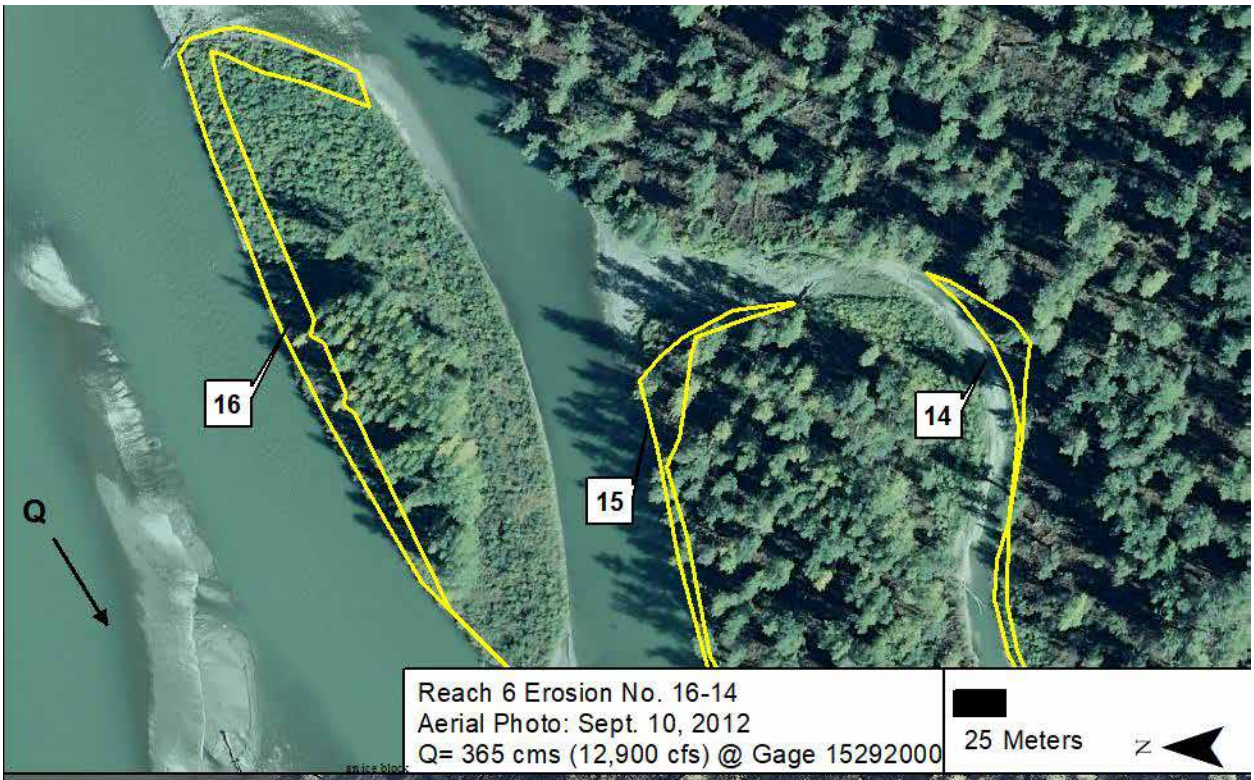

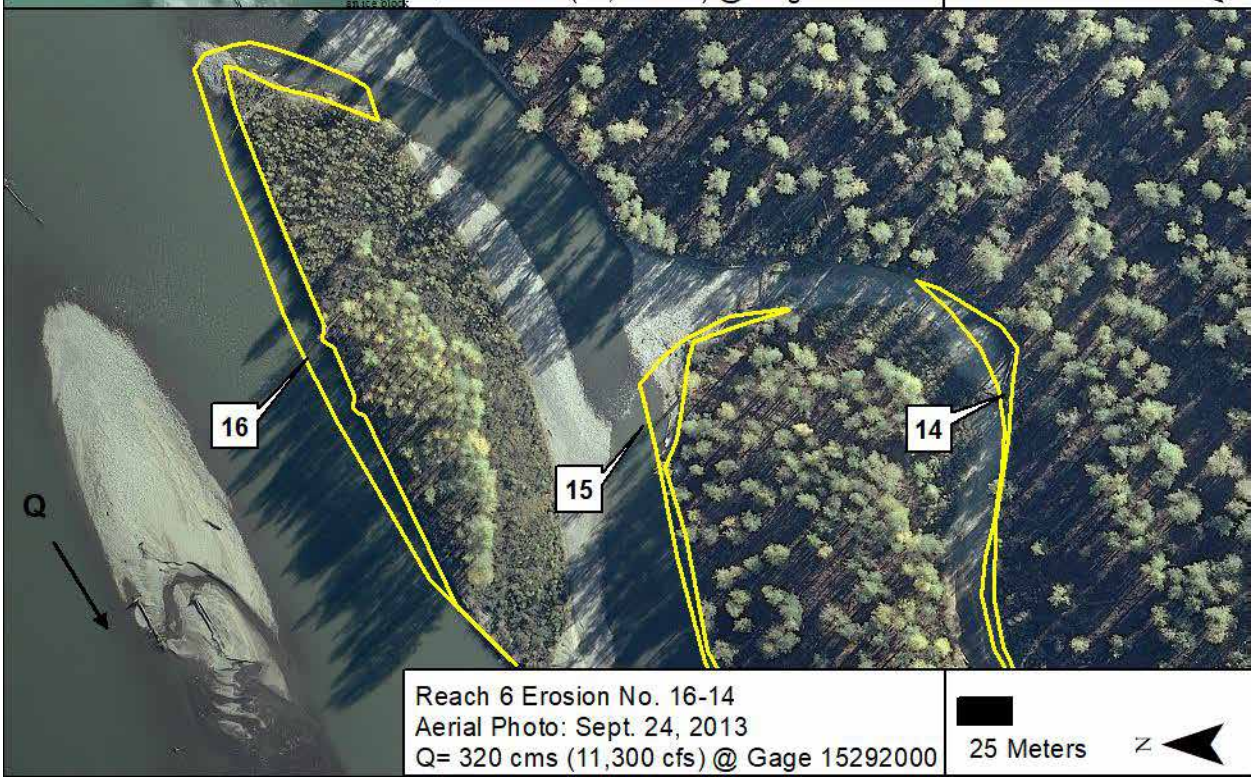

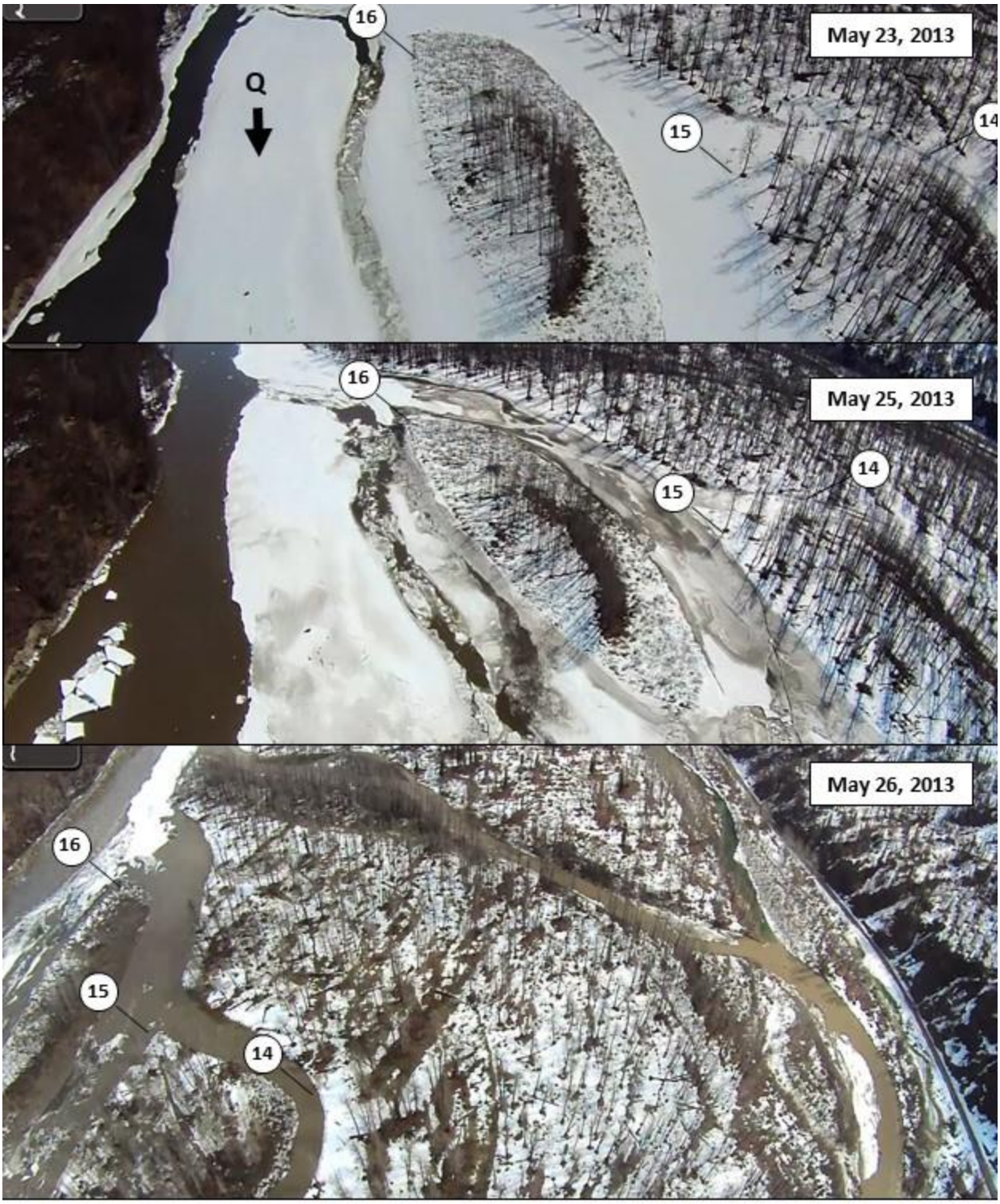
May 23, 2013
Q
16
15
14
May 25, 2013
16
15
14
May 26, 2013
16
15
14

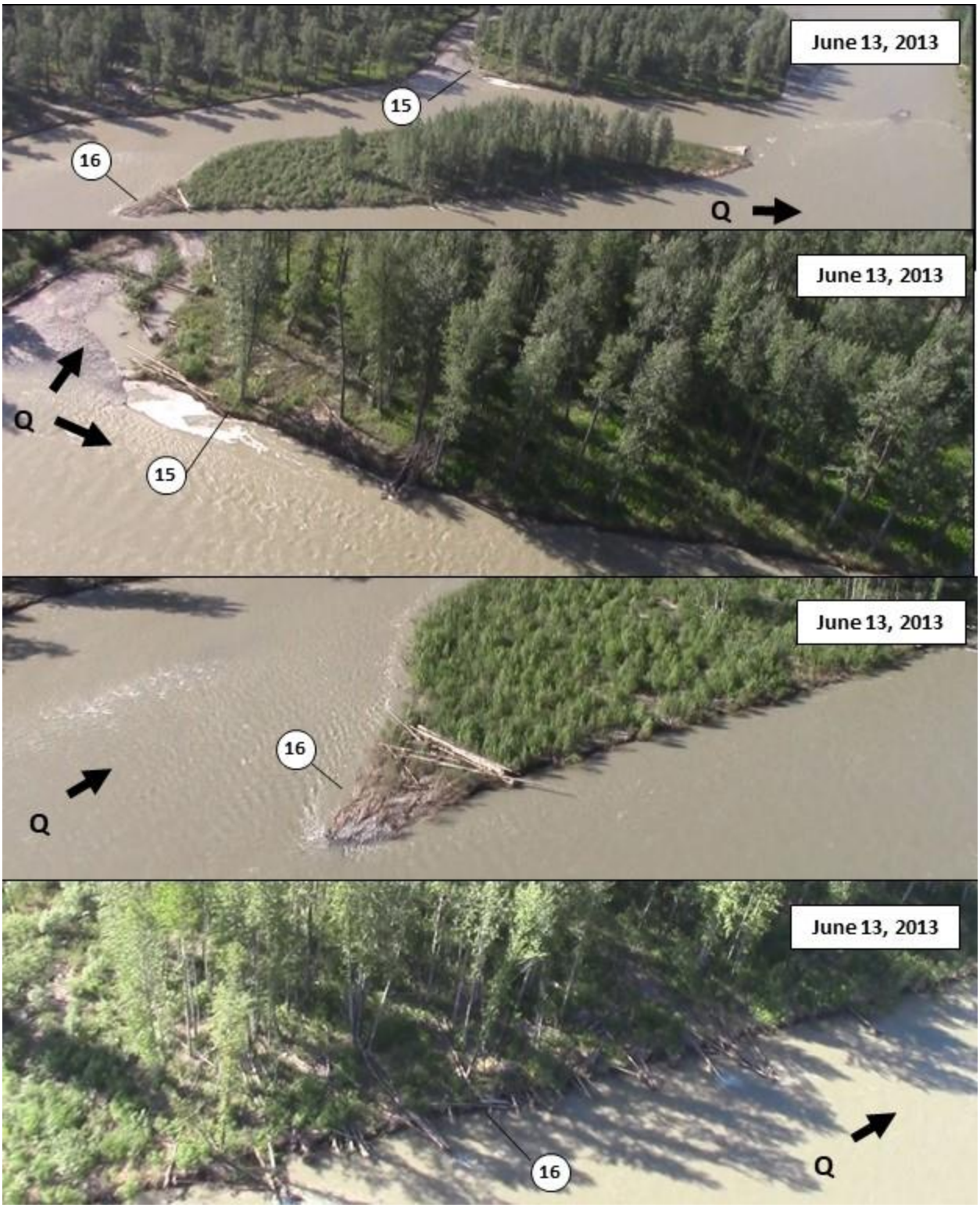
June 13, 2013
15
16
Q
June 13, 2013
Q
15
June 13, 2013
16
Q
June 13, 2013
16
Q

B.1.25 Erosion Location No. 13

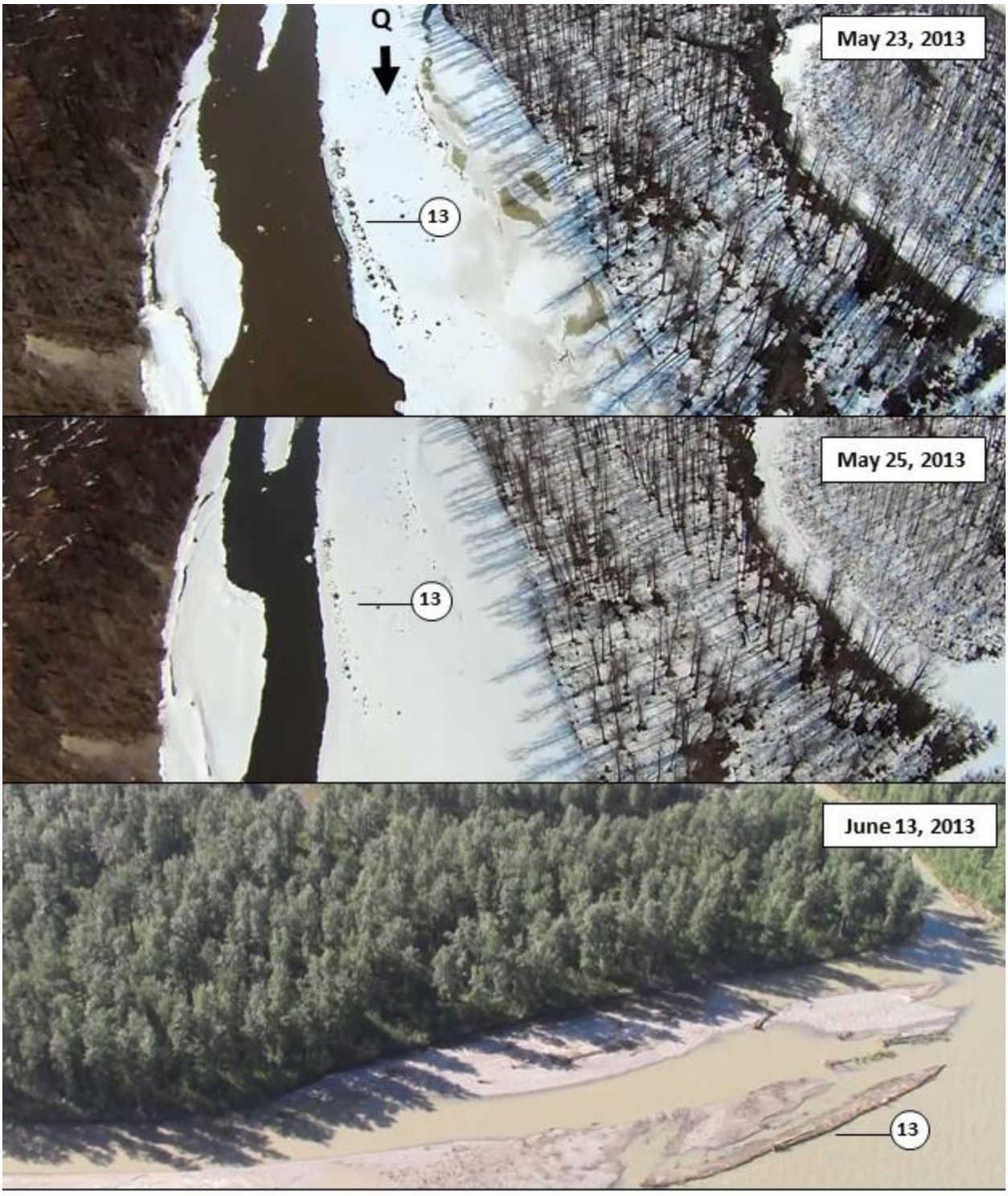
Q
May 23, 2013
13
May 25, 2013
13
June 13, 2013
13

B.1.26 Erosion Location No. 12

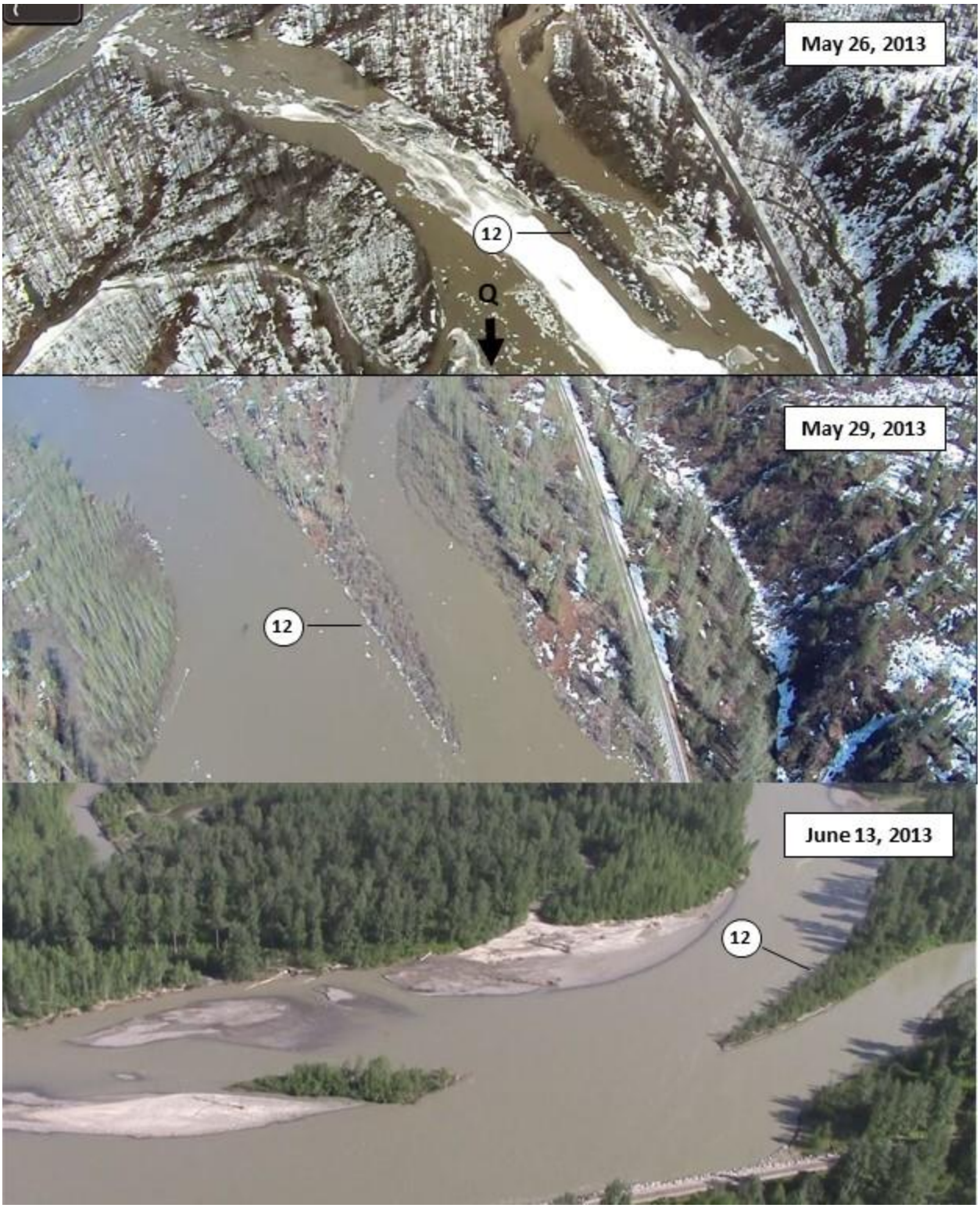
May 26, 2013
12
Q
May 29, 2013
12
June 13, 2013
12

B.1.27 Erosion Location No. 11

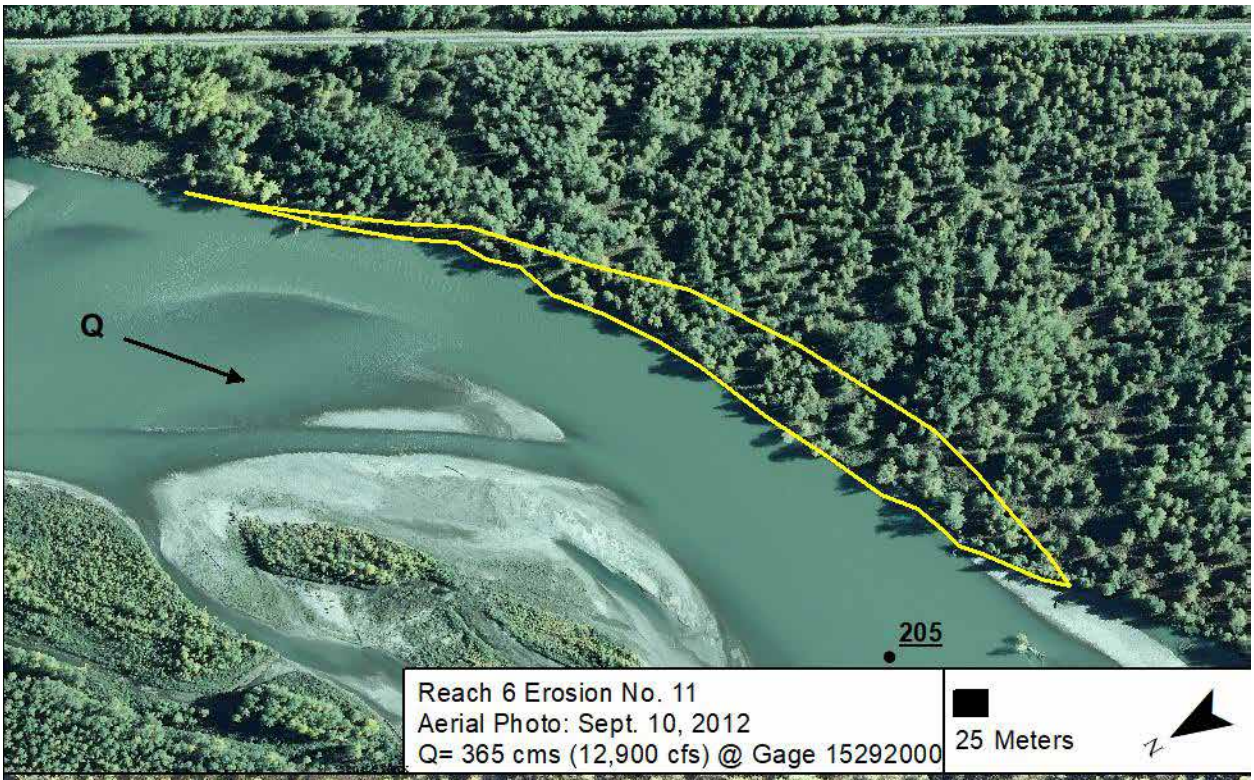

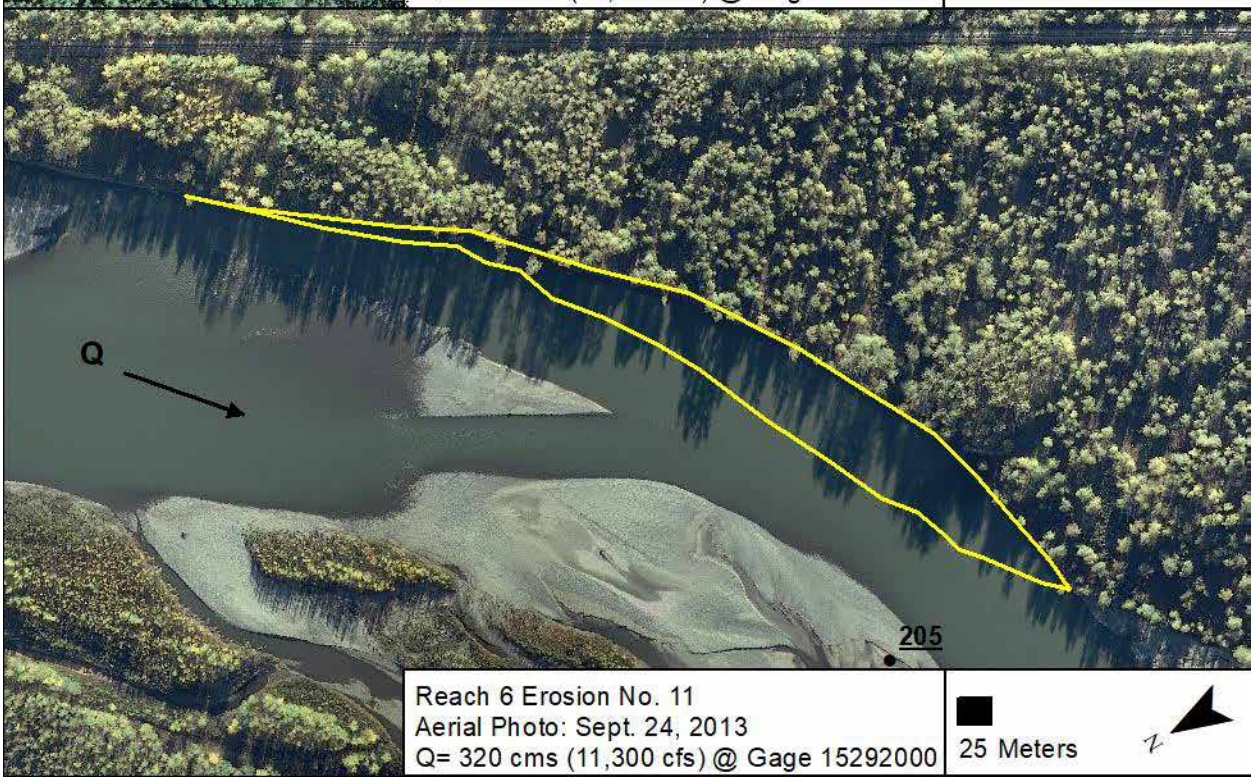

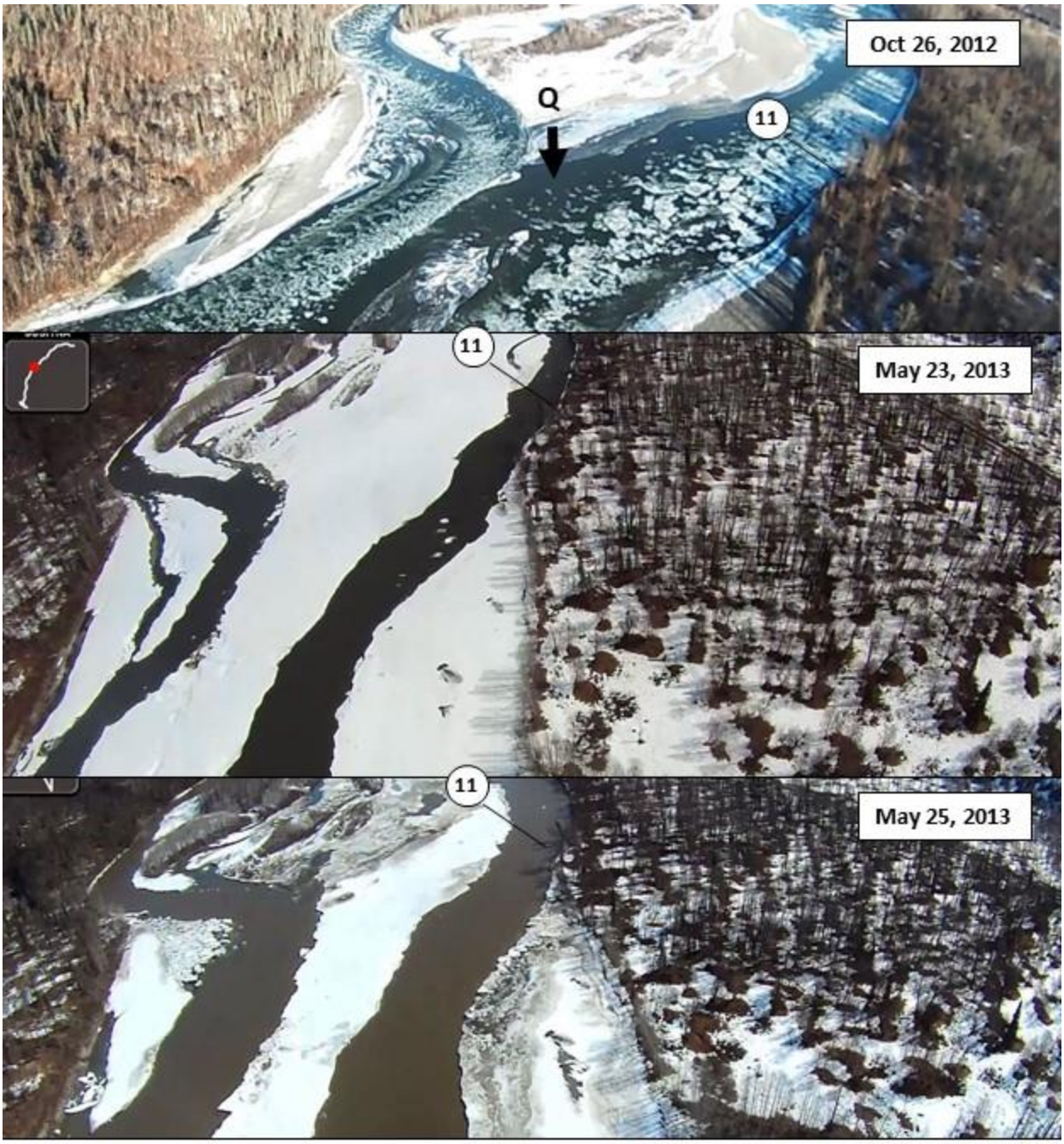
Oct 26, 2012
Q
11
11
May 23, 2013
11
May 25, 2013

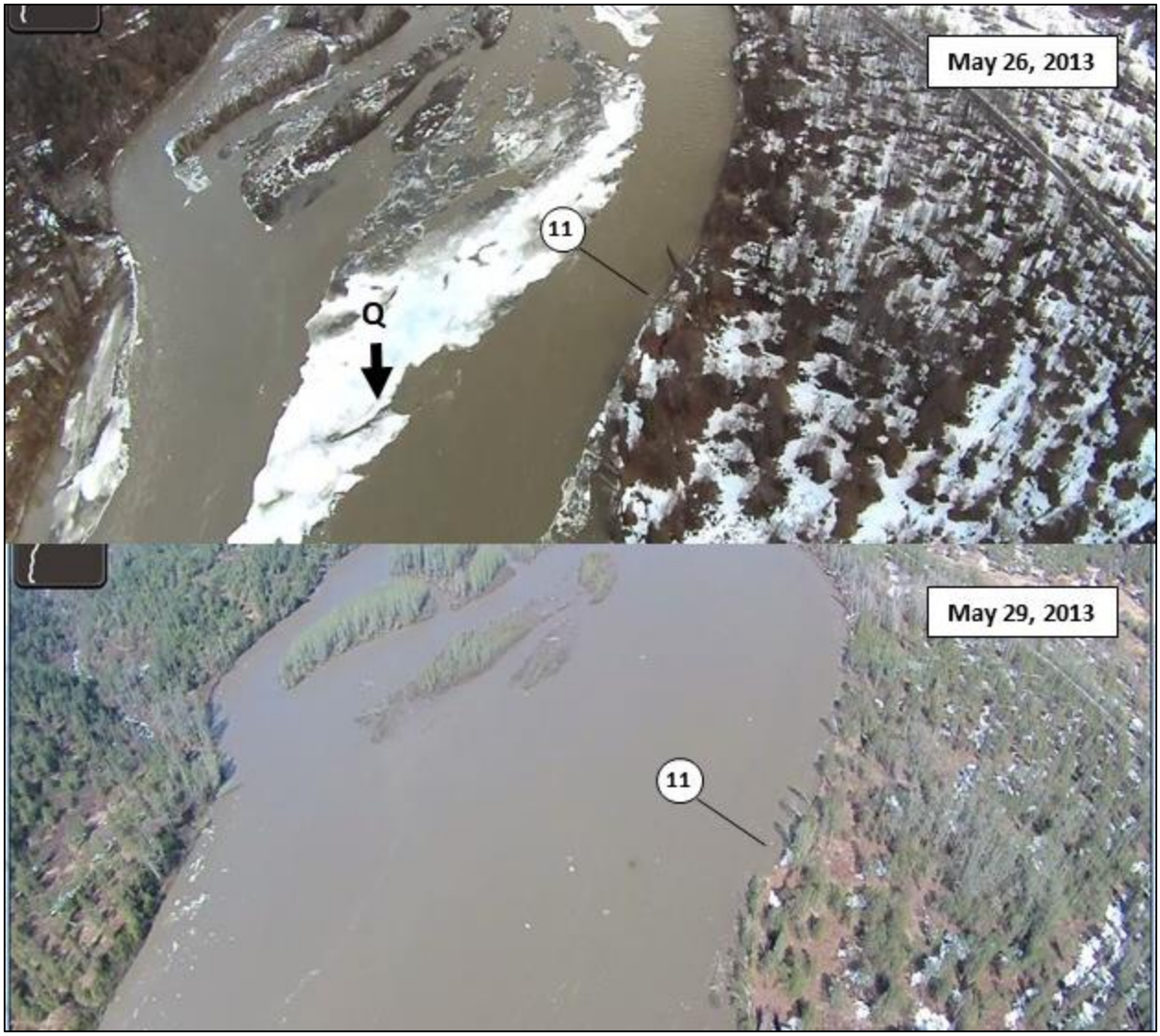
May 26, 2013
11
Q
May 29, 2013
11

B.1.28 Erosion Location No. 10

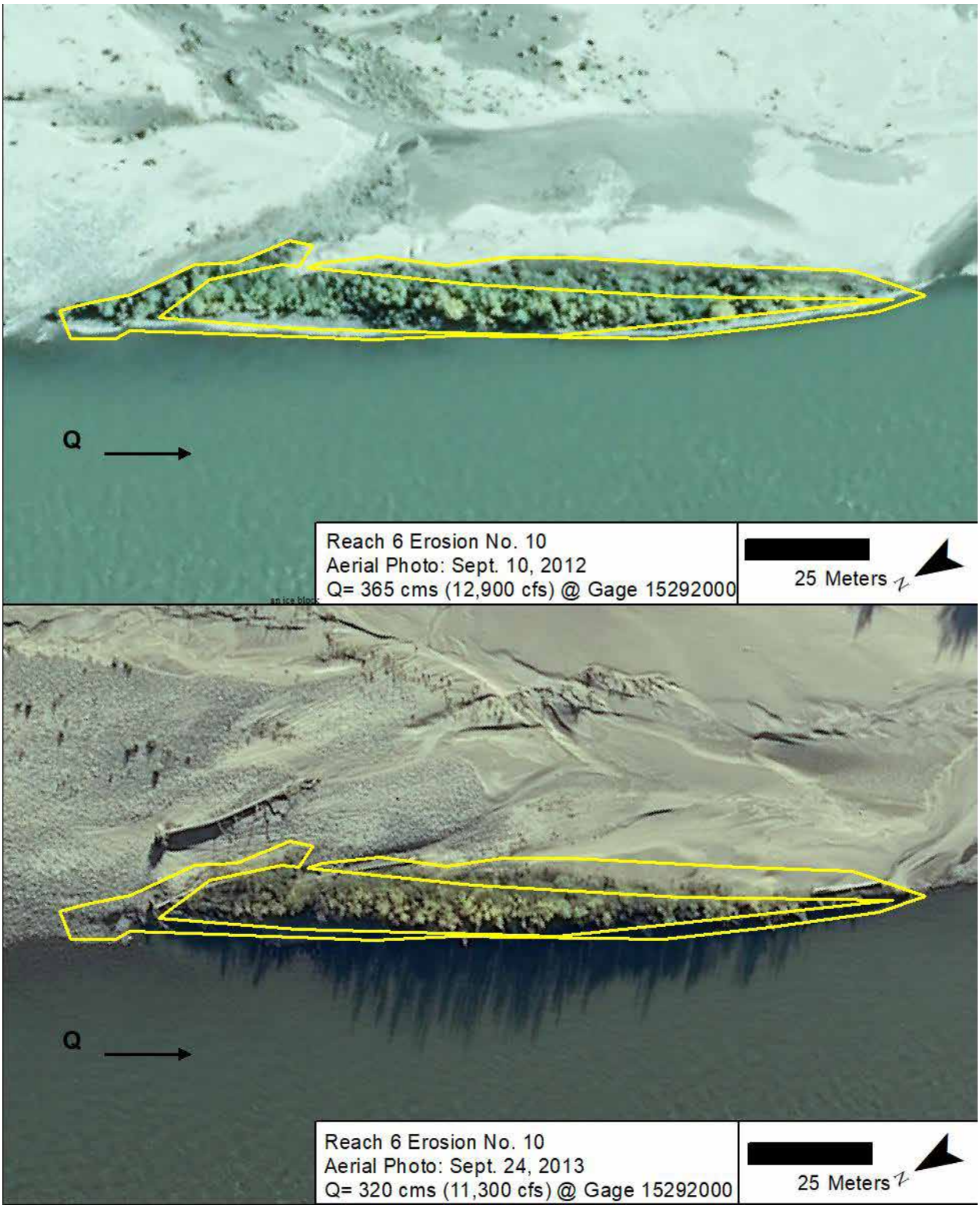

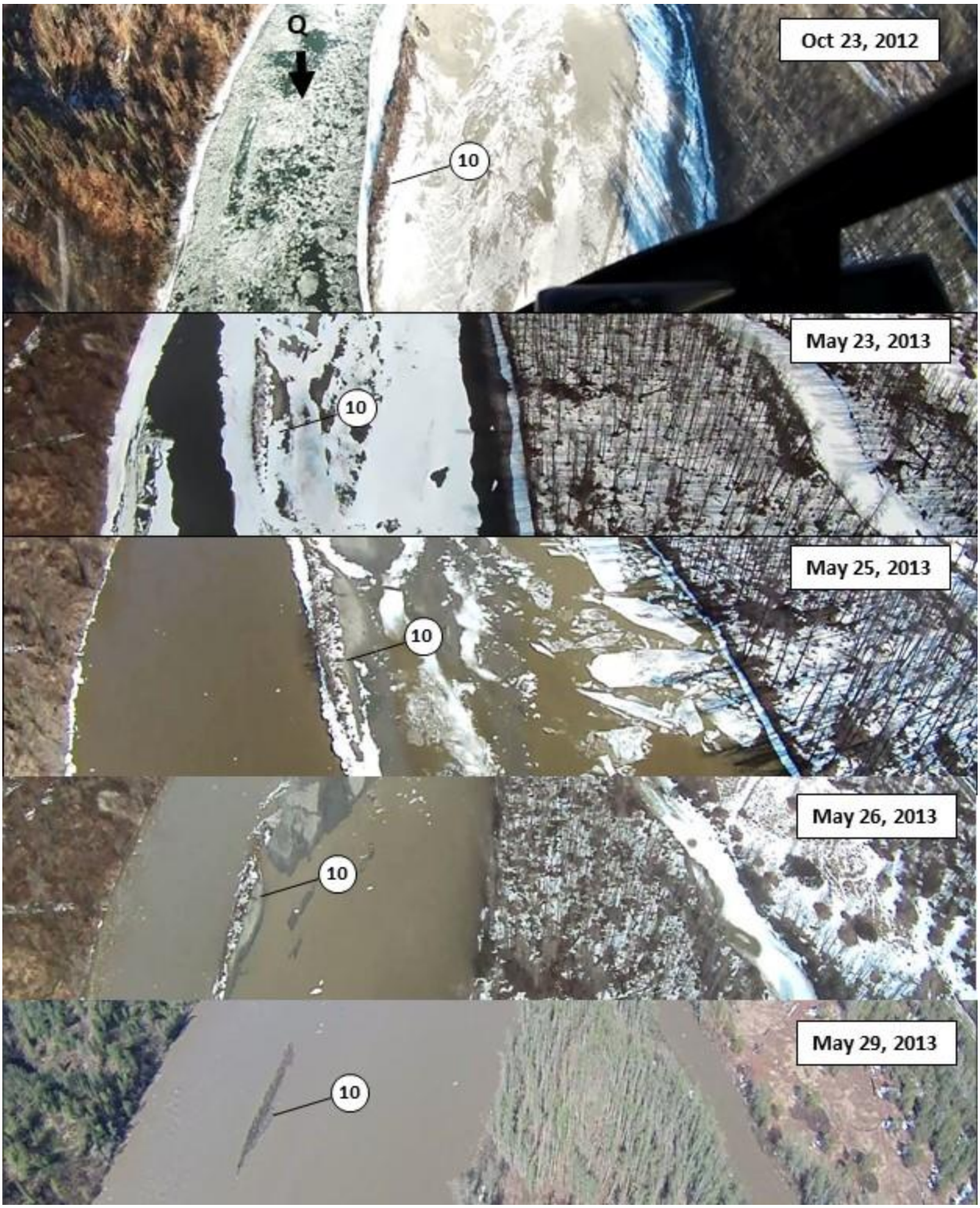
Q
Oct 23, 2012
10
May 23, 2013
10
May 25, 2013
10
May 26, 2013
10
May 29, 2013
10

B.1.29 Erosion Location No. 9

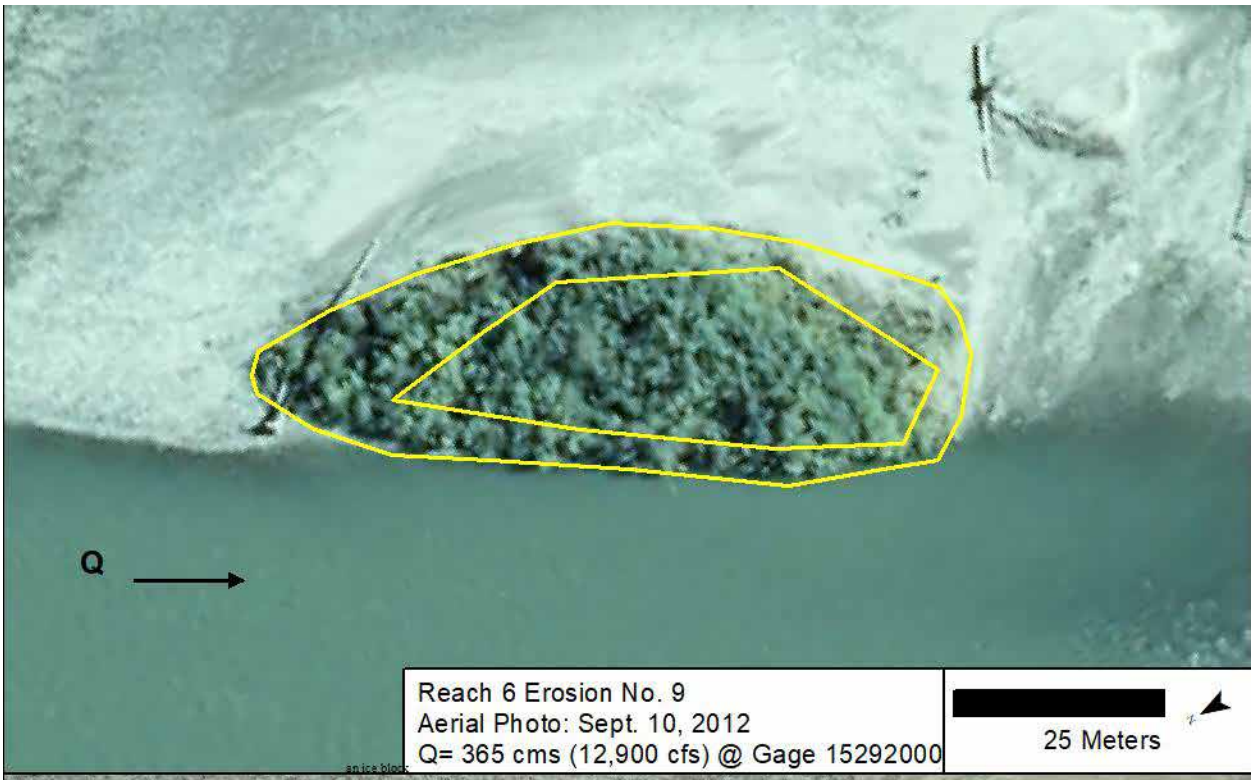

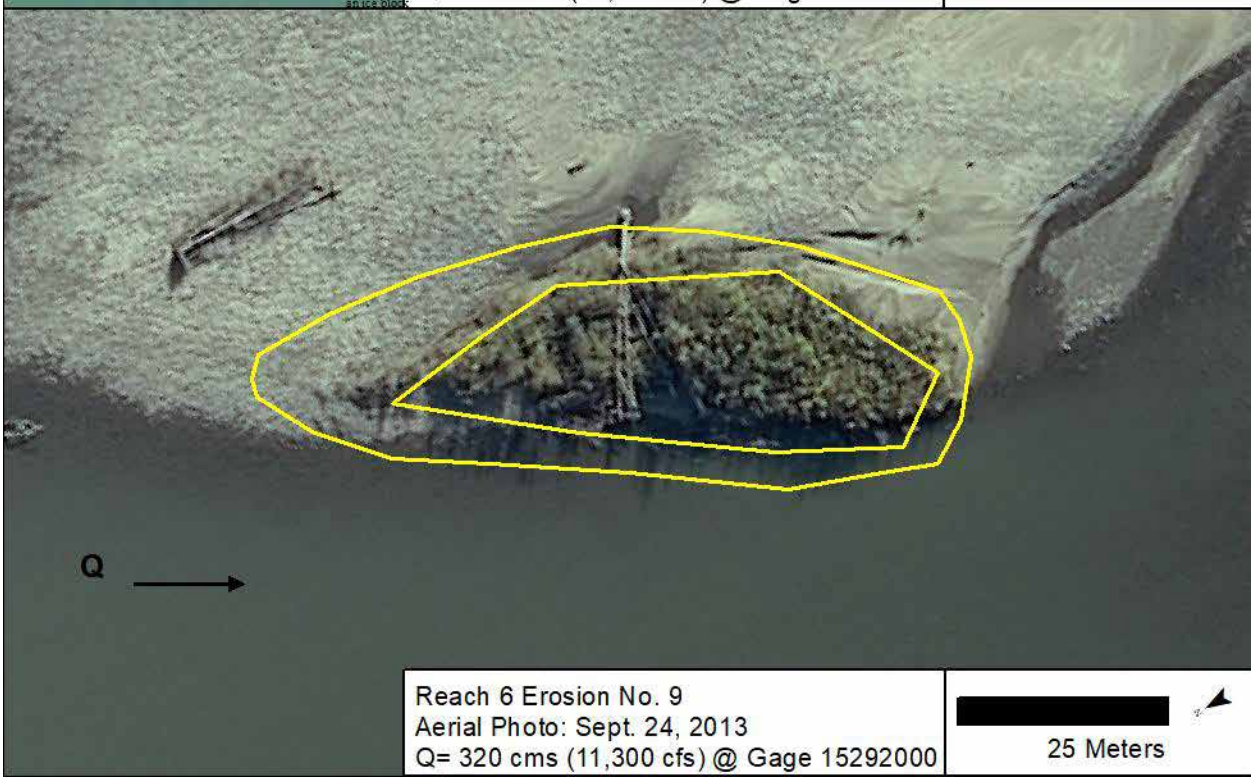

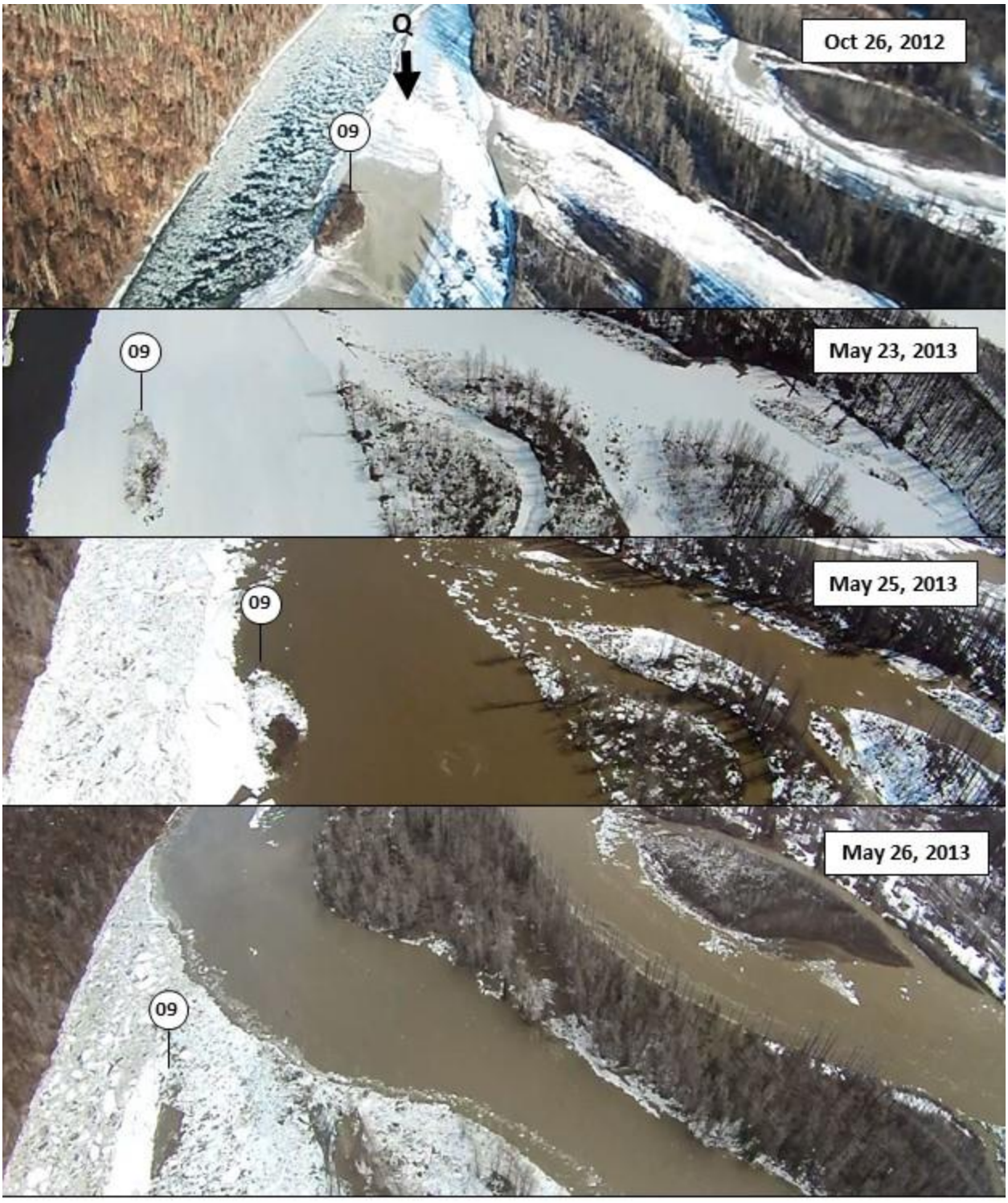
Q
Oct 26, 2012
09
09
May 23, 2013
09
May 25, 2013
09
May 26, 2013

B.1.30 Erosion Location No. 7-4

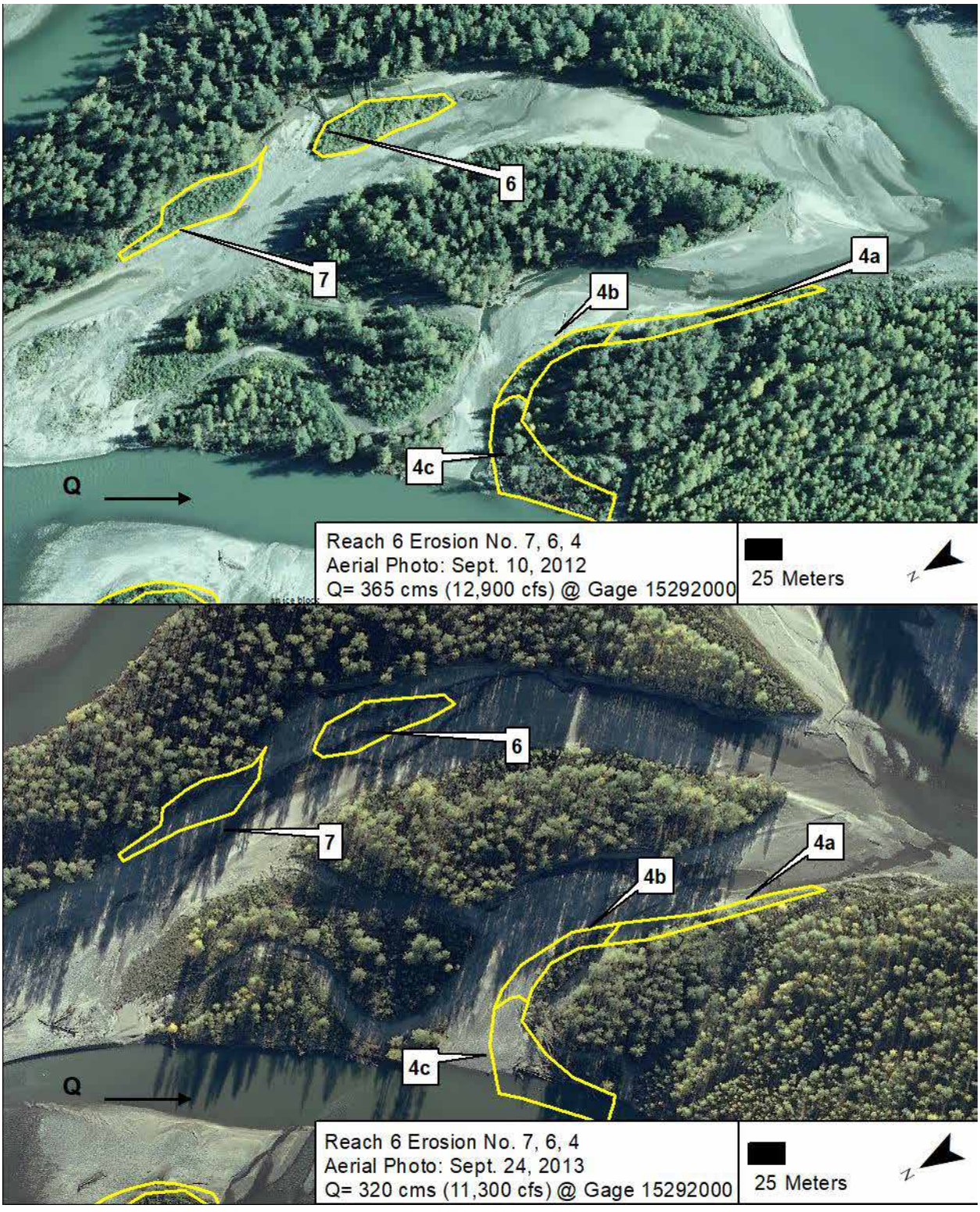

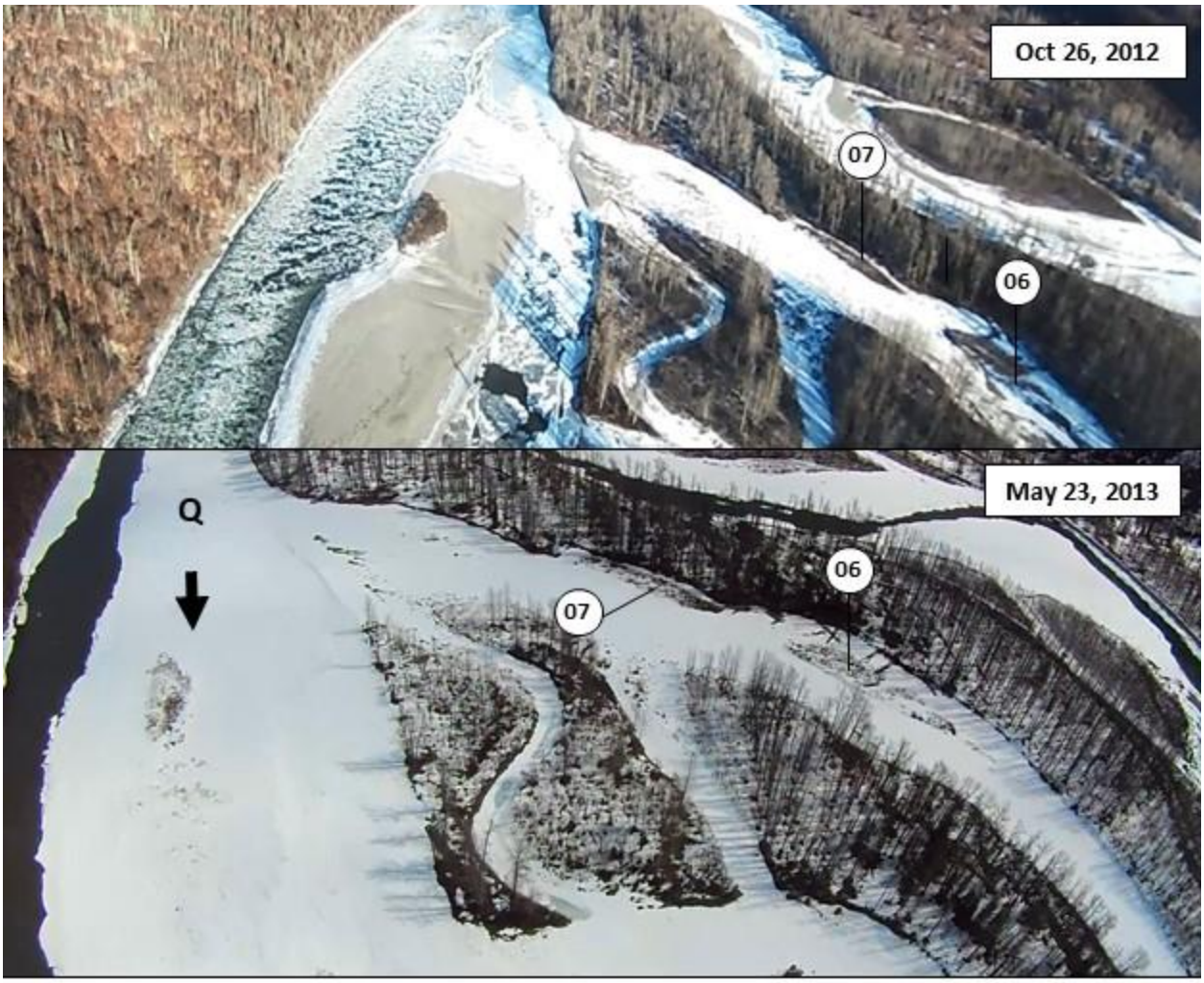
Oct 26, 2012
07
06
May 23, 2013
Q
06
07

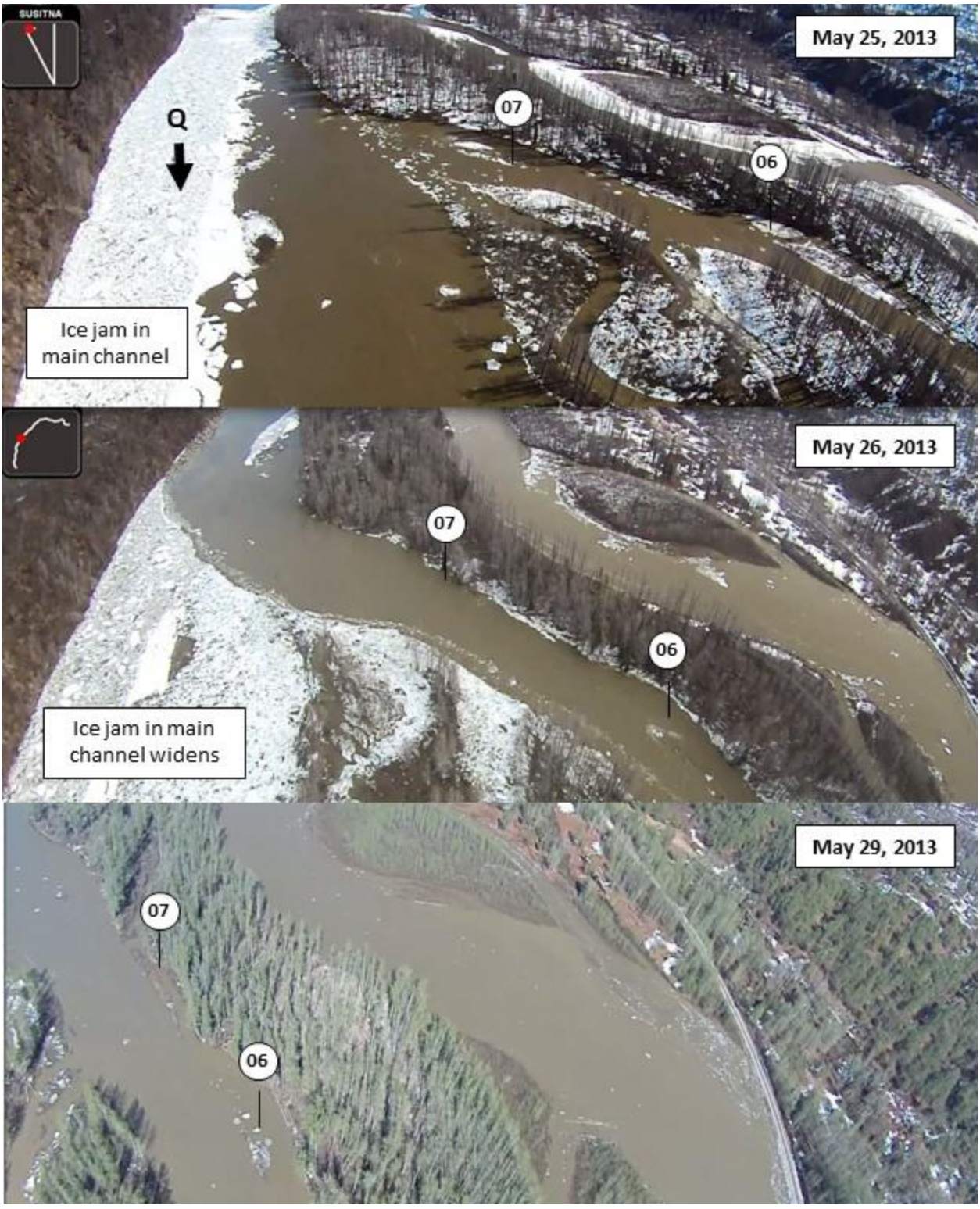
SUSITNA
May 25, 2013
Q
07
06
Ice jam in main channel
May 26, 2013
07
06
Ice jam in main channel widens
May 29, 2013
07
06

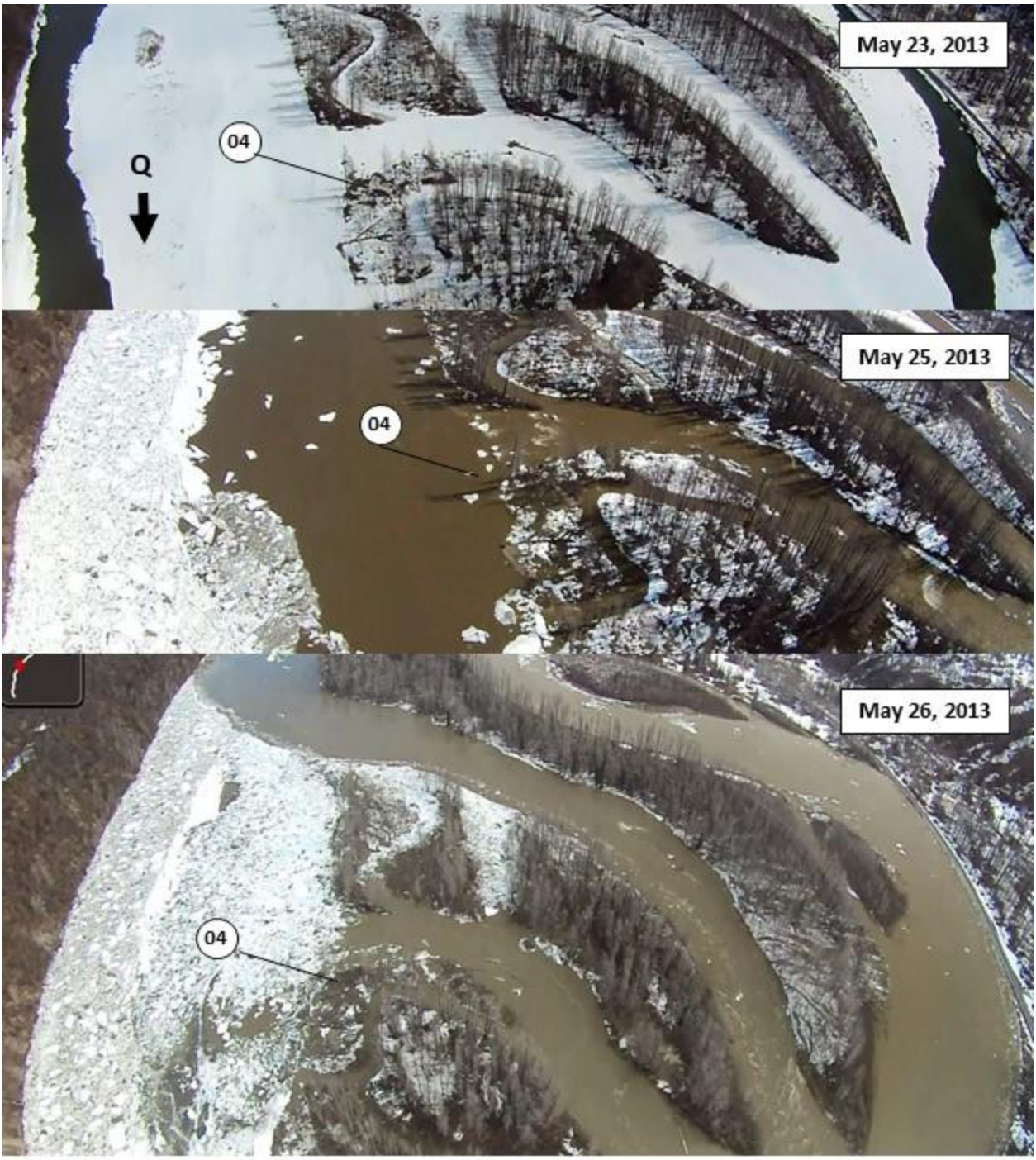
May 23, 2013
04
Q
May 25, 2013
04
May 26, 2013
04

B.1.31 Erosion Location No. 3

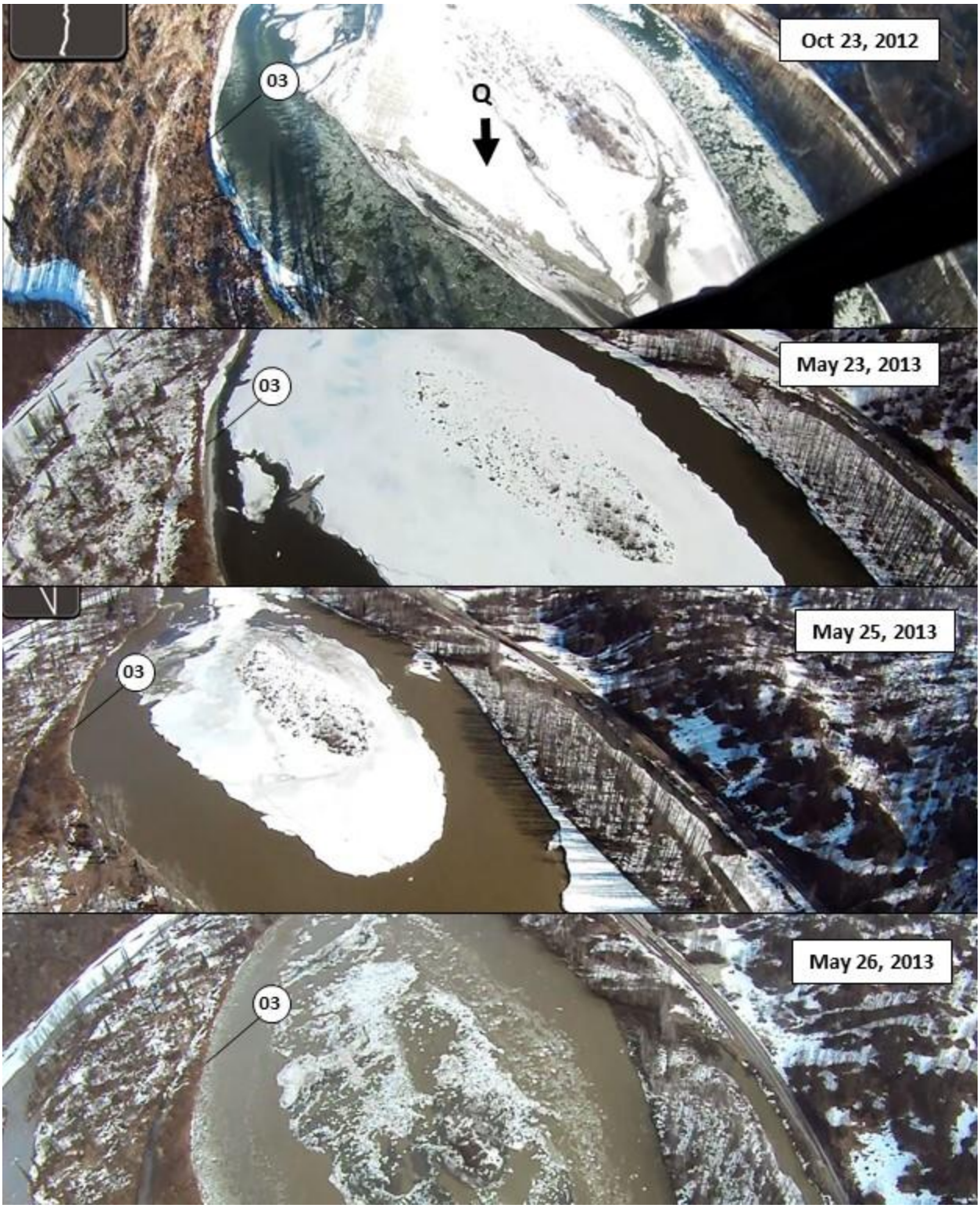
Oct 23, 2012
03
Q
May 23, 2013
03
May 25, 2013
03
May 26, 2013
03

B.1.32 Erosion Location No. 2

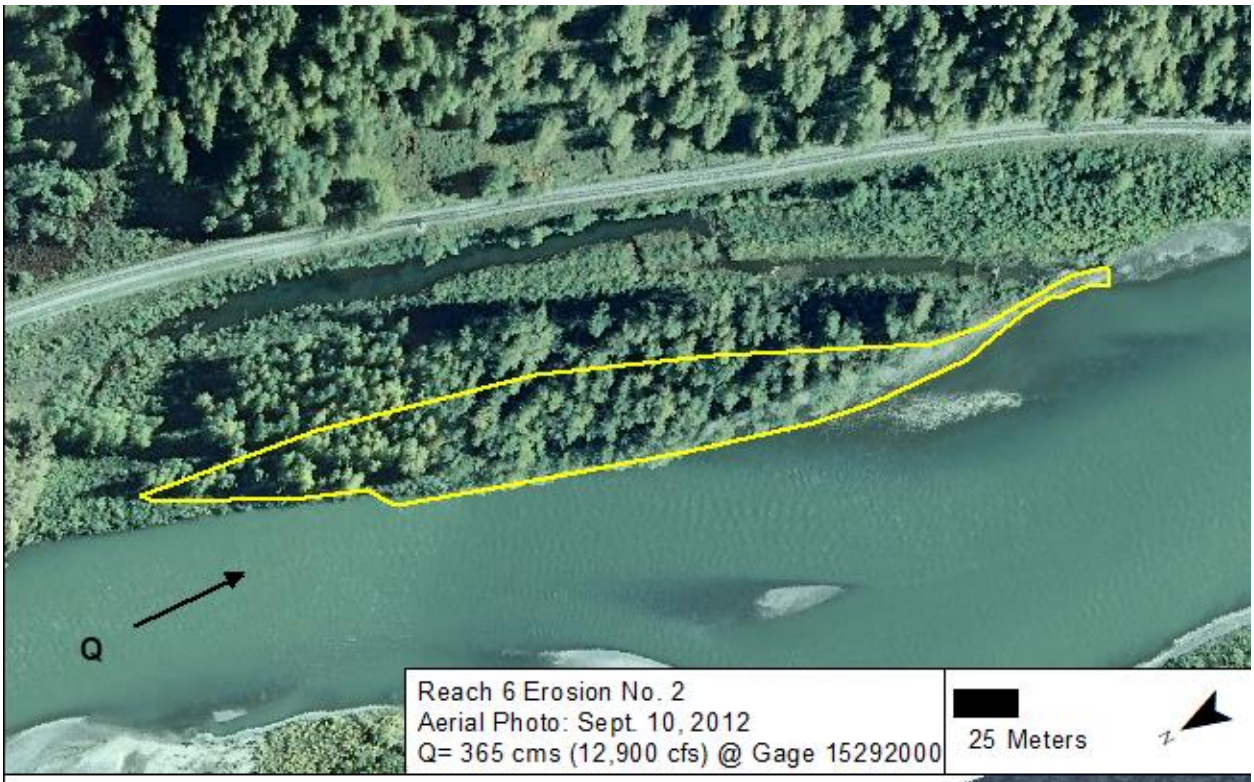

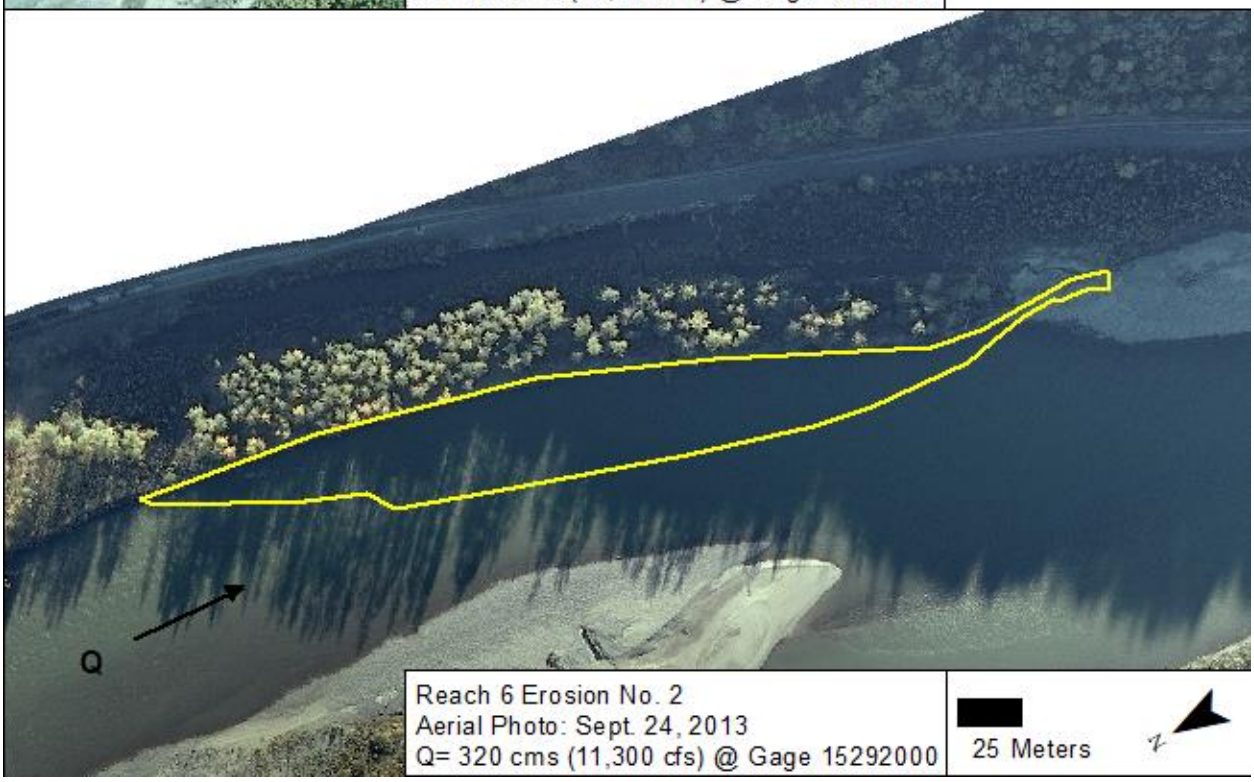

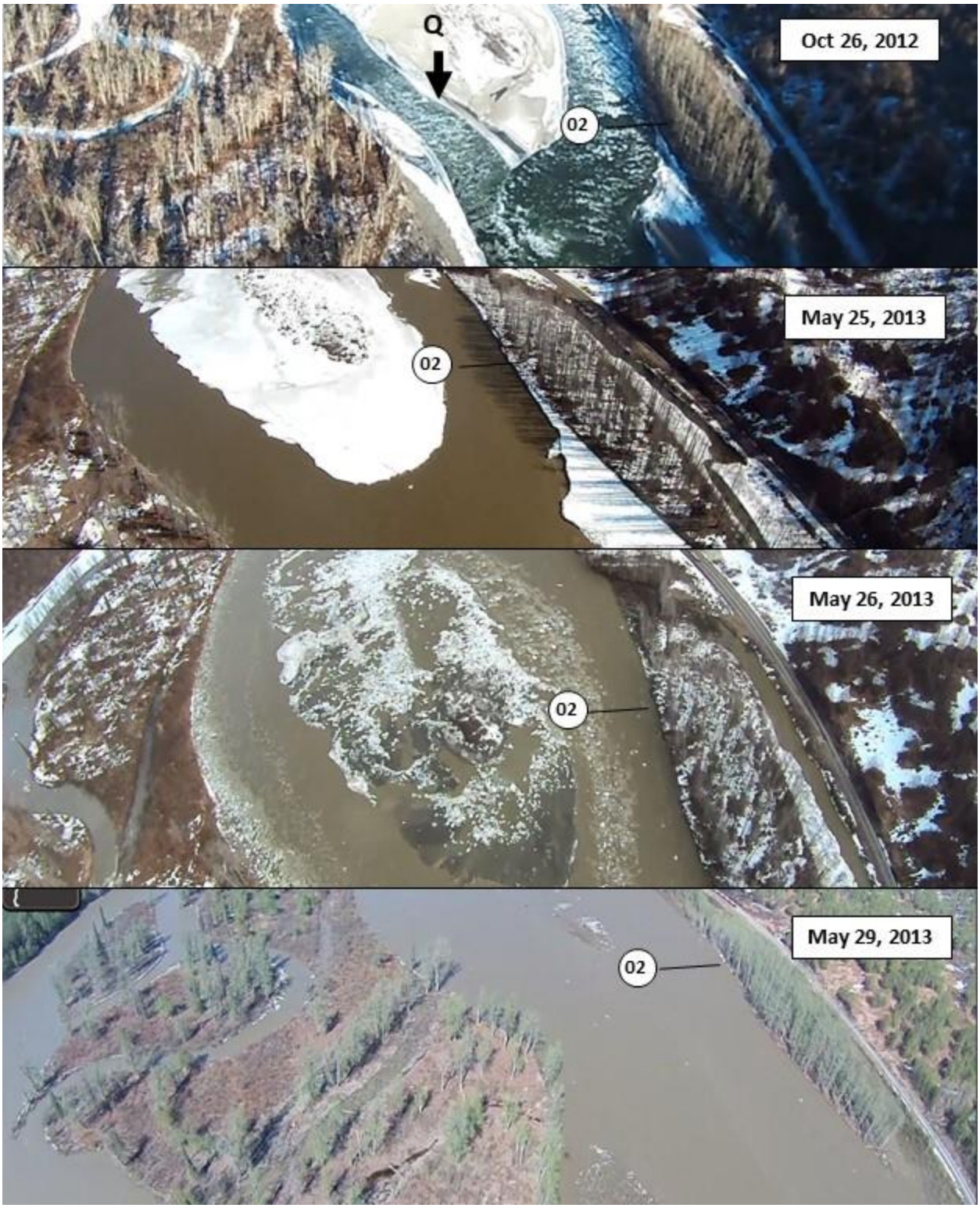
Q
Oct 26, 2012
02
May 25, 2013
02
May 26, 2013
02
May 29, 2013
02

B.1.33 Erosion Location No. 1

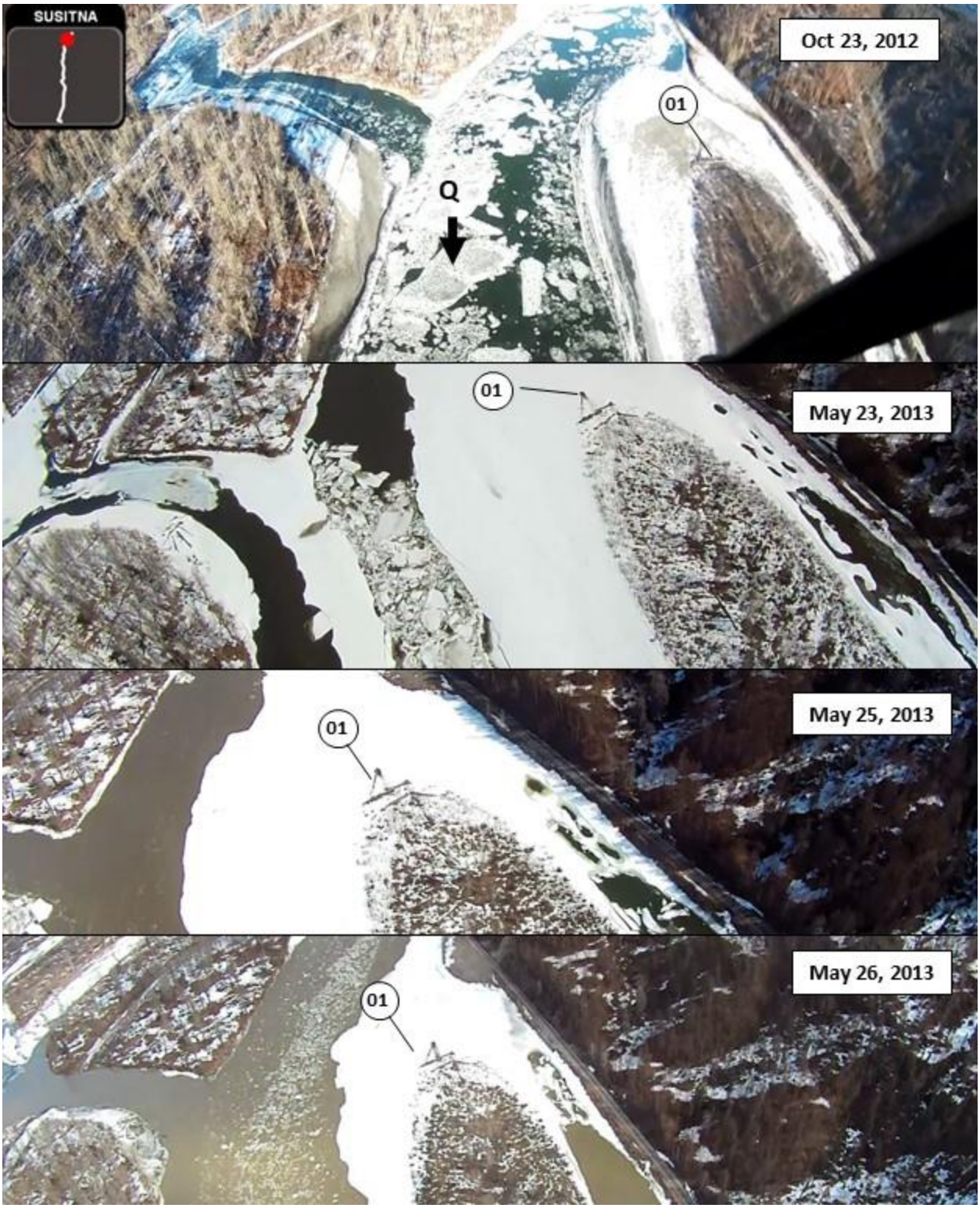
SUSITNA
Oct 23, 2012
01
Q
01
May 23, 2013
01
May 25, 2013
01
May 26, 2013

B.2 Reach 7

B.2.1 Erosion Location No. 13

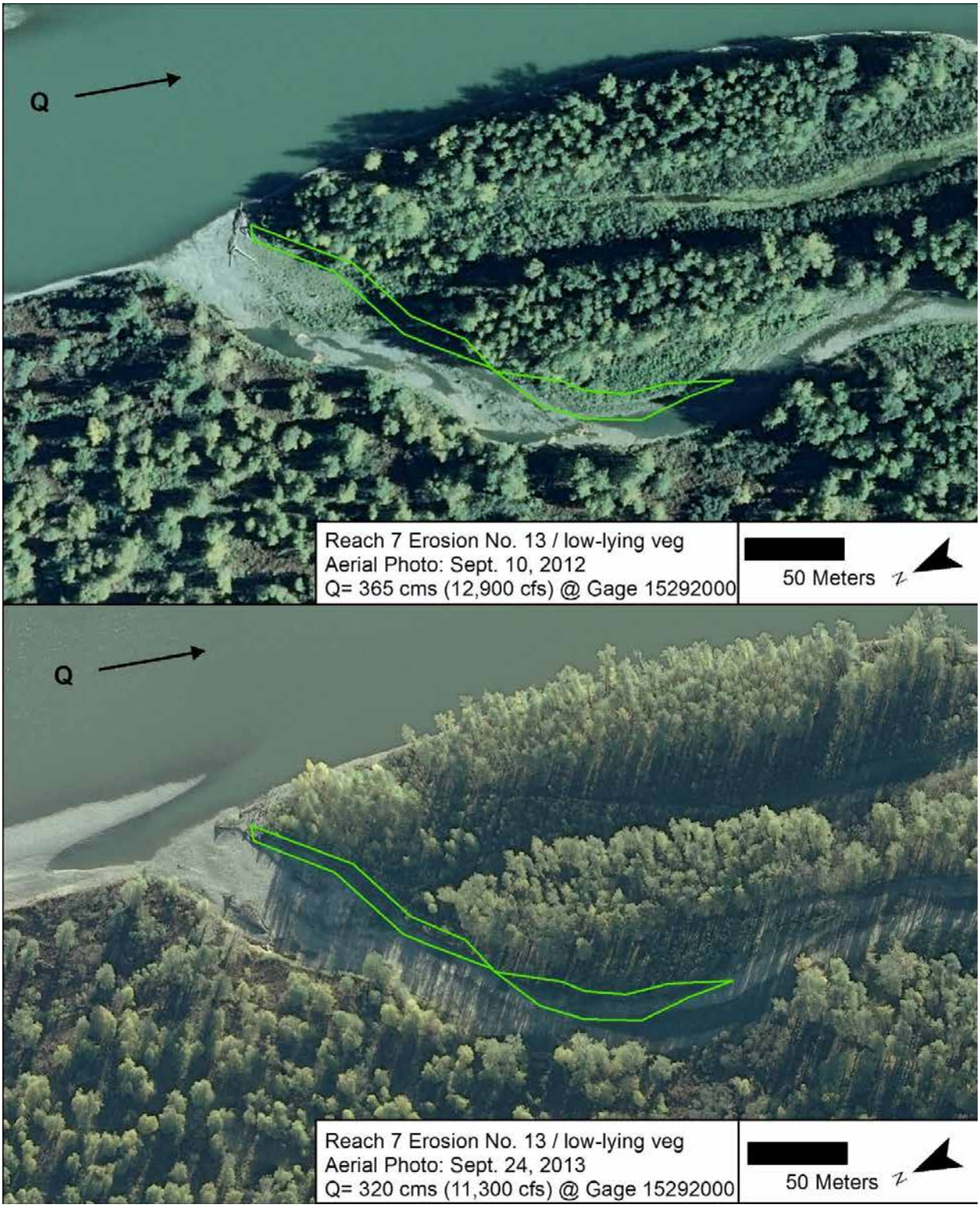

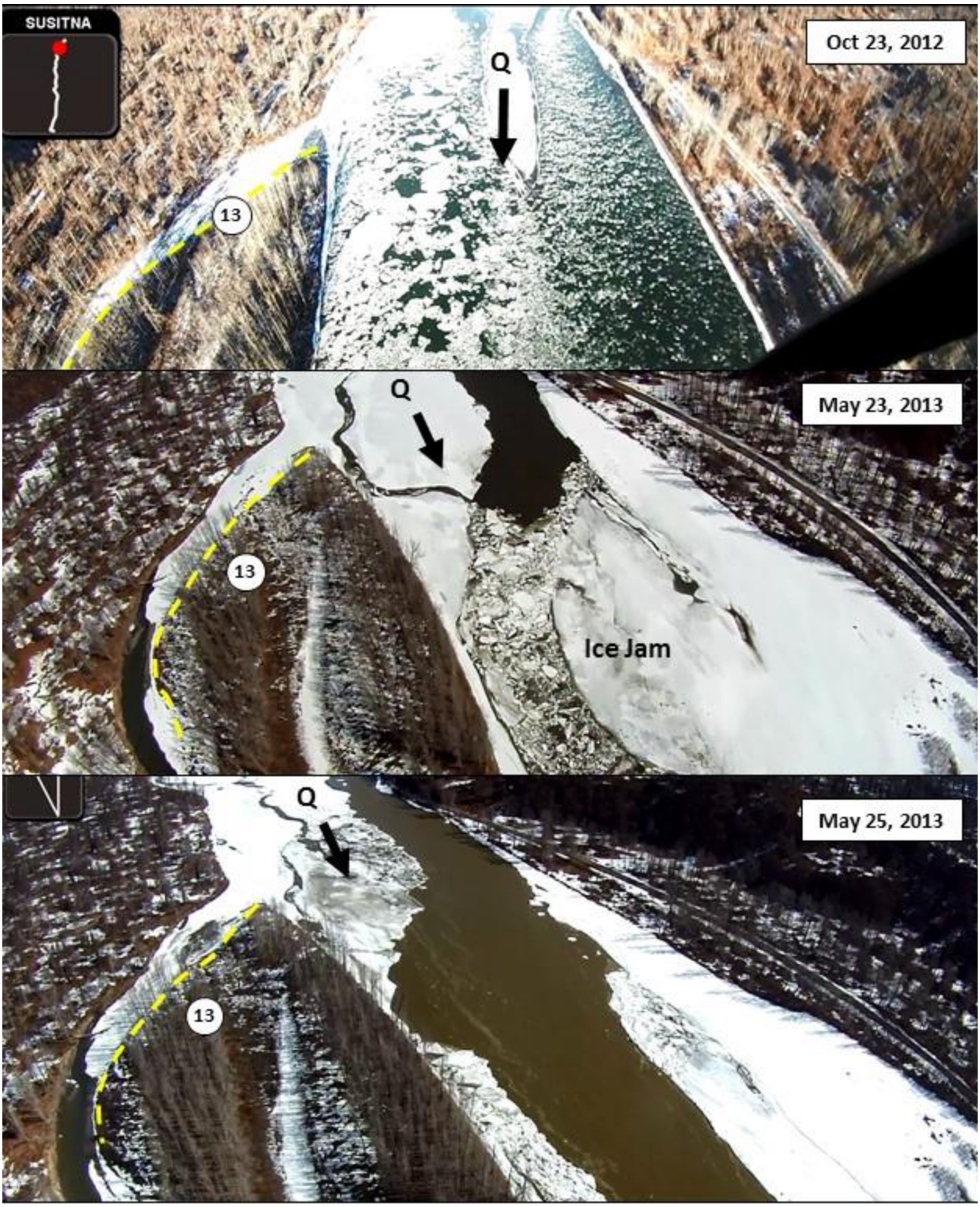
SUSITNA
Oct 23, 2012
Q
13
May 23, 2013
Q
13
Ice Jam
May 25, 2013
Q
13

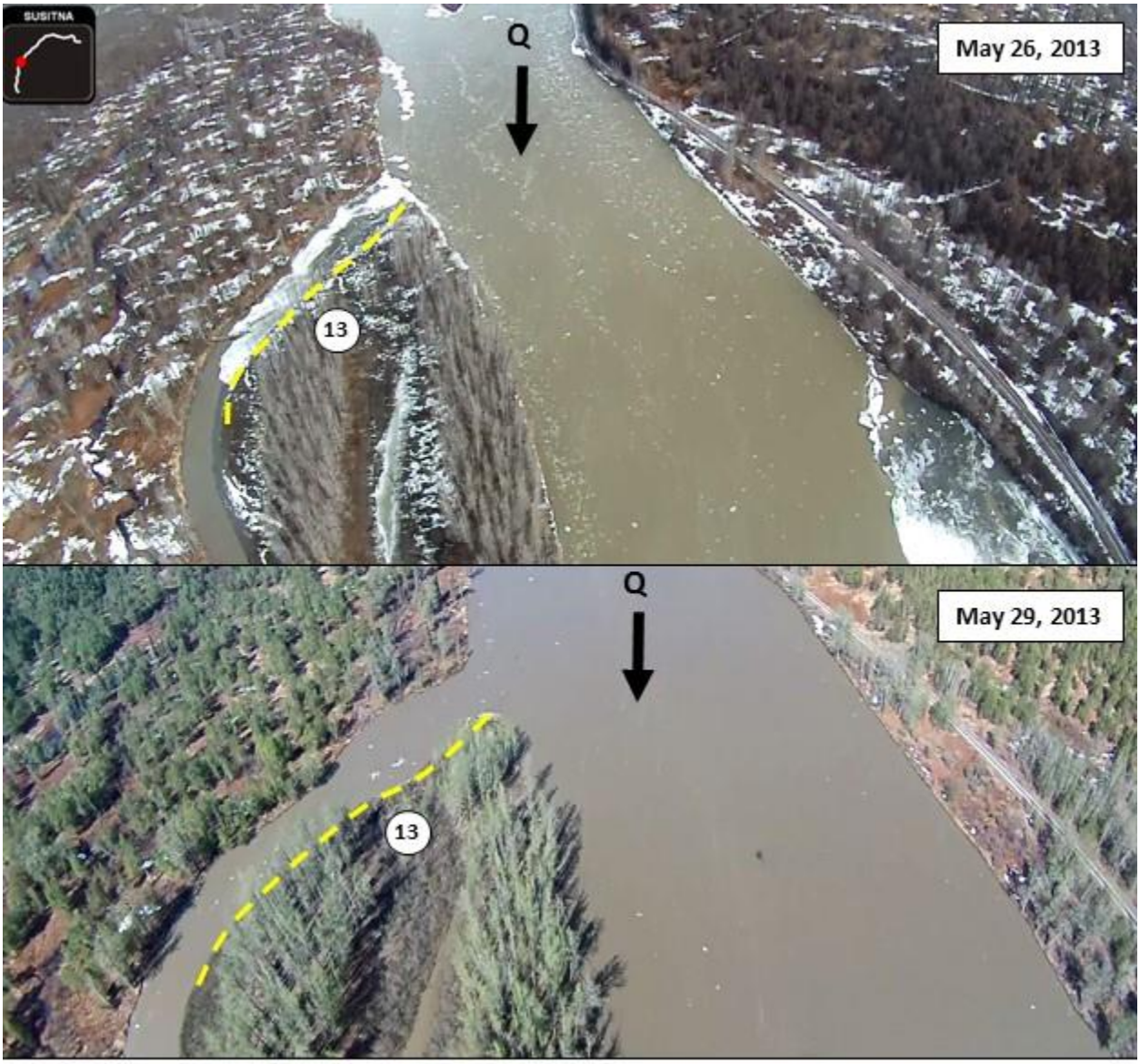
SUSITNA
Q
May 26, 2013
13
Q
May 29, 2013
13

B.2.2 Erosion Location No. 11 and 12

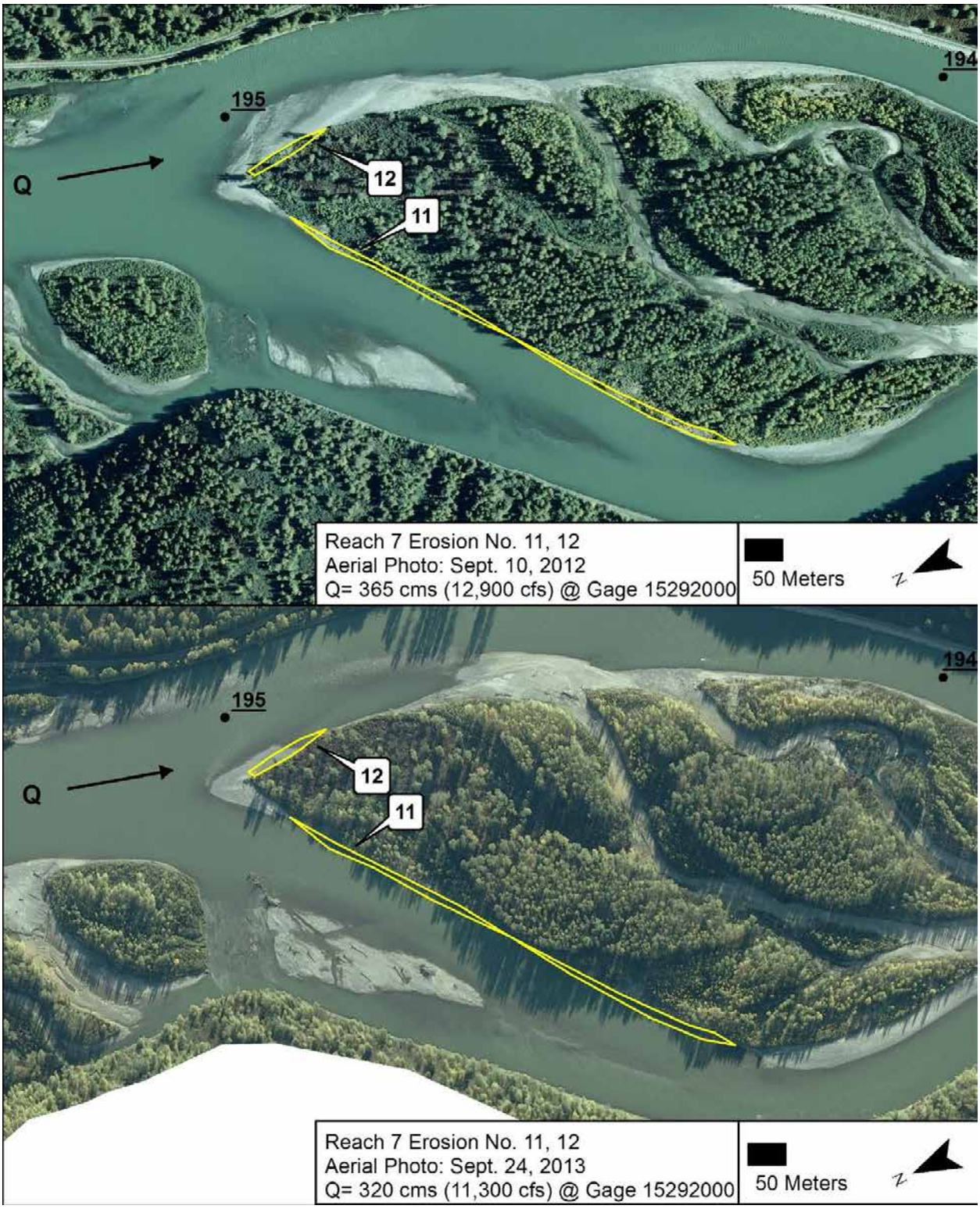

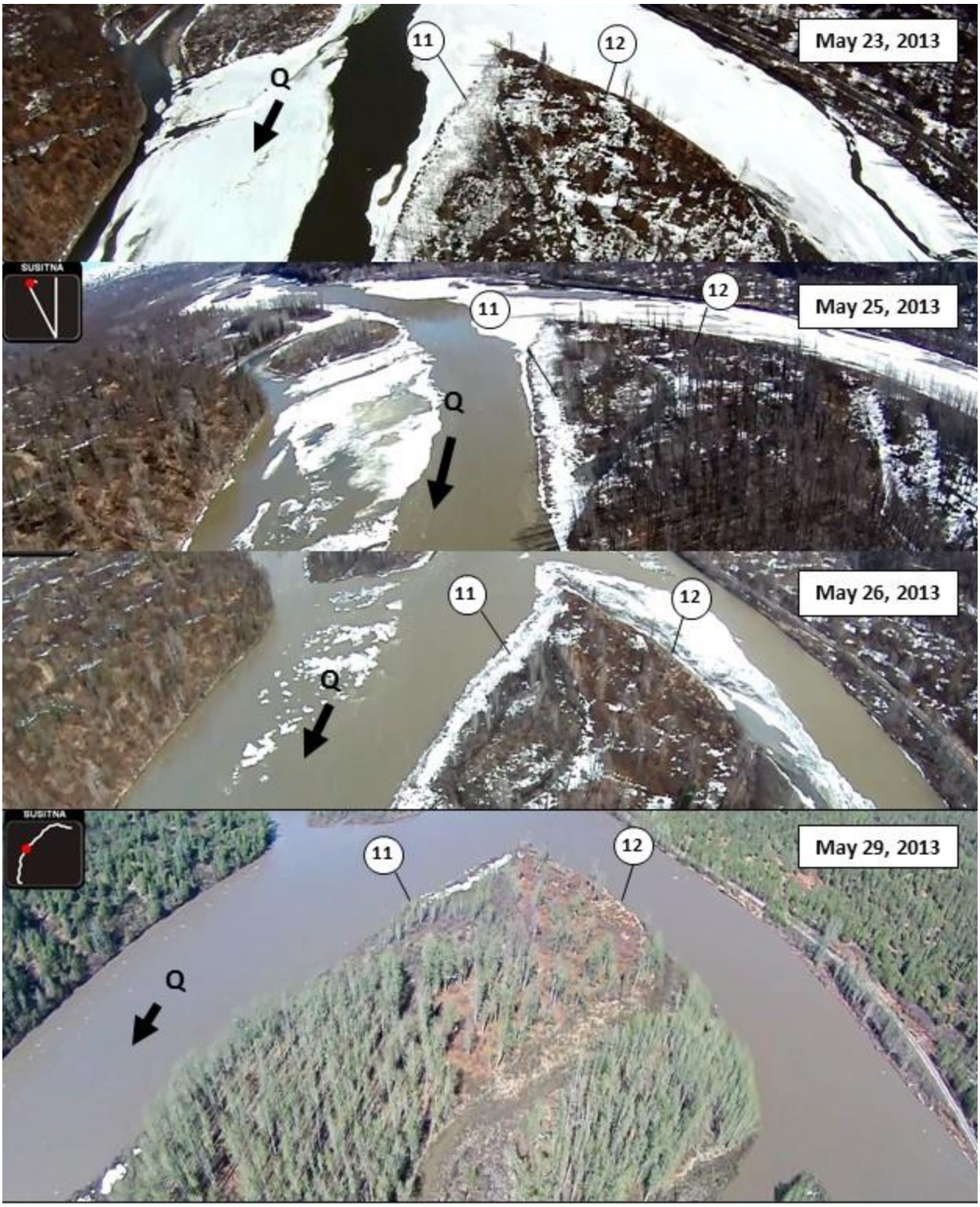
May 23, 2013
11
12
Q
SUSITNA
May 25, 2013
11
12
Q
May 26, 2013
11
12
Q
SUSITNA
May 29, 2013
11
12
Q

B.2.3 Erosion Location No. 10

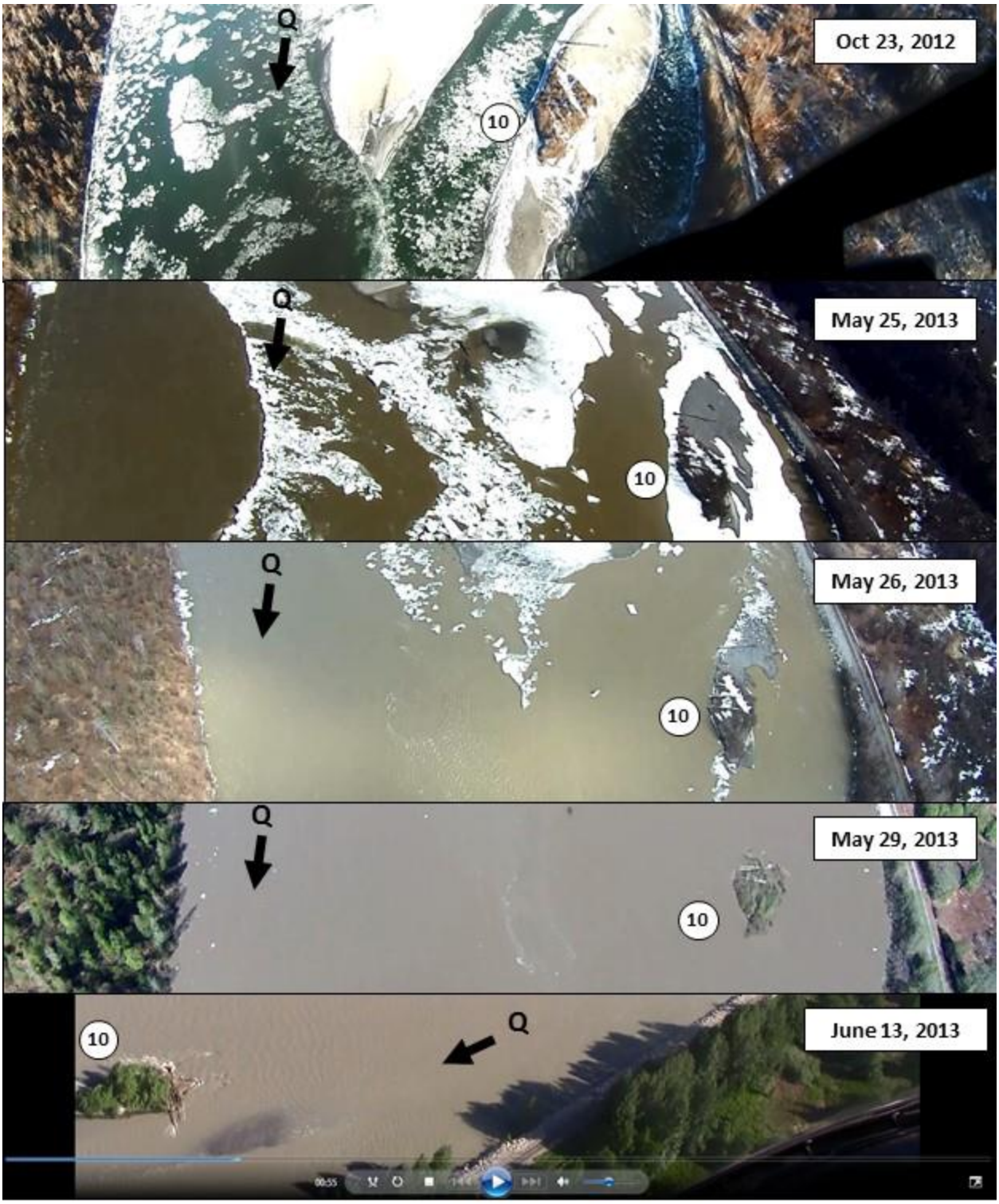
Q
Oct 23, 2012
10
Q
May 25, 2013
10
Q
May 26, 2013
10
Q
May 29, 2013
10
10
Q
June 13, 2013

B.2.4 Erosion Location No. 9, 8, and 7

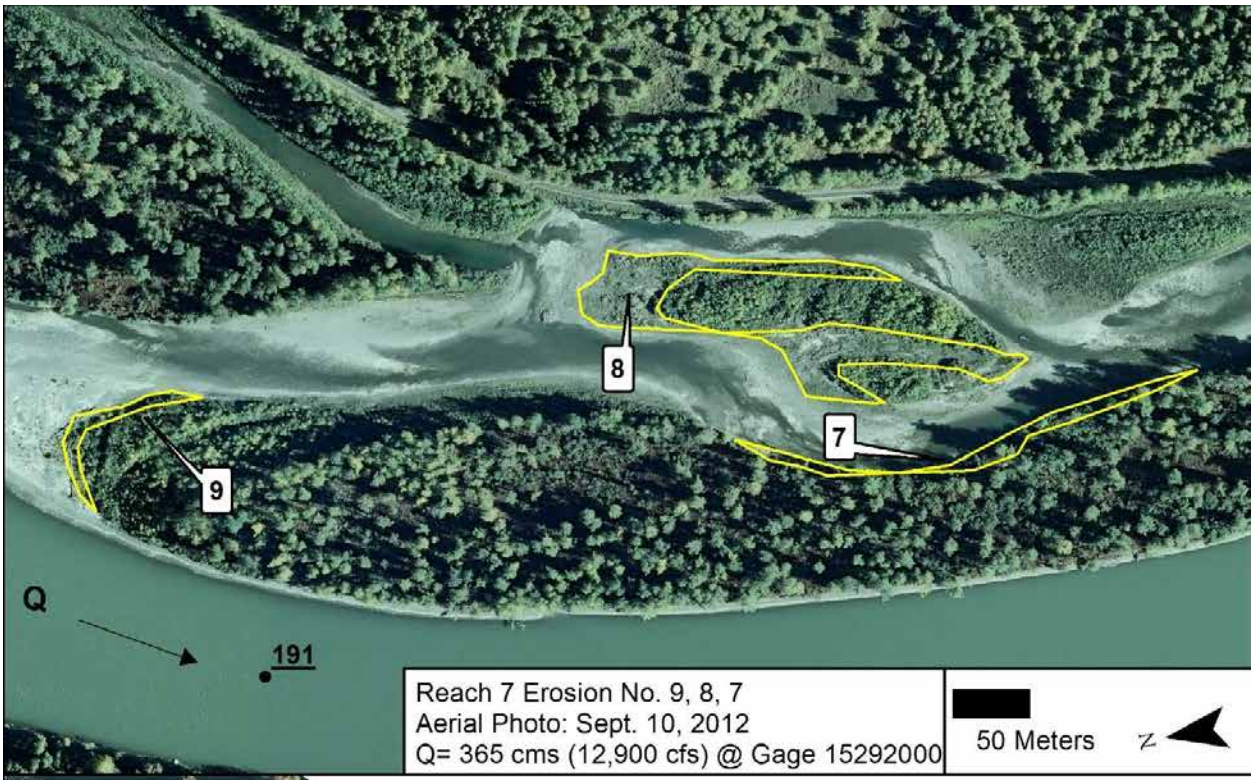

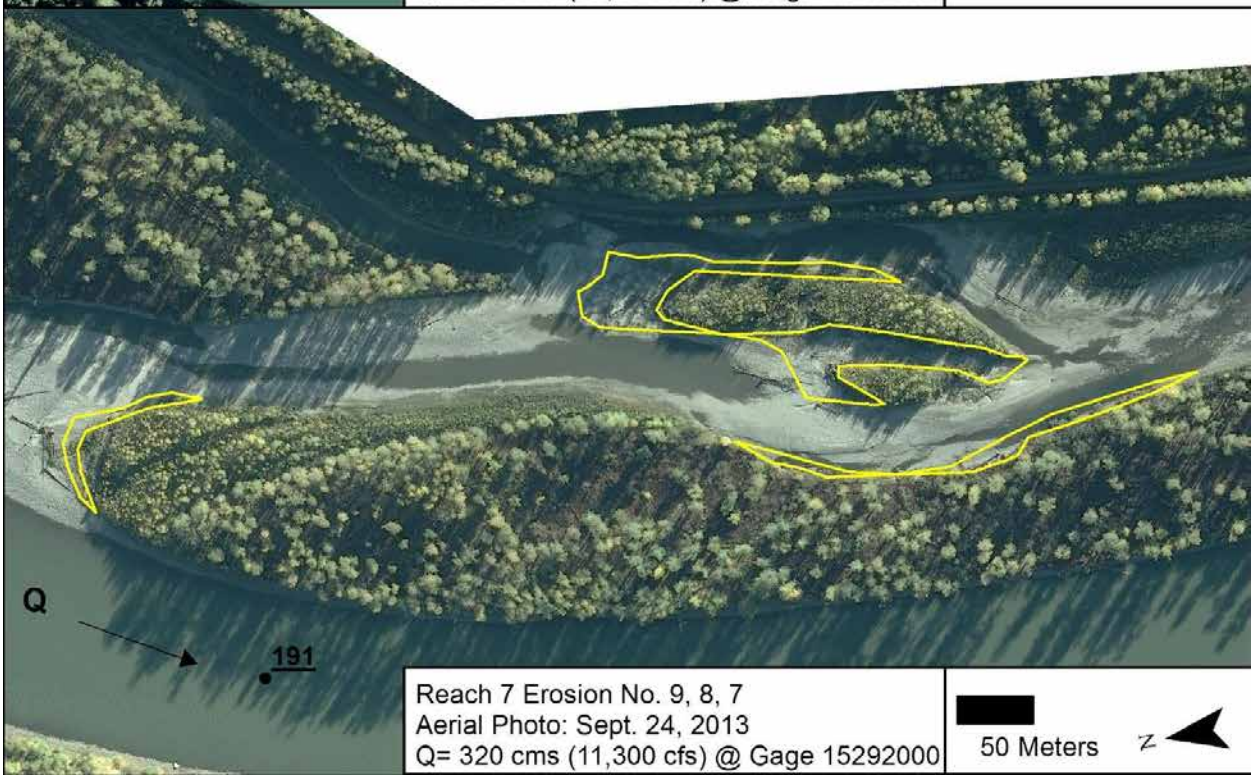

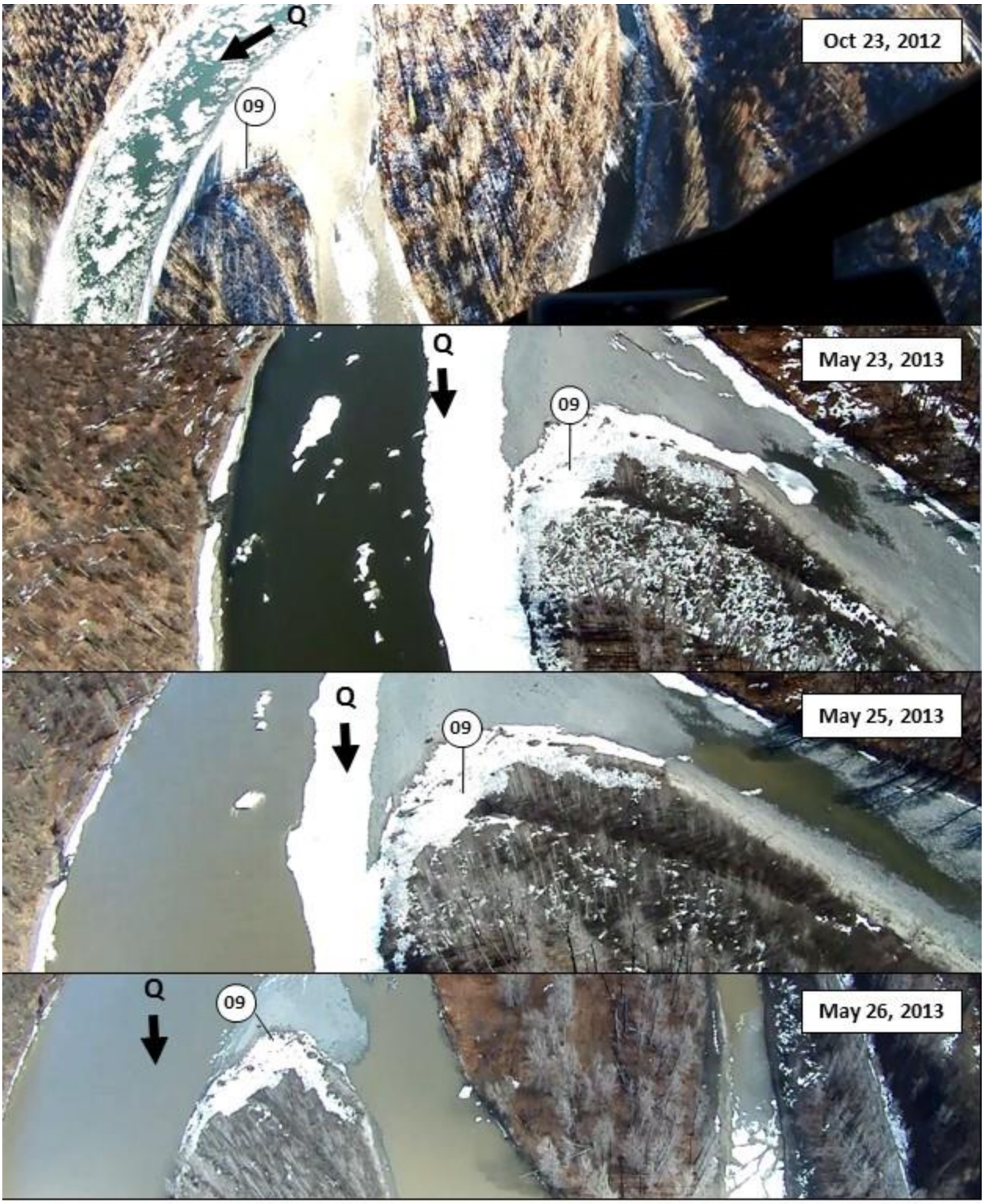
Q
09
Oct 23, 2012
Q
09
May 23, 2013
Q
09
May 25, 2013
Q
09
May 26, 2013

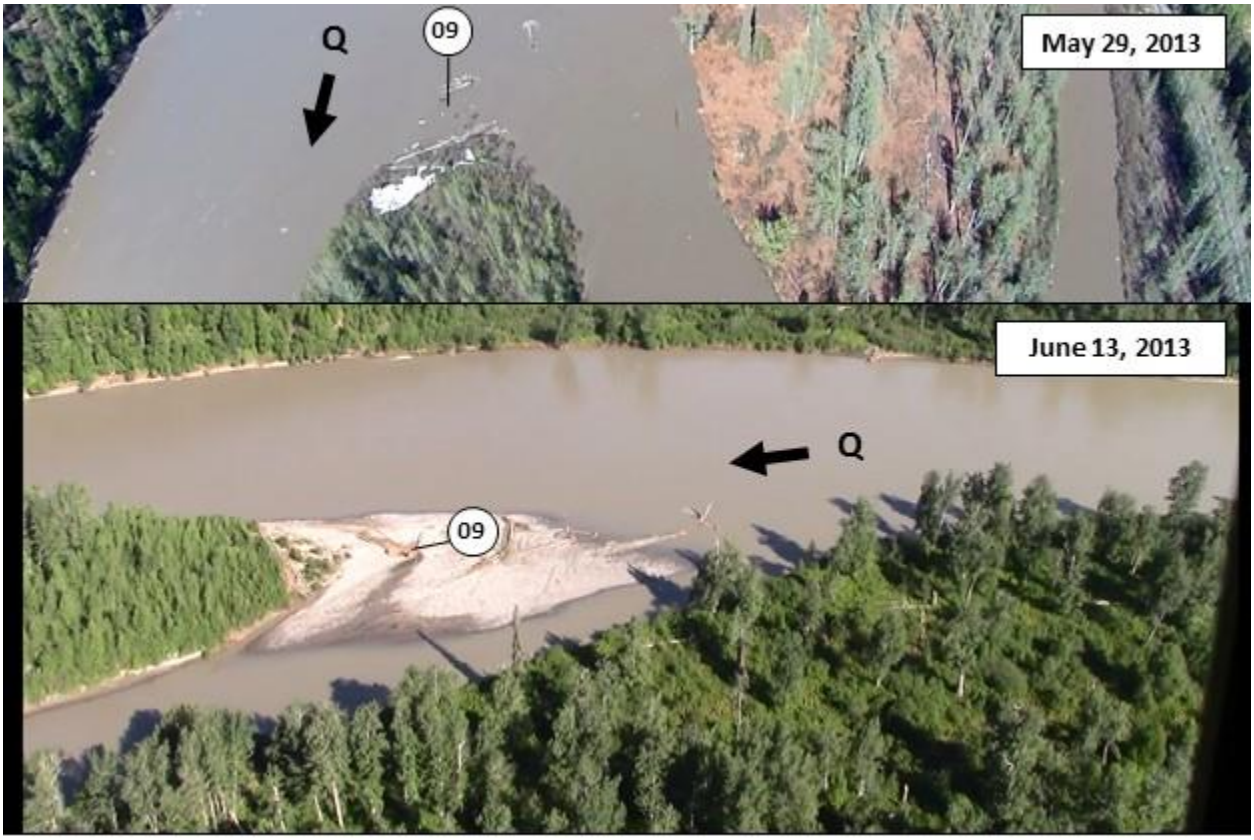
Q
09
May 29, 2013
June 13, 2013
Q
09

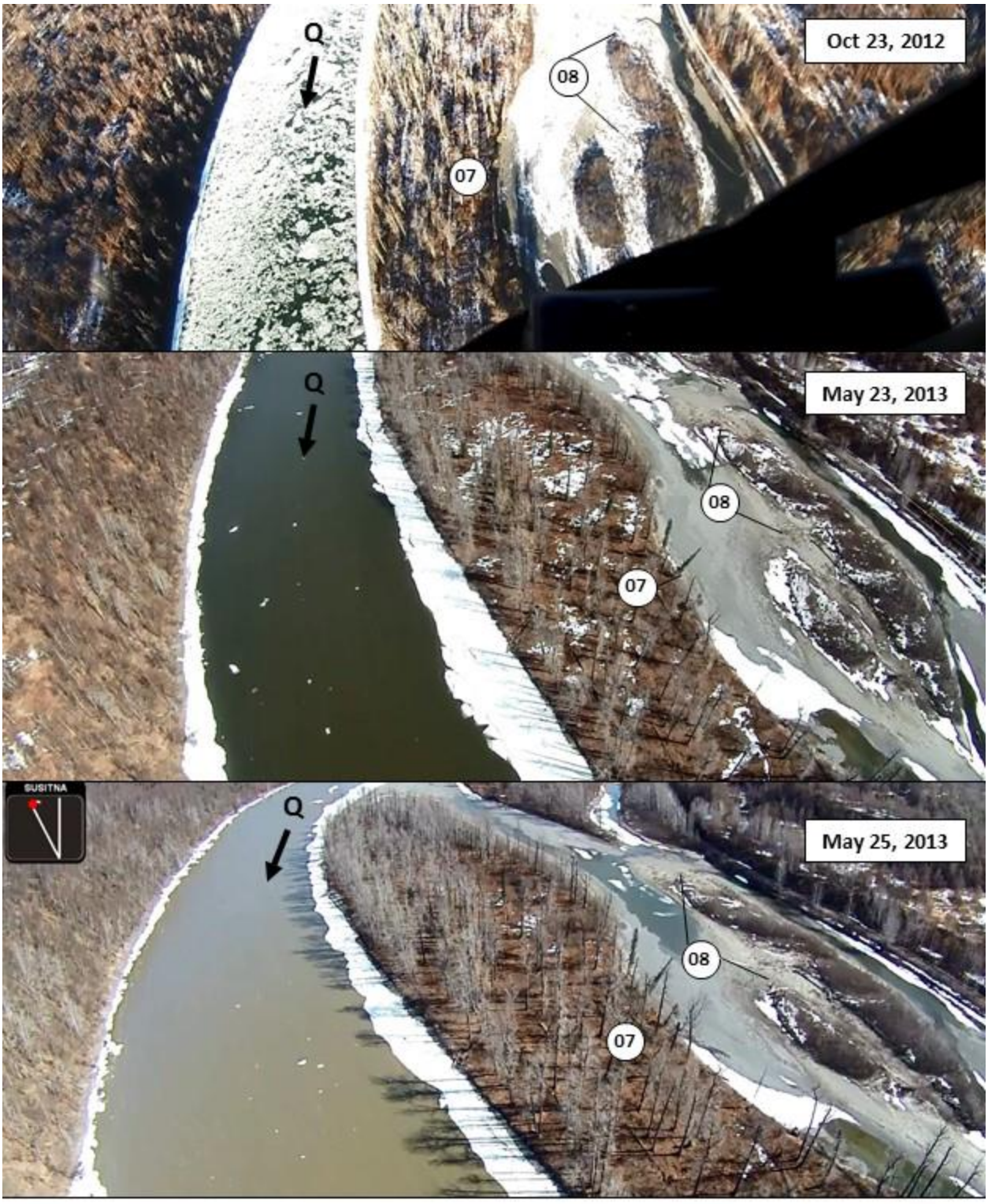
Q
Oct 23, 2012
08
07
Q
May 23, 2013
08
07
SUSITNA
Q
May 25, 2013
08
07


Q
May 26, 2013
08
07
Q
May 29, 2013
08
07
07
June 13, 2013
08
Q

B.2.5 Erosion Location No. 6 and 5

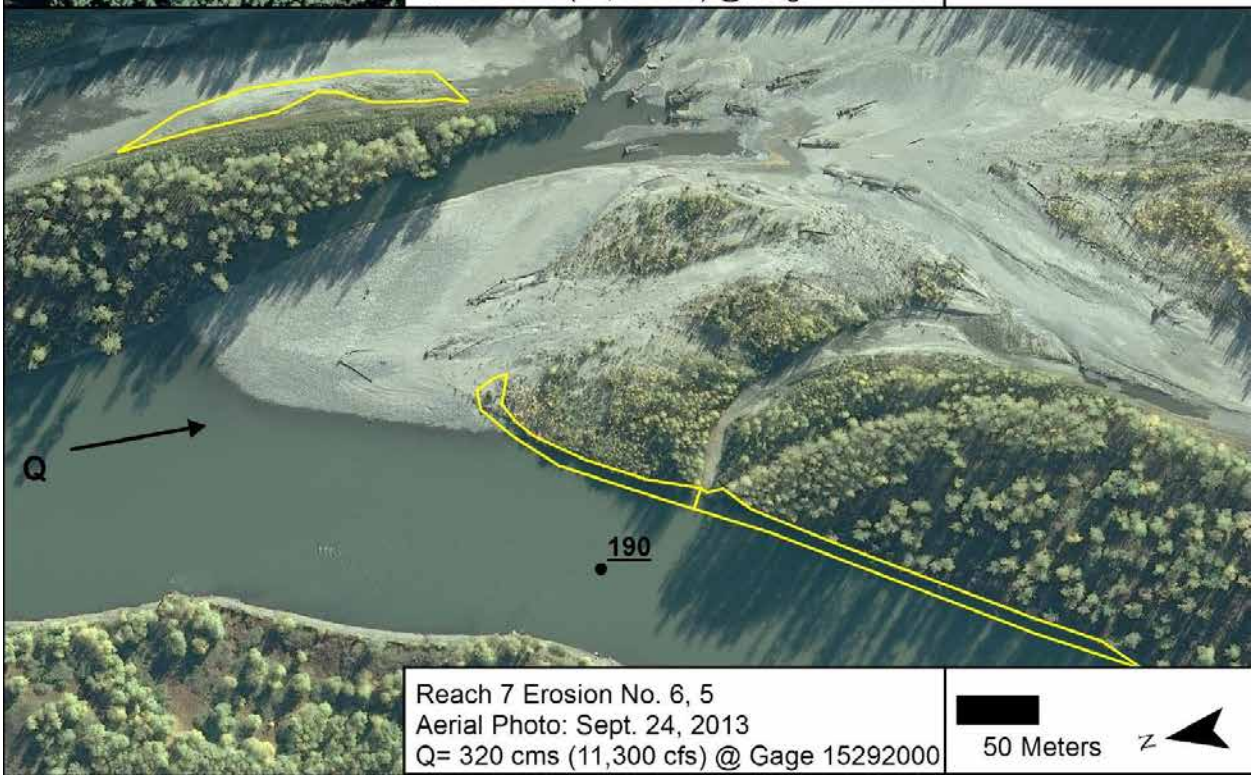


SUSITNA
Q
Oct 23, 2012
06
SUSITNA
Q
May 26, 2013
06

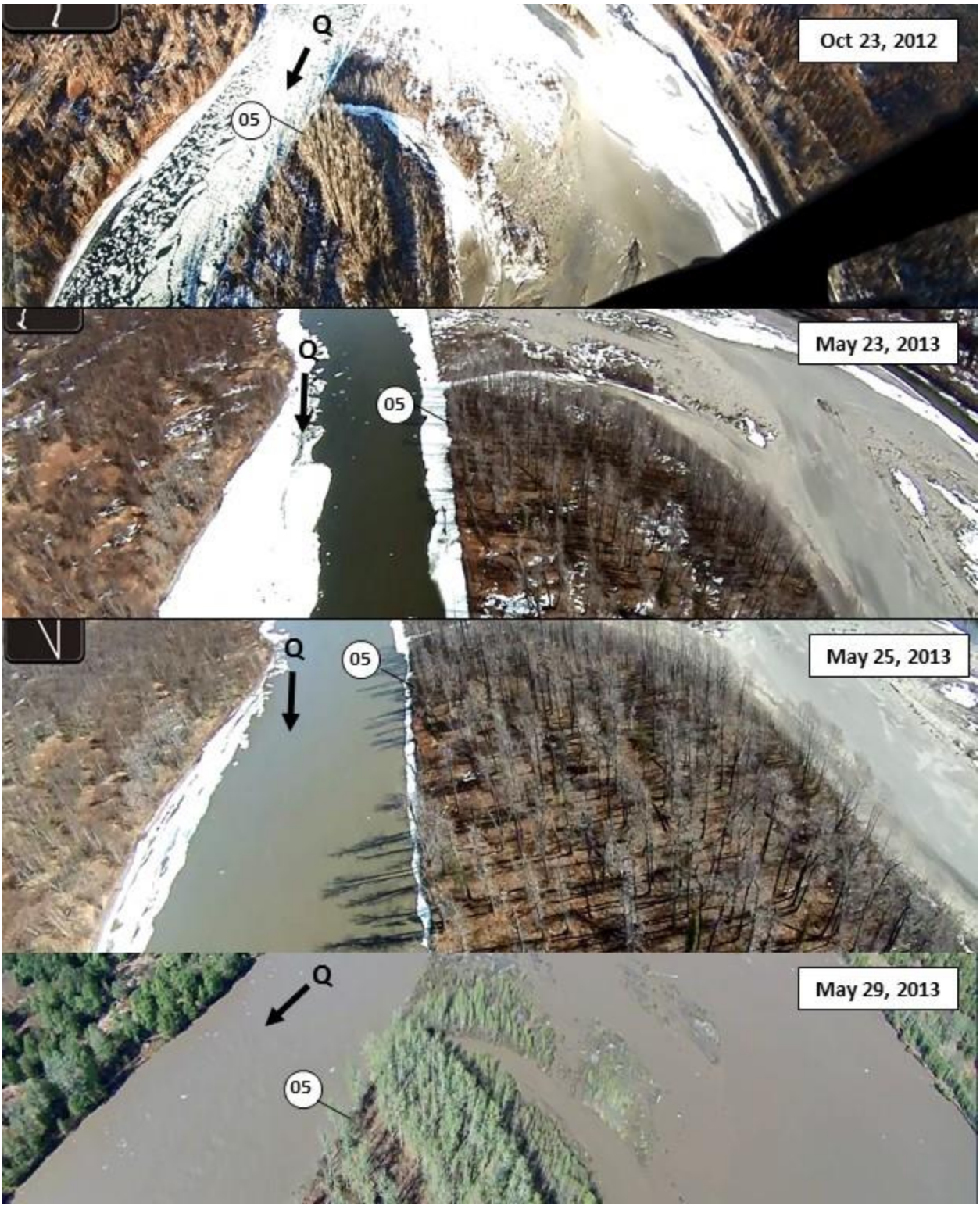
Q
05
Oct 23, 2012
Q
05
May 23, 2013
Q
05
May 25, 2013
Q
05
May 29, 2013

B.2.6 Erosion Location No. 4

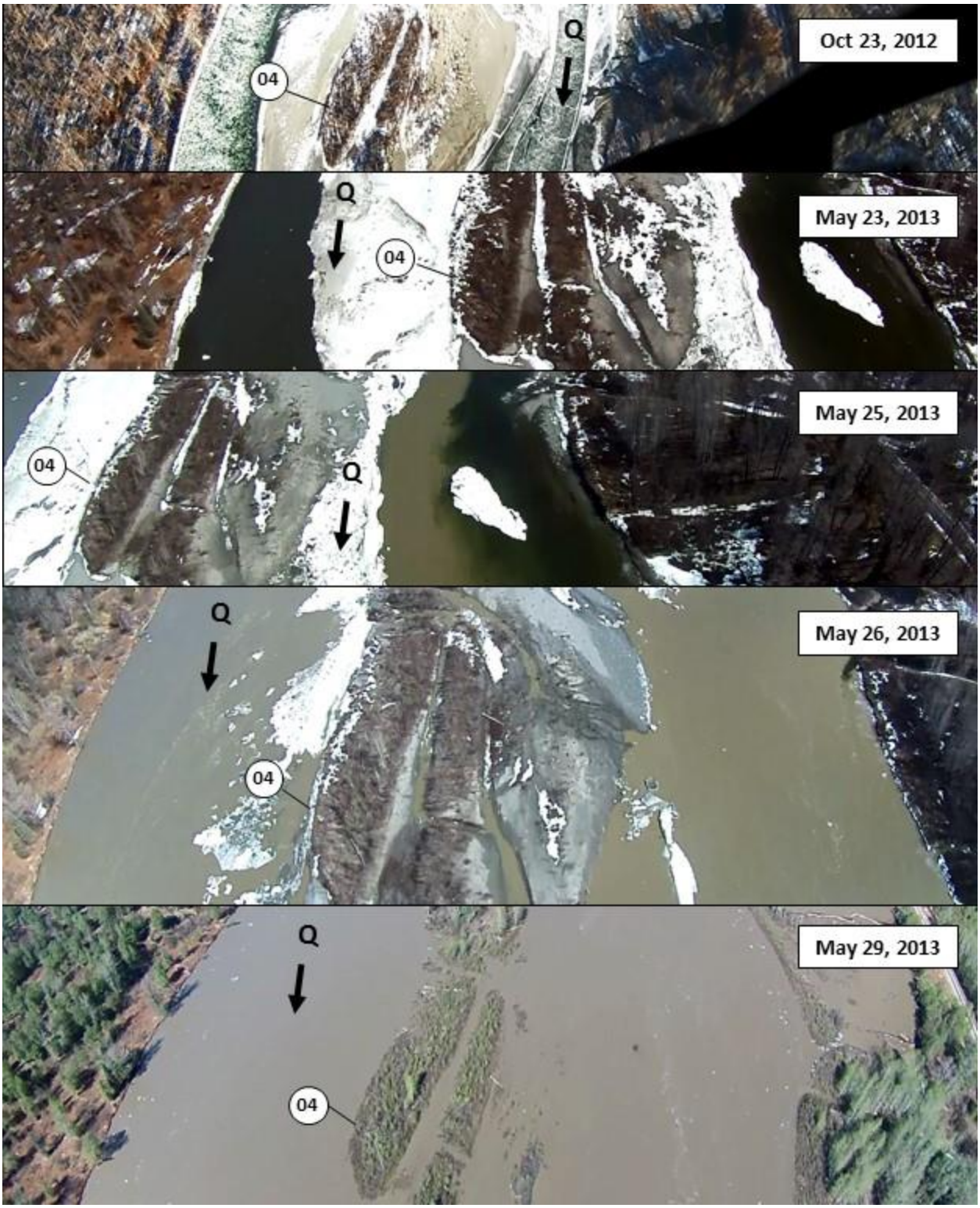
Oct 23, 2012
Q
04
May 23, 2013
Q
04
May 25, 2013
04
Q
May 26, 2013
Q
04
May 29, 2013
Q
04

B.2.7 Erosion Location No. 3

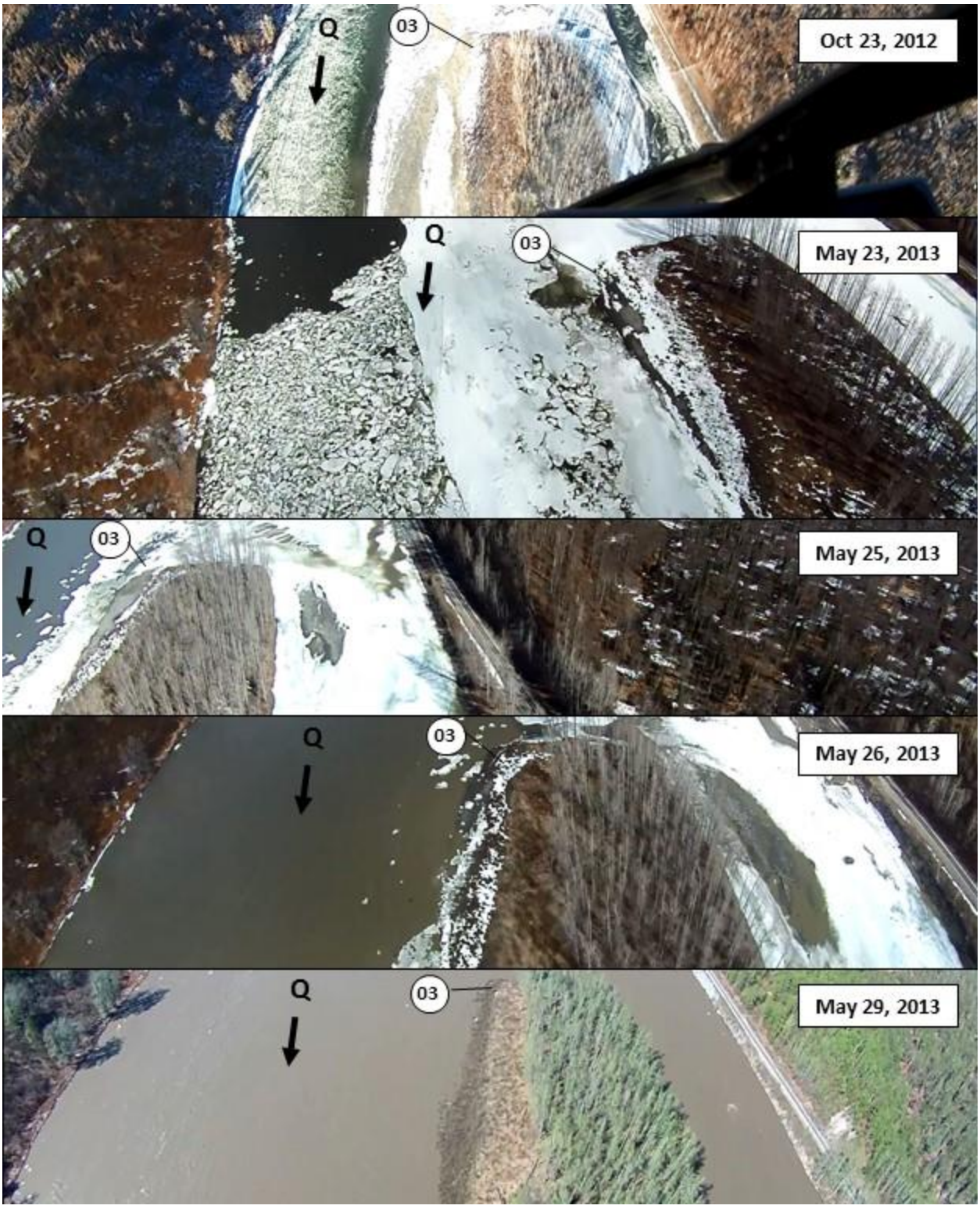
Q
03
Oct 23, 2012
Q
03
May 23, 2013
Q
03
May 25, 2013
Q
03
May 26, 2013
Q
03
May 29, 2013

B.2.8 Erosion Location No. 2

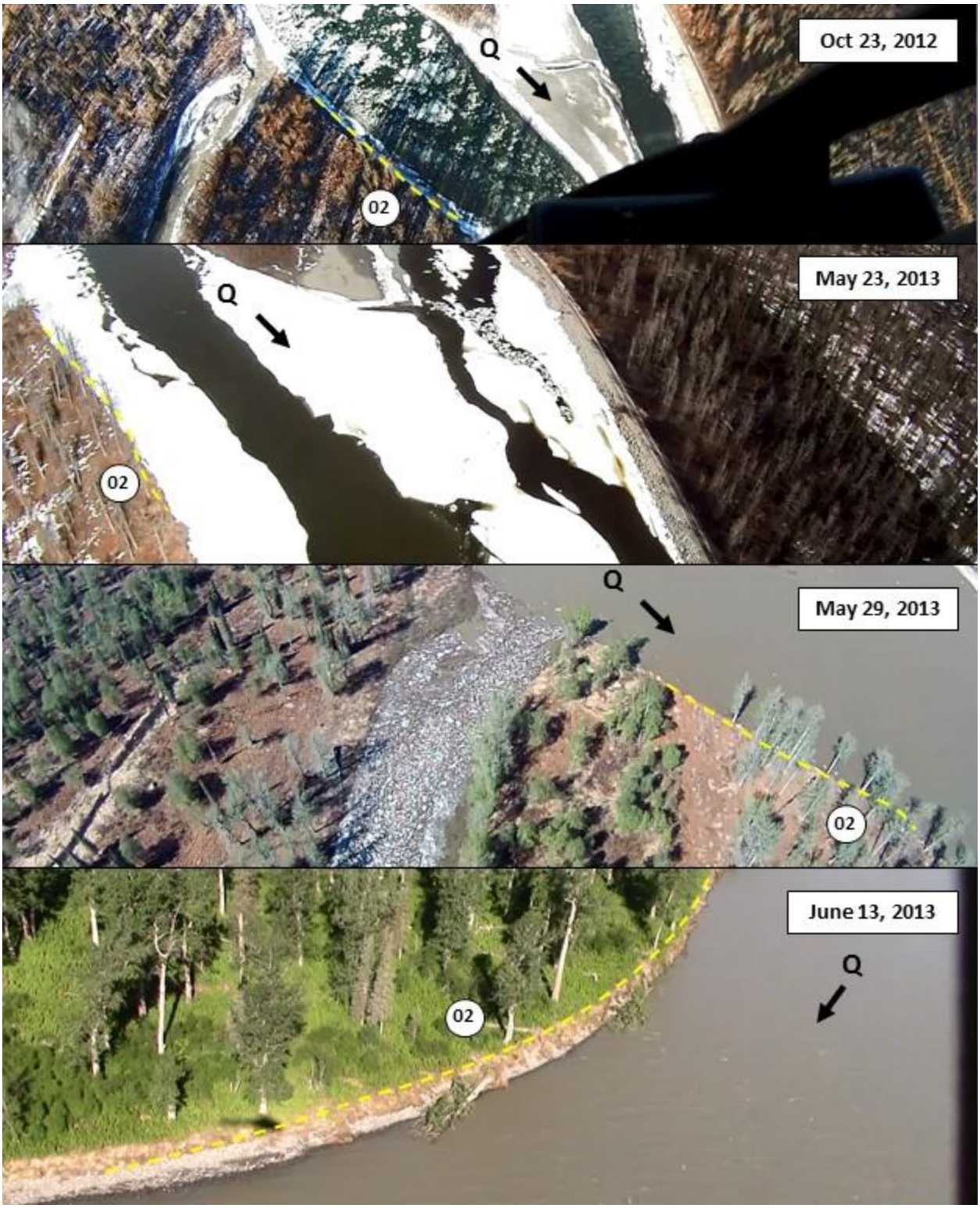
Oct 23, 2012
Q
02
May 23, 2013
Q
02
May 29, 2013
Q
02
June 13, 2013
Q
02

B.2.9 Erosion Location No. 1

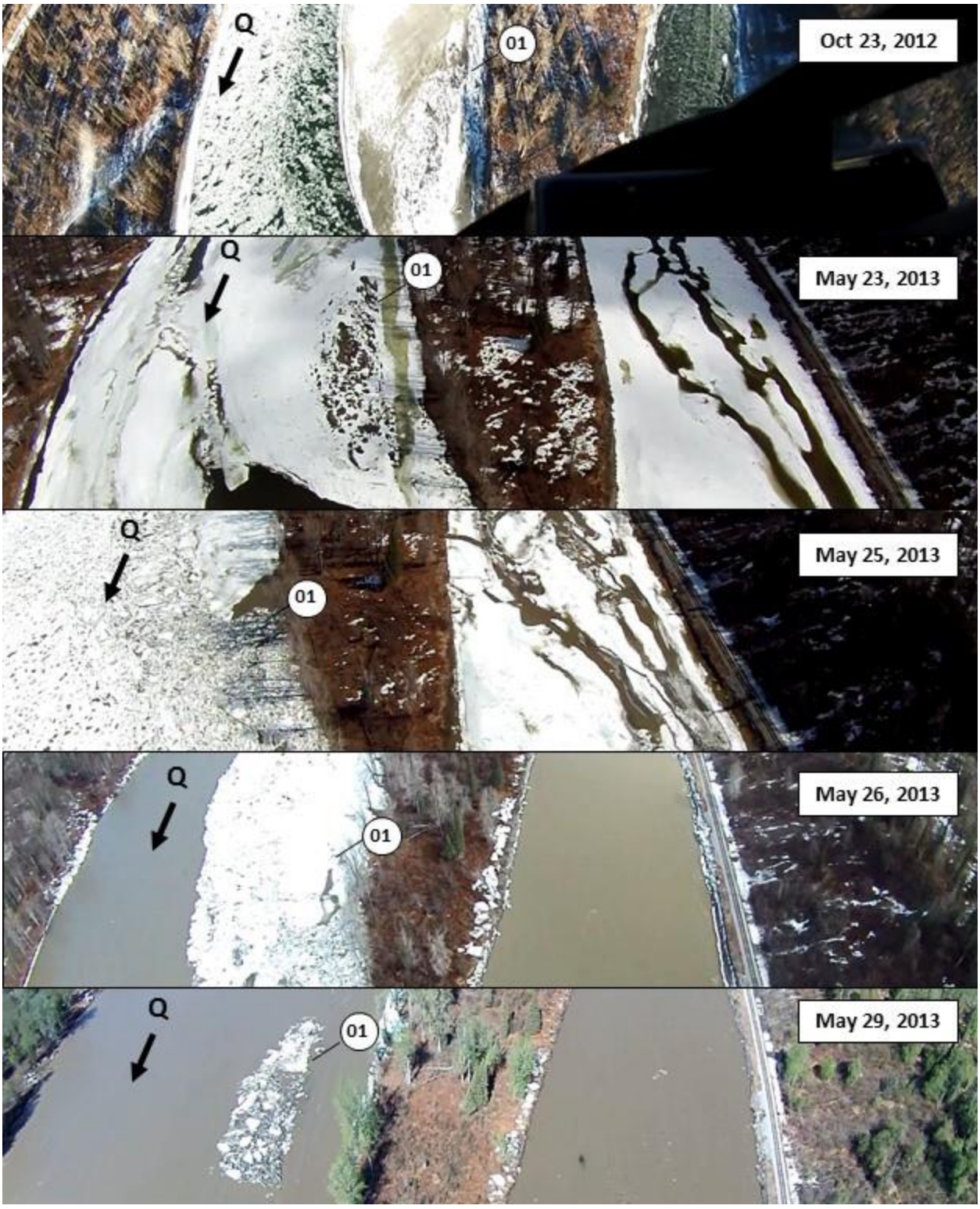
Q
01
Oct 23, 2012
Q
01
May 23, 2013
Q
01
May 25, 2013
Q
01
May 26, 2013
Q
01
May 29, 2013

APPENDIX C: STRESS FROM IMPACTING ICE RUBBLE AND ICE FLOES

As this thesis shows, flow-driven ice rubble and floes impact the banks of the Middle Susitna River and thereby trigger bank erosion. The purpose of the brief analysis this appendix presents is to –

1. Evaluate the approximate magnitudes of impact forces exerted by ice rubble and floes typical of those observed on the Middle Susitna River;
2. Demonstrate that the stress associated with impact by an ice block or floe can exceed the shear stress needed to hydraulically entrain coarse, cohesionless sediment or shear bank material; and,
3. Show that the stress level associated with impacting ice blocks (i.e., ice rubble), is often comparable, though usually does not exceed, the strength of tree-root reinforced bank soil and/or frozen banks.

For a single, drifting ice floe impacting a bank or bar, the magnitude of the impact stress exerted by the floe can be estimated in approximate terms as:

$$\sigma = \frac{(virtual\ mass\ of\ ice\ floe * deceleration) + (water\text{-}pressure\ force)}{bank\ contact\ area}$$

Here, virtual mass of an ice floe can be estimated as

$$virtual\ mass = \ mass\ of\ ice\ floe + C * mass\ of\ fluid\ displaced\ by\ ice\ floe$$

with,

$$mass\ of\ ice\ floe = floe\ volume * \ \rho_{ice}\ , \text{ and,}$$

$$C = added\ mass\ coefficient$$

Deceleration is estimated as,

$$deceleration = (v_1 - v_2)/\Delta t$$

Also, here, water-pressure force is attributable to water thrust ahead of the ice mass. This force is neglected here, because the ice mass is relatively thin such that water can be readily displaced vertically.

The increment of time associated with ice mass impact is

$$\Delta t = time\ for\ ice\ block\ to\ come\ to\ a\ stop \approx \frac{x}{v_{avg}}$$

With, $x = distance\ for\ ice\ block\ to\ come\ to\ stop$, and $v_{avg} = \frac{v_1+v_2}{2}$

The aforementioned equations are difficult to calculate accurately, for several reasons. Notably, the mass of water displaced by a large floe moving along a relatively shallow river channel is difficult to calculate accurately, and changes with proximity to bank. The added-mass coefficient characterizes the mass of water displaced as an ice floe decelerates on approaching a channel bank. Values of added mass are difficult to determine accurately, and indeed change as the floe approaches close to a bank. Further, floe sizes vary in size and shape. Moreover, the actual contact area is hard to assess. Therefore, as the present effort focuses on an approximate level of force, added mass is neglected.

For this analysis, v_2= 0 m/s, and v_1 is assumed to be water flow velocity. An annotated figure of this process is presented in Figure C-1.

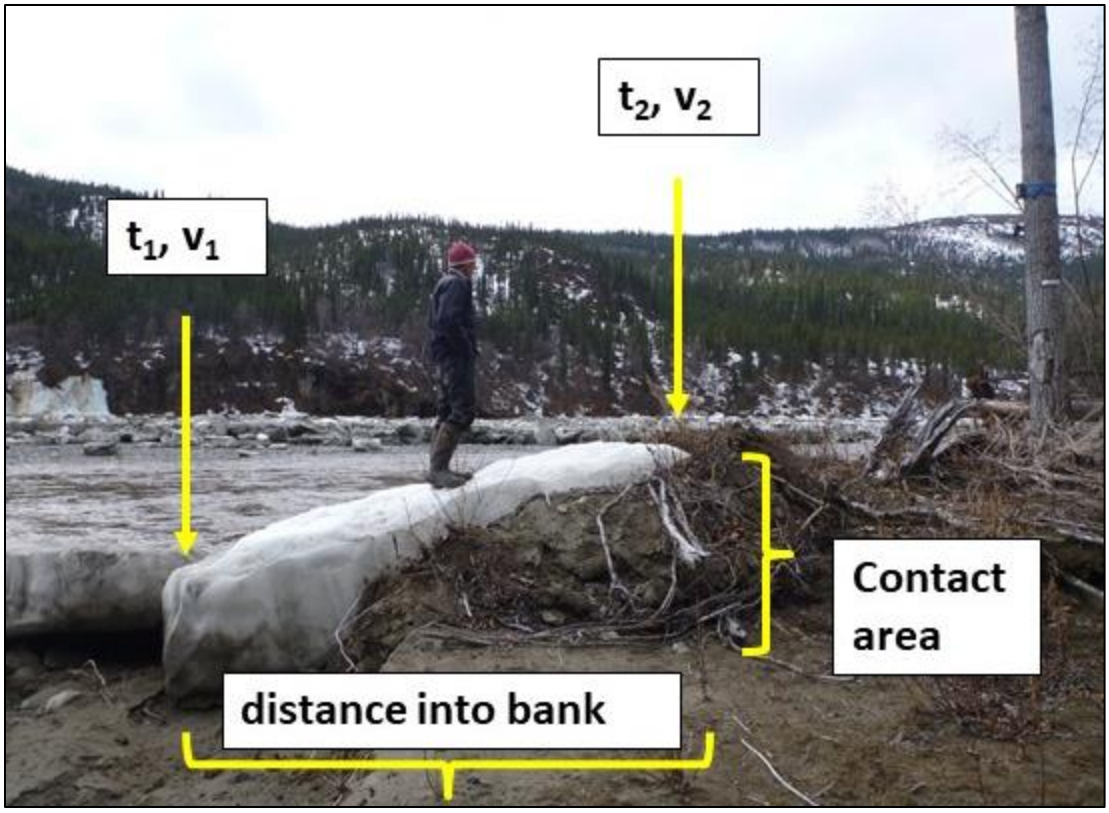

Figure C-1. Annotated photograph of ice block impacting bank on Susitna River, Alaska. Estimated dimensions of ice block are 4m in length, 1 m in width, and 1m in thickness. The photo was taken May 9, 2012 by HDR, Inc.

Stress was plotted for varying ice block sizes (1 m^3 to 1,000 m^3) over a series of water flow velocities ranging from typical open-water flows (equal to 1 m/s) up to extreme flow velocities associated with ice jam breaks (equal to 5 m/s).

An example calculation for an ice floe 10m in length, 10m in width, and 1m in thickness (100 m^3 in volume) is presented below:

$$\sigma = \frac{virtual\ mass\ of\ ice\ floe * deceleration}{bank\ contact\ area}$$

Virtual mass of a 100 m^3 ice floe is estimated as

$$mass_{ice} = volume_{ice} * \rho_{ice}$$

$$= 100m^3 * 916.7\frac{kg}{m^3}$$

$$= 91{,}670\ kg$$

Deceleration of an ice floe conveyed by water flow at 3 m/s is solved for by,

$$deceleration \approx (v_1 - v_2)/\Delta t$$

$$\Delta t = time\ for\ ice\ block\ to\ come\ to\ a\ stop \approx \frac{x}{\frac{v_1 + v_2}{2}}$$

$$deceleration \approx \frac{(v_1 - v_2)}{\frac{x}{\frac{v_1 + v_2}{2}}},$$

Here, $v_2 = 0\frac{m}{s}$:

$$decleration \approx \frac{v_1^2}{2 * x} = \frac{\left(3\frac{m}{s}\right)^2}{2 * 2m} = 2.25\ m/s^2$$

Bank contact area is equal to ice floe width multiplied by ice floe thickness. In this example bank contact area is equal to 10m^2. Therefore, the horizontal component of stress imparted onto a bank via an ice block is:

$$\sigma = \frac{91{,}670\ kg * 2.25\ m/s^2}{10\ m^2} = 20{,}625\ Pa = 20.6\ kPa$$

The foregoing analysis does not consider situations in which ice blocks are pressed by an accumulation of ice rubble, rather than being flow-driven. In this situation, the force exerted by the ice block depends on the stress exerted by the pressure transmitted through the accumulation.

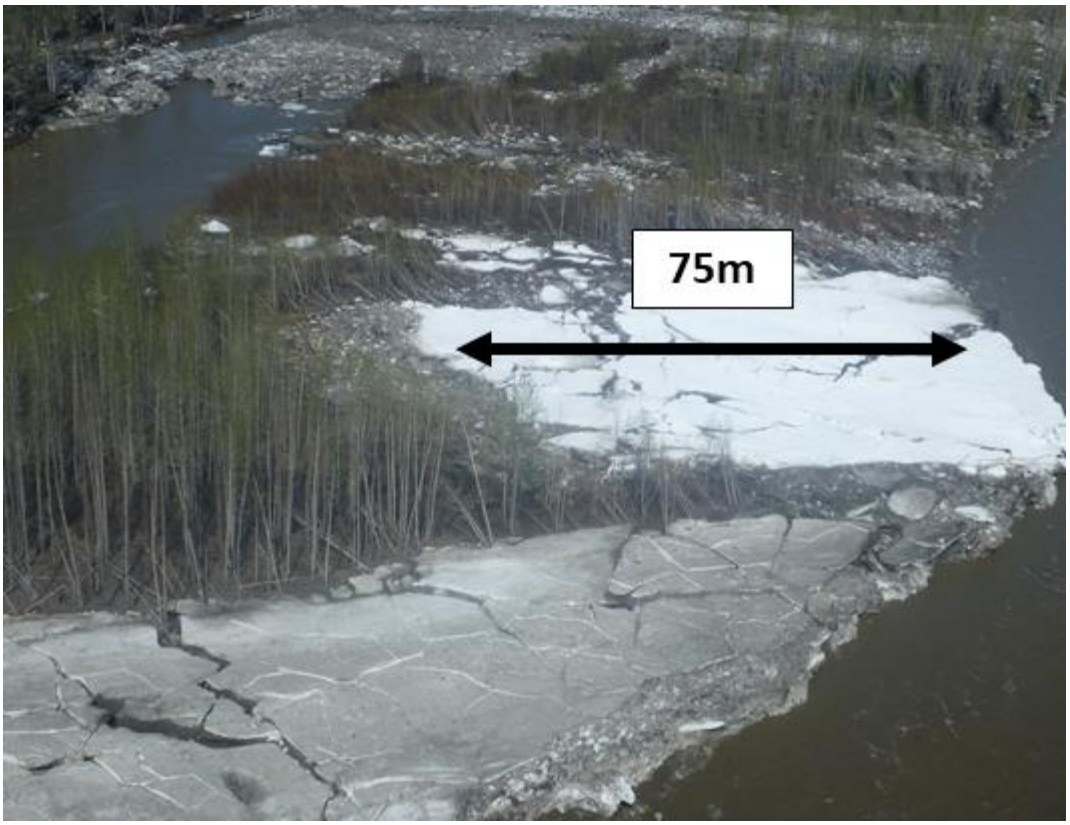

Figure C-2. Ice floes alided with and shoved over a vegetated bar in the Middle Susitna River. The ice floes failed in flexure, as the sheet-cracking indicates. This photo was taken May 29, 2013 by HDR, Inc.

Observations of ice floes that failed in flexural, as exemplified in Figure C-2, indicate that an upper level of force was reached when floes impacted banks. An upper level of force can be estimated by determining the force required to fail the floe in flexure. Flexural failure estimates the vertical component of ice impact on a bank as:

$$N = V/\cos(\alpha)$$

Here,

$$V = vertical\ component\ \ of\ floe\ failing\ in\ flexure,\ \text{and}$$

$$\alpha = bank\ angle\ .$$

The horizontal component of ice impact on a bank, H, is then estimated as:

$$H = N * \sin(\alpha)$$

Literature values of ice floes failing in flexure range from 300 kPa to 500 kPa (Ashton, 1986). Therefore, for a bank angle of 45 degrees, the upper limit of horizontal force can be estimated as:

$$H = \frac{300\ kPa}{\cos(45)} * \sin(45) = 300\ kPa$$

$$H = \frac{500\ kPa}{\cos(45)} * \sin(45) = 500\ kPa$$

However, as flexural strength is multiplied by tangent of the bank angle, gradual banks will be subject to lower impact forces than more vertical banks. Example bank angles are indicated in Figure C-3.

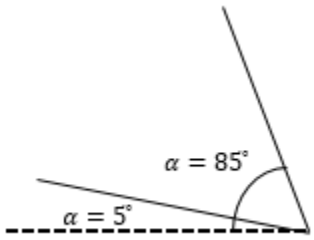

Figure C-3. Possible bank angles, measured from the horizontal plane (dashed line).

A lower threshold for impact stress for a bank angle of 5 degrees, and flexural strength of 300 kPa is estimated as:

$$H = 300kPa * \tan(5) = 26.25\ kPa$$

An upper threshold for impact stress for a bank angle of 85 degrees, and flexural strength of 500kPa is estimated as:

$$H = 500kPa * \tan(85) = 5{,}715\ kPa$$

The maximum force exerted by an ice block is associated with the force it takes to fail the ice. Most ice floes on the Susitna River during the ice-breakup of 2013 appeared to fail in flexure (see Figure C-2). Approximations of the upper and lower limits of the horizontal force associated with flexural failure are plotted for ice floes (Figure C-7 through Figure C-9). Additionally,

approximations of the upper and lower limits of crushing failure are plotted for both ice rubble and ice floes (Figure C-6 through Figure C-9). Values of crushing failure were derived from Niehus (2002) for ice near spring breakup.

Ice blocks and floes of all sizes yield high impact stresses that can gouge banks, mobilize large particles, plow over trees, and cause lateral bank erosion. Even small ice blocks (1 m^3) are able to move large sediment particles (greater than large cobbles), even when moving at modest flow velocities before contact with the bank (i.e., 1 m/s). This mechanism, in part, explains the distribution of large, loose boulders along the bank and on the floodplain; loosely distributed cobbles are also a product of anchor ice attachment, which decreases their net weight and makes them somewhat easier to transport by water flow.

Tree-root systems increase bank strength. In a field study, Simon and Collision (2002) found various diameter of tree roots to increase bank soil strength from 2,000 to 8,000 Pa and some grass roots to increase soil strength from 6,000 to 18,000 Pa. Wu (2013) summarizes observed shear strength from a range of soil types reinforced by vegetation; values are consistent with those of Simon and Collision (2002) and range from 1,000 to 12,000 Pa. These resistance values are within the magnitude of force that small ice blocks may exert along the bank. If an ice block impacts a root-reinforced bank, roots may fail at smaller contact areas, leading to localized erosion, but may not fail over larger contact areas.

It appears that impacting ice blocks less than 10 cu. meters can mobilize large sediment particles and cause some bank erosion, however reach-wide effects are likely limited. Limited reach-wide effects may be due to the increased bank strength by root-reinforced soil. Ice blocks greater than 10 cu. meters (i.e., ice floes), which were observed during the 2013 dynamic ice breakup on the Susitna River, are likely more dominant in driving bank erosion than smaller ice

blocks. A photograph of an ice floe 75m in length moving into a vegetated bar and active floodplain surface is shown in Figure C-2. Comparison with Figure C-1 shows that, whereas a much smaller ice block only causes localized gouging of the bank, a large floe can over-ride meters of bank.

The effects of frozen soil on bank resistance are unclear. In many boreal environments, frozen cohesive bank soil is partially entrained by flow, leaving an intact "shelf," that eventually fails. The topic of ice impacting banks with varying degrees of vegetation and with frozen and unfrozen soil requires further research.

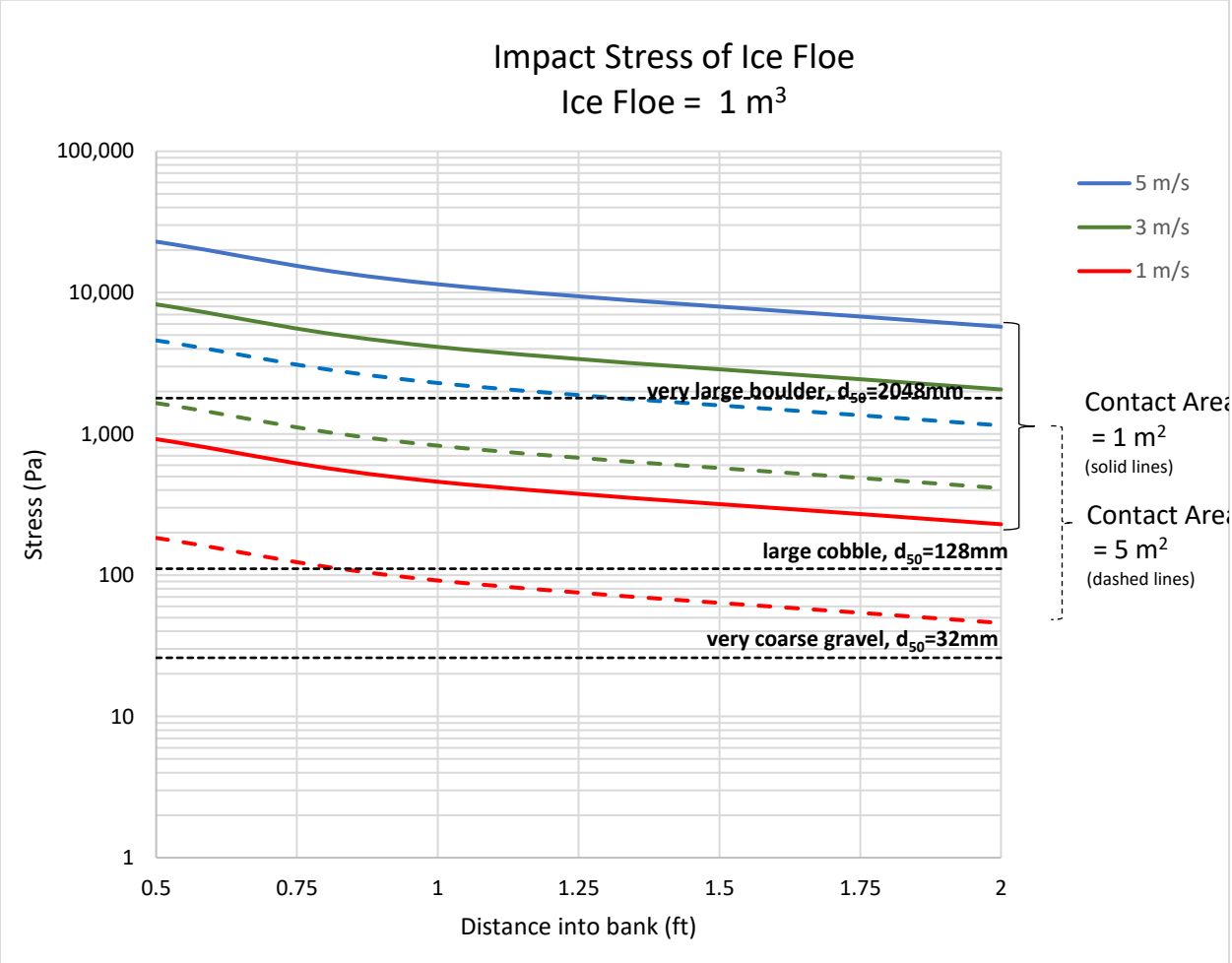

Figure C-4. Stress impact of a 1 cu. meter ice floe at varying velocities and contact areas.

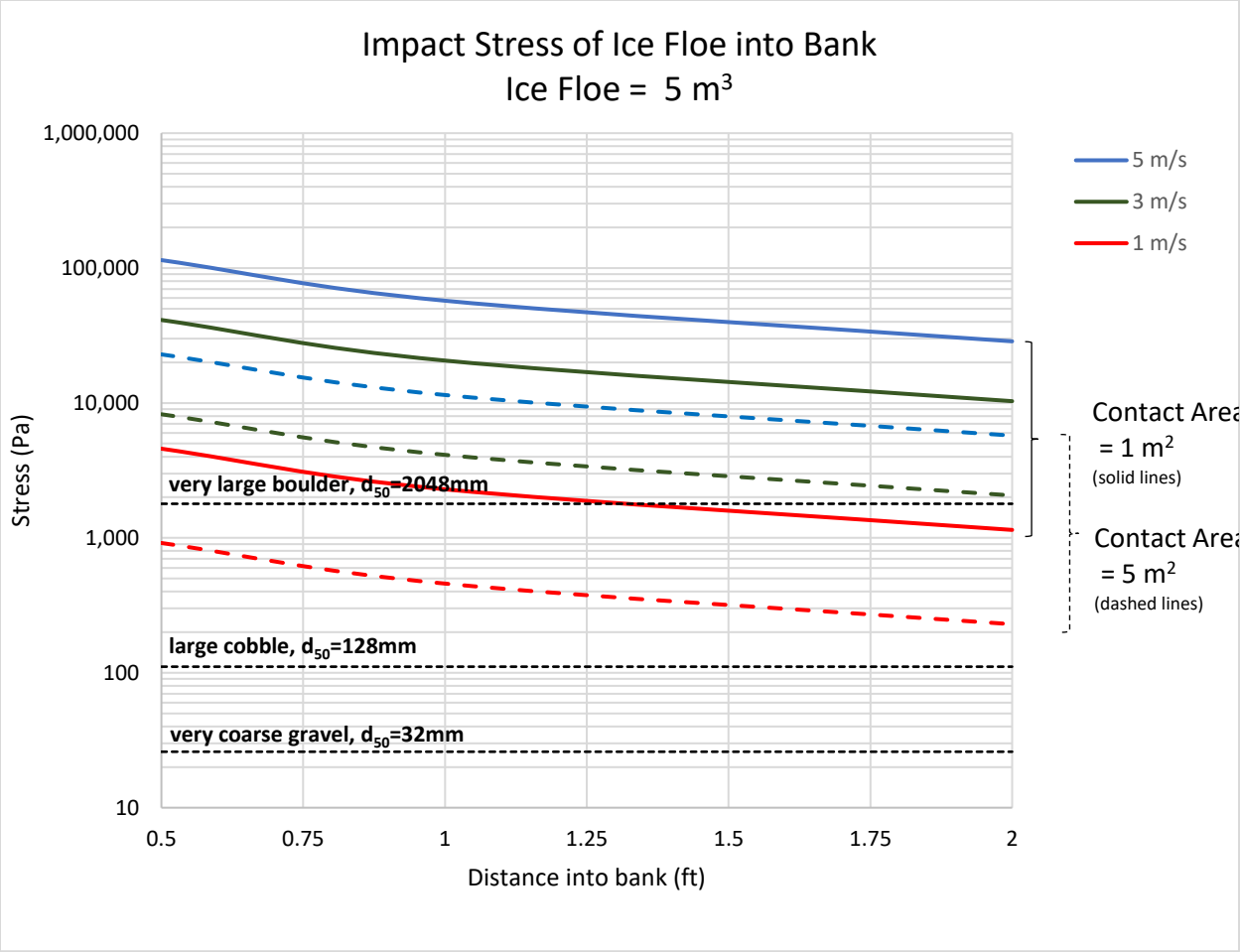

Figure C-5. Stress impact of a 5 cu. meter ice floe at varying velocities and contact areas.

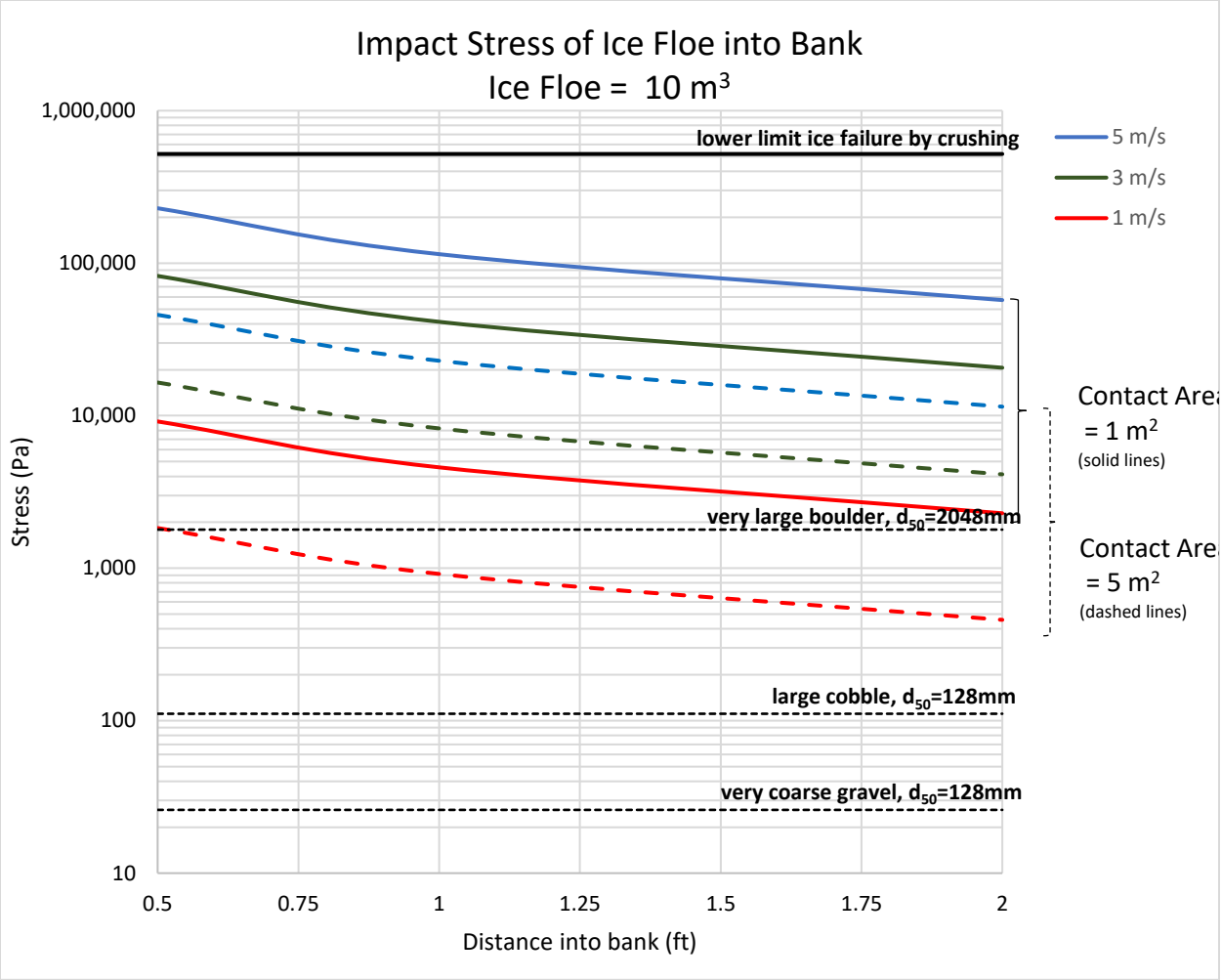

Figure C-6. Stress impact of a 10 cu. meter ice floe at varying velocities and contact areas.

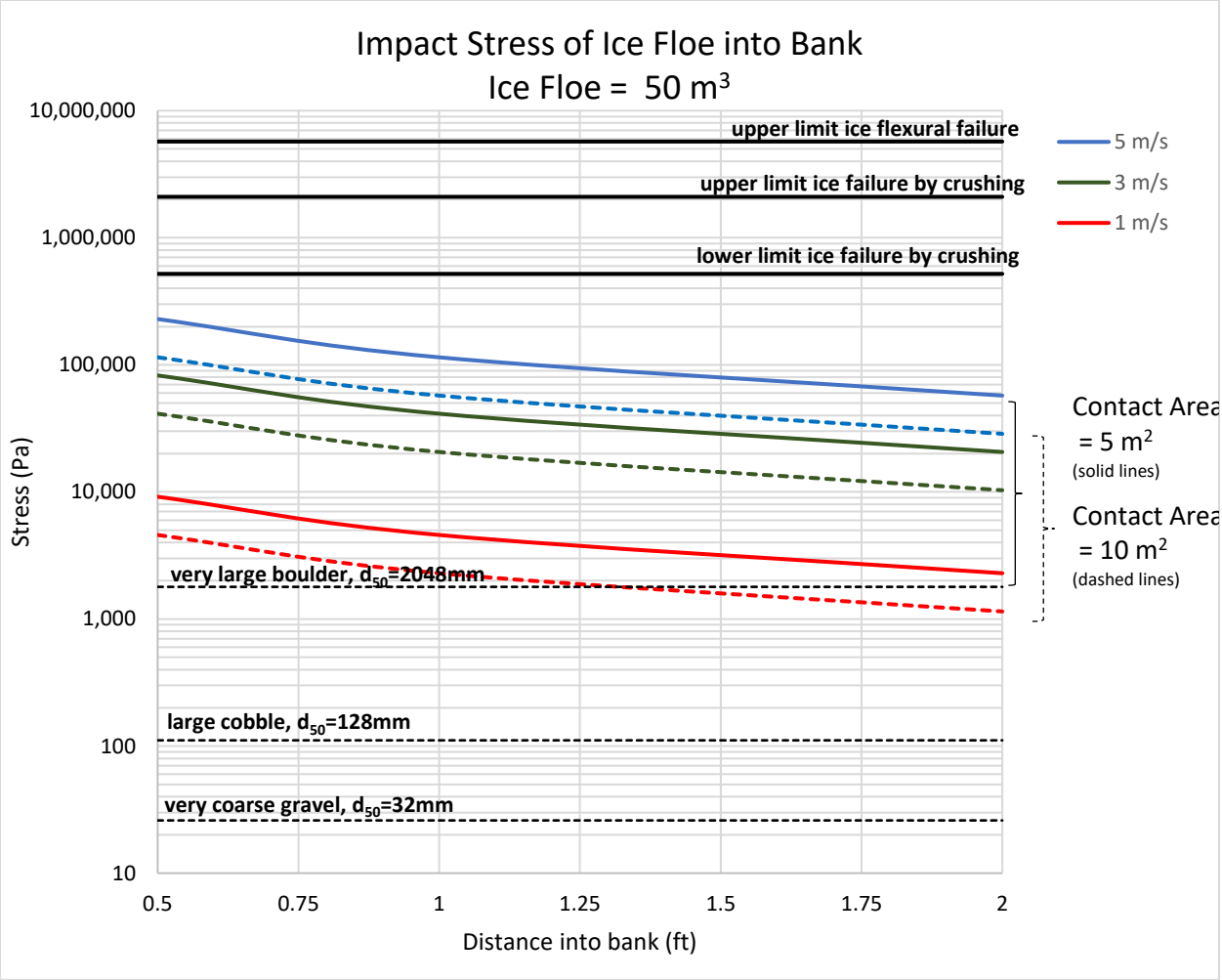

Figure C-7. Stress impact of a 50 cu. meter ice floe at varying velocities and contact areas.

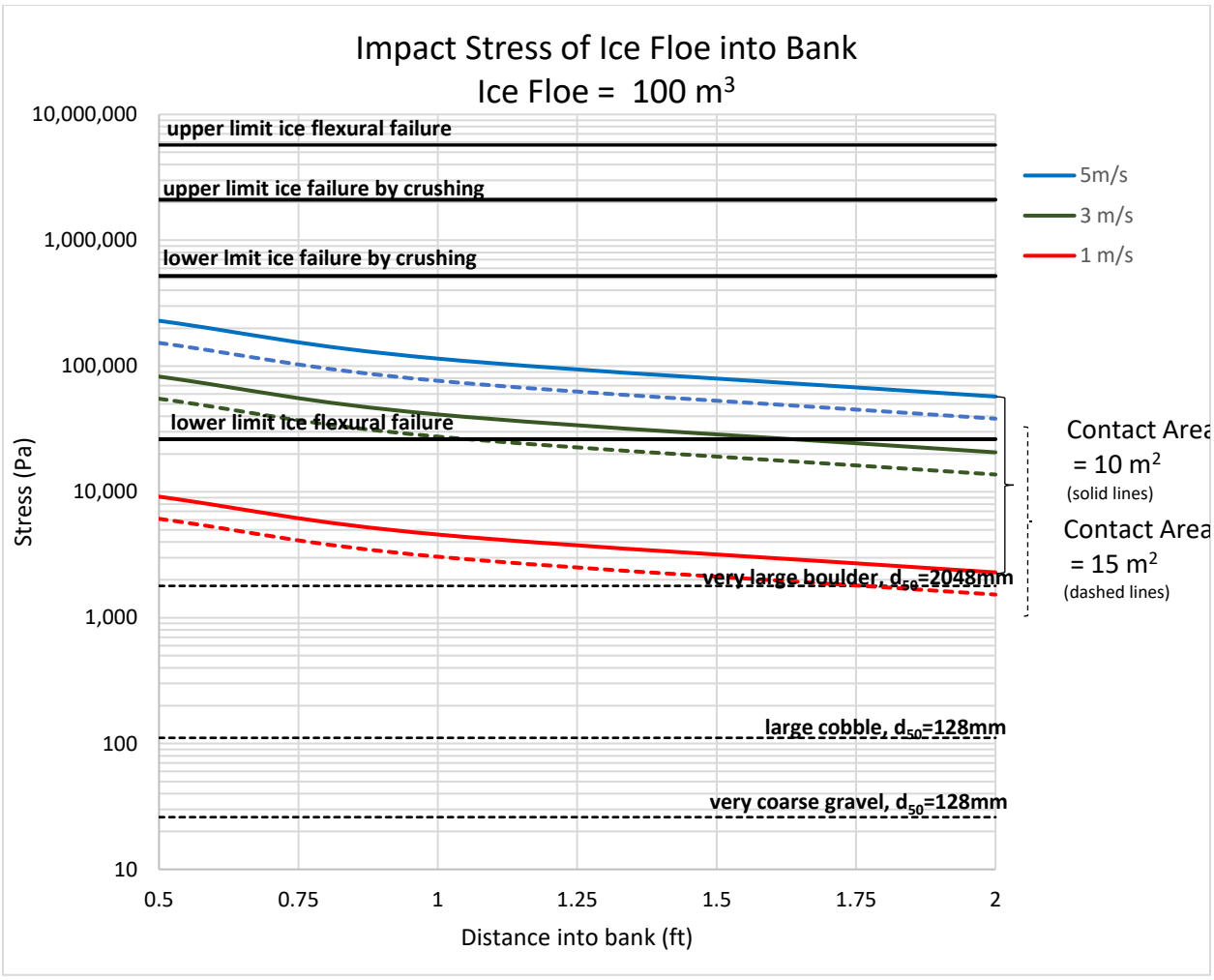

Figure C-8. Stress impact of a 100 cu. meter ice floe at varying velocities and contact areas.

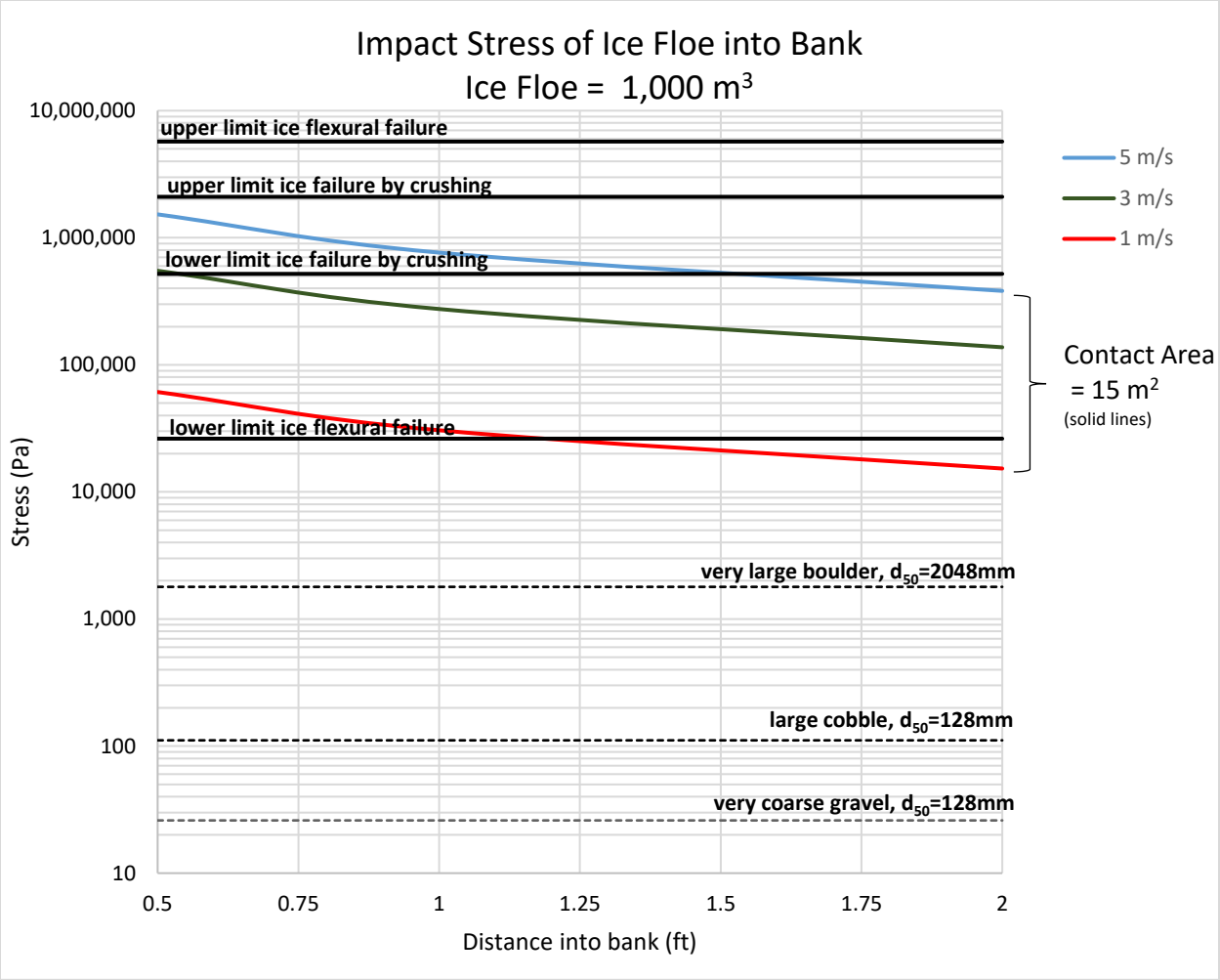

Figure C-9. Stress impact of a 1,000 cu. meter ice floe at varying velocities and contact areas.

APPENDIX D: NUMERICAL MODELING

D.1 Introduction

A two-dimensional hydraulic model (SRH-2D) was developed for approximately 4 km on the Susitna River (RK 210 to RK 206). The goal of the fixed-bed model was to simulate hydraulic characteristics in complex flow patterns in order to quantify flow distribution, lateral feature breach (i.e. overtopping), erosion and deposition based on existing and with-project hydrologic, sedimentologic, and ice-regimes (Tetra Tech, 2015d). This existing model was selected in order to analyze shear stress distributions and water surface elevations under simulated main channel blockages.

The geometry of the existing model (Tetra Tech, 2015d) was modified to simulate blockage in the main channel from ice and diversion into secondary channels. Open-water hydraulic modeling was performed over a range of typical (10,000 to 21,000 cfs; 283 to 595) and extreme (30,000 and 40,000 cfs; 850 and 1,133 cms) discharges during ice-breakup (Jon Zufelt, HDR Inc., personal communication)

While the model simulates steady-state open-water hydraulic conditions, it is a useful tool to provide clues into flow redistribution and subsequent shear stress values under a hypothetical main channel ice jam.

As the existing model was developed in imperial units (i.e. feet, pounds, cfs), the use of imperial units are maintained for this analysis. Where possible, metric units are also presented.

D.2 Study Area

The selected study area is a sub-reach of Reach 6, from approximately RK 210 downstream to RK 206. This sub-reach is referred to as Focus Area 128 (Slough 8A) according to the proposed project (Tetra Tech, 2015bb). The region has a wider valley bottom, and a side channel complex consisting of both wide and narrow secondary channels.

D.3 Methods

Methods for developing and running ice-jam blockage numerical models are elaborated in the following subsections: geometry (Section D.3.1), roughness (Section D.3.2), hydrology (Section D.3.3), and model comparison (Section D.4.1).

D.3.1 Geometry

Two scenarios were developed to simulate flow redistribution from an ice-jam.

- Channel blockage between RK 208 and RK 206.5 diverting flow into a wide secondary channel (i.e. side channel), referred to as "Jam 1"; and,
- Channel blockage near RK 208.5 diverting flow into a narrow secondary channel (i.e. side slough), referred to as "Jam 2".

To modify the 2D model geometry, a polygon was drawn in GIS to represent the outer boundary of the ice-jam. Polylines were drawn along the adjacent bank confinements which consisted of a floodplain on river left and the toe of the bedrock slope on river right. Elevation data were extracted to the polylines using 2014 LiDAR (Tetra Tech 2015b). A triangulated irregular network (TIN) of the main channel blockage was created using the ice jam boundary area and polylines with extracted elevation data. Elevations from the main channel blockage TIN were applied to the 2D model mesh nodes within the ice jam boundary area and merged with existing geometry outside of the ice jam boundary area.

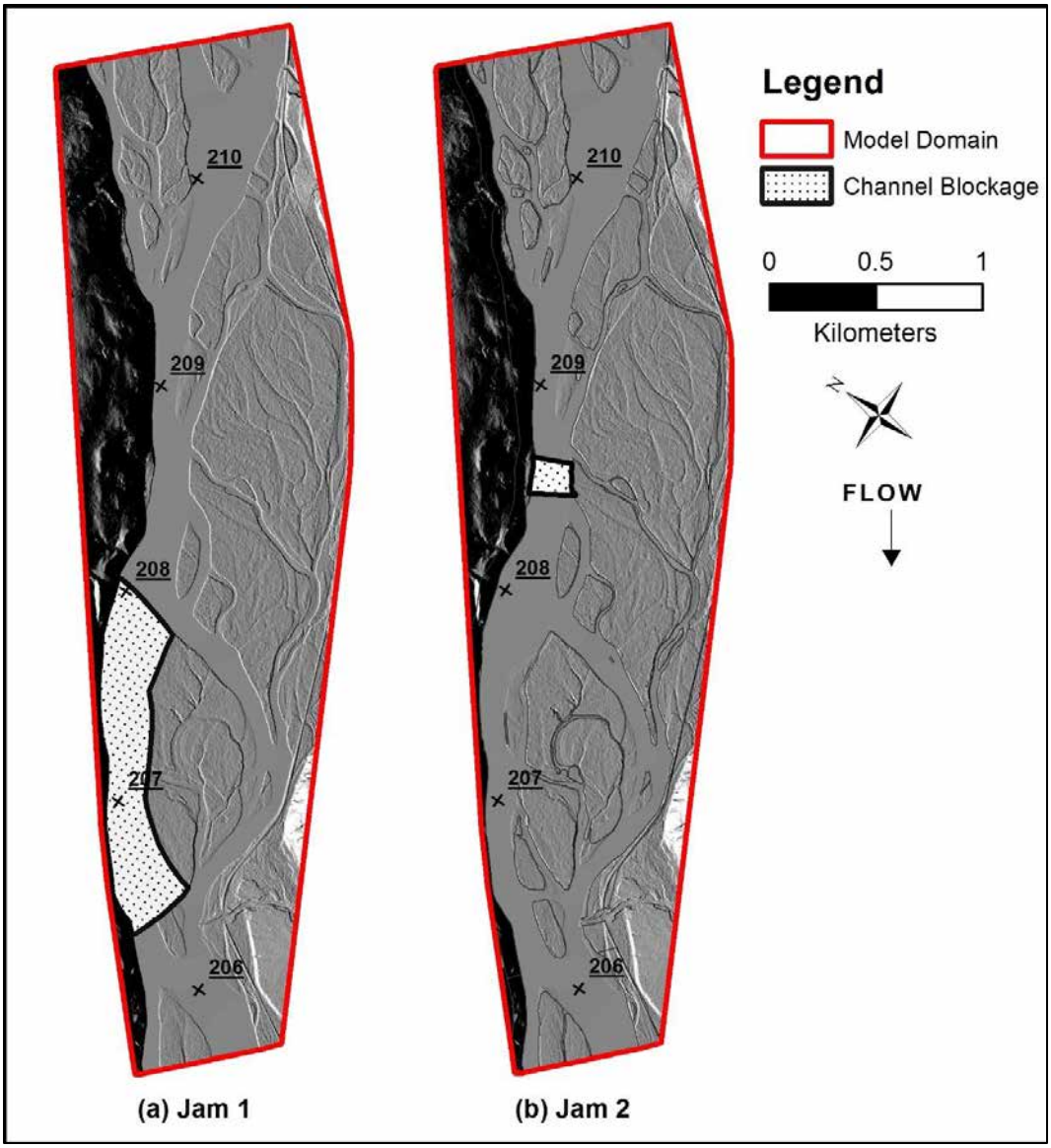

Figure D-1. Model Domain and locations of channel blockages for Jam 1 (a) and Jam 2 (b).

D.3.2 Roughness

Manning's n values for ice jams range from 0.01 up to 0.10 depending on jam thickness and the type of ice forming the jam whether loose frazil, frozen frazil, or sheet ice (United States Army Corps of Engineers, 2016). Roughness values for the existing 2D hydraulic model were set to 0.03 for the main channel, 0.04 for gravel bars and toe of bedrock and 0.17 for the overbank of a mature floodplain (Tetra Tech, 2015d). As most of the modified mesh nodes were within the

main channel or defined as a gravel bar with roughness values of 0.03 and 0.04, no modification to roughness values was deemed necessary from the existing model.

D.3.3 Hydrology

A range of flows were selected that encompass typical historic break-up flows for minor through extreme ice-jam breakups (Jon Zufelt, HDR Inc., personal communication). Steady-state models were run for each of the following flows:

- 10,000 cfs (283 cms)
- 15,000 cfs (425 cms)
- 21,000 cfs (595 cms)
- 30,000 cfs (850 cms)
- 40,000 cfs (1,133 cms)

D.3.4 Model Comparison

The main channel blockage models were compared to un-changed geometry models under open-water conditions to identify difference and trends in geomorphic surface inundation, secondary channel inundation, and shear stress values. In addition, shear stress values in areas that eroded between the 2012 to 2013 period, and were located within the model domain, were compared between models with no-blockage to the two models simulating ice-blockage.

D.4 Results and Discussion

Model comparison results are first presented for specific locations within the model domain and second for general trends in shear stress redistribution. Locations that eroded in the 2012 to 2013 period are compared between the existing conditions scenario and two jam scenarios in Figures D-2 through D-4. The intent of this comparison is to identify whether a main channel blockage would result in sufficient shear stress to mobilize the bank toe at any of the observed erosion locations. For illustration of shear stress throughout the model domain (and not solely

known erosion locations), shear stress distribution maps over the range of ice-breakup discharges are presented in Figures D-5 through D-14.

Locations that eroded in the 2012 to 2013 period and exist within the model domain are shown in Figure D-2. Each erosion location is assigned a numeric identifier (12 through 20), that is consistent with the erosion locations presented in Section 5.2. Shear stress was evaluated at each known erosion location for the two main channel blockage scenarios over the range of ice-break up discharges (10,000 cfs to 40,000 cfs; 283 cms to 1,133 cms) and compared to shear stresses with no channel blockages for the range of historic open-water discharges (10,000 cfs to 98,000 cfs; 283 cms to 2,775 cms). The bed shear stress comparison between Scenario 1 and existing conditions is shown in Figure D-3 while Scenario 2 is shown in Figure D-4. Erosion locations denoted with an asterisk (*) indicate the scenario is a main channel blockage. The results show the increase or decrease in average bed shear stress at the banks based on a main channel blockage and subsequent redistribution of flow.

Shear stresses at known erosion locations under Scenario 1 (main channel blockage and flow diversion into a wide secondary channel) increased at two erosion locations (i.e. location 12 and 14). Locations 12 and 14 were situated downstream from the main channel blockage on the outside of the bend in secondary channels, where the addition of flow diverted from the main channel was the most pronounced. Locations closest to the jam (locations 15 and 16), had a reduction in shear stress, which is a result of backwater reducing the local velocity gradient. Location 13 was within the main channel blockage area, and as expected, had a reduction in shear stress for the blockage scenario. The remaining erosion locations (locations 17 through 20) did not have much change in shear stresses; this is likely due to the distance from the jam location of more than 1.5 km.

For Scenario 2 (main channel blockage and flow diversion into a narrow secondary channel) no erosion locations were found to exceed bed shear stress values compared to those from open-water existing conditions; this is largely due to the fact that no erosion locations downstream from the jam were situated in the flow diversion zone (locations 12 through 16). The extensive backwater effects caused by the location of the jam in Scenario 2 (confined channel sub-section) illustrate the extent of flooding that can occur in the overbanks as well as the distance backwater effects can occur in the channel. Backwater effects are observed for nearly 1 km upstream of the jam, contributing to the large reduction in bed shear stress at erosion locations 17 through 20.

Under existing conditions, only erosion locations 17a and 17b had shear stress values that exceeded the critical threshold for the typical sediment grain size at the bank toe (64mm). No other erosion locations had shear stress values that could exceeded the critical threshold even at the 100-year peak flow event (98,000 cfs; 2,775 cms). While flow diversion due to Jam 1 was able to increase the bed shear stress at two locations, it was not sufficient to exceed the critical threshold. The numerical modeling indicates that flow diversion from ice-jams alone did cause the observed bank erosion between 2012 to 2013.

Shear stress maps of each modeling scenario compared to existing conditions is presented in Figures D-5 through D-9. The change in critical diameter and shear stress for each modeling scenario compared to existing conditions is presented in Figures D-10 through D-14. Diversion of flow into both the wide and secondary channels resulted in overtopping of the adjacent floodplain surface. As expected, the magnitude of overtopping was more pronounced for flow diversion into the narrow secondary channel. In both jam scenarios, flow diversion from hypothetical ice jams, revealed trends of locations that were more or less prone to erosion. Increased shear stresses were

observed at three types of locations while decreased shear stress was observed at one. Each trend is presented below:

1. Increased shear stress in existing secondary channels, sufficient to mobilize the channel bed material,
2. Increased shear stress at the downstream ends of depressions or overflow channels on the floodplain surface,
3. Decreased shear stress upstream of the ice jam.

Each of these types of locations are labeled with a numeric identifier (i.e. 1, 2, or 3) in Figures D-10 through D-14.

As seen in the change in critical dimeter and shear stress maps in Figures D-10 through D-14, one of the main effects of a main channel blockage and flow diversion is its ability to locally concentrate flow through side channels (Trend 1) as well as its ability to concentrate in preferential flow paths along the floodplain (Trend 2). Flow diversion has the potential to inundate side channels and side sloughs at discharges that may not otherwise convey water, and in some locations, is capable of mobilizing bed material. If flow diversion is coupled with ice rubble, secondary channels may experience higher bed stresses along the channel bed and bank than during any other open-water event. Diversion of flow and ice into secondary channels, can cause the periodic scour of low-lying vegetation and may contribute to maintaining the current channel width or enlarging the channel.

The downstream ends of secondary channels that now convey water coalesce with the convergence of flow across the floodplain creating local regions of increased shear stress and possible scour (Trend 2).

While shear stress values may not be sufficient to erode vegetation across the floodplain surfaces from water flow alone, when diverted overbank flow is coupled with vegetation removal by ice, the shear stresses may then be sufficient to entrain and erode into the finer-grained overbank materials (Trend 3). Pathways of increased shear stresses along the overbanks are pronounced where adjacent to the main channel ice jams. If a jam were to occur in a region that had limited area to diffuse diverted flow, shear stresses through the overbank may be much higher and coupled with enough strength-competent ice blocks, able to cause significant dissection of geomorphic surfaces or lateral bank retreat.

Lastly, backwater effects from the two jam scenarios cause a significant reduction in shear stress (Trend 3). While the jam holds, this process limits local erosion upstream and downstream of the jam, and creates preferential areas for aggradation in the overbanks.

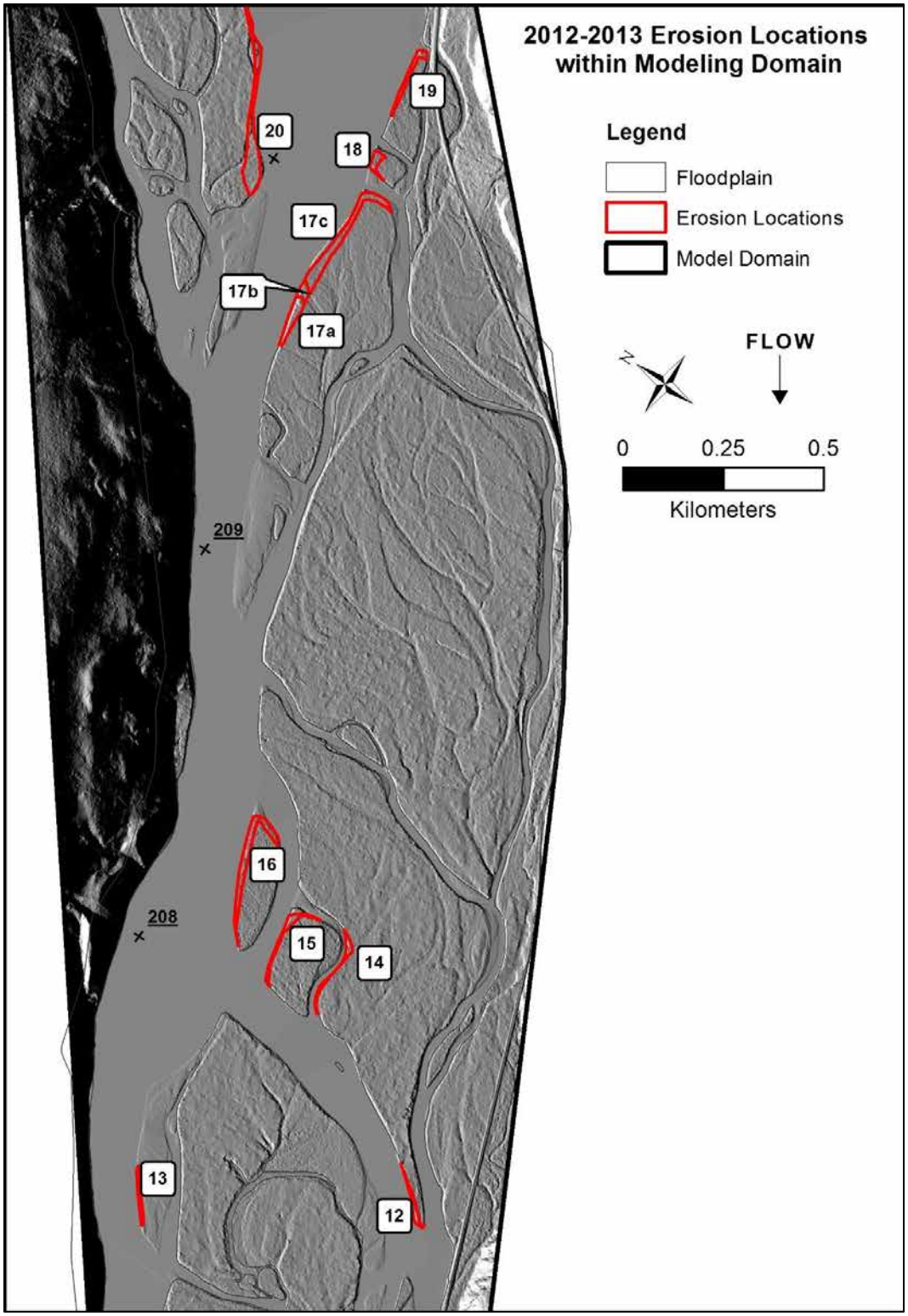

Figure D-2. Locations of erosion between the 2012 to 2013 period within the 2D model domain. Numeric identifiers for each erosion location correspond with locations presented in Section 5.2.

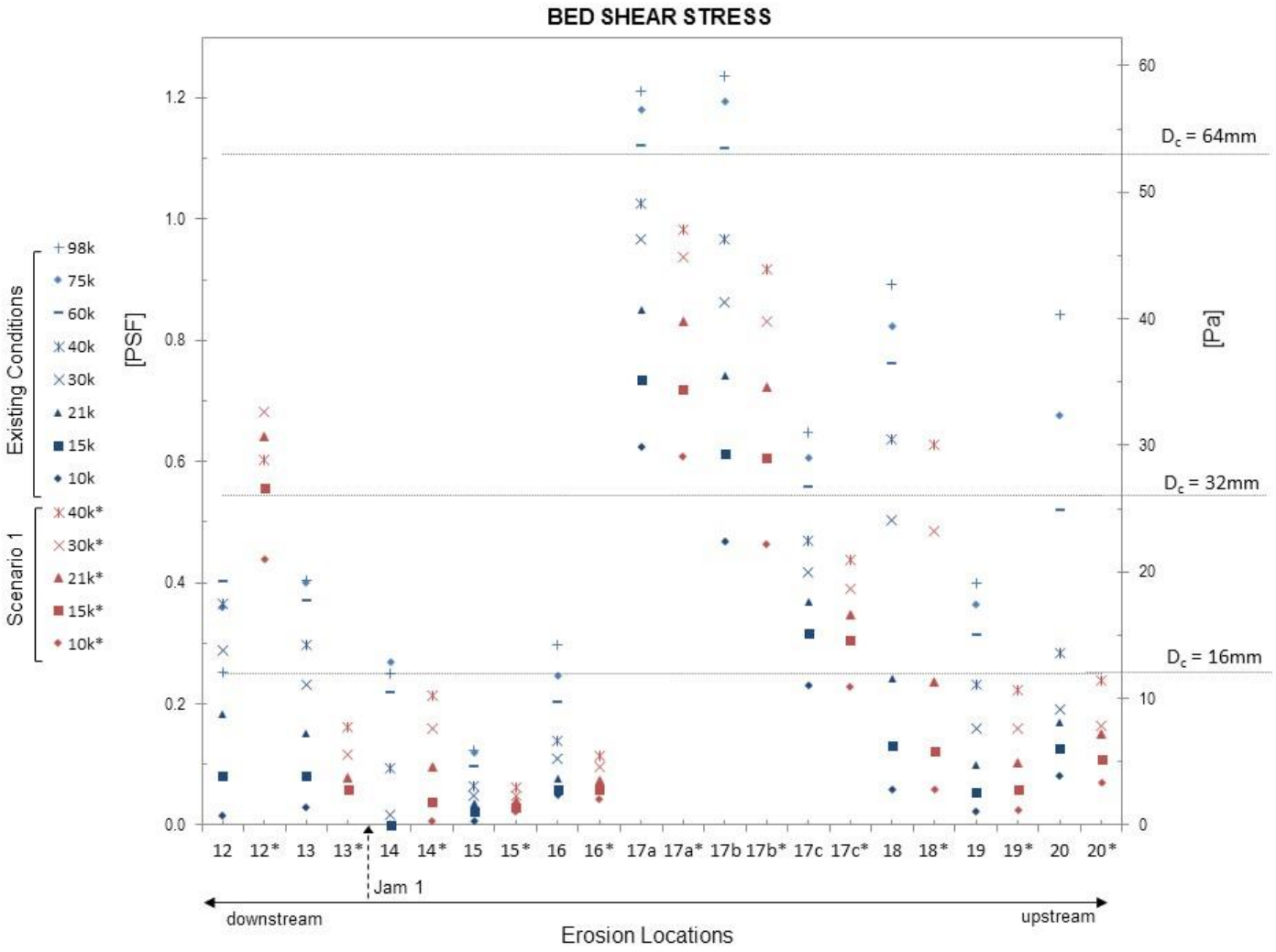

Figure D-3. Bed Sear Stress at Observed Erosion Locations (shown in Figure D-2) from Existing Conditions and Scenario 1 of Simulated Main Channel Blockage. Critical shear stress for various grain sizes are presented.

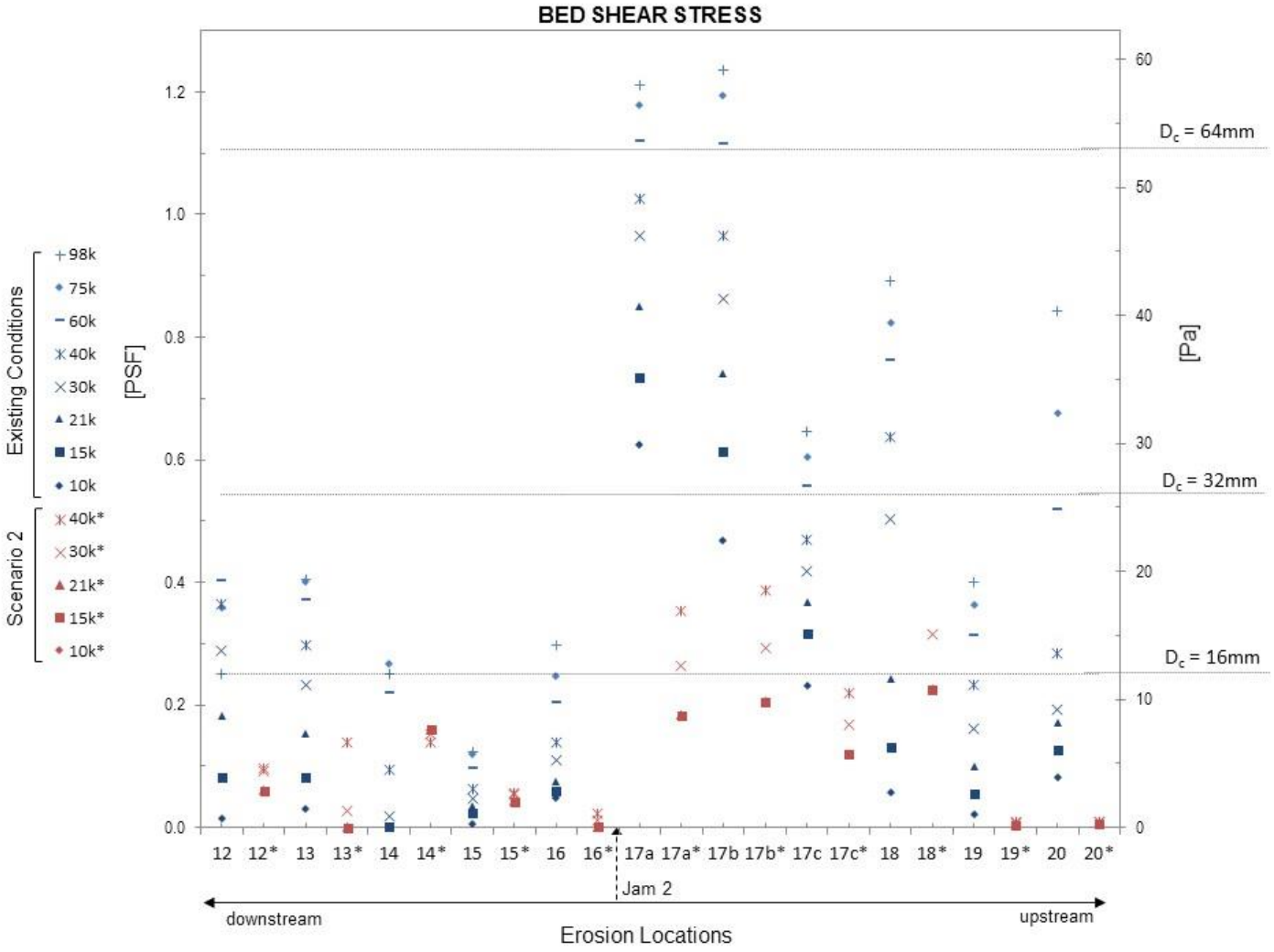

Figure D-4. Bed Sear Stress at Observed Erosion Locations (shown in Figure 4.16) from Existing Conditions and Scenario 2 of Simulated Main Channel Blockage. Critical shear stress for various grain sizes are presented.

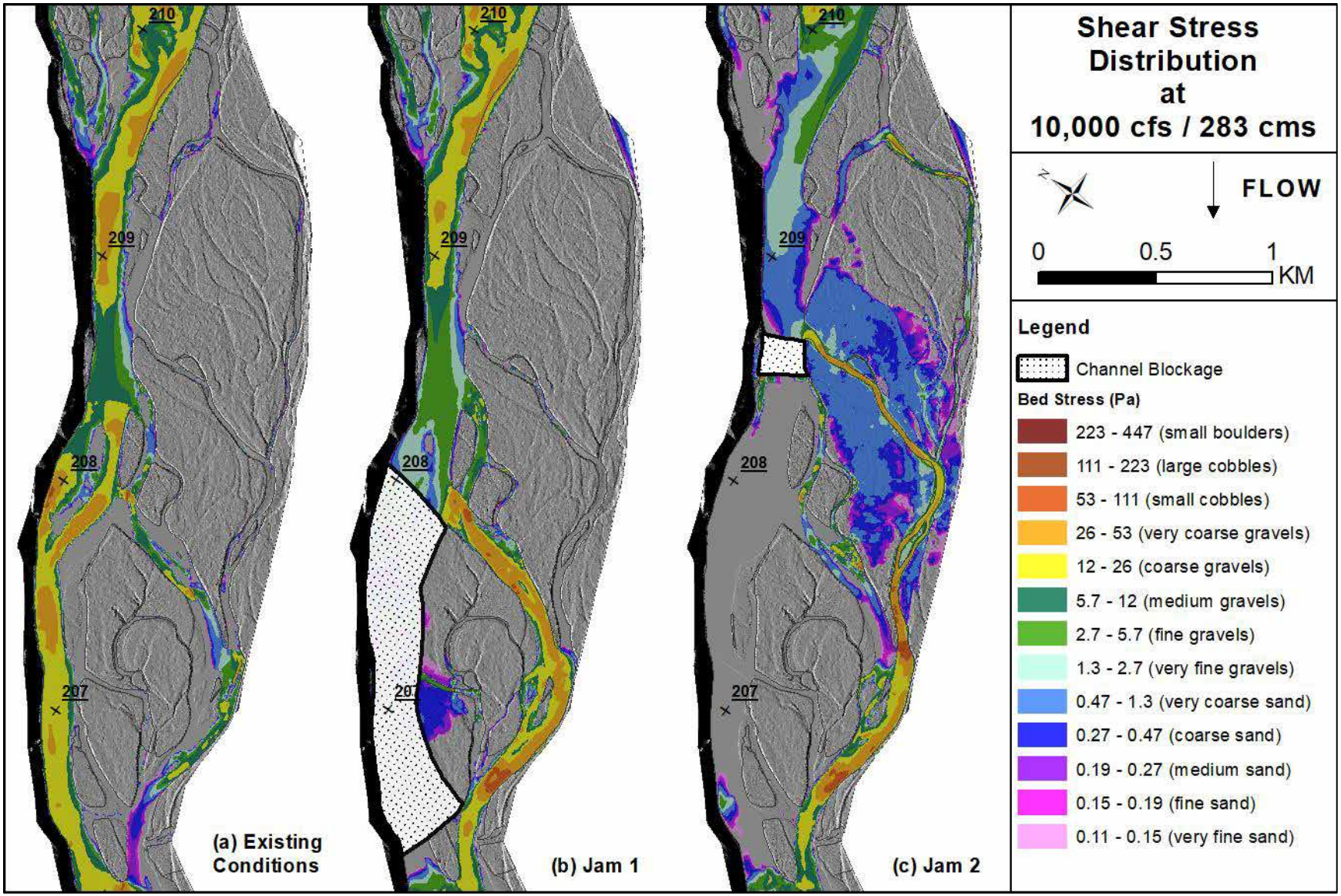

Figure D-5. Shear stress for two scenarios of flow diversion into secondary channels compared to existing condition at 283 cms.

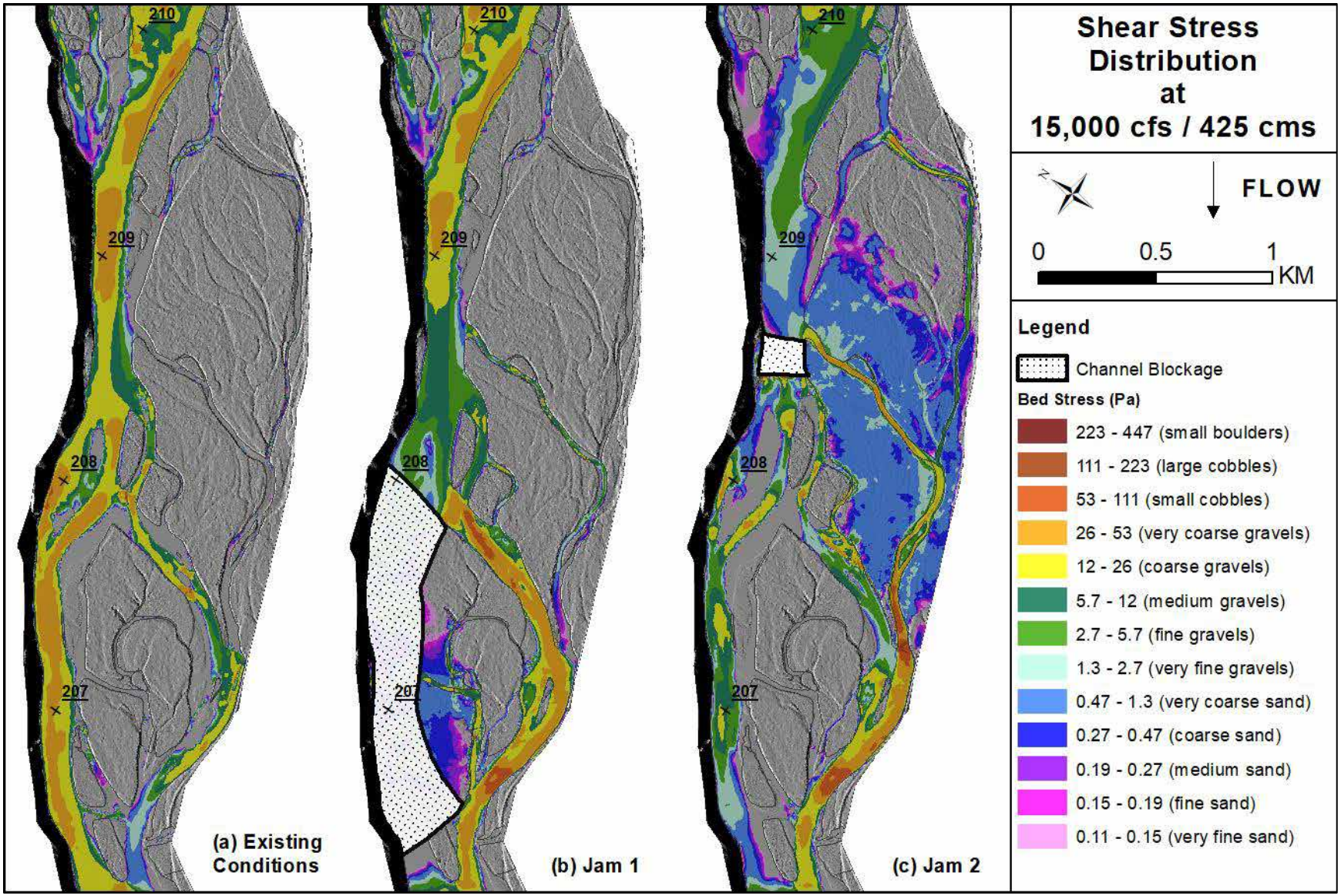

Figure D-6. Shear stress for two scenarios of flow diversion into secondary channels compared to existing condition at 425 cms.

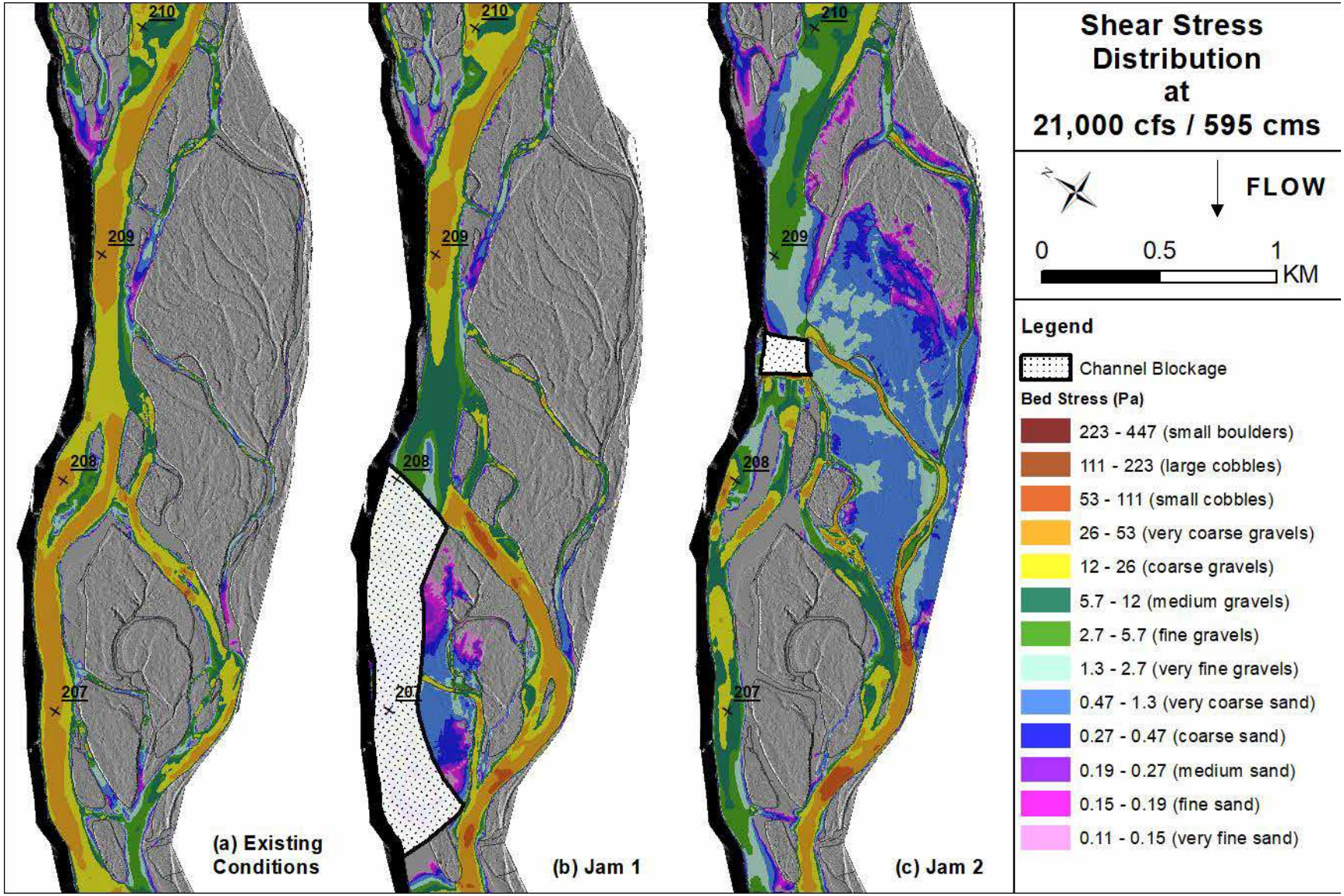

Figure D-7. Shear stress for two scenarios of flow diversion into secondary channels compared to existing condition at 595 cms.

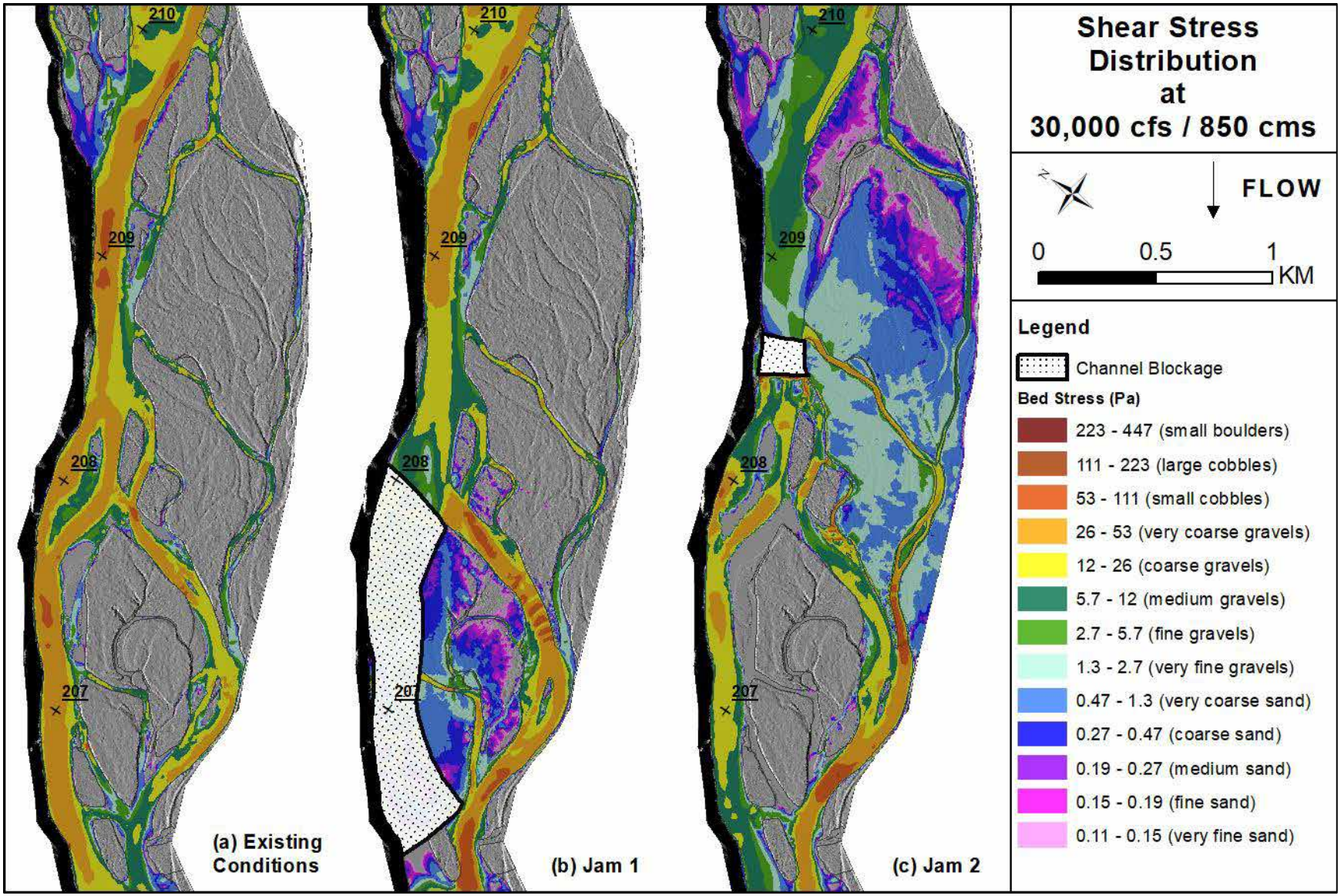

Figure D-8. Shear stress for two scenarios of flow diversion into secondary channels compared to existing condition at 850 cms.

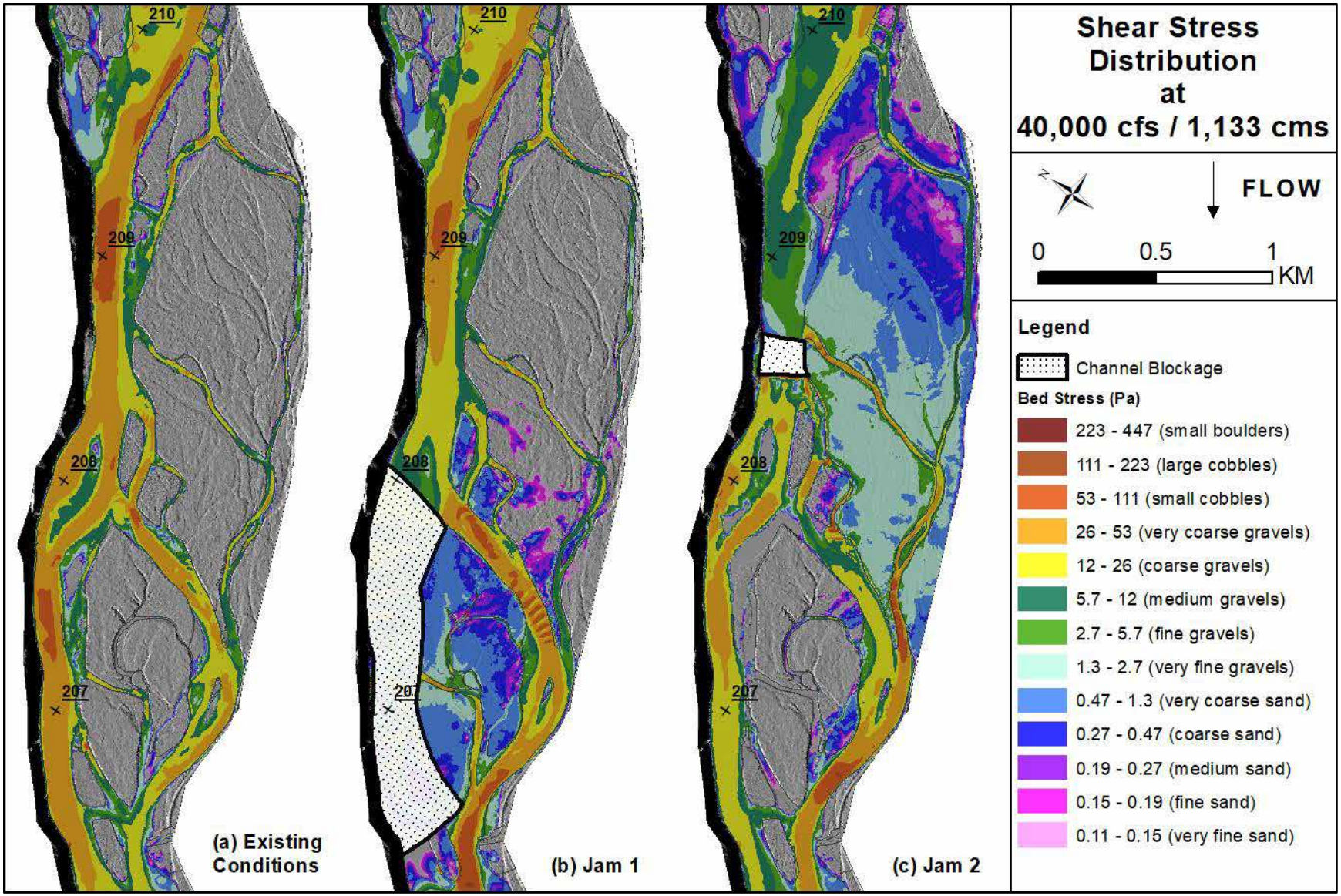

Figure D-9. Shear stress for two scenarios of flow diversion into secondary channels compared to existing condition at 1,133 cms.

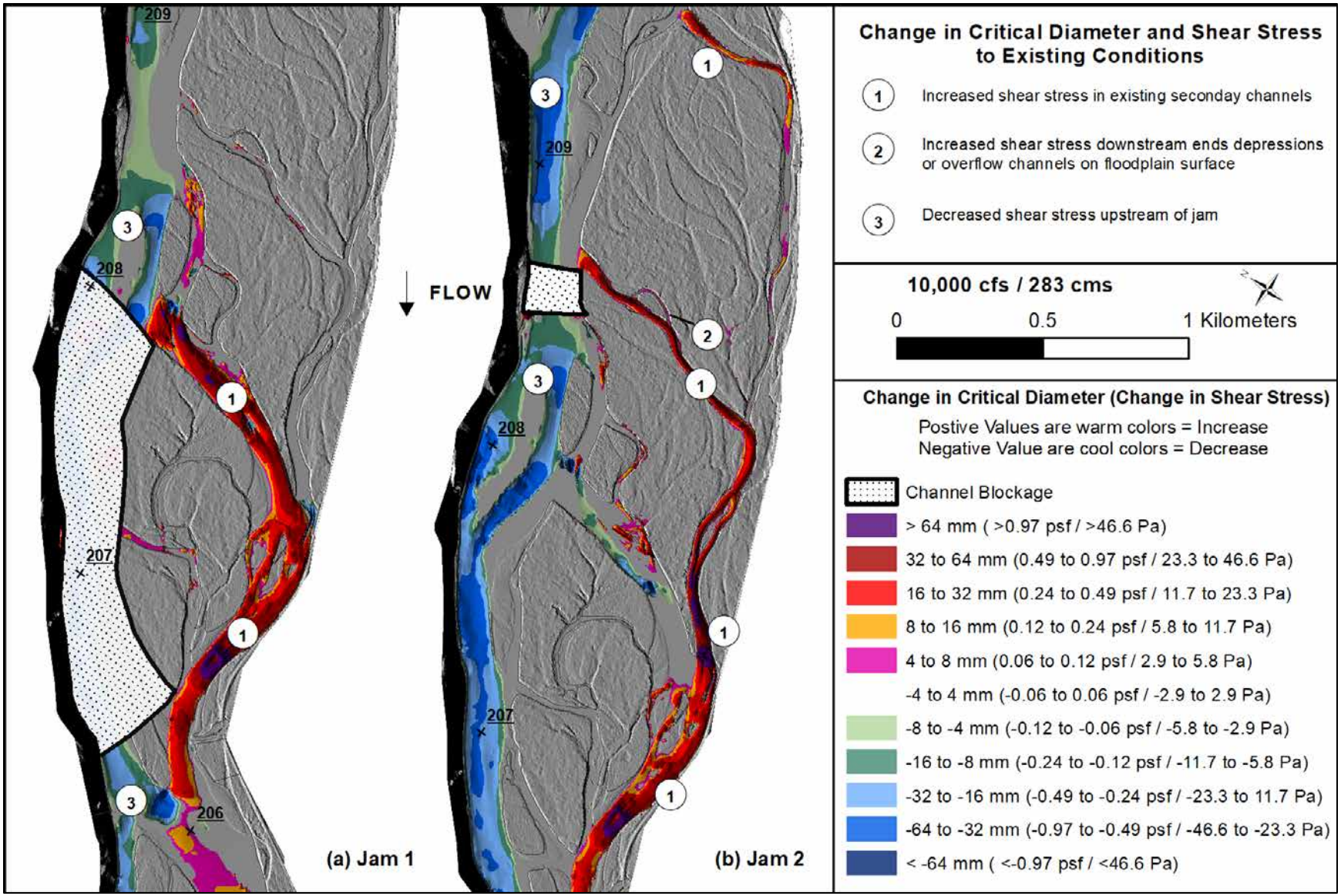

Figure D-10. Change in critical diameter and shear stress from two channel blockages compared to existing conditions at 283 cms.

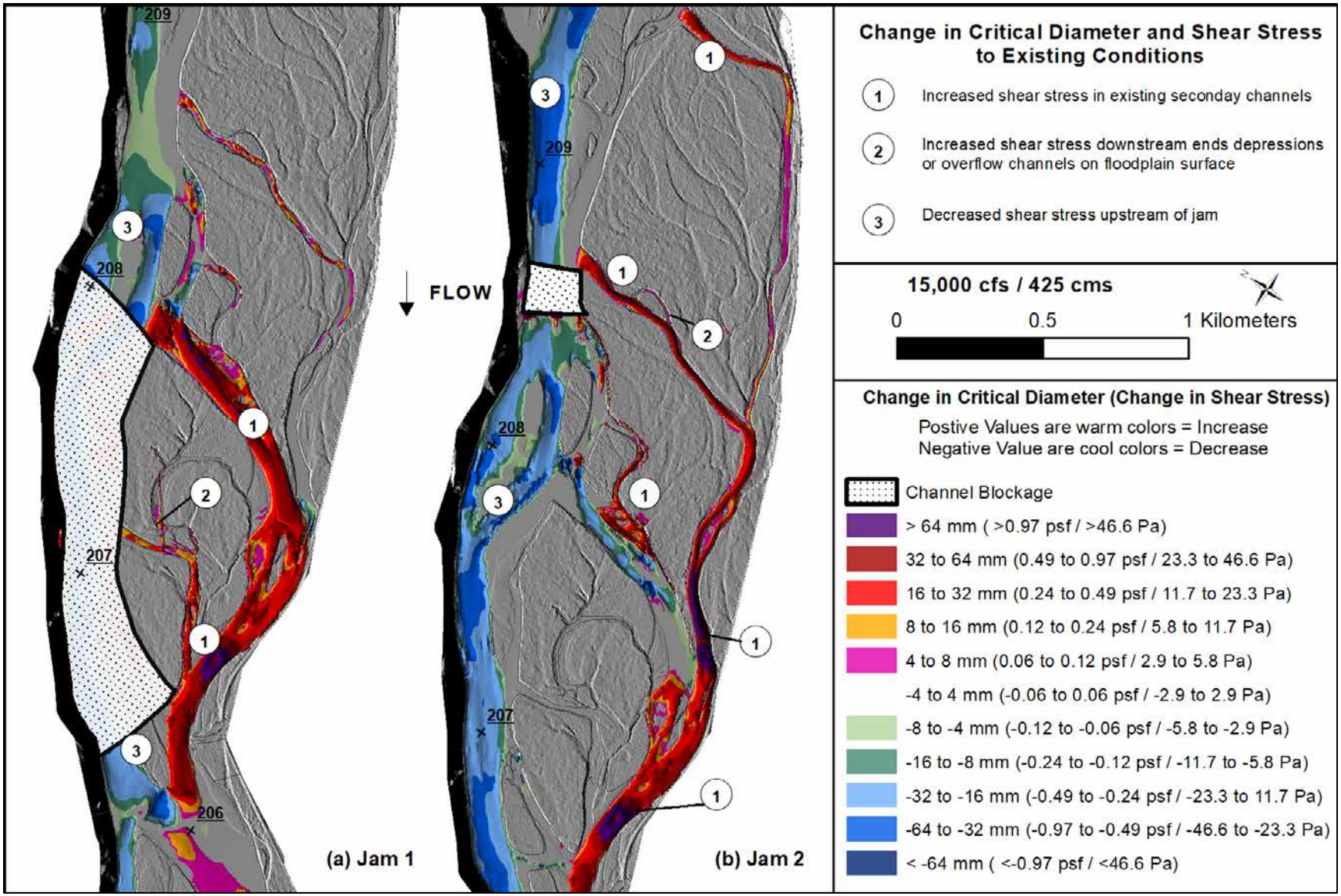

Figure D-11. Change in critical diameter and shear stress from two channel blockages compared to existing conditions at 425 cms.

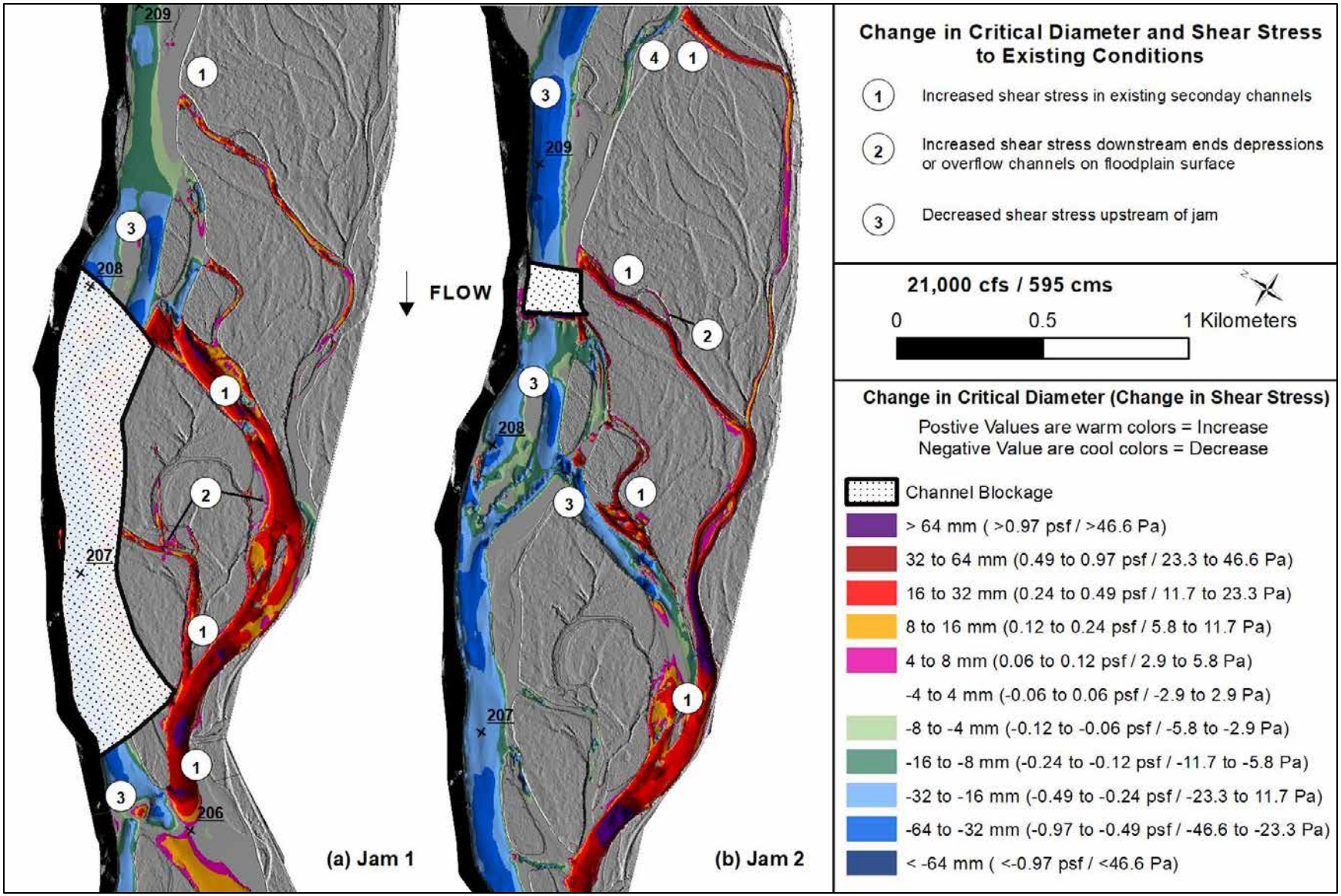

Figure D-12. Change in critical diameter and shear stress from two channel blockages compared to existing conditions at 595 cms.

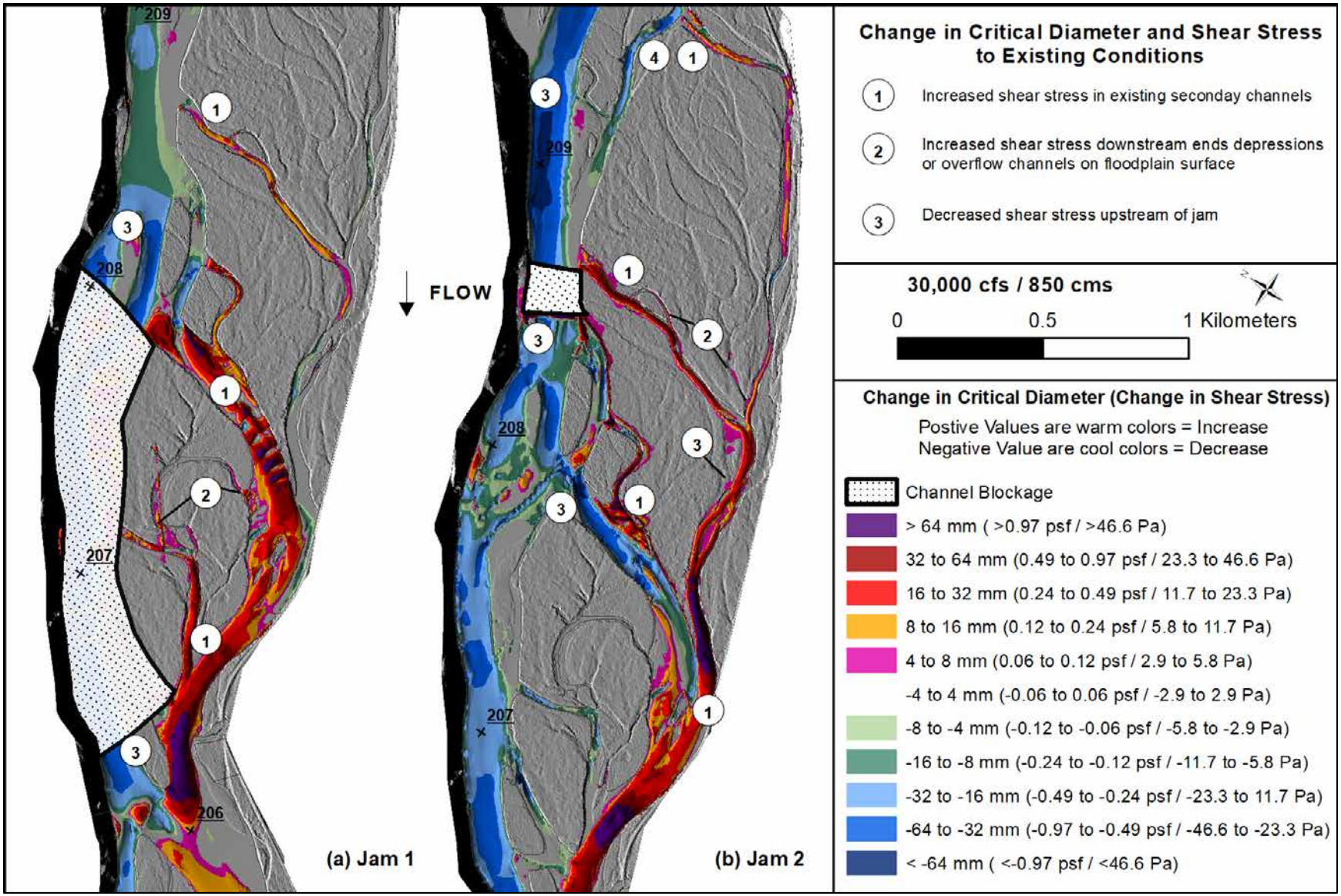

Figure D-13. Change in critical diameter and shear stress from two channel blockages compared to existing conditions at 850 cms.

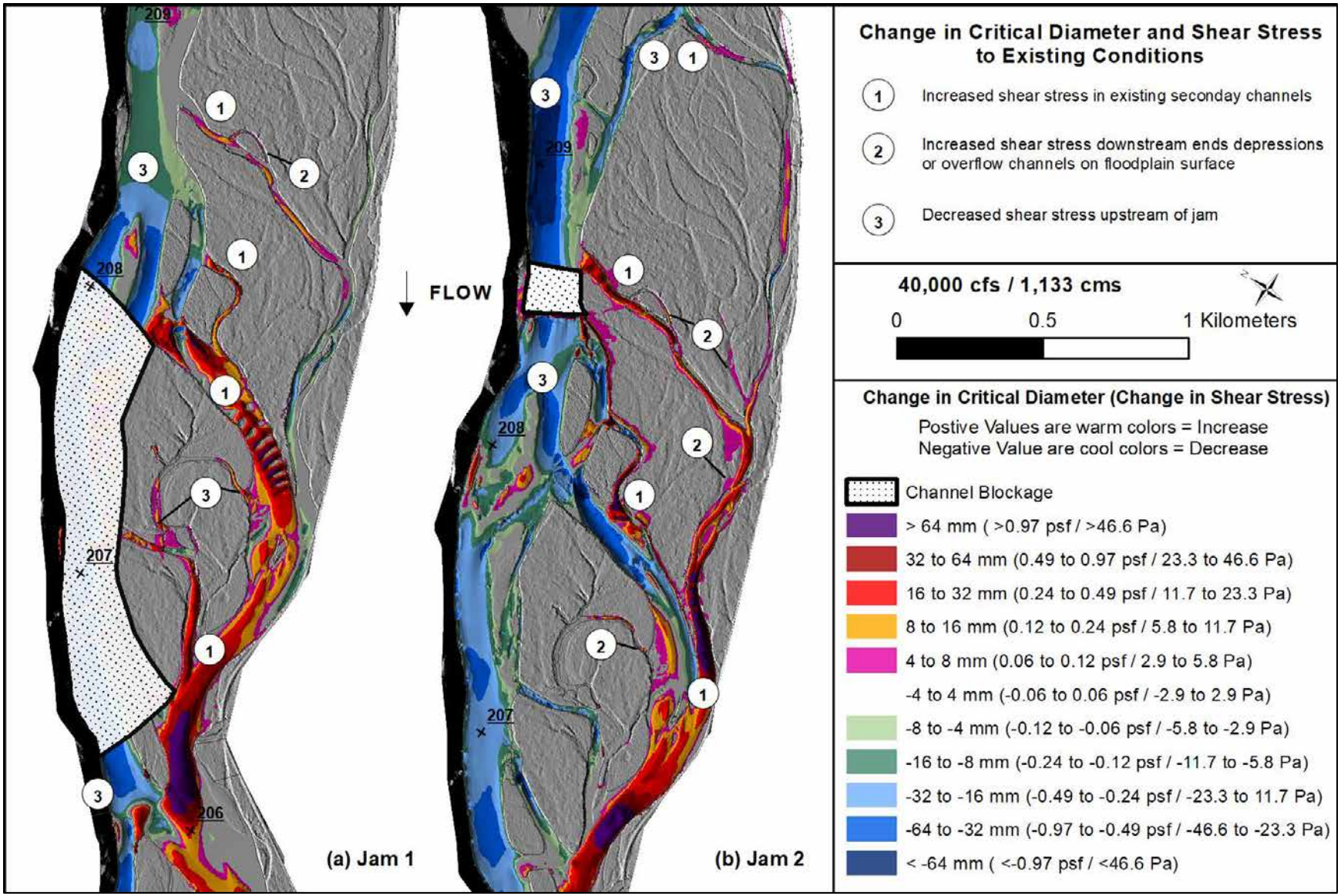

Figure D-14. Change in critical diameter and shear stress from two channel blockages compared to existing conditions at 1,133 cms.